jpl ———————————————➤

FEB 197°

RECEIVE
NASA STI FACILITY

JET PROPULSION LABORATORY
CALIFORNIA INSTITUTE OF TECHNOLOGY
PASADENA, CALIFORNIA

LIST OF AUTHORS

Chapter	Principal Author	Contributors
1. Introduction	W. F. Carroll	
2. Summary	J. D. Ingham	
3. Sail Film Material Requirements for HCRM	W. M. Rowe	F. Bouquet/ W. Steurer
4. Technical Program		
4.1 Basic Sail Film	M. N. Sarbolouki/ W. M. Rowe	W. F. Carroll
4.2 Coatings and Thermal Control	W. M. Rowe	E. E. Luedke/ W. A. Meuller/ R. B. Somoano
4.3 Joining, Handling and Processing	W. M. Rowe/ H. E. Marsh	G. Harbord/ S. H. Kalfayan
4.4 Sail Film Performance	E. Cuddihy/ S. D. Hong/ W. M. Rowe	F. Bouquet/ W. F. Carroll/ W. Dowler/ A. Gupta/ R. Klemetson/ O. Mayes/ M. N. Sarbolouki
4.5 Supporting Structures	W. Steurer	R. Bamford
5. Conclusions and Recommendations	W. F. Carroll	

FOREWORD

This is the final report on the Sail Film Materials and Supporting Structures for a Solar Sail — A Preliminary Design prepared by the Jet Propulsion Laboratory, California Institute of Technology, Pasadena, California. The effort was supported by technology work at NASA-ARC, NASA-LaRC, NASA-MSFC, and by various industrial contracts. The report covers the entire materials portion of the Solar Sailing Development Program conducted over the period October 1976 through July 1977 (FY 1977).

The NASA-HQ personnel responsible for coordination of this materials program were G. Deutch, A. Henderson and B. Achhammer whose suggestions and recommendations contributed significantly to the effort.

The materials development task of the Solar Sail Advanced System Technology program at JPL was performed under the auspices of the Applied Mechanics Division with W. F. Carroll as the Task Manager. Supporting technical personnel at JPL were drawn mainly from the Applied Mechanics and the Control and Energy Conversion Divisions. A partial list of the supporting technical personnel from the other NASA centers who contributed to the program were as follows:

Ames Research Center	Langley Research Center
J. Parker	W. Slemp
A. Heimback	V. Bell
K. Johnson	

Marshall Space Flight Center

R. Gauss
A. Whittaker

Many individuals at JPL participated in the engineering investigations and laboratory analyses that made the sail materials development effort a success. Their contributions are acknowledged below:

F. Bouquet	basic film, system performance
H. Broyles	basic film, system performance
W. Dowler	system performance
R. Fraser	coatings
R. Feadors	system performance
A. Gupta	system performance
R. Gauldin	system performance
G. Harbord	joining and handling
S. Kalfayen	joining and handling
R. Klemetson	system performance
R. Landel	basic film, system performance
D. Lawson	system performance
P. Lindenmeyer	basic film
O. Mayes	system performance

R. Mueller   coatings and thermal control
R. Somoano   coatings and thermal control
J. Stevens   system performance

G. Varsi   basic film, system performance
E. Yen   basic film, system performance

Industrial contractors and institutions who made significant contributions to the sail materials development effort either directly by performing laboratory development and materials testing or indirectly by providing test materials and data were as follows. A list of each of the individual contributors at these organizations would be very difficult to compile. Contractor reports are listed in Appendix III.

Battelle Columbus Laboratories . . .   Columbus, Oh
Boeing Aerospace Co. . . . .   Seattle, Wa.
Brookhaven Laboratories . . . . . .   Long Island, N. Y.
Ciba-Geigy Corp. . . . .   Ardsley, N. Y.
E. I. duPont . . . .   Wilmington, Del.
Dyne Optics . . . .   Corona Del Mar, Ca.
Endurex Corp. . . . .   Mesguite, Texas
Ferro Corp., Composites Div. . . .   Culver City, Ca.
General Dynamics, Convair Div. . . .   San Diego, Ca.
GM Vacuum Coating Laboratories . .   Newport Beach, Ca.
King Seeley Corp. . . . .   Winchester, Mass.
Keim Precision Mirrors . . . .   Burbank, Ca.
Midwest Research Institute -
North Star Div. . . . .   Minneapolis, Minn.
Optical Coating Laboratories, Inc. .   Santa Rosa, Ca.
Richmond Corp. . . . .   Redlands, Ca.
Rockwell International
Science Center . . . .   Thousand Oaks, Ca.
Surface Activation Corp. . . . . . .   Syosset, N. Y.
Surface Science Laboratories . . . .   Palo Alto, Ca.
P. J. Schweitzer . . . .   Lynn, Mass
TRW Defense and Space
Systems Group . . . .   Redondo Beach, Ca.
University of California
at Los Angeles . . . .   Los Angeles, Ca.

CONTENTS

FIGURES

TABLES

SOLAR SAIL DISTRIBUTION

K. Atkins	180-700	3095	M. Jacobs	291-208	7062
R. Bamford	157-410	4225	R. Jacobson	FT-D328	5066
A. Beck	138-310	4575	J. James	180-901	3580
A. Berglund	233-307	5111	W. Jaworski	157-102	3126
C. Berglund	171-301	6995	S. Kalfayan	84	3233
R. Boain	156-220	2947	J. Kievit	158-224	6142
F. Bouquet	157-507	4482	J. King	180-703	7546
J. Brayshaw	157-316	4007	R. Klemetson	125-159	7736
H. Broyles	67-201	5557	A. Klumpp	FT-D315	6795
F. Bristow	180-200	5011	R. Landel	67-201	4402
W. Carroll	157-507	5309	W. Layman	157-205	3023
F. Collella	180-201	7006	D. Lawson	233-119	5609
E. Cuddihy	67-201	3188	P. Lyman	157-205	3730
G. Coyle	158-224	6514	E. Marsh	198-326	3599
D. Dipprey	198-102	2099	H. Marsh	67-201	3170
W. Dowler	125-159	3169	W. Mueller	84	2420
W. Downhower	180-401	5453	B. Murray	180-905	3405
W. Eklund	180-704	2946	M. Neugebauer	183-401	4110
F. Felberg	180-500	4241	R. Newburn	183B-365	2319
R. Frazer	183B-104	4613	R. Norton	138-310	5440
L. Friedman	180-701	6015	W. O'Neill	156-217	2476
C. Gates	180-801	6354	R. Parks	180-404	3442
R. Gauldin	125-159	4543	R. Ploszaj	233-306	4429
M. Gayman	158-224	6142	D. Rea	180-901	6243
R. Goldstein	122-123	3943	G. Robillard	169-533	7780
S. Gunter	198-112A	4097	G. Rodriguez	198-326	4057
K. Gupta	144-218	3114	W. Rowe	157-507	2898
H. Haglund	180-701	2831	W. Ruff	158-224	3589
T. Hamilton	180-801	6313	M. Salama	138-310	3041
N. Haynes	180-901	2260	M. Sarbolouki	67-201	3204
A. Hibbs	180-703	2430	C. Sauer	156-220	4875
S. Hong	67-201	5794	C. Savage	157-315	6580
J. Ingham	67-201	4401	J. Schmuecker	158-224	2866

SOLAR SAIL DISTRIBUTION (Cont'd)

L. Schumacher	T-1201	4627	G. Varsi	125-159	6390
D. Smith	156-217	4877	B. Wada	157-507	3600
R. Somoano	122-123	2213	A. Wilson	144-218	2429
W. Steurer	157-507	5017	J. Wilson	180-401	3270
J. Stevens	158-224	4796	J. Wright	156-220	7503
L. Stimpson	157-102	3683	E. Yen	122-123	
M. Trubert	138-310	6448	D. Yeomans	FT-D412	2870
C. Uphoff	156-220	3054			

AMES

J. Parker
A. Heimback
K. Johnson

GODDARD

R. Farquhar

JOHNSON

M. Fagey

LANGLEY

V. Bell
W. Boyer
O. Childress
W. Slemp

NASA HQ

B. Achhammer
G. Deutsch
J. Disher
A. Henderson
D. Herman
N. Hinners
J. Kramer
S. Sadin
M. Salkind
P. Tarver
A. Timothy
R. Wallace
J. Yardley
T. Young

MARSHALL SPACE FLIGHT CENTER

R. Gauss
K. Johnson
A. Whittaker

Chapter 1

INTRODUCTION

In November 1976, NASA initiated an effort to examine solar sailing technology with a mission to rendezvous with Halley's Comet. Since the mission would require a new project start in FY '79 (Oct. 1978) in order to meet an early 1982 launch date, the purpose of the study was to design and to demonstrate project technology readiness by the summer of 1977.

The background of Solar Sailing and details of the complete system design are described in Refs. 1 and 2.

The critical "enabling technology" for a Halley Comet Rendezvous Mission (HCRM) is an ultra-light, highly reflecting material system capable of operating at high solar intensity (high temperature, high radiation dose) for long periods of time.

When the program was initiated in late 1976, a target area density of 4.5 gm/m^2 had been established for the Sail material system (basic film, joints, coatings, reinforcement/rip stop). The Sail was required to operate more than 1 year at 0.3AU (11 suns); the equilibrium Sail temperature at that solar intensity, based on estimated properties, was 370°C. Furthermore, films (similar to those which have been fabricated for space instrument covers) requiring production and handling in a controlled laboratory environment were unacceptable. The total area of the flight HCRM Sail was nearly 10,000,000 ft^2; with scrap and test and spare hardware, twice this quantity was required.

By July 1977, feasibility had been demonstrated for a Sail material System (film, joints, coatings) with an area density of only 3.3 gm gm/m^2, producible in the required quantities and capable of operating at 0.25 AU (16 suns), with an equilibrium temperature of 250°C. It might have been possible to go closer to the sun (with higher

thrust at a higher temperature) for the film, but this was not necessary for a successful mission and was beyond the demonstratable limits for the structure and spacecraft.

Analyses and experiments late in the study indicated a reasonable probability of achieving a Sail material system with an area density approaching 1.6 gm/m^2. In fact, extrapolation of technology to such a density was more sound and defensible than the original target of 4.5 gm/m^2 had been in Nov., 1976.

The success of the Sail materials program and the data reported here is the result of coordinated four-center NASA (JPL, ARC, LaRC, MSFC) studies and cooperative and subcontracted efforts by a large group of industrial, research and academic organizations.

As a tool for planning, management and reporting, the materials program was organized into five major subdivisions with the first four addressing the film materials. The main technical body of this report, chapter 4, follows this organization. The major subdivisions are:

(a) Basic Film

(b) Coatings and Thermal Control

(c) Joining and Handling

(d) System Performance (failure mode analysis, radiation effects, etc.)

(e) Supporting Structures Assessment for the Heliogyro

REFERENCES

1. Friedman, L.D., et al., "Solar Sail Development Program - Final Report," JPL Report 720-9, Vol 1, January 30, 1978.

2. Friedman, L.D., et al., "Solar Sailing - The Concept Made Realistic," AIAA 16th Aerospace Sciences Meeting, Paper No. 78-82, January 1978.

Chapter 2

SUMMARY

The Advanced Systems Technology (AST) materials effort for the Solar Sail, consisted of activities in five principal areas: (1) Basic film materials and their properties, (2) radiative coatings and their properties, (3) Sail material joining methodology (4) space environmental stability/performance assessments and (5) supporting structures assessment for the Heliogyro.

In the area of basic film materials, an exhaustive survey was performed with the help of other NASA centers, an industry conference for film producers, and a contracted effort at Battelle-Columbus Laboratories. A first choice, basic film was selected, which met all mission requirements. This material was Kapton H, a thermosetting polyimide manufactured by E.I. duPont.

A series of target properties was established for the basic polymer film which included an areal density of ≤ 3 g/m^2 (this value had evolved from an earlier requirement of 3.6 g/m^2 at the start of the program), thermal stability range of -130 to 250°C, thermal cycling capability of 1600 cycles between 210 to 250°C, high radiation resistance, tensile strength of 28,000 to 35,000 KN/m^2 and tear initiation resistance of about 0.1 N/μm. Five candidate polyimides were identified and ranked in the following order on the basis of their properties and processing characteristics: The prime candidate, Kapton, directly manufactured by duPont (to meet the thickness requirement), chemically etched Kapton, plasma etched Kapton, and two thermoplastic polyimides: Ciba-Geigy B 100 (or possibly P 100) and Upjohn 2080. On the basis of available data and preliminary test results, directly manufactured Kapton was initially selected for the benchmark Solar Sail design. But further thermal stability testing was performed on this material and the Schweitzer processed B-100 to satisfy missing data requirements. The conclusions were: (1) the initial properties of Kapton are superior to those of B 100; (2) Some B 100 properties improved on aging, but never exceeded those of Kapton; (3) at 250°C Kapton is significantly better

than B 100; (4) at 270°C both materials are at their best, and B 100 improves, apparently by cross-linking after about 10 days exposure; (5) Both films meet the target properties at 250 to 270°C; at 305°C B 100 properties begin to deteriorate and Kapton is superior.

Although B 100 has some advantages, e.g. potentially more producible in ultrathin thicknesses, lower density and lower cost, it was not proposed as the baseline material for the HCRM primarily because much less technical data was available than for Kapton and it had not been produced commercially in large quantities.

The criteria for selection and evaluation of Sail film coatings were established. They included high reflectance and specularity on the front (sun facing) surface, durability, capability to survive long-term space exposure, light weight, low cost, high thermal emittance (on the back surface), capability to provide radiation protection to the organic film, and sufficiently low resistivity to dissipate space charges.

Coatings were evaluated by examination of the technical literature, theoretical analysis and detailed test measurements. To assist in this area, a thermal radiative property measurements program was performed at TRW Defense and Space Systems Group. Aluminum (1000Å) was selected as the baseline reflective coating over silver because of its better performance in the UV region, better tarnish resistance and lighter density. On the basis of data gathered from incoming receiving tests by TRW on commercially procured aluminized polymer films over a period of several years, a criterion for a minimum solar reflectance of 0.88 was established. Aluminum also satisfies the other criteria mentioned above. Several thermal coatings effectively increased the emittance (>0.6) of the backside of the Sail film and thus lowered the maximum operating temperature of the Sail during the near-sun encounter to an acceptable value (for polymer films) of 250°C. Initial estimates of Sail operating temperature were 370°C. Chromium (125Å) was selected as the baseline backside coating. Indium-tin-oxide (ITO) and carbon, evenly dispersed through the polymer material, are alternatives. Carbon

coatings were found to be relatively unsatisfactory in most respects. ITO (1500Å) is considered to be a viable candidate, especially if the emitting side coating were required to be of a greater thickness to afford better radiation protection (the emittance enhancing characteristics of the chrome is considerably reduced at thicknesses greater than 125Å).

Losses arising from sublimation and sputtering by solar protons of either aluminum or chromium were estimated to be small and are not considered to be a problem. Although some limited data were obtained, the capability or lack of capability of the emitting side coatings to adequately protect the polymer film from damaging charged particle radiation was not well established. The protection afforded by the aluminum reflector coating (1100Å) however, appeared quite adequate. The most serious existing reservations about the reflective and emissive coatings are potential degradation of specular reflectivity and emissivity during handling, storage and exposure to the space environment.

Several coating processing methods were examined, e.g. physical vapor deposition, ion beam sputtering and ion plating. While all these methods appeared feasible, increased and/or improved production facilities would be required, especially for large volumes of chromium. The physical vapor deposition method was selected as the baseline process primarily because it was the most commercially developed technique for applying the quantities of film coatings required for the Sail production schedule for HCRM.

Various joining methods were evaluated and tested for bonding Sail film segments. Although considerable advancement in technology would be necessary, a method was developed that demonstrated the feasibility of a continuous, high-speed "heat seal" type adhesive joint. Calculations established that over 400 miles of seams would be required just to join Sail segments (for either the Heliogyro blades or the square Sail configuration).

A thin bond line of ≤ 3.8 μm (0.15 mil) was developed for the modified butt type, adhesive joint. Commercially available bonding equipment was located that could be modified to perform the bonding process and a 4' x 5' demonstration panel was fabricated. The adhesive selected, duPont NR150B2G, was found to adequately meet the strength requirements for the joint. Provisions were made in the joint design to tightly control the amount of exposed adhesive on the sun-facing side of the Sail to minimize thermal problems.

Necessary further technology advancements that would be required for Sail fabrications include the capability for handling large quantities of the fragile, ultrathin films during Sail fabrication while retaining the critical optical and thermal properties.

Simulated space radiation testing was conducted on Sail film materials at the Boeing Co., Brookhaven Labs, NASA-MSFC, NASA-ARC and JPL. The bare Kapton was sufficiently thermally stable at temperatures up to 300°C. However, it was found to be readily degraded by UV at temperatures of 260°C and higher. Exposure of bare Kapton and B100 film in vacuo, at 11 suns solar UV intensity and 1.3 KeV protons resulted in film blackening and carbonizing. Despite attempts to control the test temperatures, it was apparent that thermal runaway had occurred based upon the extent of thermal degradation that was observed. This was mainly attributed to deficiencies in the test design. While these tests on uncoated samples were plagued by thermal runaway, resulting in the predominance of very high temperature effects, the results did not indicate that particulate radiation (and UV) would result in significant degradation of coated Kapton.

Test results on Kapton stability were also taken from the literature and from experimental results obtained as part of the materials evaluation program. These were analyzed to also help to predict the thermal stability of Kapton during a HCRM. These analyses indicated that Kapton would have adequate thermal stability, especially if the film were thermally annealed prior to Sail fabrication to prevent potential hydrolytic degradation.

Additional investigation of the kinetics of degradation and mechanical properties indicated a close correlation between chemical degradation and deterioration of mechanical properties, and showed that mechanical integrity would be adequate for the mission by a large margin of safety. For Kapton, creep at 50 psi and 250°C was estimated to be 3.3×10^{-3} in/in and thermal expansion (from -100 to 250°C) was estimated to be 1.02×10^{-2} in/in. Thermal shrinkage (nitrogen atmosphere, 264°C, 3 days) was -3.3×10^{-3} in/in.

Analysis of limited thermal aging data for the baseline adhesive joint indicated that while the shear strength of the joints was more than adequate at elevated temperatures, that there appeared to be lowering trends at sub zero temperatures (although joints were still stronger than the parent material). Test data examined were for relatively short aging times (18 days) however, and further experimental work would be required before valid conclusions could be reached.

Other materials evaluations were concerned with materials to be used as supporting structures for the sail film. Graphite-polyimide composites were selected for all the major structural components of the Heliogyro. These include the tubular truss center body, blade retention structures, battens and tendons. The tendons would require high tensile strength fiber, e.g. HTS, Celion 6000, Thornel 300 or Modmore II. The other components require high modulus fiber, such as HMS or GY'70. Because of its superior high temperature properties NR-150-B2G was selected as the preferred polyimide, although some problems were anticipated with regard to reproducible curing. The only critical environmental condition was believed to be the temperature profile to be expected during the mission. Analyses indicated that the highest transient temperatures ($\sim$320°C) would be encountered in the hub structures. Therefore the use of NR-150-B2G would be mandatory. The battens would be covered with heat shields, so the maximum estimated temperature would be about 260°C, which would allow the use of other polyimides. The maximum temperatures for the tendons of 224°C (normally), with excursions to 245°C for a total of 96 hours allow a substantial safety margin.

The feasibility of producing 1 mil tape for the edge tendons was established. The tensile strength would allow a safety factor of 2.5 at the start of the HCRM, falling to a minimum of 1.2 after progressive micrometeoroid damage based on a prevailing conservative meteoroid model. It was also determined that production of the tubular structures would be feasible.

Chapter 3

SAIL FILM MATERIALS REQUIREMENTS FOR HCRM

With the discovery of a rendezvous trajectory for a HCRM,[1] JPL began an intensive study of the potential readiness of Solar Sailing. The assessments of this study were positive and an advanced technology development program was initiated in November, 1976. The development effort included the following considerations:

(a) Sail materials

(b) Sail size, established by mission performance (e.g. characteristic acceleration, readiness date, etc.)

(c) Weight and storage constraints imposed by Shuttle bay capabilities and spacecraft component weights

(d) Materials (Sail film and other material weights)

(e) Operating temperature limits - reflectivity of the sun-facing surface, space environment survivability and manufacturability

Figure 4-7 gives the equilibrium temperature vs heliocentric distance of vehicle materials for various values of emittance. It is readily seen that the temperature limits of many polymers would be exceeded as the heliocentric distance shortens for certain estimated parametric values of emittance 'e.g. the emittance of some films were estimated at 0.2 to 0.3). The initial best estimate in November 1976 for the emittance of a polyimide Sail film was ∿.3 which corresponded to an equilibrium temperature of 370°C (beyond the design limits of the material) at a heliocentric distance of 0.3. Through improvements in thermal control technology, it was later possibile to decrease both the heliocentric distance and the Sail equilibrium temperature by the time of the July 1977 technology review.

The combination of the desired spacecraft performance parameters and mission environmental requirements dictated an initial set of functional design requirements for the Sail film material.

Although two configurations for Sail design were initially being considered for the program, the Square Sail was dropped as a candidate for the Halley mission in May 1977 as a result of a preliminary design analysis at JPL, and the Heliogyro Sail was selected as the baseline design concept.

With respect to the Sail film materials however, the type of Sail configuration played a lesser role in determining functional design requirements than with the maintenance of properties during pre-launch, launch and deployment. The latter appeared easier to achieve with the Heliogyro. The primary environmental criterion was the high thermal radiation during the near-sun cranking orbit; other environments of significance were UV and high-energy radiation as well as chance micrometeroid encounters.

3.1   FUNCTIONAL DESIGN

The mission profile for Halley was based on certain Sail performance parameters that were, in turn, based on desired Sail film material physical, thermal, optical and electrical properties. For example, at the time of the technology review in July 1977, the maximum allowable area density for the basic film without coatings, ripstop, etc., was calculated to be ∿3.0 g/m^2 to maintain desired spacecraft velocity and payload capabilities. Early program requirements were 3.6 g/m^2, which was reduced as other program requirements grew. This meant that if a material such as duPont's Kapton H film were used (with a density of 1.42 g/cc) it would have to be a little less than one-tenth mil (∿2 microns) thick to meet the 3.0 g/m^2 requirement. The minimum thickness Kapton film commercially produced was over three times this thickness (7.5 microns).

The thermal requirements for the film were also severe. As earlier indicated, calculations predicted that the temperature of aluminized polymer films would reach approximately 370°C during the 0.3 AU solar distance cranking orbit (assuming α s for the aluminized side as 0.16 and an emittance of 0.3 for the back side of the film). At

these temperatures Kapton polyimide appeared to be the only possible polymer candidate and even it looked very questionable when considering the four year duration of the mission with extended times at 0.3 AU.

The early optical and electrical property requirements for the Sail film did not appear as difficult to meet. A total reflectance value of 0.85 for the metallized film surface appeared to be achievable as did an electrical resistivity of 10^6 Ω/square.

Sail film mechanical properties were dependent upon the Sail configuration. For the Square Sail (which was considered the most stringent of the Sail design concepts with respect to the loads on the film), these were as follows:

      (a)   Tensile Yield Stress = 0.2 psi minimum

      (b)   Elastic Modulus = 43,000 psi minimum

      (c)   Bend Radius = 0.002 in* maximum

      (d)   Rip Stop = 0.5 lb**

3.2   MAINTENANCE OF PROPERTIES

3.2.1   Pre-launch

During the Sail film development effort, there was little analytical time devoted to determining the pre-launch mechanical requirements which included fabrication and handling stresses.

The reason being that these would be dependent upon final decisions on processing methods employed, stowage configuration, and spacecraft design. Since the Heliogyro Sail configuration was selected in late May 1977 to be the design, these parameters had not been sufficiently defined at the time that work was curtailed on the program

---

*Bend radius without creasing
**Minimum force without rip propagating through rip stop.

to allow much effort in determining pre-launch conditions. A quick assessment revealed that there did not appear to be any significant show stopper type problems with the individual Sail blades of the Heliogyro.

3.2.2 Launch and Deployment

The same was the case for launch and deployment loads. Preliminary analyses indicated that the magnitude of these loads was within the limits of the mechanical property requirements that were established earlier for the Square Sail.

3.2.3 Mission Environment

Activity directed toward the mission environment was analytical in nature and was based on the projected mission profile. Considerations were given to the following:

(a) <u>Charged Particles</u> - A primary concern at the beginning of the mission was the possible degradation of the thin, basic film structure or its reflective coating due to impact of energetic charged particles. Initially, of course, the trajectory and the radiation environment were unknown and an effort was undertaken to define important components. The major sources of the charged particles were assumed to be:

(1) Earth's Radiation Belts

(2) Solar Wind

(3) Solar Flares

(4) Cosmic Rays

For the Solar Sail to be feasible, it was mandatory that the radiation exposure of the film be kept below damage levels for polymers. These damage levels were only approximately known from previous reactor technology. If the polymer film were to be exposed to higher radiation dose levels than initially predicted,

thicker metallized protective coatings would be
required to reduce the level of radiation exposure
to the polymer.

The approach used in this portion of the mission environ-
ment study consisted of the following:

(1)   determination of the total fluences and peak
        flux of charged particles as a function of
        energy over the 4 year mission.

(2)   computer simulation of the corresponding
        nuclear particle dose profile through the
        basic film.

(3)   determination of the Sail requirements based
        upon trade-off results of the above theoreti-
        cal data.

Simultaneously, a combined environment test program
to irradiate potential film candidates was undertaken
to confirm the reality of the degradation over a
range of interest.

(b)   Solar Intensity - In addition to the protons, elec-
        trons and meteroids found in space, the Solar Sail
        materials will be exposed to electromagnetic radia-
        tions from the solar surface. It was found desirable
        to have the Solar Sail go into the sun as close as
        possible for the following reasons: (1) maximum thrust
        for the Sail is achieved (2) the orbital periods are
        less and (3) energy changes can be acquired at a faster
        rate. Early mission trajectories took the spacecraft
        into a heliocentric distance of 0.3 AU, which, as ear-
        lier discussed, appeared to be the temperature limit
        for the materials. This was later reduced to 0.25 AU.
        The Sail, in order to achieve rendezvous with Halley,
        must completely turn ("crank") its orbital plane so
        that the spacecraft flies retrograde, as does the
        comet. Thus, the term, "cranking" orbit was coined to

describe the operation where the Sail cranks over the solar pole for an approximate 400 day time period to achieve the proper retrograde position and characteristic acceleration.

The electromagnetic spectrum of the sun consists primarily of the following major components (1) Ultraviolet, (2) Visible and (3) Infrared radiations, and is relatively constant for a fixed solar distance. The intensity of all three components vary inversely as the square of the solar distance and, in the cranking orbit (0.25 AU), is 16 times that at 1 AU. Outside the Earth's atmosphere, the solar constant is 1.98 calories $cm^{-2}min^{-1}$, and, therefore, the intensity at 0.25 AU is 31.7 calories-cm^{-2}-min^{-1}. Approximately 8% of this value is due to the damaging ultraviolet component; thus the Sail film material must be protected. The sun side coating must reflect most of the ultraviolet component to maintain temperature. The reflector must be specular to maximize thrust; the coating must also reflect or absorb the UV component of this energy to protect the basic polymer film.

(c) Meteoroids - During the mission the external surfaces of the spacecraft will be impacted by meteoroids. According to the present state of knowledge, meteoroids have an average material density of 0.5 g/cm^3 and will impact with a relative mean velocity of 32.6 km/sec. Since very little information exists as to any preferred direction of the meteoroid paths, particularly in the vicinity of the sun, a conservative directionality factor of 1 was adopted. As to the meteoroid flux, which is basically inversionally proportional to particle size, a number of models are existing, only partially supported by measurements in the near-earth region. On the basis of rather conservative flux

models, the fluence in terms of particles/m^2 over the mission duration was defined as follows:

Particle Mass M	Integral Fluence (Particles/m^2 of Mass Greater than M)
10^{-10}	4.6×10^3
10^{-9}	1.9×10^3
10^{-8}	5.9×10^2
10^{-7}	1.3×10^2
10^{-6}	2.3×10^1
10^{-5}	1.9×10^0
10^{-4}	9.8×10^{-2}
10^{-3}	5.4×10^{-3}
10^{-2}	3.2×10^{-4}
10^{-1}	2.2×10^{-5}
1	1.4×10^{-6}

Figure 3-1 identifies the integrated fluence as related to particle diameter for the regime of interest with regard to potential damage, ranging from particle diameters of app. 10^{-1} to 10^{-4} cm. Below this range, particles are too small to cause significant damage, while the encounter probability of particles greater than 0.1 cm diam. is extremely low.

The extent and significance of the damage generated by meteoroid impact depends on the configuration, the material, and the functional characteristics of individual components.

The expected damage to the _film_ may be divided into three modes:

(1)   Minute surface degradation by craters with a diameter of less than $\lambda/4$.
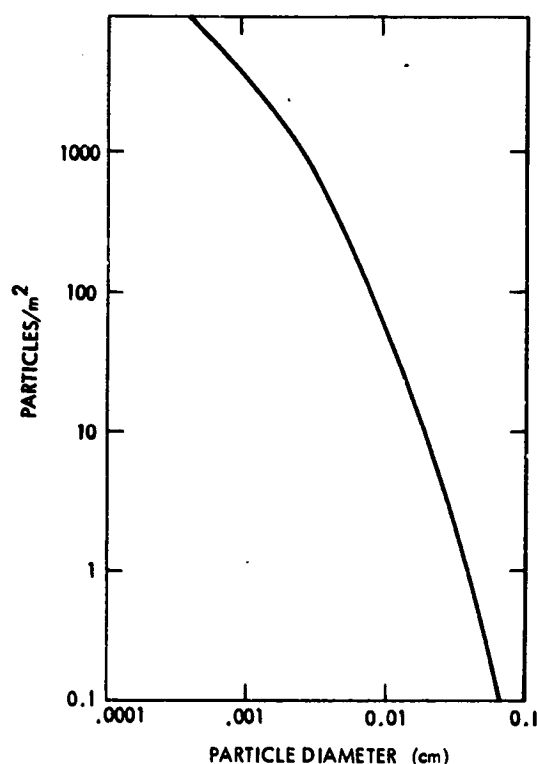
Figure 3-1. Mission-Integrated Meteroid Fluence
as Related to Particle Diameter

(2)   Penetration of the aluminum coating without
       significant damage to the film.
(3)   Penetration or puncture of the film (and
       coatings).

The fraction of the sail area affected by each mode is
identified in Figure 3-2. Since the area fraction
affected by all three modes is less than 0.027%, the
reduction of reflectance and sail efficiency are
negligible. Penetration and puncture of the film
may be of concern in the case of a highly stretched
film material where it may cause tearing between rip-
stops. The tentatively selected Kapton film is con-
sidered insensitive to puncture.
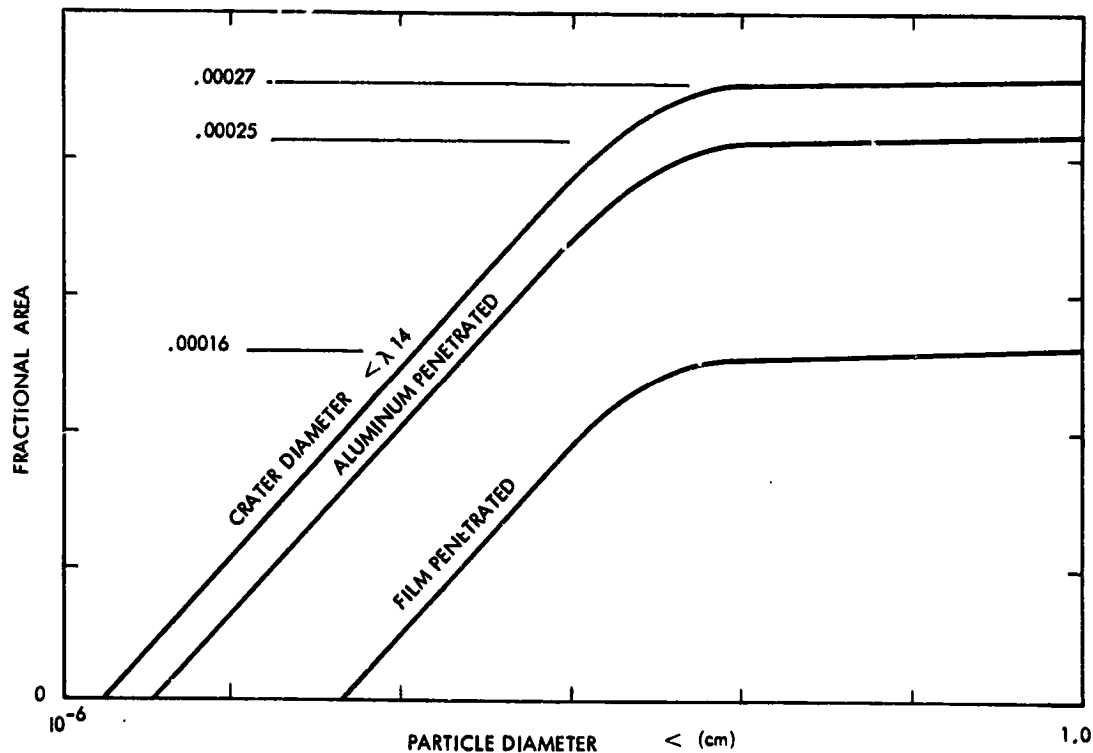
3-8

Figure 3-2.   Effects of Meteoroid Impacts on Sail Film
and Affected Area Fractions

The majority of structural components is likewise
insensitive to meteoroid damage, due to appreciable
thickness and/or extremely low surface area. The
sole exception are the tendons (blade edge members)
due to the combination of an appreciable surface area,
high stress and the use of unidirectional composite
material of low thickness. In this case meteoroid
damage is the primary design criterion, as discussed
in detail in Section 4.5.4.7.

REFERENCES

1. Wright, J.L., "Solar Sailing: Evaluation of Concept and Potential", Battelle Memorial Institute Report No. BMI-NLVP-TM-74-3, November 1974.

Figure 3-2. Effects of Meteoroid Impacts on Sail Film
             and Affected Area Fractions

The majority of structural components is likewise
insensitive to meteoroid damage, due to appreciable
thickness and/or extremely low surface area. The
sole exception are the tendons (blade edge members)
due to the combination of an appreciable surface area,
high stress and the use of unidirectional composite
material of low thickness. In this case meteoroid
damage is the primary design criterion, as discussed
in detail in Section 4.5.4.7.

REFERENCES

1. Wright, J.L., "Solar Sailing: Evaluation of Concept and Potential", Battelle Memorial Institute Report No. BMI-NLVP-TM-74-3, November 1974.

Chapter 4

TECHNICAL PROGRAM

To achieve a Solar Sail design by August 1977 containing all
the technical advancements required for a HCRM, an intensive materials
technology development effort was initiated in November 1976. The pre-
vious section on materials requirements for the Sail discussed the tech-
nical challenges that were involved. This section of the report will
deal with: (1) selection of the basic film material and the characteri-
zation of its properties, (2) coatings and thermal control investiga-
tions, (3) joining and handling studies, (4) Sail film system perform-
ance evaluations and assessments and (5) supporting structures for the
Sail film. Work reported in the latter area is primarily devoted to the
Heliogyro since the design of the Square Sail had not matured to a level
where significant inputs were made by the materials team. The majority
of the support structures technology concepts that were performed for the
Square Sail, was done by contracted efforts. (Refs. 1 and 2.) These were
aborted when the decision was made to pursue only the Heliogyro Sail.

4.1   BASIC SAIL FILM

4.1.1   Candidate Survey

In order to meet the mission performance requirements, it was
mandatory that the weight per unit area of the Sail film be as low as
possible. Based initially on design considerations for a very large
area ($\sim$775,000 square meters) Square Sail, the area density for the
film (minus any coatings or reinforcing strips) was established at
3.6 grams per square meter. This number was subsequently reduced to
3.0 g/m^2 when technology advancements made it feasible. Both the Square
Sail and the ultimately selected Heliogyro design shared this require-
ment. Not only did the basic Sail film have to be lightweight, other
requirements imposed on it were that it be:

   (a)   optically smooth.

   (b)   capable of being coated with and compatible with
         specular metallic and other thermal/optical coatings.

(c)   stable in the space environment (with appropriate
       protective coatings) for long periods of time while
       exposed to high solar intensity and charged particle
       irradiation

(d)   temperature resistant (with appropriate protective
       coatings) to withstand 11-16 times the solar intensity
       on earth (0.3 to 0.25 A.U.) for 1-1/2 to 2 years.

(e)   available in sufficient quantities for manufacture,
       coating and assembly into a very large total area
       (∿1.6 million square meters) to meet the Sail produc-
       tion schedule.

Table 4-1 summarizes the initial target technical require-
ments that were determined to be necessary for the basic film material
for the Heliogyro blades. As mentioned, the area density was later
reduced to 3.0 g/m^2. Using these requirements as a guide, potential
material candidates were surveyed and screened. This was a combined
effort between the various NASA centers engaged in the program plus a
contracted study by the Battelle-Columbus Laboratories (under the direc-
tion of JPL). Early in the program (Jan. 1977), an industry conference
organized by the New York Polytechnic Institute was held in Washington,
D.C. to develop technical strategy and recommend the most viable candi-
dates. This conference included representatives from such companies as
duPont, Cellanese, Union Carbide, Monsanto, Allied Chemical, IBM and
Sheldahl. The results of the conference were very useful in the selec-
tion of candidate basic film materials that could be used for a HCRM.

Initially all types of materials that could be made into
films were considered but, primarily because of the area density require-
ment, it soon became apparent that polymers were the best candidates if
they could meet the thermal and space radiation requirements. Figure 4-1
shows the relationship between the film density in grams per cubic
centimeter and film weight per square meter for various polymers. The
only metal candidate that appeared to be practical from an overall
properties standpoint was aluminum and it's density (at 2.8 grams per
cubic centimeter) was such that the film (or foil) would have had to be

Table 4-1. Target Technical Properties of the Sail Film

A. Physical

    1.   Area Density ≤ 3.6 g/m^2

    2.   Thickness Uniformity ±10%

B. Thermal

    Thermal Stability range -130 to 250°C

    Thermal Cycling Capacity 1600 cycles, 210-250°C

C. Radiation

    1.   Metallized film must endure a total of 210,000 Solar UV hrs.

    2.   Metallized film has to withstand a total of 2×10^{10} Rads (Si)

D. Mechanical

    1.   Overall dimensional change between -130 to 250°C must be ∿1.5% (thermal expansion, residual shrinkage, elastoplastic deformation)

    2.   Ultimate tensile strength 28,000 - 35,000 KN/m^2 (4-5 Kpsi)*

    3.   Tear initiation resistance

       ∿1.0 N/μ (350 lb/inch). Applicable during entire mission.

---

*(actually encountered only during handling and unrolling of blades). During flight the load is ∿2 psi.

0.04 mils in thickness to meet the target area density. At these ultrathin thicknesses, the durability and crease resistance of metals are very questionable. Table 4-2 lists density, weight and thickness considerations for some metals.

The major difficulty anticipated with polymers for a Halley Mission were their reportedly poor (for this mission) radiation and elevated temperature resistance. Early predictions on the temperatures to
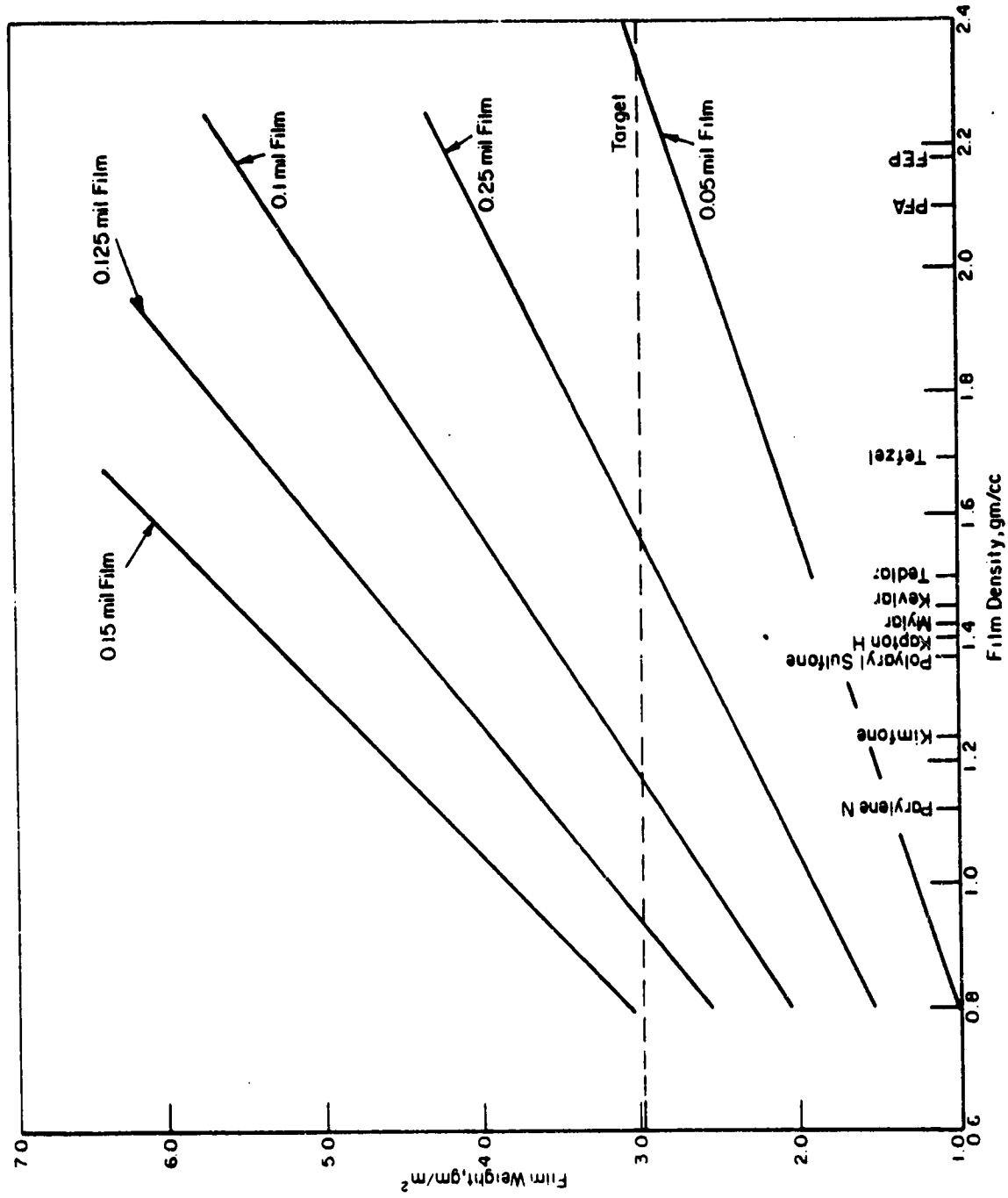
Figure 4-1. Correlation of Film Weight per Square Meter with Density of Thickness

Table 4-2. Metals as Film Materials

Metals	Density gm/cm^3	Weight of Film Per m^2 of Thicknesses, gms			Thickness in Microns of Film at Which the Weight is 4 gm/m^2	Melting Point ^{o}C
		1μ	5μ	10μ		
Lithium	0.53	0.53	2.7	5.3	7.5	180
Magnesium	1.74	1.74	8.7	17.4	2.3	650
Beryllium	1.85	1.85	9.3	18.5	2.2	1277
Aluminum	2.7	2.7	13.5	27.	1.5	660
Copper	8.96	8.96	44.8	89.6	0.45	1083
Silver	10.5	10.5	52.5	105.	0.4	961
Gold	19.3	19.3	96.5	193.	0.2	1063

coated films during a 0.3 AU cranking orbit were of the order of 350°C. This was beyond the range (for continuous use) of practically all polymer films. Kapton type polyimides appeared to be the only material with any possibility of meeting this constraint. However, data was very limited on its long term temperature stability, and also, there were further unknowns about its space radiation stability for the intended mission. The general chemical and thermal inertness properties of this polymer however, were superior to most of the other candidates.

It was not until a breakthrough occurred in obtaining promising emittance coatings for the films, thereby allowing lower operating temperatures when the Sail was in near sun orbit, that it actually appeared feasible to employ polymers for the Sail application. Another contributing factor were studies that indicated feasible methods to join Kapton (which was known to be a difficult material to bond).

The aforementioned coating and joining technology developments are discussed in subsequent chapters.

Concurrent with the development of coatings that permitted the operating temperatures of the Sail film to be kept under 250°C at a heliocentric distance of 0.3 AU, a decision was made by Mission Design

to decrease this distance to 0.25 AU to further increase Sail performance and to provide more margin in mission launch parameters. At 0.25 AU the operating temperature of the Sail film (with a suitable emissive coating) would be of the order of $250^{\circ}C$, which was still within the operating temperature range of several polymers. However, testing was performed up to, and above, $300^{\circ}C$ to evaluate feasibility of missions closer to the sun in the event weight, reflectance or other goals could not be achieved for the Sail; and to demonstrate margin.

4.1.2   Assessment of Basic Film Candidates

Conceptually the Sail film could have been constructed of either a single monolithic component or a composite material, e.g. a film reinforced with an integral scrim or webbing. Thus, initially, the following matrix was designed to verify the various possibilities (see Table 4-3).

The results of such an approach were that both monolithic and composite film material appeared technically feasible. However, on the basis of current technology and availability, the monolithic concept appeared more practical and expedient. The various organic films and fiber formers, inorganic fibers and composites that were considered are tabulated in Tables 4-4, 4-5, 4-6, 4-7, and 4-8. The biggest technical challenge for a fiber reinforced scrim or web appeared to be the achievement of a good bond between the scrim and the matrix film. Material incompatibilities existed between available fibers and candidate films, e.g. thermal expansion differences and non-wetting characteristics.

Therefore, attention was directed towards finding suitable monolithic film candidates which could be screened with respect to their ability to satisfy the requirements of the Sail. These requirements included material properties as well as availability and manufacturability. Methods for reinforcement of monolithic films were investigated separately and are covered under joining and handling. The majority of the commercial films that were identified were considerably thicker than the initial nominal thickness requirement of 2.5 micron (0.1 mil)

Table 4-3. Material Selection Approach

Single Component (Monolithic)			Composite			
	Organic	Inor-ganic	Org. Film	Org. Fiber	Inorg. Film	Inorg. Film
Film Former	+	+				
Org. Film			+	+	+	+
Org. Fiber			-	+	-
Filament	-	-				
Inorg. Film					+	+
Inorg. Fiber						-

+ Indicates feasibility

projected for the Sail. Only a few polymer types, e.g. the
polysulfones and the polyxylenes, were routinely produced in the ultra-
thin thickness range and these did not appear to demonstrate sufficient
elevated temperature stability for the Sail application. The various
films initially considered as potential candidates are listed in
Table 4-4. The tabulation includes materials available commercially in
film form as well as those that are potentially producible in this form.

4.1.3   Selection of Primary Candidate Film Materials

Because of the critical schedule for the sail program (which
called for a HCRM launch in late 1981), the decision was made to concen-
trate on materials which most nearly conformed to or exceeded the tem-
perature and radiation requirements and could also be most readily
developed into the proper thickness range. One particular group of
polymers met these requirements the best. These were the thermosetting
and thermoplastic polymides typified by duPont's Kapton H, Upjohn's 2080
and Ciba Geigy's B100 and P100 respectively.

Discussions with duPont to interest them in directly produc-
ing their Kapton H film to the desired 0.1 mil thickness were initially
nonproductive. However, as the project gained more momentum, duPont

Table 4-4. Summary of Properties of Some Organic Films

Film Designation	Polymer Type	Heat Resistance, °C (ASTM D-759)	Density, g/cc	Folding (ASTM D-2176)	Tear, g/mil (ASTM D-822)	Tensile Strength, psi x 10³ (ASTM D-882)	Tensile Modulus, psi x 10³ (ASTM D-882)	Radiation Resistance Sunlight UV	Radiation Resistance Gamma	Radiation Resistance Neutron/Electron	Minimum Thickness Available mils	Comments
Kapton (0.25-mil) (DuPont)	Polyimide	400	1.42	10,000	8	25	430	Excellent	Flexible 4.16 x10⁹ Rads	Elongation 50% 6x10⁹ Rads	0.12	Shrinkage 0.3% at 480 F/8 yr; no decomposition 200 C/3x16⁻⁶ Torr
Mylar (DuPont)	Polyethylene terephthalate	150 max recommended	1.38-1.40	14,000	12-15	25	550	-	-	-	0.12	Moisture affects stability at high temperature
Kynar (Pennwalt)	Polyvinylidene fluoride	150 max recommended	1.75-1.78	-	-	6-8	120	Excellent	10⁸r	-	1 (?)	No oxidation or thermal degradation at 150°C/5 yr
Astrel 3o0/620 Astrel 650 (Carborundum)	Polyaryl sulfone	260 service temp	1.36	-	-	-	-	Darkens	1.2x 10⁸ Rads No Change	-	-	(a)
FEP Teflon (Type A) (DuPont)	Fluorocarbon	200	2.12-2.17	10,000	125	2.7-3.1	70	Excellent	-	-	0.5	No degradation at 200 C/10,000 hr; heat-sealable
Halar (Allied)	E-CTFE	180	1.66-1.68	-	-	7-10	250	Excellent	-	-	-	-
Udel (Union Carbide)	Polysulfone	150-170 service range	-	-	-	10-13	360-720	-	-	-	-	-
Parylene (Union Carbide)	Polyxylylene	-	1.1-1.12	-	-	6.5-10	-	-	-	-	-	Excellent for film gage control
Aclar (Allied)	Polychlorotri-fluoroethylene	180-200 service range	2.1-2.2	-	12-30 (D-689) varies direction	4.5-6.0	150-300	Excellent	-	-	0.5	Heat-sealable; no change UV-vacuum

Table 4-4. Summary of Properties of Some Organic Films (Continuation 1)

Film Designation	Polymer Type	Heat °C Resistance, (ASTM D-759)	Density, g/cc	Folding (ASTM D-2176)	Tear, g/mil (ASTM D-1922)	Tensile Strength, psi x 10^3 (ASTM D-822)	Tensile Modulus, psi x 10^3 (ASTM D-822)	Radiation Resistance Sunlight UV	Radiation Resistance Gamma	Radiation Resistance Neutron/Electron	Minimum Thickness Available mils	Comments
Tefzel (DuPont)	E-TFE	150-180 service range	1.70	-	-	7.5	130	Excellent	-	-	~0.25	-
Tedlar (DuPont)	PVF	100	1.38-157	-	-	7-18	250-375	Excellent	-	-	0.5	Film made by casting. Some varieties heat-sealable; Embrittles at 150°C/3000 hr
Lexan (G-E)	Polycarbonate	135 heat distortion	1.2	250-400	20-25	9	290-300	-	10^8 yellow low no embrittlement	5×10^7 r stable; 30% loss elongation	-	-
Teflon PFA (DuPont)	Fluorocarbon	260 service range	2.13-2.16	>1,000,000 (D-643)	40-70	7000	60-80	-	-	-	-	-
	PBI	(b)	-	-	-	-	-	-	-	-	-	(c)
	Polyphenyl quinoxaline	>150	-	-	-	-	-	-	-	-	-	(d)

(a) Although neither 3M, who developed the resin, nor Carborundum, who has licensed the resin for sale, have made commercial films. The properties are such that melt casting undoubtedly would be unsatisfactory. Solubility properties, however, are such that solution casting should be successful.

(b) High-temperature resistant material with little change in properties to 250°C.

(c) Although Celanese has demonstrated solution casting of PBI films, they do not produce films commercially

(d) Developmental material. Adequate supply doubtful

Table 4-5. Organic Film Formers

Materials	Temperature and Decomposition	Radiation and UV	Processing	Disadvantages and Concerns
Polimides Kapton-Poly (diimide-other) (duPont)	~300°C Very Good	RAD.-Excellent;UV?	Solution Cast	Shrinkage
JPL-LARC	~300°C Very Good	RAD.-Excellent;UV?	Chem. Etched	Shrinkage
ARC	~300°C Very Good	RAD.-Excellent;UV?	Plasma Etched	Shrinkage Stability
CIBA-GEIGY B100	250°C Very Good	RAD.-Excellent;UV?	Solution Cast	Shrinkage
UPJOHN 2080	250°C Very Good	RAD.-Excellent;UV?	Solution Cast	Shrinkage
TRW (Kapton type)	250°C Very Good	RAD.-Excellent;UV?	Electrodeposition	Shrinkage
PARYLENE (Union Carbide)	~210°C Good	RAD.-Excellent;UV?	Vapor Deposition	Adhesion Difficult
PBI (Celanese)	~300°C Very Good	RAD. Excellent; UV Poor	Solution Cast	Processing? Effect of H_2O
Polyester: Bisphenol + Isophthalic Acid (-sovolta)	Good	RAD. Good; UV Prob. Poor	Solution Cast	Availability?
Polysulfone:Kimfone (P.J. Schweitzer)	~160°C Fair	RAD. Good; UV Poor	Solution Cast and Stretched	Shrinkage, Thermal Resistance

Table 4-5. Organic Film Formers (Continuation 1)

Materials	Temperature and Decomposition	Radiation and UV	Processing	Disadvantages and Concerns
MYLAR (duPont)	<150°C Poor	RAD. Good; UV Poor	Solution Cast and Stretched	Shrinkage, Thermal Resistance
Fluorosilicone	>230°C Good	RAD. Good; UV?	Cast or Milled and Curred	May not retain coating
Nomex	<250°C Good	RAD. Good; UV Poor	Paper Process	Not made as film
Teflon	270°C Good	Poor, UV O.K.	Latex is cast or sprayed & sintered	Flows, high density
Kynar	~160°C Good	Good, UV Good	Melt entruded	High density, thermal resistance
Polyphenylquinoxa-lene (PPQ)	~250°C	RAD. Good; UV?	Solution Cast	Availability
Tradlon (Polyparabanic acid) (Exxon)	~150°C	RAD. Good; UV?	Solution Cast	Thermal Stability

Table 4-6. Organic Fiber Formers

	Thermal Properties	Radiation & UV	Processing	Disadvantages
PBI Polybenzimidazole	It retains 20% of its strength after 300 hrs @ 304°C in air. Degrades faster in air than in vacu.	Has serious UV problem (80% strength retention after 6 wks in weatherometer at room temperature). Radiation resistance o.k.	Finished polymer solution spun into N_2 atm and later stretched @ 900°F	Minimum 10-12μ in yarn form; fibrids φ = 3 1μ Very hydrophilic & absence of H_2O causes brittleness. It is not crosslinked. Its UV resistance is inferior to Kapton.
BBB Polybisbenzimidazobenzo Phenanthroline	It retains 50% of its strength 360°C after 30 hrs in air. Degrades faster in air than in vacu.	Radiation resistance is o.k. Its UV features are better than PBI	Finished polymer solution spun and later stretched	Minimum fiber diam is 10-12μ in yarn form. It is not a crosslinked material. Not available commercially. Inferior to Kapton but better than PBI.
Kapton Type Polyimide	It retains 60% of its strength 200°C in air. (~10^2 hrs) 350°C evolves CO_2. Degrades faster in air than in vacu.	Its UV not reported but probably is better than Kapton if it can be crosslinked. Radiation: o.k.	Polyamic-acid is solution spun and later transferred into polimide. The fiber has not been crosslinked but it can be done	Minimum Fiber diam is 10-12μ in yarn form. Its properties are equivalent to Kapton.
Nomex-Aromatic Polyamides (Nomex & Fexlar)	Its maximum recommended use is 200°C for periods several years in air. Retains 50% of its strength @ 300°C after 300 hr in air	Radiation: o.k. U.V. very poor	Finished polymer is solution spun & stretched	Minimum fiber diameter is 10-12μ in yarn form Inferior to Kapton

N ~ 50 : 50

KEVBR

No woven or non-woven fabric is available which is less than 25μ thick or weigh less than 88/me

Table 4-7. Inorganic Fibers

		Processing	Advantages	Disadvantages
Monofilaments (Continuous Filaments)	Quartz	Heated rod is stretched	available > 1 μ, strong; low density. Could probably be woven into a grid	$\alpha_f < \alpha_p$
	Carbon	Charring of polymeric monofilaments	Strong, electrically conductive, low density	+ minimum diameter is 25μ; $\alpha_f < \alpha_p$
	Metals	drawing of hot wire thru die; spinning	flexible, can be woven. A woven grid of < 1g/m² can be made	high density, minimum diam. 12.5μ temperature, $\alpha_f > \alpha_p$
	Glass	melt extrusion	medium density	brittle, minimum diam is 25μ $\alpha_f \sim \alpha_p$
Yarns (Continuous Filaments)	Glass	melt extrusion	medium density 1" mesh, $\Phi = 3.8\mu m$; 1.5 g m⁻²	minimum fiber diam. is 3.8μ; fiber separation
	Carbon	Same as carbon monofilament	medium density	minimum fiber diam. is 8μ; fiber separation
	Metals	same as metal monofilaments	smaller diameter (0.7μ) light woven mesh can be made aid for static problems	high density fiber separation
Staples (short filaments)	Glass	melt extruded & blown	All these fibers are available in sub-micron size and can easily be incorporated into a 2.5μ film. They give local ripstop. Eliminate the fabric formation process. If metal wires are chosen electro-static dissipation and charge asymmetry will be eliminated	Since the fibers are not continuous they don't provide long range ripstops & film still may require some additional macro-network.
	Quartz	multifilaments are drawn & then chopped; spinning		
	Metals			
	Carbons	Carbon yarns are chopped		
	Asbestos	mining; mining and digesting		

Note: Almost all inorganic fibers are viable candidates, i.e. have good thermal, radiation and UV resistance. Almost all have the problems of: Mismatch of expansion coef. with polymer: Adhesion, Density, Brittleness, if film is made on a paper or a grid stretching becomes impossible.

α_f - coefficient of thermal expansion fiber
α_p - coefficient of thermal expansion polymer

Table 4-8. Composites

	Remarks
1. KAPTON-type with KAPTON type tape ripstops	Matching technology
KAPTON-type with BBB type tape ripstops	Expansion Coefficient Mismatch
2. Parylene on PBI Paper	Tear resistance Adhesion
KAPTON type on Nomex Scrim	Degradation
3. KAPTON with deposited metal ripstops	Fabrication Environmental Resistance Expansion Coefficient
4. Polymer with a. inorganic mesh b. include microfibers	Tear resistance Handling/static Expansion coefficient Mech. properties
5. Metal film with deposited metal ripstops	Under investigation Mech. properties
6. Aluminum film on chromel scrim Aluminum film on glass scrim	Electrostatic Environmental resistance

agreed to a contract (under the direction of NASA-LARC) to pursue the feasibility of such an endeavor. Their initial attempt at producing the 2.5 micron (0.10 mil) film resulted in material approximately 3.3 micron (0.15 mil) thick. However, they gained enough confidence from their experience in this first run to predict that they could directly produce film of the desired thickness in quantities to meet the Sail schedule.

Based on the foregoing, directly produced Kapton became the prime candidate film material. As a backup, if for any reason duPont should not have been able to produce the film, there were three options. Two of these included two processing methods for reducing the thickness of commercially available 7.5 micron (0.3 mil) Kapton: 1) chemical etching and 2) plasma etching. The third option was an alternate material - Ciba-Geigy B 100 thermoplastic polyimide. The advantages and disadvantages of the final four major candidates, according to ranking are shown in Table 4-9.

Table 4-9. Major Basic Film Candidates as of July 1977

Material	Candidate's Rank	Mfgr. Method	Advantages	Disadvantages
DuPont Kapton	1.	direct produced (proprietary method)	Best high temperature polymer. It has been around for more than a decade and a wealth of information is available about its properties. Very good radiation resistance	1. Not commercially available, high production costs for ultrathin gauges.
	2.	chemically etched		2. May not be as good as virgin Kapton.
	3.	plasma etchea		3. May become too costly
Ciba-Geigy Thermoplastic polyimide B100	4.	direct produced by solvent or water casting	Lower density (20% lighter than Kapton); Suitable thermal properties. Its Tg can be varied if so desired. Heat sealable, easy to cast thin film. Lower potential costs for fabrication into ultrathin gauge film	new material, not enough known about long term properties. Not made into 2.5μm thick films commercially
Ciba-Geigy Thermoplastic polyimide P100	5.	direct produced by solvent or water casting	same as B 100 but with higher thermal resistance	same as B 100 and resin is still in experimental stage

The chemical structure of the two final candidates are as follows:
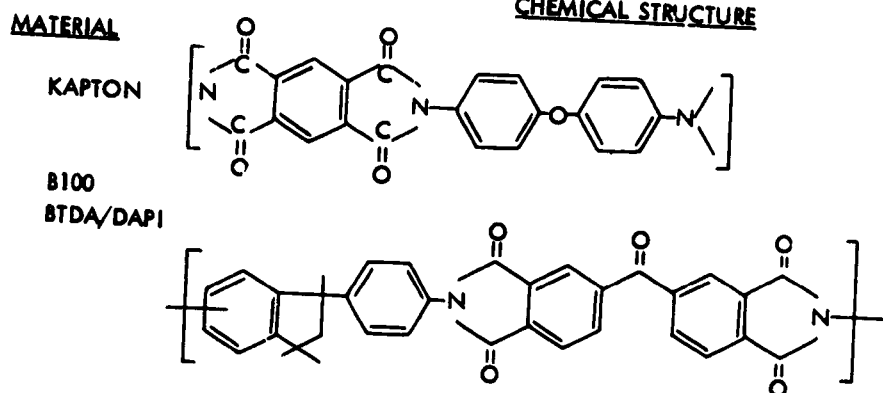
4.1.4   Mechanical and Thermal Property Characterization of Candidate Films

Subsequent to the screening of the potential film materials which narrowed the candidates to two (Kapton and B100), an effort was initiated to more completely characterize their pertinent mechanical and thermal properties. This began with a thorough search of the available literature followed by a testing program designed to provide required missing information.

(a)   Literature Search

The literature search encompassed making contact with the manufacturers of the materials to solicit available data and also surveying the open literature for work by other investigators. Table 4-10 summarizes the salient information that was obtained from the literature search.

Initially, three polyimide materials were under consideration. Besides Kapton and B100, Upjohn's 2080 thermoplastic resin was also a candidate. However this material did not withstand simulated space radiation as well as the others (see chapter on Sail Film System

Table 4-10.   Basic Properties of Kapton and B100 Polyimides

Property	Kapton	B100
1. Physical		
• Density	1.42g/cc	1.16g/cc
• Thermal Expansion Coefficient (Machine Direction)	$2 \times 10^{-5}/°C$ between -200 to 300°C	$5.25 \times 10^{-5}/°C$ between -200 to 300°C
2. Thermal		
• Glass Transition, Tg	400°C	318°C
• Service Temperature Range (insitu)	-270 to 400°C	-270 to 300°C
3. Radiation		
Gamma Radiation	No problem up to 3×10^8 Rads (Si)	Not known
UV	Not known	Not known
4. Mechanical		
Tensile Strength, newtons/cm^2 (psi)	17,500 @ 25°C (25,000)	7770 @ 25°C (11,100)
	11,900 @ 200°C (17,000)	2730 @ 260°C (3900)
Modulus, newtons/cm^2 (psi)	301,000 @ 25°C (430,000)	252,000 @ 25°C (360,000)
	18?,?00 @ 200°C (260,000)	315,000 @ 260°C (450,000)
Elongation at Break, %	70 @ 25°C	10.2 @ 25°C
	90 @ 200°C	54.9 @ 260°C
Tear Initiation Strength, newtons/micron	0.2 @ 25°C	
5. Water Absorption, %	2.9	2.9

Performance) and also was found to require the use of undesirable solvents (OSHA standards) in its manufacture so it was not given further consideration.

(b)   Test Program

The purpose of the test program for the basic film material was primarily to obtain missing mechanical property data. This data was needed to provide design information for the Sail. The properties measured as a function of temperature are tabulated in Table 4-11. The measurement method employed is also shown. Some physical properties as a function of temperature, e.g. thermal coefficient, were also measured.

The results of the measurements are included in Table 4-12. The material used for these measurements were the direct manufactured 3.7 micron (0.15 mil) Kapton from duPont and the Ciba-Geigy 3.0 micron (0.12 mil) B100 polyimide. The B100 film was solvent cast by the Peter Schweitzer Division of Kimberly Clark.

The strength data reported in the table are noted decreases or increases in that particular property over the temperature range through which the spectrum was tested.

4.1.5   Manufacturing Requirements for Basic Film

Along with the various physical and mechanical property requirements for the basic film, there were also requirements for its fabrication. The 2.5 micron thickness limit for the material was initially beyond the state-of-the-art for the most desired candidate, Kapton H film from duPont. Thus it was very apparent that a great deal of technology development was necessary to obtain candidate films of the required thickness once that viable candidates had been identified based on their physical, mechanical and space radiation properties. A second criteria was the availability of the resin and its subsequent

Table 4-11. Mechanical and Thermal Property Measurements vs
Temperature for Kapton and B100 Film

Property Measured at Various Temperatures		Measurement Method
	Static	Instron Tester
1. Tensile Modulus		
	Dynamic	Rheovibron
2. Yield Strength		Instron Tester
3. Ultimate Tensile Strength		Instron Tester
4. Ultimate Elongation		Instron Tester
5. Elongation at Yield		Instron Tester
6. Stress-Strain Curve vs T		Instron Tester
7. Tear Initiation Strength		Instron Tester
8. Tear Propagation Strength		Instron Tester
9. Creep		Creep Analyzer
10. Thermal Expansion Coeff		Rheovibron
11. Thermal Transitions		Rheovibron
12. Shrinkage		Dimension Measurement

fabricability in sufficient quantities to meet the rigid demands of
the Solar Sail program schedule whicn called for a launch in late 1981
(over 1.6 million square meters of coated film was needed for the total
program). Because polyimides were identified as having the best poten-
tial for the Solar Sail film material, a concentrated program was
devoted to assess the producibility of film from these materials. There
were two prime candidates, duPont's Kapton H and Ciba Geigy's B 100.
For the Kapton (because of high manufacturing costs for the ultrathin
gauge film and to guard against the possibility that duPont might have
trouble making it) alternate methods for achieving the ultrathin mater-
ial were investigated. These included plasma and chemical etching of
readily available (and less costly) thicker film.

Table 4-12. Mechanical Properties vs Temperature (Bare Films)

Property and Temperature Range	Direct Produced Kapton	B100 (Made by Schweitzer)
1. Dynamic Tensile Modulus from -200 to 300°C	73% decrease	74% decrease
2. Thermal Transitions (-200 to 300°C	-90°C and +120°C	-90°C and +160°C
3. Expansion Coefficient from -200 to 300°C	2.5×10^{-5}/°C M.D.[1] $3\text{-}5.6 \times 10^{-5}$/°C T.D.[2]	5.2×10^{-5}/°C M.D.[1] 5.8×10^{-5}/°C T.D.[2]
4. Ultimate Tensile Strength from -60 to 280°C	50% decrease	71% decrease
5. Static Tensile Modulus from -60°C to 280°C	20% decrease	51% decrease
6. Tear Initiation Strength from -60 to 280°C	60% decrease	40% improvement
7. Shrinkage		
8. Creep (Al/Cr* metallized) 240 to 300°C	Instrument inaccuracy prevents firm conclusion but thus far no noticeable creep has been seen	

[1]M.D. - Machine direction

[2]T.D. - Transverse direction

*Aluminum on one surface, ∿1000A; Chromium on opposite surface, ∿125A.

4.1.5.1 Direct Manufactured Film. The first choice for a material and manufacturing method was the direct solvent casting technique used to produce the Kapton H film. duPont has shown its capability in producing 3.3 micron film and a high probability of making 2.0 micron film. An estimated schedule for meeting the HCRM schedule with the duPont 2.0 micron, basic film is shown in Figure 4-2.
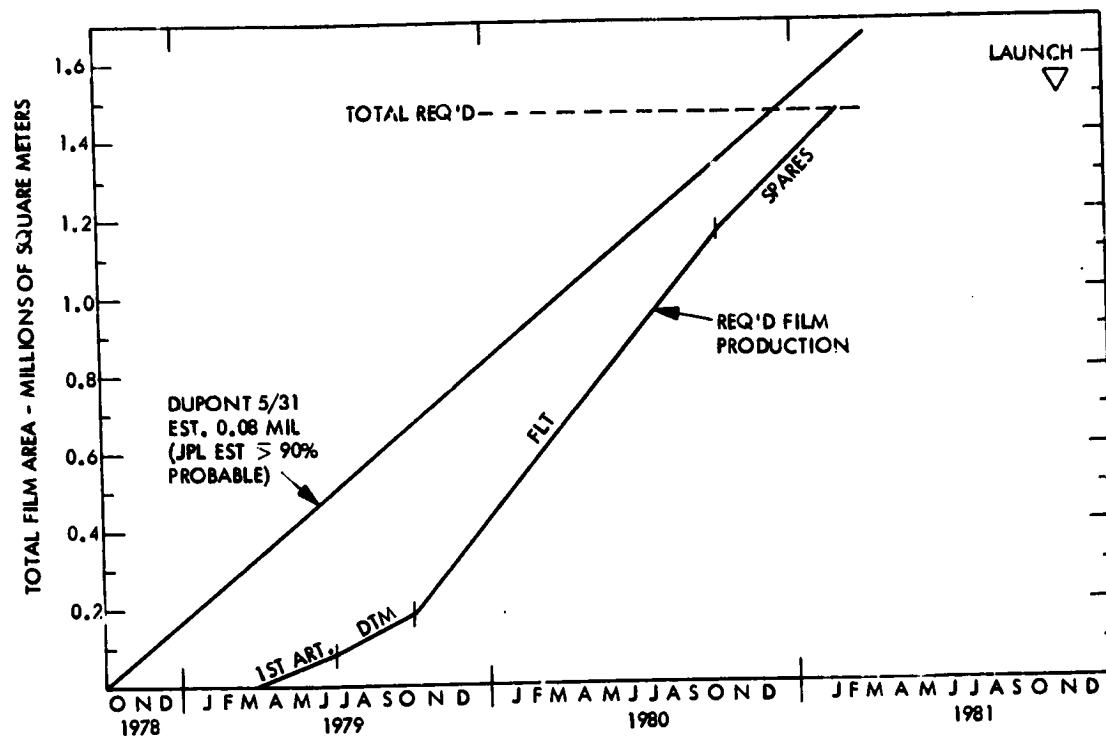
Figure 4-2.   Solar Sail Materials Film Production for HCRM

The alternate material choice for the Sail film was Ciba-Geigy's B-100 polyimide.   This resin can be made into ultrathin films by both solvent casting and water casting techniques.   Figure 4-3 depicts the solvent cast technique.   The feasibility of making 2.5 micron film from the B-100 resin was demonstrated by P. J. Schweitzer Co. using a combination of solvent casting and stretching.   A similar schedule (to the one done with DuPont) for delivering the B-100 film was developed with Schweitzer.

The water casting technique was tentatively explored by the Midwest Research Institute, Minnetonka, Minnesota.   Basically the technique consists of dissolving a polymer in a water soluble solvent and casting the solution on a water surface.   An ultrathin membrane forms spontaneously as the solvent dissolves in the water.   The difficult part of the process appears to be in successfully retrieving the polymeric film from the water surface without damage while maintaining the ability

4-21
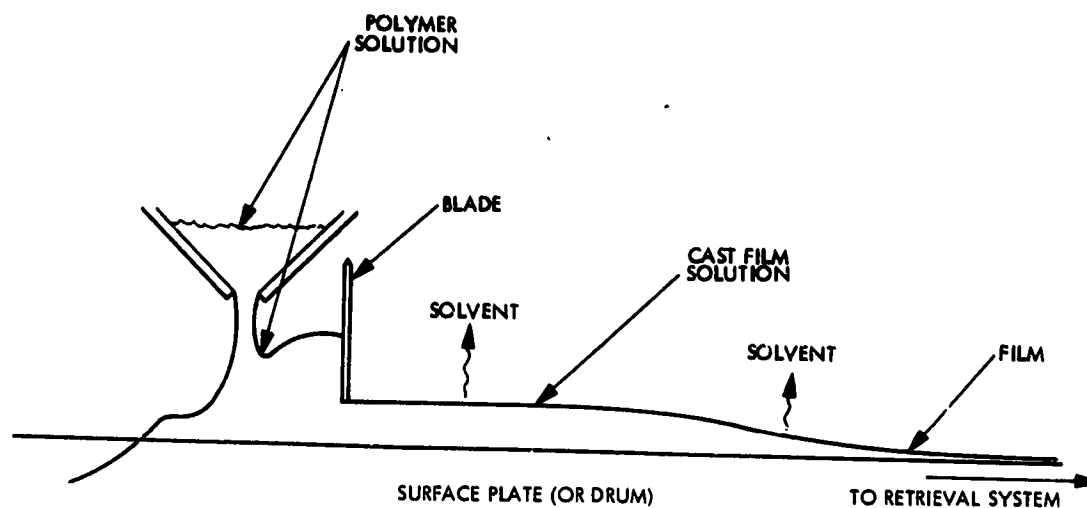
Figure 4-3. Solvent Film Cast Schematic.

to subsequently apply reflective and emissive coatings. MRI was awarded
a small development contract to establish the feasibility of this film
making process. A schematic diagram of a pick up system is shown in
Figure 4-4. Successful, continuous runs (∿100m) of the Ciba-Geigy B 100
and P 100 films were made with thicknesses of 1.0 to 2.0 micron. The
film is retrieved on paper, from which it must be removed to metallize
one side (one side could be metallized while on the paper).

4.1.5.2   Reduction in Thickness of Heavier Gauge Films. Backup
methods for obtaining 2 micron Kapton film included reducing the thick-
ness of heavy gauge material by plasma and chemical etching. The feasi-
bility of the plasma etching method for reducing the 7.5 micron thick,
commercially available Kapton film to 2.5 microns was established by the
Surface Activation Corporation in work sponsored by NASA-ARC, (Ref. 3).

Chemical etching techniques employing alkaline solutions
were investigated by JPL and demonstrated on a batch basis to be viable.
This method was employed to obtain a majority of the 2 micron thickness
Kapton samples for evaluation studies. Figure 4-5 is a plot of the
etching rate versus potassium hydroxide bath temperature for two differ-
ent solution concentrations.
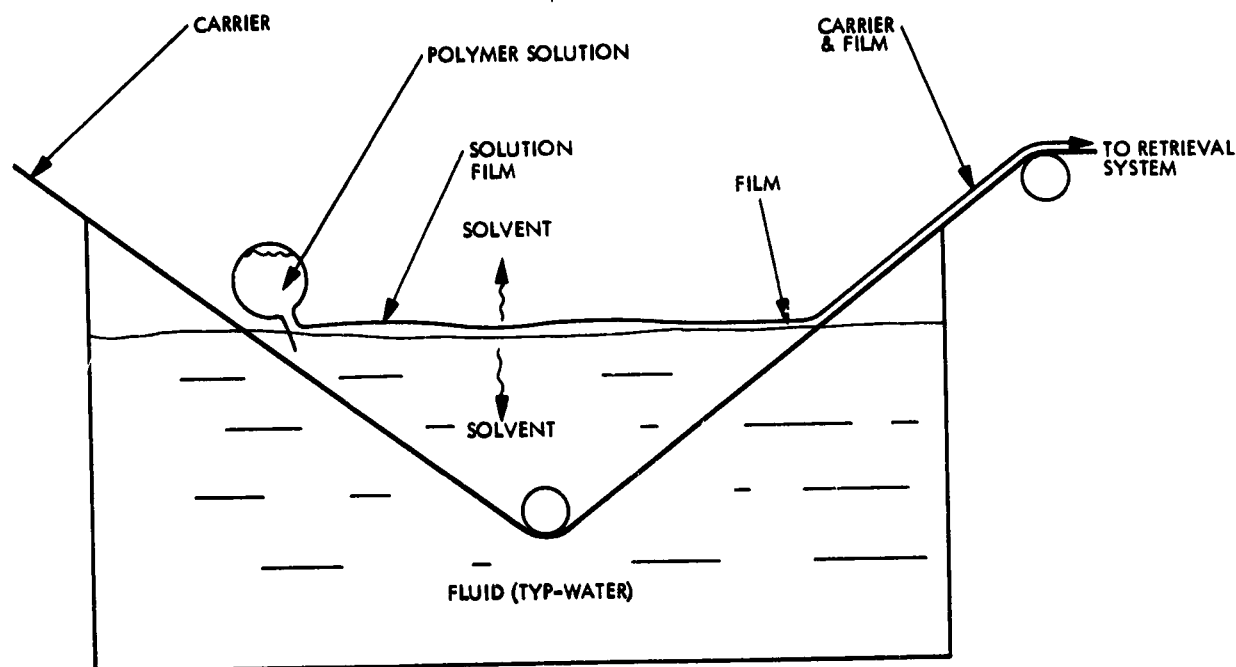
Figure 4-4. Water Cast Schematic

There are several advantages to the chemical etching

process:

(1) readily available supply of heavier gauge Kapton film

(2) potential savings by utilizing lower cost, heavier gauge film

(3) can serve as intermediate step for preparing surface for metallization.

The limitations of the process that need to be worked

include:

(a) initial control of the film thickness is presently limited to ±10%.

(b) residual side effects to the basic polymer requiring additional treatments to the film

(c) methods for handling processed film to account for mechanical expansion

(d) probable high facility costs.

4-23
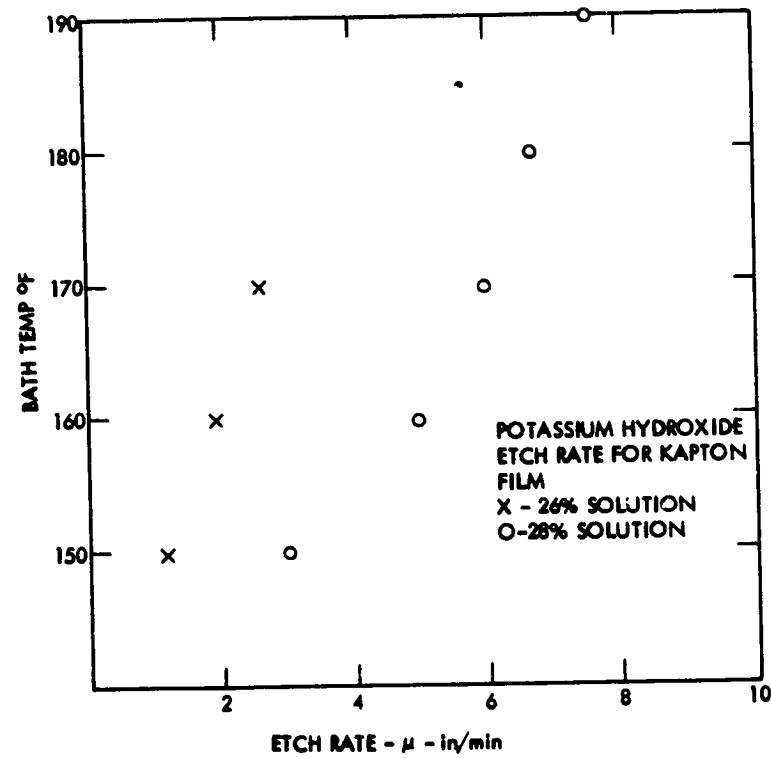
Figure 4-5.   Etching Rate versus Bath Temperature for Kapton Film

Plans were in process to further develop both the chemical and plasma etching techniques through contracted technology development efforts had the Solar Sail program continued.

REFERENCES

1. Weis, R., "Preliminary Design and Fabrication Assessment for Two Solar Sail Candidates - Final Report", Document No. 0003-70065, ILC Dover, July 4, 1977.

2. Daniels, J.B., et. al., "Preliminary Solar Sail Design and Fabrication Assessment - Spinning Sail Blade and Square Sail Sheet, Final Report." JPL Contract No. 954721, June 22, 1977.

3. Howe, R.E., "Feasibility of Continuous Plasma Etching of Kapton Film for Solar Sail Project," Order No. A41901B (GP), Surface Activation Corp., June 1977.

4.2 COATINGS AND THERMAL CONTROL

4.2.1 Background and Technical Requirements

The sun facing surface of the solar sail must be specular and highly reflective to maximize the photon momentum impulse (force) and must also be resistant to degradation by the solar and space environment for periods up to four years. The high levels of irradiation are especially of concern because of the nearness of the approach of the spacecraft (0.25 AU) during its projected two year cranking orbit around the sun (Figure 4-6).

To maintain acceptable equilibrium temperatures for the deployed Sail in a near-sun cranking orbit, it is mandatory that the $\alpha_1/\varepsilon_{1+2}$ ratio for the Sail be low; e.g., 0.1 to 0.2. This factor is defined as the ratio of the solar absorbtance, α_1, of the sun facing side of the Sail divided by the sum of the emittances of the sun facing side (ε_1) and the back-side (ε_2).

This is derived from the relationship:

$$T_S^4 = \frac{\alpha_S}{\varepsilon_1 + \varepsilon_2} \cdot \frac{G}{\sigma}$$

where:

T = absolute temperature

α_S = front surface absorbtance

ε_1 = front surface emittance

ε_2 = back surface emittance

σ = Stefan – Boltzmann Constant

G = solar intensity factor

With the parameters G, σ, and α being defined for a given condition either ε_1 or ε_2, or both, must be increased in order to decrease T.
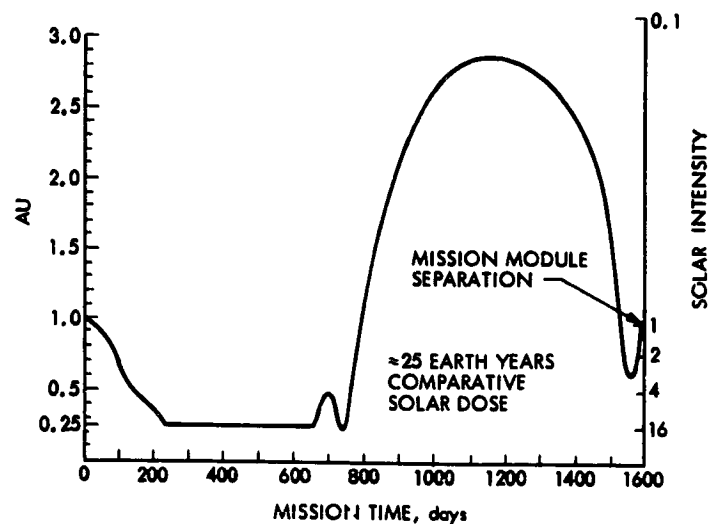
Figure 4-6. Solar Intensity Profile

The need for a low $\alpha_1/\varepsilon_{1+2}$ ratio for the Solar Sail is illustrated in Figure 4-7 which is a plot of temperature versus heliocentric distance with the $\alpha_1/\varepsilon_{1+2}$ ratio as a parameter. The equilibrium temperature for aluminized 2.5 micron Kapton with an $\alpha_1/\varepsilon_{1+2}$ ratio of 0.42 is (from Figure 4-7) approximately 370°C at 0.25 AU, but at this temperature Kapton becomes brittle and loses its mechanical strength. Thus, it is apparent that the emittance of the back side of the Sail film, or possibly that of the front side, must be increased.

The thermal aspects are not the only concern. The extreme thinness of the polymeric Sail material make it particularly susceptible to the degrading effects of charged particle and UV radiation. Therefore, the solar-side coating or coatings have to be of sufficient density to impede charged particles from the solar wind, absorb UV radiation, and be mechanically stable.

$$T_S^4 = \frac{\alpha_S}{\epsilon_1 + \epsilon_2} \cdot \frac{G}{\sigma}$$

KAPTON DESIGN LIMIT

$\alpha_S = 0.16$

$\epsilon_2 = 0.30$ $\epsilon_1 = 0.03$

$\epsilon_2 = 0.50$

MYLAR DESIGN LIMIT

$\epsilon_2 = 0.70$

DISTANCE FROM SUN - AU
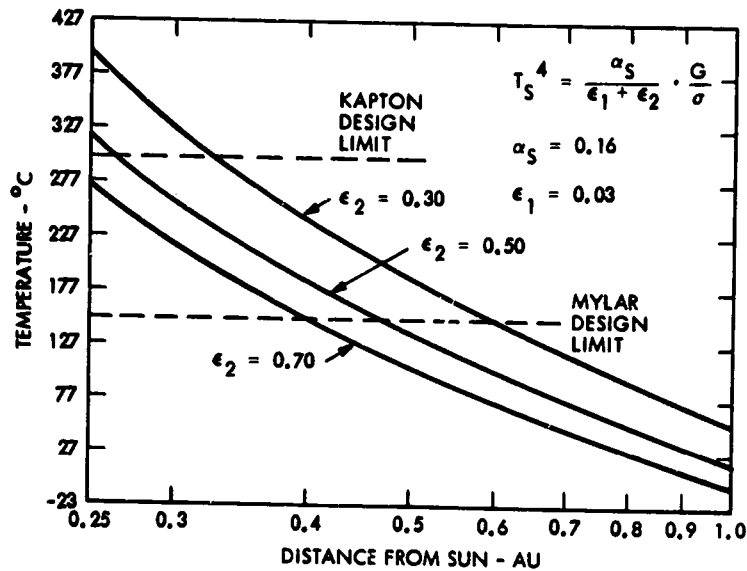
Figure 4-7.   Sail Film Temperature vs AU

Another requirement is that the coating system be sufficiently low in electrical resistivity to dissipate the electrostatic charges built up in the sail film during the fabrication-through-development phases as well as in space. The basic film being a dielectric, has high electrical resistivity. The various requirements for the coating are summarized in Table 4-13.

4.2.2   Survey and Selection of Candidates

Using the foregoing coating requirements as a guide, various candidate coatings were examined. These coatings were divided into two types: sun-side high solar reflectance coatings and back-side high emittance coatings.

Table 4-13. Summary of Solar Sail Film Coating Requirements

A. Physical

- Weight ~ 0.45 g/m^2 (includes all coatings)

- Electrically conductive

- Provide protection to Sail polymer film from charged particle and UV radiation levels predicted.

B. Chemical and Mechanical

- Tarnish- and corrosion-resistant during handling, storage, and pre-launch

- Good mechanical integrity over temperature range of -130 to 250°C and during temperature cycling of 1600 cycles at 210-250°C.

D. Optical - Thermal

- High spectral reflectance (0.88) for sun-side over life of mission to reduce thermal absorption

- High specular reflectance component (0.9) to maximize solar thrust

- High hemispherical emittance ($\varepsilon_2 = 0.6$) for the back side to achieve the requisite low value of $\alpha_1/\varepsilon_{1+2}$.

4.2.2.1 <u>High Solar Reflectance Coatings</u>. A survey of the literature revealed that aluminum and silver were the best reflective coating candidates for the Sail application. As seen in Figure 4-8, silver has a higher overall spectral reflectance than aluminum, but it has an abrupt transparent window in the UV region. This window would allow UV radiation to penetrate and possibly degrade the underlying polymer film. Other disadvantages of silver are its relatively high density (3 times that of aluminum), high cost and its susceptibility to tarnishing in the prelaunch environment. Combinations of silver and aluminum appeared attractive; however, the need for a protective over-coating for the silver was still present, and the cost was high.

In the area of what would be available on a commercial basis in reflective coatings, TRW made a survey of aluminized films that they had procured over a recent three year period (primarily for thermal
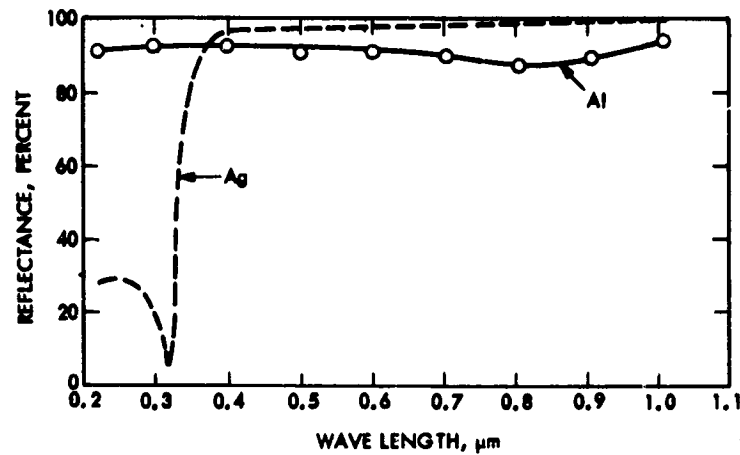
Figure 4-8. Spectral Reflectance of Al and Ag

control applications) where quality control records had been kept of
solar reflectance values. The data (shown in the histogram in
Figure 4-9) indicated that commercially applied, vapor deposited
aluminum coatings yielded large percentages of solar reflectance values
in the range of 0.88 to 0.91. Based on these data, a criterion was
established for a minimum spectral reflectance of 0.88 for aluminized
coatings.

Preliminary calculations of the necessary thickness required
for the reflective coating to provide UV and charged particle protection
revealed a minimum of 1000Å for aluminum. Later computer simulations
of the absorbed radiation dose over the HCRM showed that 1100Å would
be necessary. This is discussed in the section on sail system perform-
ance. Figure 4-10, which plots film thickness as a function of optical
transmittance for aluminum and silver, illustrates that silver must be
applied thicker to achieve equal opacity.
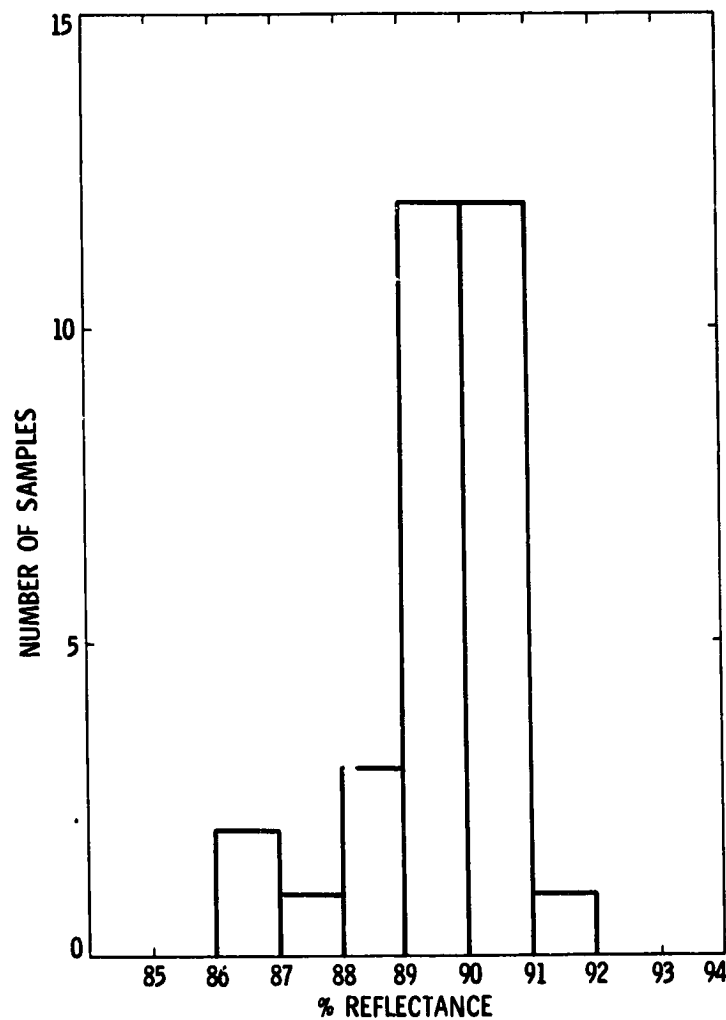
Figure 4-9. Solar Reflectance of Commercially Aluminized Kapton Film

During the course of the investigation, several candidates for protective overcoats for the reflector were identified. These included:

- MgF_2
- Al_2O_3
- SiO_x
- $In/Sn\ O_x$

Such coatings need the following characteristics:

- Non-absorber of solar energy

- Non-degrading
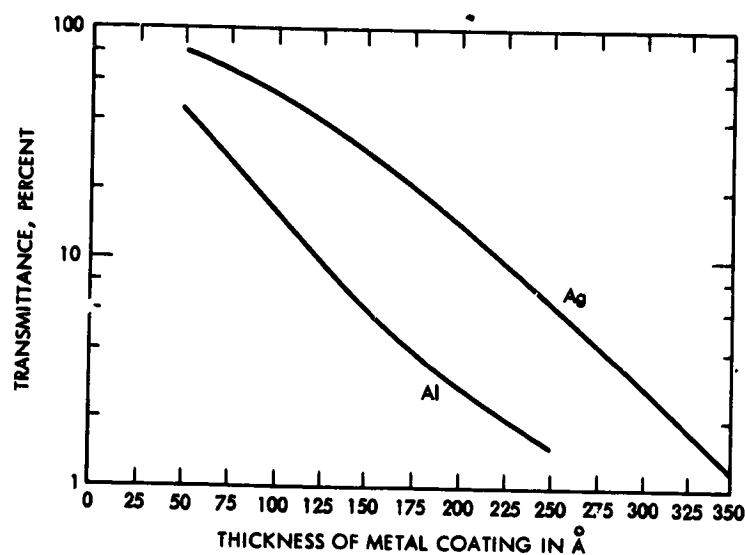
Figure 4-10.   Transmittance-Coating Thickness Relation of Ag and Aℓ

- Non-generator of damaging secondary radiation

- Compatible with reflector coating

- Mechanical and chemical integrity

Most of the work performed was in ion plated coatings. However, at the time that effort was discontinued on the program, it had not been clearly determined if overcoats would be required.

4.2.2.2   High Emittance Coatings.   A number of approaches were considered to increase the Sail emittance.   The major materials combinations are shown in Figure 4-11.   The coating thicknesses shown are illustrative and varied with coating material.   The duPont polyimide film, Kapton, is shown as the polymer film material since it was the baseline concept and was used for the great majority of samples and tests that were performed in this part of the program.   Tests were conducted on 2.5 micron or thicker polymer film.   Later in the program, mission design requirements dictated   change to the thinner 2.0 micron Kapton film which, at that time, appeared feasible for duPont to manufacture.
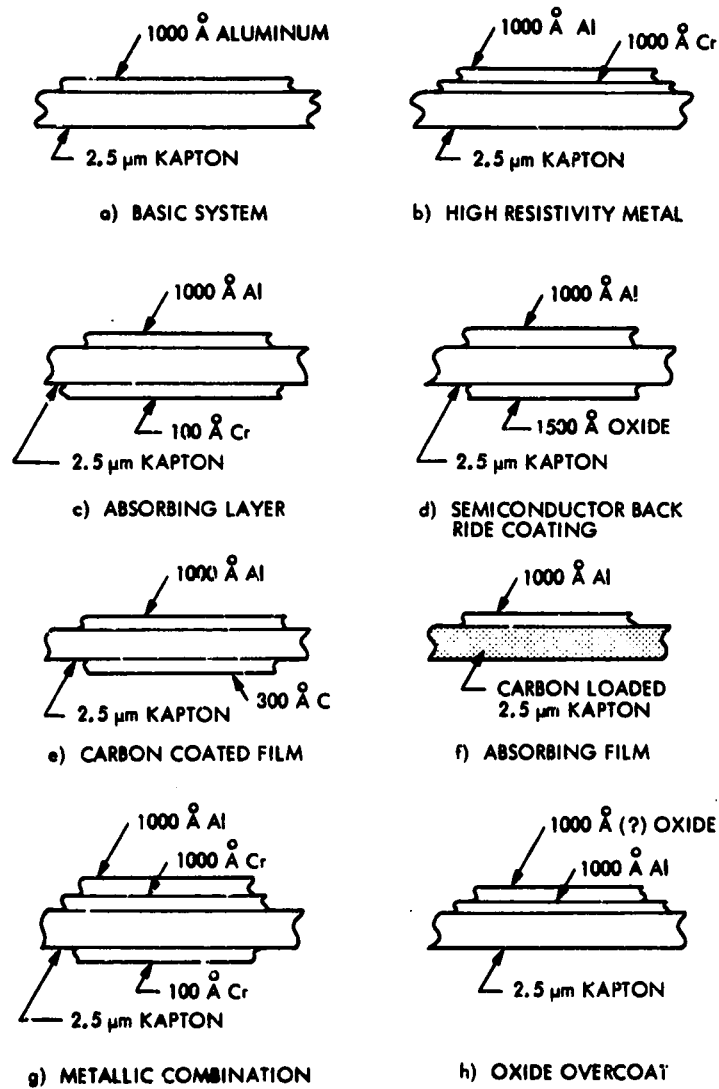
Figure 4-11. Approaches for Increasing Emittance of Polymer Film

Concept (a) is the simplest (aluminized Kapton). As mentioned previously, the emittance sum, ε_{1+2}, is too low to prevent high film temperatures and thus limits the vehicle solar approach.

Concept (b) was to introduce a layer between the Kapton and aluminum with an electrical resistivity higher than that of aluminum, since from the Hagen-Rubens approximation $\varepsilon \sim \sqrt{\rho_e}$, where ρ_e is the electrical resistivity. Several high-resistivity metals were considered for this application with chromium and nichrome alloys being preferred for their stability and availability.

Concept (c) was to introduce absorbing-emitting material in the form of a thin metal layer located one quarter of an emitted wavelength from the opaque metal reflective coating. This concept capitalized on the fact that the Kapton base film was a partially transparent dielectric with the requisite thickness. The infrared interference system so constructed enhances the emission. The absorbing material must be present in sufficient quantity to absorb or emit, but not so thick as to become a reflector and hence a poor emitter.

Concept (d) was the same basic idea, but with a thicker semiconductor for the absorber, because the thickness would not be so critical.

Concept (e) was carbon in place of an oxide semiconductor.

Concept (f) is related to Concepts (c), (d), and (e), but the absorbing material, carbon, is distributed throughout the Kapton film to avoid spectral tuning of the infrared interference effect. The carbon also acts as a scattering medium to promote absorption by the Kapton.

Concept (g) was simply a combination of Concepts (b) and (c), and was felt to offer the optimum in benefit.

An overcoat on the reflecting side, Concept (h), is widely used to increase emittance of evaporated films and solar cells. However, it requires a relatively thick coating and is subjected to the severe solar environmental conditions.

Concept (f) is based on the addition of fillers (e.g., carbon black) to the base polymer. Such fillers to the basic film would also serve to increase its UV resistance. As with the reflective coating, the resistivity of the backside coating must be reasonably low $(R \approx 10^{10}$ ohms/square) in order to dissipate static charges. This requirement made it difficult to consider fillers as the only means of increasing emittance. Therefore, the major effort was concentrated on coatings.

4.2.3 MEASUREMENTS

The need for concepts to increase the emittance of ultra-thin Kapton film was initially deduced from extrapolated data, since there was no thin material available for measurement. Coatings development and testing was actually initiated using 7.5 micron Kapton before processing techniques were developed to produce thinner gage material. As the program developed and more representative samples were prepared, more detailed thermophysical property measurements were made.

4.2.3.1   Sample Fabrication. Nominal 2.5 micron Kapton H films were made at JPL by etching thicker (7.5 micron), readily available material in a sodium hydroxide bath as discussed in 4.1.5.2. Generally, there was some slight variation from specimen to specimen in terms of total thickness, but these were inconsequential as long as they were identified. Vapor deposited coatings were applied to the samples by TRW, Optical Coating Laboratories, JPL, Keim Precision Optics, and Dyne Optics. Ion plated coatings were p_pared by Endurex Corp.

Since coatings were applied under both laboratory controlled and commercial conditions, there was some concern as to the accuracy of the reported thicknesses and quality (e.g., purity) of the materials being applied. All vapor deposited coatings applied at TRW were accompanied by thickness calibration specimens which were coated simultaneously, overcoated with aluminum and then measured using a Varian 980/4000 interferometer.

Carbon-filled polyimide samples were prepared by NASA-LaRC. A solution-cast film of a Kapton type polyimide was produced with a 10% by weight carbon black loading. This sample was subsequently front side aluminized and back side coated with 100Å chromium. Additionally, some samples of protective overcoats for reflective coatings and a duplex coating of silver over aluminum were prepared by Endurex.

4.2.3.2   <u>Measurement Techniques</u>. At the start of the testing, all emittance data were taken using a Gier Dunkle Emittance Inspection Device, Model DB100. Because this device yields a near-normal measurement of the infrared reflectance, correlation was necessary with the more accurate (but more time consuming) Calorimetric Hemispherical Emittance Device or with a Paraboloid Reflectometer which measures near normal spectral reflectance. Examination of the data revealed that the DB100 consistently gave results that correlated well with the more sophisticated methods. Thus, the DB100 was employed for screening candidate emittance coatings, and the more complicated calorimetric and spectral measurements were reserved for those coating systems that appeared the most promising and for which more thorough data compilation was desired.

The devices used to measure thermophysical properties are described as follows:

(a)   <u>Solar Reflectance/Absorptance</u>

Values of near-normal directional spectral reflectance at wavelengths from 0.28 to 2.5 microns were measured using a Beckman DK2A Spectrophotometer with an Edwards, et al.[1]-type integrating sphere

reflectometer. These data were then integrated over the Thekaekara[2] solar irradiance spectrum to obtain values of solar reflectance. Values of solar absorptance were obtained by subtracting values of solar reflectance from unity, since solar transmittance was zero.

To determine effects of elevated temperature on the solar absorptance, another test was performed. Samples were mounted inside small fused silica "test tube" vacuum chambers attached to a small aluminum disc to which a Kapton/nickel foil heater had been bonded. The temperature was monitored with a thermo-couple while the sample was heated to the test temperature, in vacuo. The sample, in its evacuated holder, was then inserted directly into the integrating sphere reflectometer, where directional reflectance of the sample was measured. In order to account for any unexpected contaminant deposits that might accrue on the glass during the test, the sample was mounted in such a way that it could be moved to allow the 100 percent beam to pass through the glass tube.

The scattering characteristics (contributing to loss of specularity and therefore Sail thrust) of the reflected energy from the Sail material were also of concern. A series of measurements were made in an attempt to quantify the specular reflectance of a JPL-supplied "benchmark"* film material was measured with the TRW bi-directional reflectometer shown schematically in Figure 4-12. The angular nomenclature used is shown in Figure 4-13. The measurement was made at 0.6 microns (which is near the peak of the solar spectrum). Approximately 35 percent of the solar spectrum lies below this wavelength. This particular wavelength was selected as

---

*The "benchmark" film system as defined henceforth in this report consists of a 2.5 micron (0.1 mil) Kapton film with 1000Å of Al as the reflective coating and 125A of Cr as the emissive coating.
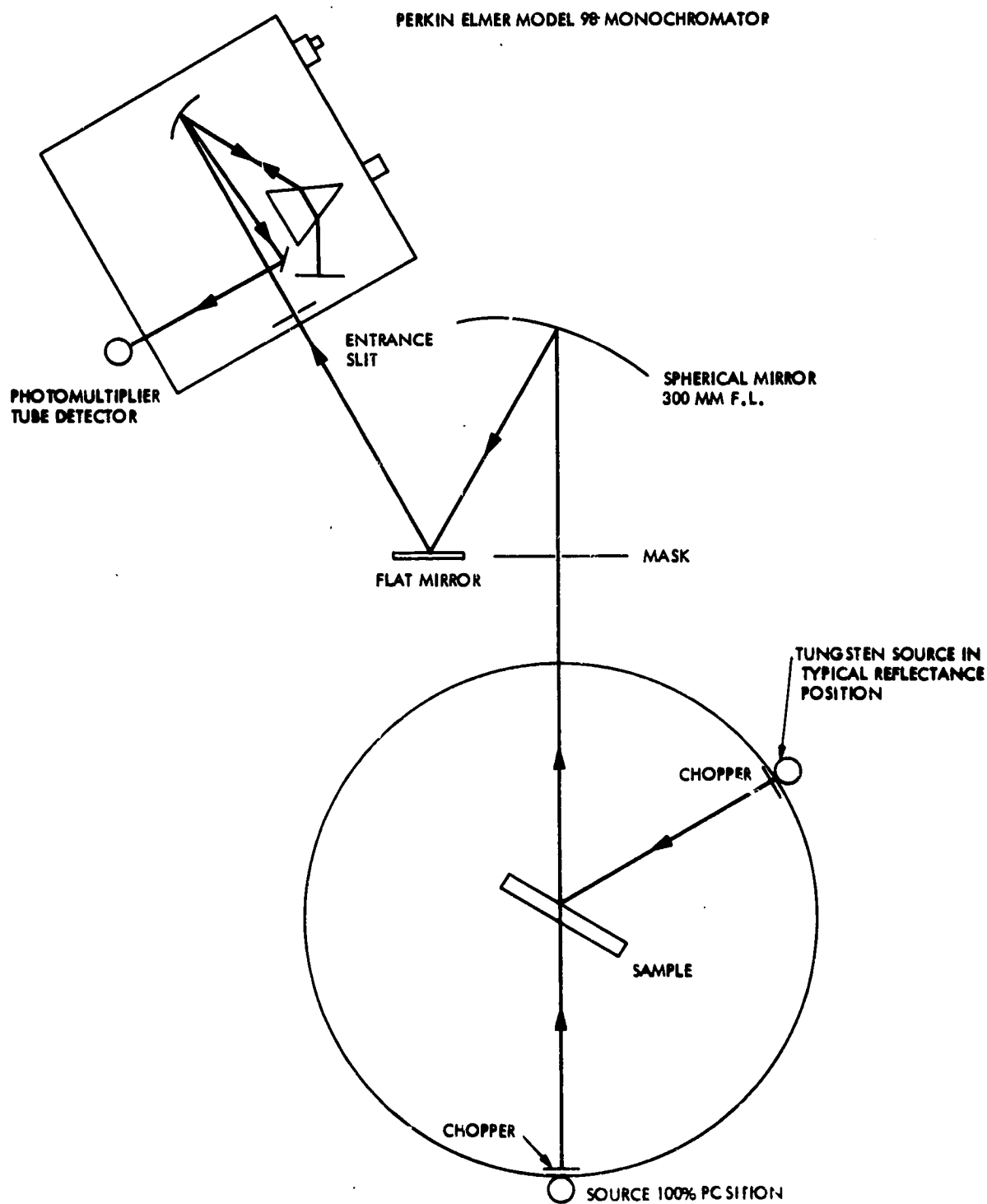
Figure 4-12. Schematic Representation of the TRW
Bidirectional Reflectometer
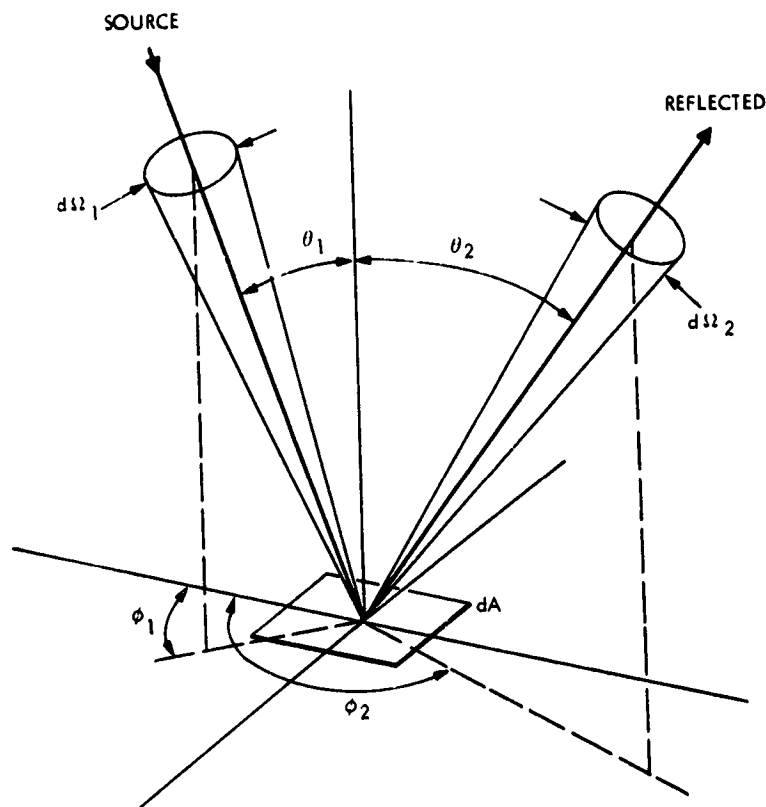
Figure 4-13. Geometry of Radiation Incident and
Leaving a Differential Area

a conservative single point to measure, since at longer
wavelengths the surface of the material would be more
specular.

The sample was mounted in a special holder,
designed to place the film in tension and maintain the
surface smooth and flat. The amount of tensile force
used to accomplish this was not measured, but was
assumed to be similar to what might be obtained on a
Sail blade segment. The measured values for solar
absorptance and near-normal emittance of aluminized
material taken from an adjacent portion of the same
coated film yielded values of $\alpha_s = 0.12$ and $\epsilon_Q = 0.01$.
These were taken for reference purposes.

In another test to determine the degree of
specularity of the uncrinkled aluminized film, minor

modifications were made to the Integrating Sphere Reflectometer. The area of aperture opening was effectively increased through the use of circular blank masks on the inside wall.

Then the decrease of the diffuse reflectance component (Rd) was monitored as a function of the polar (1/2) angle of the reflected energy. For nominal measuring applications this polar angle is 5.3°. With the masks the angle was increased to 8.5° and then to 10.6°. At these angles, the diffuse reflectance decreased from an initial reading of 0.227 at 5.3° to 0.035 at 10.6°.

(b) Emittance Inspection

The Gier Dunkle Instruments Model DB-100 Infrared Reflectometer[3] was used to determine the emittance of several film surfaces. This instrument was calibrated using vacuum deposited gold and 3M Velvet Black Paint as reference surfaces. The gold surface has been measured relative to a National Bureau of Standards vacuum deposited gold standard and found to have a near-normal infrared reflectance of 0.990. The 3M Velvet Black has been measured by a variety of techniques (Ref. 4-16) and found to have a reflectance of 0.080.

(c) Emittance Using Directional Spectral Reflectance

Values of near-normal directional spectral reflectance at wavelengths from 2.0 to 26 microns were measured using the TRW Paraboloid Reflectometer[9]. These spectral data were then numerically integrated over the Planckian 80°F Black Body irradiance curve to obtain the reflectance of the material to an 80°F black body source. These integrated reflectance values were then subtracted from unity to obtain near-normal 80°F emittance.

(d) ## Hemispherical Emittance by Calorimetric Techniques

Determination of values of hemispherical emit-
tance were made using calorimetric methods taking due
account of the inherent errors[6]. Two 4 inch by 4 inch
pieces of the metallized films were bonded to 4-inch
square heater/substrate assemblies, and the electrical
power required to maintain the specimen at specific
temperatures while in an evacuated bell jar with
liquid nitrogen-cooled walls was metered.

4.2.3.3 Thermophysical Property Data

4.2.3.3.1 Solar Absorptance/Reflectance. The solar absorptance of
aluminized Kapton was found to be essentially independent of temperature
over the range 20 to 285°C in vacuo. Both smooth and crinkled samples
were measured with the results summarized in Table 4-14. An interesting
phenomenon which appears in the spectral data is a decrease in the
characteristic 0.8 micrometer absorption band of aluminum at the higher
temperature.

The specular reflectance data presented in Table 4-15 illus-
trates that the aluminum coated, smooth, Kapton surface was strongly
specular: at small angles 5 degrees off the specular angle the relative
reflectance is down 3 orders of magnitude. Data for in-plane incidence
is shown in Figure 4-14. This Figure is an expanded <u>polar</u> plot of the
data. The surface normal of the sample is indicated by the $\bar{n}$ symbol.
All data was taken with the incident beam 10° off normal (in the region
-20 to $+7^o$, the source obstructs the reflected beam measurement cannot
be taken). At -20 and -30°, however, the measured signal was less than
0.001% and could not be measured accurately.

Data taken out of the plane of incidence ($\phi_2=+90^o$) indicates
that there is actually somewhat less side scatter out-of-plane. The
$\phi_1=10^o$, $\phi_2=10^o$, $\phi_2=90^o$ point, for example, could be compared to the
$\phi_1=10^o$, $\phi_2=20$, $\phi_2=180^o$ point. The in-plane 10°-off-specular value is

Table 4-14. Effect of Temperature on Solar Absorptance of Aluminized Kapton

Test Condition	Smooth[1] Aluminized 0.1 mil Kapton Film	Crinkled[2] Aluminized 0.1 mil Kapton Film	Aluminized Kapton Film	Smooth[1] Aluminized 0.1 mil Kapton Film
In Air, Out of Tube		0.19_7[3]	0.12_0	
In Air, In Tube		0.18_8		
In Vac, In Tube, T=20°C	0.12_6	0.18_8		0.14_0
In Vac, In Tube, T=77°C	0.12_1			
In Vac, In Tube, T=150°C	0.10_9	0.18_4		0.13_9
In Vac, In Tube, T=233°C		0.18_0		0.13_8
In Vac, In Tube, T=285°C				0.14_1
In Vac, In Tube, T=20°C		0.18_5		0.14_1
In Air, Out of Tube			0.11_1	

[1] Bonded to aluminum disc with DC 93-500 silicone rubber adhesive

[2] "Moderately" crinked by hand, then smoothed and bonded to aluminum disc using DC 93-500 adhesive

[3] Solar Absorptance data considered accurate to ±0.01; third figure shown depressed to indicate trends

Table 4-15. Relative Bidirectional Reflectance Data for
Benchmark Solar Sail Material

ϕ_1	ϕ_2	θ_1	θ_2	$\rho-\%$
0	180	$-10°$	-30	<0.001
			-20	<0.001
			$+7$	0.38
			8	1.1
			9	6.6
			10	100.00
			11	11.4
			12	1.86
			13	0.51
			14	0.21
			15	0.21
			20	0.018
			25	0.006
			30	0.002
0	90	-10	10	0.003
			20	0.0015
			30	<0.001
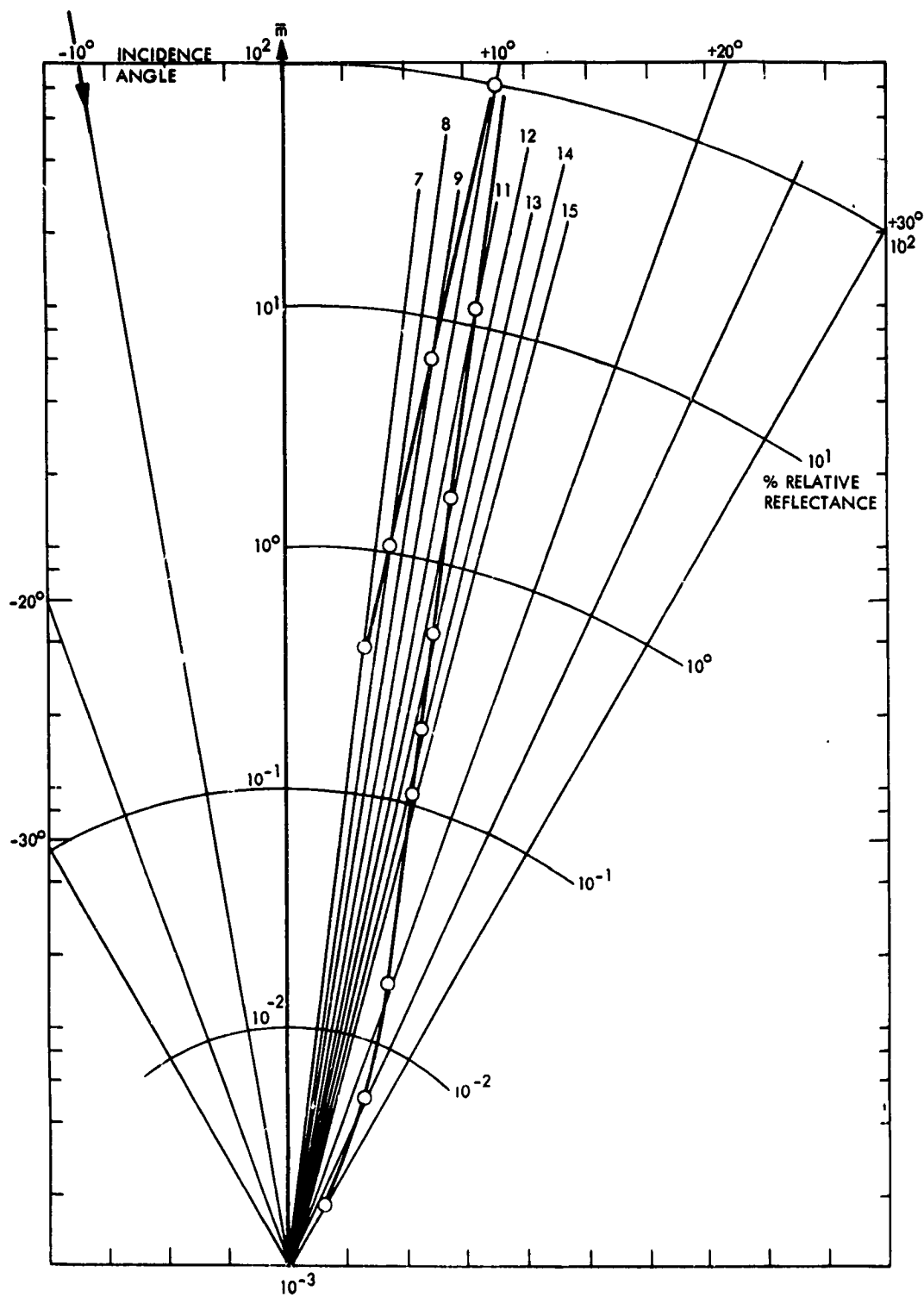
Figure 4-14. Relative Bidirectional Reflectance of Smooth
Aluminized 0.1 mil Kapton, $\;_1=$, Logrithmic
Plot

0.18 percent, while the out-of-plane 10°-off-specular value is 0.008 percent 20°-off-specular values are 0.0020 percent and 0.0015 percent in and out-of-plane.

The data for the other test for determining the degree of specularity of uncrinkled (smooth) aluminized Kapton is shown in Table 4-16. From these data, a preliminary value for the specular reflection coefficient of aluminized Kapton was estimated. The value of 0.98 was calculated based on the three measurements and the following basic assumptions.

(1) specular reflection is a function of surface roughness only

(2) both the slope of the infinitestimal surface area of the membrane and the reflected light intensity can be described by the same distribution function

Two different distribution functions were applied to process the data; the cosine and the normal. Both approaches produced the same value for the specular reflection coefficient that is used for calculating the thrust imposed on the Sail film by the photon impulse (momentum).

4.2.3.3.2 Emittance. Emittance data for selected samples is presented in Tables 4-17 to 4-19. The nomenclature used to describe each sample is based on the sketch at the rear of the table. Table 4-17 presents data for several thin polymer films. The scatter in the data is believed to be the result of variations in film thickness. Sample A4 was measured calorimetrically to verify the DB100 readings and to determine temperature effects. The calorimetric data at 38°C agreed quit: well. Sample A2 was measured spectrally in the TRW Paraboloid Reflectometer and once again the data agreement with the DB100 was very good. The conclusions from these measurements: (1) the ultrathin polymer films ($\sim 2\mu m$) alone do not have high enough emittance to meet the requirements for a 0.25 AU mission, and (2) all emittance measuring techniques gave similar results.

Table 4-18 summarizes data for thin film metal enhanced films of configurations Figure 4-11 b, c, and g. Chrome, 50/50 nickel-

Table 4-16. Decrease in Diffuse Reflectance as Function f
Polar Angle Increase

Reflectometer Aperture	No Mask (1" square)	Small Mask (1.12" dia.)	Large Mask (1.4" dia.)
Polar angle for Specular Reflectance Measurement (α)	5.3°	8.5°	10.5°
Solar Reflectance (r)	0.864	0.864	0.864
Diffuse Reflectance (R_d)	0.227	0.098	0.035
Normalized Specular Reflectance (R_s)	0.737	0.887	0.959

chrome and 80/20 nickel-chrome were used as the absorbing layer. The
resistivity metal (Cr) under aluminum did not greatly increase the emit-
tance, and (2) an absorbing layer of nominally 100Å of chrome or nichrome
on the backside of the Kapton did nearly double the emittance. Fig-
ure 4-15 presents measurements, made early in the program, that estab-
lished the feasibility of concept (c) and provided the selection of
optimum Cr coating thickness. The hemispherical emittance of samples A4
and CR9 was measured to verify DB 100 readings and to determine emittance
at elevated temperatures. Figure 4-16 shows a value of 0.62 at 280°C
for CR9 and 0.34 for A4.

Table 4-19 summarizes data for Indium/Tin Oxide and carbon
coatings on Kapton. Carbon coated samples did not yield results compar-
able to the metals tested. Indium/tin oxide coatings were comparable
to Cr coatings, but required much longer deposition times to achieve
the thicker coatings.

Another promising method for increasing the emittance of the
back surface was that of using a filler of carbon black in the base
resin film. A solution-cast film of Kapton type polyimide, prepared by
NASA LaRC, that contained 10% by weight carbon black had a hemispherical
emittance of 0.55. When 100A of chromium was subsequently vapor
deposited on the back side, the emittance increased to 0.7. There
were problems, however, in manufacturing large volumes of film in this
manner.

Table 4-17. Emittance of Aluminized Polymer Films

Sample Number	Description[1]	SS 2 Mat'l	SS 2 Thick.	SS 1 Mat'l	SS 1 Thick.	SPF Mat'l	SPF Thick.	εC Mat'l	εC Thick.	Emittance ϵ_Q [2]	Emittance ϵ_N [3]	Emittance ϵ_H [4]
A1	STD Alumi-nized Kapton, 0/Al/K/0	-	-	Alum.	Nom 1500Å	Kapton	0.3 mil.	-	-	0.45		
A2	Etched Kapton, Aluminized, 0/Al/K/0	-	-	Alum.	Nom 1500Å	Kapton	0.1 mil.			0.35	0.38	
A3	0/Al/K/0	-	-	Alum.	16000Å	Kapton	Nom 0.1 mil.	-	-	0.26		
A4	Etched Kapton Aluminized 0/Al/K/0	-	-	Alum.	Nom 1500Å	Kapton	0.1 mil.	-	-	0.29		0.30/ 38°
A5	Alum Tef (TFE) 0/Al/TFE/0	-	-	Alum.	Nom 1500Å	TFE Teflon	0.1 mil.	-	-	0.25		
A7	Lap Joint 0/Al/K/ADH/	-	-	Alum.	Nom 1500Å	Karton Adhe-sive Kapton	0.1 mil.	-	-	0.53		

[1] 0 is no coating; K = Kapton; Al = Aluminum; etc., starting from sun side: SS2/SS1/SPF/C

[2] Measured with gier dunkle DB100, Nominal 38°C value

[3] Calculated from spectral reflectance data

[4] Hemispherical emittance measurement at 38°C

Sun Side Coating 2 - SS 2
Sun Side Coating 1 - SS 1
Substrate Polymer Film - SPF
Emitting Side Coating - .C
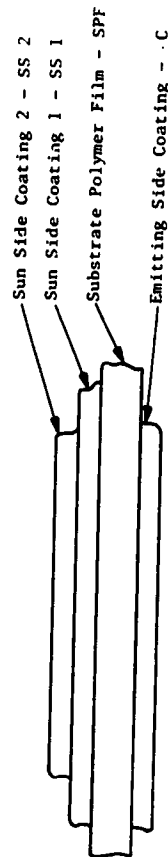
Table 4-18. Emittance of Chrome/Nickel — Enhanced Films

Sample Number	Description[1]	SS 2 Mat'l	SS 2 Thick.	SS 1 Mat'l	SS 1 Thick.	SPF Mat'l	SPF Thick.	C Mat'l	C Thick.	Emittance ε[2]	ε[3]	ε_H[4]
Cr 1	O/A./K/Cr	-	-	Alum.	Nom 1500Å	Kapton	0.3 mil.	Chrome	483Å 250Å 135Å 50Å 0	0.41 0.51 0.64 0.61 0.45		---
Cr 2	Al/Cr/K/O	Alum.	1150Å	Chrome	1150Å	Kapton	0.1 mil.	-	-	0.37	0.47	
Cr 3	Al/Cr/K/O	Alum.	1600Å	Chrome	1950Å	Kapton	0.15 mil.	-	-	0.37		
Cr 4	Al/Cr/K/Cr	Alum.	1700Å	Chrome	2000Å	Kapton	0.1 mil.	Chrome	100Å	0.61		
Cr 5	O/Al/K/Cr	-	-	Alum.	1500Å	Kapton	0.1 mil.	Chrome	100Å	0.55		
Cr 6	O/Al/K/Cr	-	-	Alum.	1620Å	Kapton	Nom 0.1 mil.	Chrome	Nom 100Å	0.64	0.68	
Cr 7	Al/Cr/K/O	Alum.	1620Å	Chrome	1930Å	Kapton	Nom 0.1 mil.	-	-	0.51		
Cr ?	Al.Cr.P/Cr	NiCr	2390Å	Cr Cr	1580Å	Pary-lene	Nom 0.1 mil.	Chrome	100Å	0.39		
Cr 9	O/A./K/Cr	-	-	Alum.	1500Å	Kapton	0.11 Avg	Chrome	100Å	0.55-0.60		0.62
NiCr ?	Al/NiCr/K/O	Alum.	1700Å	NiCr 50/50	2000Å	Kapton	0.1 mil.	-	-	0.46		
NiCr ?	Al/NiCr/K/NiCr	Alum.	1700Å	NiCr 50/50	2000Å	Kapton	0.1	NiCr 50/50	100Å	0.62		

(1) O is no coating; K = Kapton; Al = Aluminum; etc.
 Starting from sun side: SS2/SS1/SPF/ C

(2) Measured with Gier Dunkle DB100, Nominal 100 F
 Value

(3) Calculated From Spectral Reflectance Data

(4) Hemispherical Emittance Measurement

Sun Side Coating 2 - SS 2
Sun Side Coating 1 - SS 1
Substrate Polymer Film - SPF
Emitting Side Coating - C

Table 4-19. Emittance of ITO and Carbon Enhanced Films

Sample Number	Description[1]	SS 2 Mat'l	SS 2 Thick.	SS 1 Mat'l	SS 1 Thick.	SPF Mat'l	SPF Thick.	cC Mat'l	cC Thick.	Emittance ϵ_Q[2]	Emittance ϵ_N[3]	Emittance ϵ_H[4]
ITO1	O/Al/K/ITO	-	-	Alum.	Nom 1500Å	Kapton	0.12	ITO	Nom 1400Å	0.59		
ITO2	O/Al/K/ITO	-	-	Alum.	Nom 1500Å	Kapton	0.08 mil.	ITO	Nom 1400Å	0.61		
ITO3	O/Al/K/ITO	-	-	Alum.	Nom 1500Å	Kapton	0.06-0.09 mil	ITO	Nom 1400Å	0.65		
C1	Carbon Coated Aluminized Kapton O/Al/K/C	-	-	Alum.	Nom 1500Å	Kapton	Nom 0.1 mil.	Carbon	350Å 150Å	0.36 0.31		
C2	Al/Cr/K/C	ALUM.	Nom 1500Å	Chrome	1500Å	Kapton	Nom 0.1 mil	Carbon	350Å 150Å	0.46 0.40		

[1] O is no coating; K = Kapton; Al = Aluminum; etc., starting from sun side: SS2/SS1/SPF/ C

[2] Measured with gier dunkle DB100, Nominal 100°F value

[3] Calculated from spectral reflectance data

[4] Hemispherical emittance measurement

Sun Side Coating 2 - SS 2
Sun Side Coating 1 - SS 1
Substrate Polymer Film - SPF
Emitting Side Coating - cC
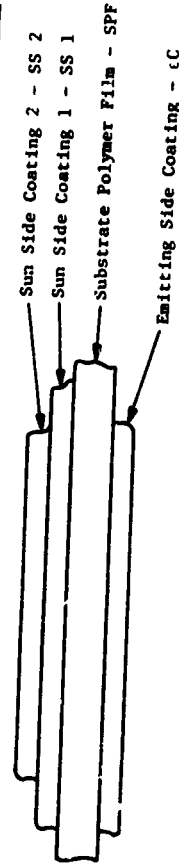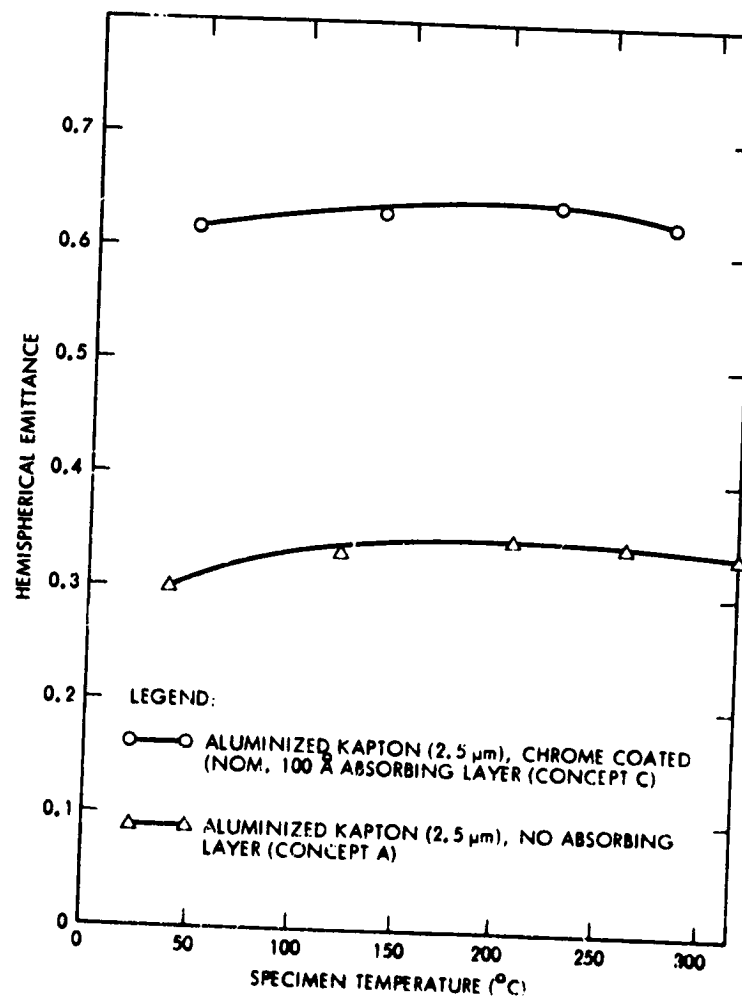
Figure 4-15. Emittance Data for Absorbing Layer Deposited on Aluminized Kapton
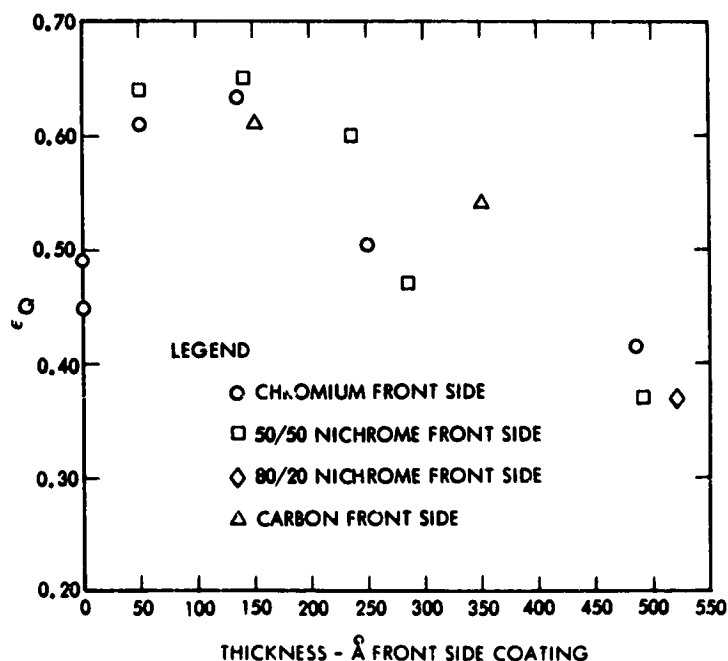
Figure 4-16.   Hemispherical Emittance of Aluminized Kapton
as a Function of Temperature

Directional reflectance data for samples A2 and CR4
(Figure 4-17) shows the interference band structure in the infrared
which causes the increased emittance for the chrome-coated samples.

4.2.4   Coating Durability

Changes in coating properties as a result of exposure to
probable HCRM environments are not known.   Short-term data indicate ade-
quate stability for the metal coatings.   Reflectance and emittance as a
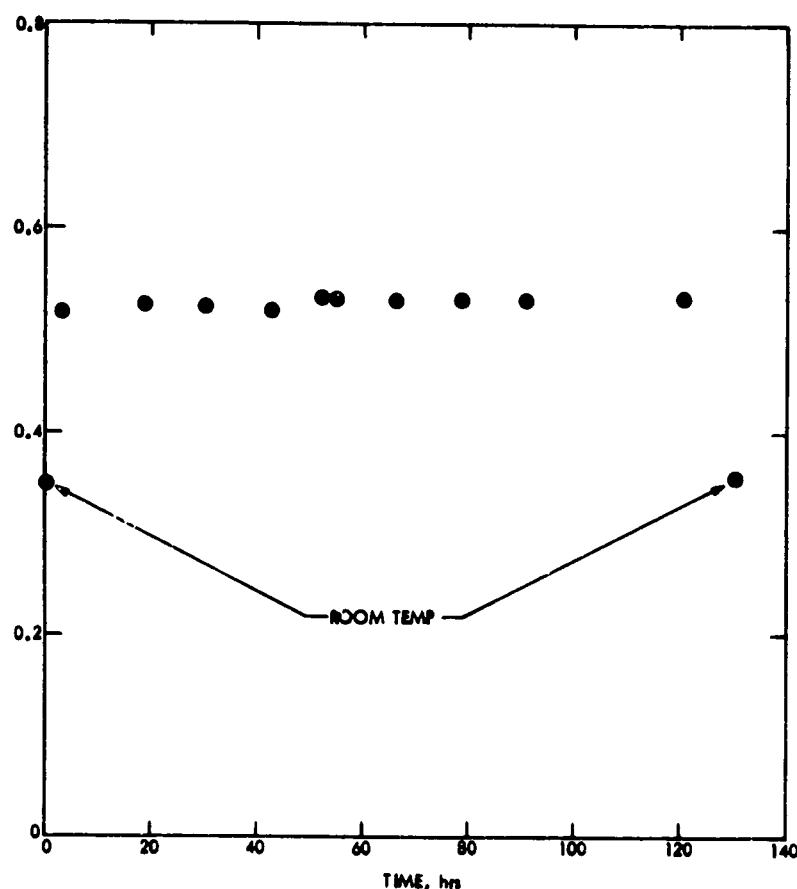
Figure 4-18. Resistivity of Aluminum Film vs. Time at 16 Suns.
Benchmark System, $T \sim 280^{o}C$, 10^{-8} Torr.

estimated at less than $1\text{Å}/year$. Stability to sputtering and sublimation
are therefore seen to be satisfactory.

The ability of the coatings as a function of thickness to
protect the polymer film from radiation has not been well established.
A radiation profile is shown along with results of some preliminary
radiation testing in the section of the report covering system
performance, where it is shown that $1100-1200\text{Å}$ of aluminum is necessary
to protect the sun-side at the polymer film from UV radiation.

The maximum resistivity necessary to avoid arcing and punc-
ture through static buildup was calculated to be about 10^{10} ohms/square.
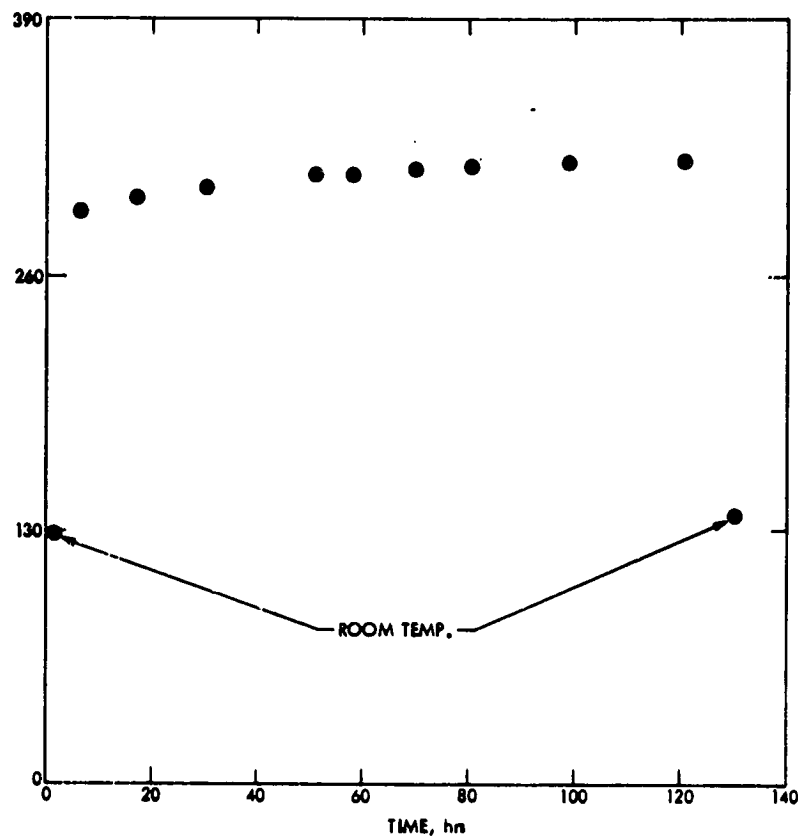
Figure 4-19. Resistivity of Chromium Film vs. Time at 16 Suns.
Benchmark System, T ~ 280°C, 10^{-8} Torr

4.2.5   Manufacturing Requirements

The technical requirements for the Sail film coatings impose
a different set of coating parameters for thin polymer films than are
normally employed for these applications. As previously mentioned, to
afford protection to the film from the solar wind and ultraviolet radia-
tion of the space environment, the reflecting side metallization must be
thicker than what is commercially applied to thin polymer films, e.g.
the minimum thickness for aluminum on the reflecting side of the Sail is
1000Å. Optical measurements late in program indicated that an increase
to 1100 - 1200Å might be advantageous to negate UV effects. This makes
it necessary to apply the coating (in the case of vapor deposited coat-
ings) in multiple passes since only a finite thickness (300 - 500Å) can
be applied with one pass without thermal damage to the thin film.

The cause is attributed to the high heat of vaporization for metal in combination with the small thermal capacity of thin polymers. The problem will be less significant as the coatings are applied with a continuous process allowing better heat dissipation from a moving metal backing (roller). However, it is a factor that must be addressed in the design of the production equipment. Additionally, because of the higher heat of vaporization of the chromium emitting side coating, the requirements for the coating equipment for this process are more stringent. In fact, during the course of the work for the Solar Sail program, no vendor was found that had a continuous coating facility for vapor depositing chromium coatings onto polymer films in widths greater than twelve inches. Other producibility considerations are the control of the coating quality, integrity and uniformity.

Since the thermal control properties of the film are derived from the chromium coating thickness, this parameter must be very closely controlled. In addition, the chemical composition (purity) of the chromium will vary with the quality of the vacuum within the chamber where the coating is being applied. Lower vacuum tends to produce slightly oxidized chromium coatings which, in turn, will have different emittance properties than the pure chromium. Large production facilities, as a general rule, tend to have poor vacuum capabilities. Since the chromium coating process will need stringent process and quality control, the development of improved metallizing equipment (over what is currently available) appears mandatory.

The physical vapor deposition (PVD) method was the major candidate process that was identified for application of the metallized coatings for the front reflector and backside emitter of the Sail film. The method was selected primarily on the basis that it has been the most thoroughly developed commercial technique and would be the most expeditious technique to develop to the point where large volumes of material could be coated with minimum modifications to existing facilities.

The availability of the proposed raw materials for applying vapor deposited coatings (aluminum and chromium) to the Sail film

appeared quite adequate and the typical production rates predicted to
be necessary to coat the film were also achievable.

Other processes such as sputtering and ion plating were also
assessed as potential methods for applying the metallization. Ion plat-
ing of Kapton film samples was performed by Endurex, Corp. The thermal
radiative properties of the samples were then measured at TRW, as part
of the measurements program previously reported.

Though limited in the scope of their effort, Endurex demon-
strated the technical feasibility of the ion-plating process to apply
metallized coatings to ultrathin polymer film for the Sail. From a
thermooptical properties viewpoint, the ion-plated samples consistently
yielded values of spectral reflectance (for silver and aluminum coatings)
and effective emittance (for chromium, etc.) which were equal to or
superior to those obtained by physical vapor deposition methods. Solar
reflectance values from ion-plated aluminum averaged near 0.91, while
emittance values from ion-plated chrome ranged between 0.68 and 0.73 on
2.5 micron Kapton, and surprisingly, show less dependence of the emit-
tance on chrome thickness than is observed for vacuum deposited chrome.
Endurex had no problem with ion-plated ITO on polymide films, and
achieved emittance values approaching 0.68. However, some of the ITO
coatings were not sufficiently conductive. Assuming that this problem
could have been solved, the ability to coat ITO was demonstrated.
Endurex also indicated that there were no unresolvable scale-up diffi-
culties with the ion-plating process. In addition, limited bond peel
test strength results were higher for these coatings than for comparable
vapor deposited ones. Sufficient data was not obtained however, prior
to culmination of the effort on the Sail program to gather conclusive
evidence.

The sputtering process offers many advantages, and according
to a Battelle report[7], has recently been developed into a high-rate proc-
ess by the use of a magnetic field over the cathode surface to enhance
plasma density. The process is known for its stable operation and,
unlike the PVD method, no rate monitor is necessary to maintain a
constant metallization rate.

REFERENCES

1. Edwards, D.K., et. al., "Integrating Sphere for Imperfectly Diffuse Samples", J. Opt. Soc. Am. 51:1279-88 (1961).

2. Thekaekara, M.P., "Proposed Specification for the Solar Constant and Air Mass Zero Solar Spectral Irradiance," IES Solar Radiation Committee, 27 August 1971.

3. Nelson, K.E., et. al., "A Device for the Rapid Measurement of Total Emittance," J. Spacecraft Rockets 3:758-760 (1966).

4. Dunkle, R.V., et. al., "Heated Cavity Reflectometer for Angular Reflectance Measurements," Progress in International Research on Thermodynamics and Transport Properties, Am. Soc. Mech. Engrs., pp. 541-567 (1962).

5. Newman, B.E., et. al., "High Temperature Reflectance Measurements with the Paraboloid Reflectometer," AIAA Paper 68-25, AIAA 6th Aerospace Sciences Meeting, January 1968.

6. Nelson, K.F., and Bevans, J.T., "Errors of the Calorimetric Method of Total Emittance Measurement," NASA SP-31, pp. 55-65, (1963).

7. Bradbury, E.J., et. al., "Survey and Assessment of Monolithic Film Materials and Associated Manufacturing Processes for a Solar Sail", Battelle Columbus Laboratories Summary Report, JPL Contract No. 954659; May 2, 1977.

720-9

4.3 JOINING, HANDLING AND PROCESSING

4.3.1 Background and Technical Requirements

In previous sections it was pointed out that the Solar Sail is a massive structure requiring large areas of ultrathin Sail film in order to gain a favorable Sail loading factor (the ratio of Sail area to Sail weight). The Heliogyro requires approximately the same sail area in its twelve individually deployed blades as the Square Sail. For each of the 7000 meter long Heliogyro blades, an estimated 7328 seams were required to join the panels. This corresponds to a total seam length of 675,000 meters (400 miles).

With these imposing figures, it was apparent that some major technology advancements in the fabrication of flexible structures would be needed and a number of tremendous technical challenges were involved in selecting a candidate method of joining the Sail film segments and in fabricating the Sail blades:

(1) large flexible space structures had been fabricated, e.g., Echo Satellite; but none as large as the Solar Sail. The Sail is 1000 times larger in surface area.

(2) films with area densities of 12 g/m^2 had been fabricated into small flexible structures; but none as light as 3 g/m^2

(3) metallized polymer films, e.g. aluminized Kapton, had been successfully joined; but joined surfaces were not required to sustain elevated temperature and space radiation exposure for long periods

Some of the technical requirements for the joining method are shown in Table 4-20. By examining these requirements and the available methods for joining and handling ultrathin films, it was apparent that serious consideration would have to be given to these factors.

Table 4-20. Target Technical Requirements for
Joining and Handling

A. Mechanical

- highly reliable, automated, fully mechanized joining system
- bond strength greater than film material
- minimum damage to coated film during processing
- overall dimensional change of joint similar to that of Sail film
- ultrathin films will require some type of support, e.g. rip-stops during handling, fabrication and deployment
- reinforcements would be required at load transfer points into the Sail structure (Square Sail) and at points of high stress, e.g. lead and trail edges of blades (Heliogyro)

B. Thermal

- thermal stability of bond must equal that of Sail film

C. Radiation

- radiation resistance of bond must equal that of Sail film

D. Electrical

- electrostatic charging of Sail film would have to be controlled and means for accomplishing this would also be required in the seam

Initial effort was devoted to a survey and assessment of known joining methods for the major Sail film material candidates at that time. This included an assessment of the various generic bonding methods for applicability to ultrathin film materials. Additionally, the current state-of-the-art in performance, efficiency and reliability of parachutes, balloons and other lighter-than-air vehicles was examined. Much of the recent research and development in the latter area; with respect to materials, handling and fabrication had been performed at or for NASA-LaRC (see Refs. 1-11).

This survey and assessment resulted in a preliminary list of the most promising joining methods which are listed in Table 4-21. There were some obvious disadvantages with the mechanical joining methods (e.g. stapling, sewing, etc.). These were as follows:

(1) Reinforcement was required along leading edges of the film to avoid tears as each hole for a thread or staple represented a stress riser. This added weight to Sail sheet.

(2) The thermal heat balance would be affected by the geometry of a thread or a staple which would make the seam temperature dissimilar (higher) than the balance of the Sail sheet.

(3) Extra weight would also be added from the introduction of the thread or staple.

Upon further evaluation and experimentation with adhesive bonding, it appeared evident that this method showed the most promise for the joining of ultrathin films. Therefore, major emphasis was placed on joint design, type of adhesive and process to be used.

Several types of bonds were expected to be utilized in the fabrication of the blades for the Heliogyro. Some are used to join the adjacent film panels of a blade, some to provide rip-stop protection in the blade panels, and still others in the fabrication of the high strength edge reinforcement members. The latter is discussed separately in another section of this report dealing specifically with the Heliogyro structure.

As earlier discussed, the basic panel segment bonds (bonding adjacent strips of film together to form larger sheets) were by far, the most numerous. Early in the program, when effort was being concentrated on the Square Sail, this particular joint received the major attention and concern. Therefore, once the major candidate bonding method was determined (adhesive bonding), effort was devoted both to selecting the type adhesive and to designing an optimum, basic joint.

Table 4-21.   Preliminary Sail Film Joining Methods

Joining Method	Comments
Adhesive Bonding	Minimum weight joint, minimum thermal problem (joint design), good material compatibility possible.
Sewing/Stitching/Lacing	Ease of fabrication process, availability of equipment, known technology.
Stapling	(Same as for Sewing/Stitchings/Lacing)

4.3.2   Evaluation and Selection of Joining Method

Since the work in the basic film materials area of this program indicated that polyimides were the major candidates for the Sail film, a survey was made to identify potential adhesives for bonding polyimide films to themselves. This survey, which included a search of the literature and contact with industry experts regarding high temperature adhesives, resulted in a list of potential adhesive candidates in the following chemical classes:

  (1)   polyimides

  (2)   polyphenylquinoxaline

  (3)   phenolic aralkyl ethers

Adhesive samples from each of these classes were obtained from manufacturers and screening tests were performed. Most of these tests were made with Kapton H polyimide film, which was the most readily available and also had emerged as the prime Sail film candidate. Early testing was performed on bare films and subsequently on metallized films after the reflective and emissive coating system (Al and Cr) had been identified. The criteria used in the screening tests for the adhesives are indicated on the following page.

Property	Criterion
Bond Strength	no failure in bond after curing
Thermal Stability	bond to be intact after aging for 24 hours at 315°C
Handling/Processing	ease of application, speed of handling, sensitivity to ambient moisture, etc.
Availability	should be commercially available in large enough quantities to support Sail fabrication schedule.

4.3.2.1   Evaluation Tests. A list of the adhesives evaluated are shown in Table 4-22. Various thicknesses of Kapton H films were employed (2.5, 7.6, 25 and 125 μm) for the screening tests. The specimens were primarily of the lap shear type, approximately 1 x 8 cm for total specimen size, with a joint area of 1 cm^2. Bond line thickness was one of the variables and thicknesses from 2.5 to 12 microns were investigated. The adhesives were generally applied by spraying with an air brush, manually brushing and then scraping (leveling) with a blade, or by the use of a Q-Tip. (cotton swab.) Prior to application of the adhesive to the Kapton surfaces, the film strips were cleaned with ethanol (100%) and air dried. Adhesive was applied to one or both surfaces of the Kapton, dried and prepolymerized (where applicable) by heat. Bonding was accomplished either by using a manual soldering iron (at 370°C) or a hydraulic platen press (where pressure and temperature were easier to control). Initial cure times varied from 10-15 seconds with the soldering iron to 30-40 seconds with the platen press at temperatures of 310-315°C.

Since the bonding process ultimately used to fabricate the Sail blade panel seams had to be, of necessity, fairly fast (2-3 meters/minute); the time required to make a strong joint was a dominant factor.

Table 4-22. Adhesives Evaluated for Solar Sail

Adhesive Designation	Type	Manufacturer	Comments
NR 150A2G	Polyimide	duPont	Good for use at 250°C T_g = 280-300°C
NR 150B2G	Polyimide	duPont	Good for use at 310°C T_g = 350-375°C
NR 150 B252X and NR 055X	Polyimide	duPont	Experimental resins, no advantage over NR 150B2G
2080D	Polyimide	Upjohn	Poor handling properties, precipitation of resin on exposure to air
TR 150-25	Polyimide-Amide	Thermo-Resist	Availability Uncertain
TR 300-25	Polyimide-Amide	Thermo-Resist	Availability Uncertain
PPQ 401	Polyphenylquinoxaline	Acurex	Unsatisfactory Bond Strength
XYLOK 210	Aralkylether + Phenol	Ciba-Geigy	Inadequate thermal stability embrittlement on aging at 310°C
Sheldahl 3P	Polyimide-Amide + Polyester	Sheldahl	Inadequate thermal stability bond failure on aging 24 hr at 310°C

Bond strength tests included tensile shear using the Instron tester in compliance with Federal Test Method Standard #175, Method 1033.IT and creep measurements under constant load. On a selective basis, tests were performed at elevated temperature in vacuum or in an inert atmosphere. The Kapton used in making up the samples had to be thicker than that used for the Sail in order to get bonds to fail in the joints during the lap shear tests.

The results of the tests indicated that satisfactory bonds were obtained with NR 150B2G and NR 150A2G adhesives made by duPont. Those made with TR150-25 and TR800-25 were also acceptable. The TR adhesives, while showing good thermal resistance on bare Kapton at temperatures of 260°C (TR150-25) and 310°C (TR800-25) were removed from consideration however when a question arose about their commercial availability in large quantities. Bonding was achieved in less than 15 seconds with the soldering iron and under 45 seconds using the platen press at 315°C. Further tests and evaluations concluded that the NR150B2G was the prime candidate for the adhesive system. This adhesive offered superior bond strengths at elevated temperature and good thermal stability over the temperature range for the HCRM.

4.3.2.2   **Joint Design.**   Concurrent with the effort to select the adhesive, work was conducted to design the basic seam that would be employed to join adjacent film panels. The major considerations were:

(1)   the joint would have to have the same thermal characteristics as the Sail film

(2)   the weight of the joint itself would have to be minimized

(3)   the joint would have to be compatible/adaptable to high speed production joining processes

(4)   voids in the adhesive would have to be kept to a minimum to avoid thermal problems.

(5)   the amount of exposed (bare) adhesive (sun side) would have to be kept to minimum to avoid thermal problems.

After studying the problems involved, a design evolved which incorporated a butt seam with an overlapping tape (doubler) on the anti-sun side of the film. This design is illustrated in Figure 4-20 which shows a 1 cm wide doubler tape of metallized Kapton film, 7.6 microns (0.3 mil) thick, adhesive bonded to butting edges of 2.5 micron (0.1 mil) thick, metallized Kapton Sail film. The bond line thickness is 3.8 microns (0.15 mil). It was calculated (Reference 12) that the gap between the two butting edges on the sun side should not exceed 76 microns (3 mils) because of temperature control considerations. Other advantages of this particular joint design were:

(a) adaptive thermal control coatings could be applied to the doubler ahead of the final joining process

(b) the adhesive could also be applied to the doubler prior to the final joining process (thus omitting a processing step on the film sheet)

(c) the doubler (with the adhesive pre-applied) could be employed as the reinforcing transverse rip-stops for the Sail film in the blade panels.

Consideration was also given to the weight that this type of joint would contribute to the spacecraft. Calculations showed that this seam would weigh approximately 0.184 g/m. With a total seam length of 675,348 m, the total seam weight would be about 124 kg. For comparison, it was calculated that for a sewn seam the weight would have been 0.204 g/m for a total of 138 kg.

4.3.2.3 Testing Program

(a) Thermal Aging

After selection of the candidate adhesive and joint design, further testing was conducted to determine the aging characteristics of the joint at various temperatures. Other tests were performed on the "benchmark" joint such as the simulated space environment testing

Figure 4-20. Benchmark Joint Configuration

at Boeing where sample joints were included with film
samples. The results of these tests showed the joint
to behave similarly to the basic films. Details of
these tests are discussed in a later section on system
performance.

Sample Preparation

Metallized lap shear specimens were made up using the
butt configuration and "benchmark" plated (1000Å of Al
on one side and 125Å of Cr on the other) 125 micron
(5 mil) thick Kapton film. Again, the thicker Kapton
was used because failure occurred in the film with the
thinner gauge films and for these test purposes, fail-
ures in the joint were sought. Bond line thicknesses
of 2 to 4 microns were employed.

An appropriate number of specimens for a statistical base could not be prepared from the same batch processes because of the lack of equipment to prepare large batches. Sheet joints were therefore prepared from small sheets of film (each 13 x 28 cm) which were subsequently cut to the specified specimen sizes. This necessitated the preparing of a large number of batches, and thus obtaining control samples from each batch, because tensile shear strengths could vary from batch to batch.

(b)   Testing and Test Results

The specimens were placed in evacuated and sealed quartz tubes which were in turn placed in ovens and aged at temperatures of 240, 270, 305 and 370°C. At certain intervals, generally every other day, specimens were withdrawn from the ovens and tested at temperatures of either -60 or 250°C.

Control specimens, that had not been aged, were tested with each group of aged specimens at either -60° or 250°C. The lap shear strengths of these control specimens, were then compared with the lap shear strength of each particular aged specimen to arrive at a shear strength ratio, S_t/S_o, where S_t = the shear strength of the test specimen and S_o = shear strength of the control specimen. These S_t/S_o ratios were then plotted versus aging time for joints aged at the four temperatures (240, 270, 305 and 370°C) and subsequently tested at either -60°C or 250°C. Figure 4-21 is the plot of aged samples that were tested at 250°C, while Figure 4-22 is the plot of those specimens tested at -60°C. Except for one case, in the samples tested at 250°C where a sample was aged at 240°C, there was an initial reduction in S_t/S_o, then an increase, followed by a gradual reduction.

The average lap shear strength values for the control samples tested at 250°C was 400 psi, while those tested at -60°C was 125 psi. Thus, even though the trends were generally toward lower
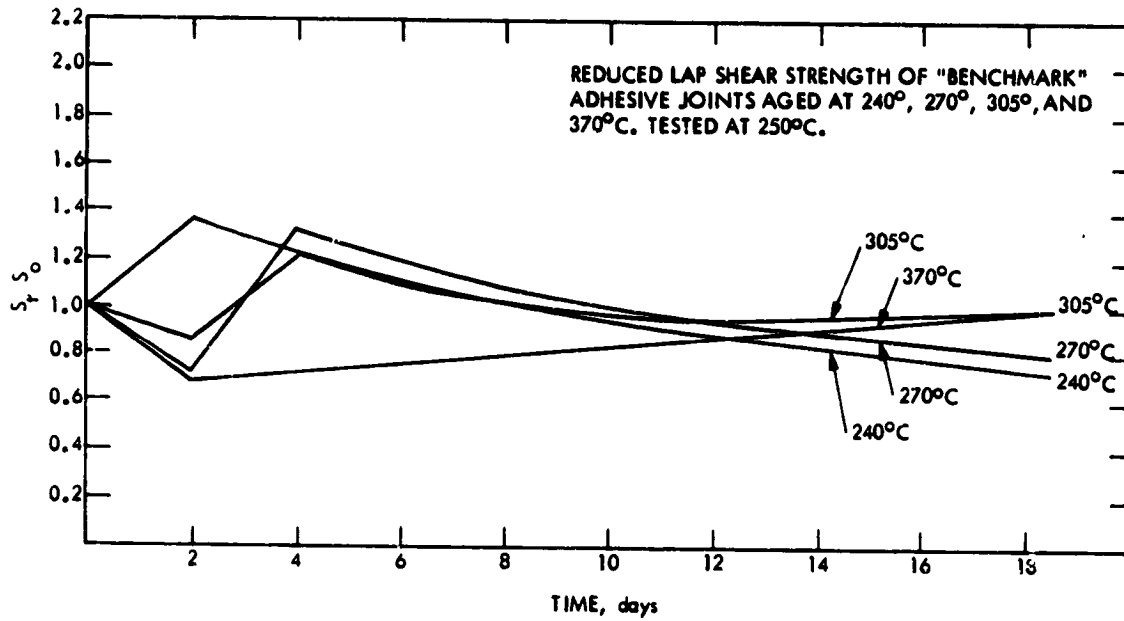
Figure 4-21.   Accelerated Aging of Adhesive Joints
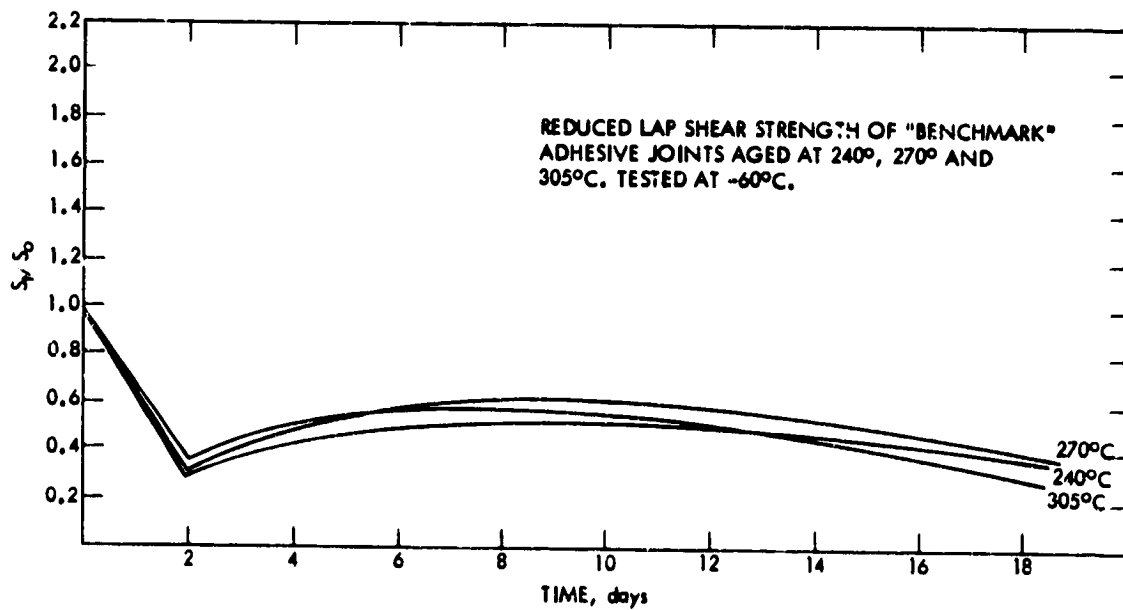
Figure 4-22.   Accelerated Aging of Adhesive Joints

S_t/S_o ratios with longer aging times, (especially at the -60^oC test temperature) the strength of the joints appeared adequate for the application where maximum loads of 0.5 psi had been projected for the film sheet while inflight. Generally, the data it 250^oC is what would normally be expected, where polymer materials that are cured at or near their use temperatures perform better than ones cured at temperatures lower than their use temperature. It is apparent that a higher temperature cure is beneficial for increasing the strength of the joint.

The trend of the data for the samples tested at -60^oC towards the lower values is not so easily explained. More analysis is needed in this area.

4.3.3   Handling and Processing

4.3.3.1   Requirements

Although it was anticipated the Sail film would receive separate handling prior to the bonding operation, e.g. application of the reflective and emissive coatings, it was perhaps in the bonding area where major concern occurred. This is where sheets of coated film are processed into Sail blade panel subassemblies and, as a result, the film would probably sustain its greatest mechanical stresses. The general problem of handling has not been previously discussed because some thought had been given to having the coatings applied to the basic film at the same point in the manufacturing cycle that Sail fabrication was performed. This would eliminate a separate handling and packaging step for the coating operation.

There were three outside contracts to study the feasibility of Sail fabrication. These were conducted under the direction of the Project Development Group of the JPL Applied Mechanics Division. These contracts basically covered Solar Sail preliminary design and fabrication assessments. Two contractors, (ILC Dover and Sheldahl) initially were conducting studies on the Square Sail configuration and one (Astro Research) on the Heliogyro. Therefore, the subject of fabrication

processing of the ultrathin, flexible Sail film received close attention by qualified personnel. These contractors are very experienced in the fabrication of lightweight, flexible space structures.

For this portion of the report, "processing" is considered as the conversion of film and adhesive into a great number of Heliogyro blade panels meeting all of the engineering requirements. Important considerations were the retention of all the properties of the Sail film required for the HCRM, e.g., reflectivity, emissivity, and long term resistance to the mechanical, vacuum, thermal and radiation environment. Also very important, were the control of dimensions and mass distribution. This was especially true of the adhesive joint where tight tolerances were required on the amount of adhesive employed and the width of the exposed gap on the sun-facing side of the butt joint.

To meet the requirements of the HCRM, all of the appropriate technology had to be developed, and a fabrication facility provided in the short time alloted by the Sail program schedule. The facility had to perform at a rate compatible with this schedule. In terms of one of the key operations, adhesive bonding, this rate corresponded to 2 to 10 meters per minute, depending upon such factors as number of shifts per day, and maintenance down-time. Notwithstanding the considerable differences between the Square Sail and the Heliogyro, the general scheme of film and adhesive processes in their fabrication would be very similar.

It is acknowledged that changes in specific raw materials could result from the findings of future research and development; however, since major attention has focused on a single set in this program, their use will be assumed in this section. The film is 2.5 μm Kapton coated with 1000Å of aluminum on one side and 125Å of chromium on the other ("Benchmark" film). The adhesive is DuPont's NR150B2G which, like Kapton, is a polyimide.

A brief outline of the required process elements is shown below. In the case of a one-piece Square Sail, the elements listed under item 2 below would be repeated many times with sub-assemblies of ever increasing size.

(1) Raw materials will be:

    (a) received,

    (b) stored,

    (c) subjected to quality control inspection and testing

    (d) delivered to work stations.

(2) At the work stations, films will be:

    (a) deployed, or partly deployed, from portable packages (probably rolls),

    (b) metallized

    (c) measured,

    (d) slit,

    (e) aligned,

    (f) bonded,

    (g) subjected to non-destructive evaluation (NDE) (not necessarily all at this point in sequence. For example, real-time NDE of bonding is contemplated).

    (h) repackaged,

    (i) delivered to another work station.

(3) Thermal treatment for additional curing of adhesive bonds.

(4) Final inspection, including weighing.

(5) Packaging for flight.

Adhesive bonding, consists of several sub-elements. The adhesive is supplied unpolymerized dissolved in a solvent. First, solution must be applied to the doubler strip in measured density (e.g., air brush spraying). Then, the applied solution is dried and prepolymerized to a tacky state by heat. Next, the two Sail sheet strips being bonded are brought together, the doubler with preapplied adhesive is fed into the operation and the entire assembly fused by pressure and heat. Our investigations indicate that sufficient strength for subsequent handling can be attained in a period of about 15 s. The additional curing (process element 3) is needed to produce in the adhesive bond the thermal resistance required of the Sail for the HCRM.

4.3.3.2   Film Handling

Early inquiries about the fabrication of light-weight flexible structures revealed the 3 g/m^2 Sail film to be considerably lighter than what had been fabricated up to that time. The chief concern was the film fragility, and particularly its poor tear resistance during handling.

However, since the inception of the Solar Sail program, considerable quantities of 2.5 micron (0.1) Kapton film were handled and subjected to a variety of testing at JPL. As a result, greater confidence was gained in handling. The two fabrication study contractors for the Square Sail, (ILC and Sheldahl) concentrated on this problem. At one time, there were plans to demonstrate the fabrication of a 2000 ft^2 Sail panel. However, this was not performed when technology development was switched entirely to the Heliogyro in late May 1977. Included in the plan were the development of methods for repairing anticipated tears. Without actual experience, a good estimate would be very difficult of the frequency of this maintenance item. The chief problem anticipated, if considerable repairing were required prior to launch, is the complication imposed on efforts to attain specified mass and mass balance on the Sail blades.

In anticipation of severe damage problems with the Sail film during processing and deployment, investigation was made of the feasibility of employing a reinforcing type of material to support the Sail. If a supporting film were needed only during manufacture of the Sail, it did not appear difficult to achieve. Kraft paper was used with success in the preparation of "benchmark" adhesive joints in an experiment with a commercial bonder. Also, a paper was employed by MRI in the retrieval of their water cast polyimide films.

As the HCRM was originally conceived using the Square Sail configuration, there was no allowance for the extra mass a permanent or a temporary supporting film would impose. However, some investigation was made into the feasibility of a temporary supporting film (one which would be discarded after the Sail was deployed). Three concepts were identified which appeared feasible, providing certain critical questions were answered:

(1)   Some polymers degrade thermally, and their degradation products are low enough in molecular weight to evaporate in the vacuum of space. The one polymer of this type that was identified, poly ∞-methylstyrene can be produced in film form. However, it is too brittle to be practical. Two avenues of avoiding the brittleness were recommended for further study, (a) plasticization or (b) replacement of the methyl group by bulkier pendant groups.

(2)   A series of film polymers was identified in a separate investigation which also degrade thermally with the aid of UV radiation. Practical use had previously been made of this technique using polybutylmethancrylate, in the

launching and deployment of a 9 meter diameter
grid sphere, passive satellite. Two questions
remained to be answered regarding the feasibility
of either of the supporting film concepts just
described. First, in the case of the Solar Sail,
the removal of the film and its degradation pro-
ducts would have to be complete. The research in
reference 13 didn't go that far because for that
mission it wasn't important. The second question
was: To what extent would the degradation pro-
ducts from the volatilizing materials contaminate
optical surfaces on spacecraft instruments as well
as the reflective side of the Sail?

(3)   Another concept considered was based on the selec-
tion of a supporting film with a unique set of
other properties. In this case the supporting
film would be very weakly attached to the Sail
film and after deployment it could be peeled off
and discarded along with other elements of the
vehicle. A bond would be achieved between the
two films just good enough to provide the required
reinforcement, but weak enough to avoid damage
during their separation. The bonding mechanism
between the two films would be made by a liquid
having a low but positive vapor pressure. The
liquid would have to be compatible with the Sail
film in the sense of not diffusing or absorbing
into it or otherwise degrading it. A major prob-
lem with this concept would be the mechanical one
of peeling, collecting and projecting the fugitive
film in a way to avoid impact with any part of the
vehicle.

4.3.3.3   Film Blocking

Thin plastic films have a tendency to cling together and
to other surfaces. Among the factors causing this phenomenon is the
static electric potential. Kapton, being a dielectric, would be expec-
ted to give trouble at 2.5 microns (0.1 mil) thickness in the uncoated
state. Qualitative observations in our experiments with metallized
films, however, indicate that the problem was not as severe. Blocking
is probably most critical during handling prior to the metallization.
If the adhesion between folded or adjoining Sail film layers prior to
blade deployment is strong enough to cause tearing or delamination or
surface damage, it can't be tolerated. Provisions have been made in the
deployment mechanism for the Heliogyro blades to minimize this problem.
The concern was much greater with the Square Sail configuration. There-
fore, some attention was directed towards conducting tests to establish
the extent of the problem of "blocking".

The ASTM tests that deal with the tendency for blocking
and with the force required to separate were reviewed. They did appear
to be directly applicable to the needs of the Solar Sail film. A com-
bination of both measurements in one test would be preferred because
they are related. A more appropriate type of test would be as follows:

(1)   Sample Preparation

Cut samples and assemble in a simple jig for
conditioning (with free ends available for
peel testing).

(2)   Conditioning

(a)   Compressive stress film mass to 30 psi

(b)   Duration: 1 day to as long as possible

(c)   Temperature: -40 to 38°C

(d)   Humidity: 0 to 50% RH

(e)   Vacuum: Start at atm.; bleed down, and hold.

(f)   Handling: "white glove" care

(3)   Peel Test

     (a)   Measure stress (lb/in) vs peel rate

     (b)   Rate: several decades

     (c)   Temperature: -40 to 38°C

     (d)   Vacuum: 10^{-7} torr

(4)   Evaluation

     (a)   Examine surfaces for blemish, delamination, and tear.

4.3.3.4   Film Creasing

Wrinkles and folded creases in the Solar Sail film are undesirable for a number of reasons. If creases are tight enough, the film itself is weakened. Creases not tight enough to weaken the film could be expected to take a permanent set on the one hand and either fracture the metallic coating or degrade the specularity of the reflective coating. Besides degrading the specularity, fractures in or missing metallic plating leave those areas of the polymer unprotected from UV and other radiation.

It appears reasonable that the Heliogyro blades might be fabricated and stowed for flight without ever subjecting the film panels to wrinkling or folding. Tight creases might be avoided in a one-piece square Sail also by the use of the concepts developed in Appendix I. Some limited testing was performed to determine to what extent deterioration occurred in the metallization (conductively and reflectively) during cyclic bending from straight to a 4" radius. Coated Mylar film (2.5 µm thick) was folded into strips and flexed 200, 400, 800 and 1600 cycles under a light load. Generally the aluminum held up well but the conductivity of the chromium decreased slightly.

4.3.3.5   Process and Quality Control

Assurance of meeting all the engineering specifications will require extensive monitoring and control in three general areas. These are: (1) quality assurance of incoming and stored raw materials, (2) controls on all process operations (automatic in many instances), and (3) NDE (non-destructive evaluation) of specific product elements during processing, adhesive joints in particular.

Film must be inspected for thickness, density, reflective and emissive coating uniformity and of coarse tears and voids. Film samples must be taken (possibly remnants from slitting) and tested destructively in a way to correlate with long-term environmental resistance properties.

Adhesive must be sampled and tested for processability (e.g., reproducability of areal density in standard spray conditions) and its capability for making the specified environmentally resistant joint.

The problems of process control for lay-out dimensions were studied by the fabrication study contracters. The Square Sail would be particularly sensitive to accumulation of errors of this type because of the necessity for approximately 1000 adhesive joints in sequence along certain dimensions. There are several dimensions in the seam joint which will have to be controlled closely, partly for overall dimension control, and partly for a variety of other reasons (reliable strength, overall mass, etc.). In particular, the unprotected adhesive in the gap of the butt joint is expected to be sensitive to the near-sun space environment. Therefore, gap width control is essential.

Total mass and mass balance from point to point (Square Sail) or blade to blade (Heliogyro) are important requirements. One process control which will be needed in order for accurate measurements of mass is the water content of the film. Kapton can absorb as much as 2.9% water. Constant control of temperature and humidity throughout the

plant is a reasonable approach. Also of concern is possible lot-to-lot variation in the Kapton film. There are opinions that variation may exist between the amounts of unreacted polymerization charge materials and/or by-products from one lot to another.

Among the conditions which must be controlled, in addition to those affecting dimensions and mass, in the adhesive bonding process; are temperature, pressure, and duration. Control of temperature and duration is also needed in the adhesive post-cure.

Monitoring and assurance of many of the required properties will be achieved by a variety of measures not requiring real-time NDE. Partly, this will be done by QA of raw materials. Other measures will include the design of machinery, particularly film handling, and process controls. The chief exception is adhesive bonds. Probably the most effective method of assuring bond quality is real-time NDE. This means that such properties as centering of doubler, butt-gap width, flash dimensions, and completeness of bond must be monitored at a rate of from 2 to 10 m/min. Qualities, such as strength and properties correlating with long-term durability can be assured by a combination of process control during bonding and destructive tests of appropriate coupons.

One or more concepts for monitoring each of the critical parameters had been identified. For example, film thickness or area density, could be monitored by a beta radiation gauge. The optical transmission or electrical resistivity of the chromium coated film would be a measure of the chromium thickness. In addition, the solar absorptance at particular wavelengths, where the values are strongly thickness dependent, is another technique for measuring the metallization thickness.

4.3.3.6   Processing Status

As other sections of this report will show, along with the reports of the fabrication study contractors, References 1 and 2, Section 4.1, established processes and equipment were identified which can

be used, perhaps with some modification, to fabricate the Sail and conduct many of the monitoring tests. Where specific needs were lacking, conceptual designs were proposed.

The adhesive bonding process received considerable attention at JPL. An adhesive with the required properties (both processing and functional) was identified. The portion of the program that remains, as with all the other material components of the Sail, is completion of the durability testing. The results of limited durability testing of the adhesive joint obtained thus far were covered earlier in section 4.3.2.3 in this section.

Other tests were conducted which tended to show that there was considerable safety factor in the "benchmark" joint. As mentioned previously, in order to perform shear tests of the adhesive joint by pulling specimens in tension, it was found necessary to substitute 125 micron (5 mil) metallized film for the 2.5 micron (0.1 mil) film and 7.5 micron (0.3 mil) doubles in order to avoid film failure. Limited creep tests showed no measurable displacement in several joints held under constant shearing loads at 235°C in vacuum for over 1100 hours. The highest loaded joint was stressed over 9 times that required in the Sail.

The processing study in particular was encouraging. As reported earlier in this section, "benchmark" joints made from "benchmark" materials were made in conventional bonding equipment. None of the problems of quality and reliability appeared to be too difficult to solve by ordinary methods. A demonstration of the fabrication of a large multibonded panel was accomplished. This demonstration Sail was fabricated by bonding four 0.3 meter wide x 2.25 meter strips of coated 7.5 micron (0.3 mil) Kapton film into a single sheet. The entire operation was performed on reasonably priced, commercially available bonding equipment that could easily be modified to perform Sail sheet bonding operations. The procedure is described in Appendix 11.

REFERENCES

1. "An Analysis and Computing Program for Three-Body Parachute Deployment Dynamics with Specific Applications to the PEPP (Balloon) Program," by V.L. Alley, Jr., and Raye C. Mathis. Langley Working Paper No. 398.

2. "Comparison Between Measured and Calculated Shroud Loads for the PEPP I Parachute Along with Predicted PEPP II Parachute Loads," by V.L. Alley, Jr., Langley Working Paper No. 399.

3. "A Study of Membrane Forces in a Truncated Sphere Under Aerodynamic Loading and Concentrated Edge Forces with Applications to the Parawing," by V.L. Alley, Jr., J.J. Mathis, Jr., and R.J. Muraca. Langley Working Paper No. 750.

4. "Decelerator Fabric Constants Required by the Generalized Form of Hooke's Law," by Vernon L. Alley, Jr., and R.W. Faison. Presented at AIAA Aerodynamic Deceleration Systems Conference, September 1970.

5. "A Stress Analysis of the Viking BLDT-1 Parachute Conopy With Emphasis on the Effects of Asymetries" by Vernon L. Alley, Jr., Langley Working Paper No. 1067.

6. "Analyses of a Yarn Reinforced Laminate for Balloon and Other Structural Uses," by Vernon L. Alley, Jr., Proceedings, Seventh ARCRL Scientific Balloon Symposium. AFCRL TR-73-0071 Special Report No. 152, January 1973.

7. "Near Optimum Parachute Clusters for Minimum Decelerator Weight to Recovery Weight" by Vernon L. Alley, Jr., NASA LWP-1112, May 16, 1973.

8. "Amplifying Ribbon Extensometer for Measuring Film and Fabric Strain" by Vernon L. Alley, Jr., and Austin D. McHatton; Presented at the AIAA 5th Aerodynamic Deceleration Systems Conference, November 17-19, 1975. Published in the Journal of Aircraft, February 1977.

9. "Investigations of Kevlar Fabric-Based Materials for Use With Inflatable Structures: by R.J. Niccum, J.B. Munson, and L.L. Rueter, Sheldahl Advanced Products Div., NASA-CR-2724, August, 1976.

10. "A Proposed Quantitative Measure of Fabric Handle and the Relative
     Characterization of Some Aerospace Flexible Materials by Handle
     Moduli," by Vernon L. Alley, Jr., and Austin D. McHatton; Presented
     at the Ninth AFGL Scientific Balloon Symposium, October 20-22, 1976,
     Portsmouth, New Hampshire. Published in Proceeding, Ninth AFGL
     Scientific Balloon Symposium, Special Report, 1977.

11. "Structural Materials Research for Lighter-than-Air Systems," by
     Vernon L. Alley, Jr., and Austin D. McHatton; Presented at the AIAA
     Lighter-than-Air Technology Conference, July 15-17, 1975. Published
     in the Journal of Aircraft, March 1977.

12. JP'. IOM 353 GEN-77-245, To W. Carroll from F. Wolf, "Aluminum
     Coating Defects on Solar Sail Film", June 9, 1977.

13. "Controlled Instability of Polymers for Grid-Type Satellites", by
     C.E. Snyder and D. Weir, Goodyear, in Rubber Chemistry and Tech-
     nology 39(4) p. 1161, 1966.

4.4   SAIL FILM PERFORMANCE

The initial investigative work and studies in this program were aimed at identifying the prime candidate film materials and coatings, and methods for fabricating coated film segments into larger panels or (in the case of the square Sail) a single one-piece structure. These initial tests and evaluations did not answer all the questions posed concerning the performance to be expected of the Solar Sail materials in the space environment. Therefore, more extensive evaluations and analytical effort was devoted towards assessing the effects of the space environment on the Sail film system. These assessments included: 1) identifying potential failure modes, 2) determining long-term life predictive methodology and 3) performing limited amounts of simulated space environment testing.

The failure modes identification effort was separated into two categories: 1) material failure modes analyses for the fabrication through deployment phase and 2) an in-space failure mode matrix for a deployed Sail. Potential failure modes were identified in these studies along with generalized requirements for special tests to determine important Sail properties affected by the various failure modes.

Predictive analyses of long-term serviceability were formulated from physical-chemical theories. Chemical degradation at various temperatures, thermal aging effects on mechanical properties and the effects of thermally induced morphological changes on the creep behaviour and thermal expansion co-efficient with respect to Kapton film were the subject of these particular modeling studies.

In the area of space effects testing, a series of experimental programs was conducted to establish the effects of the following, either singularly or in combination, on the Sail film and its bonded joints:

(1)   thermal radiation

(2)   ultraviolet radiation

(3)   gamma and neutron radiation

(4)   combined particle and ultraviolet radiation

(5)   electrostatic charge control/dissipation

Testing was performed at various locations, including NASA-ARC, NASA-LaRC, NASA-MSFC, Brookhaven Labs, the Boeing Co. and JPL.

4.4.1   Failure Mode Studies

As previously mentioned, the failure mode studies were divided into two basic categories: 1) material failure modes analyses for the fabrication through deployment phase and 2) analysis of in-space failure modes.

Potential failure modes were identified, along with general-ized requirements for tests to determine properties applicable to the various failure modes. The majority of these tests also determined desirable material properties that were used in the selection of candidate films. Thus, even though values for these properties may have already been known or under investigation, the need remained for know-ing how they would change with time, temperature and radiation in the space environment. A list of these required properties with attendant environment or test conditions is shown in Table 4-23.

4.4.1.1   Fabrication Through Deployment Failure Modes. In generating a list of expected failure modes that might occur during fabrication through Sail deployment, many assumptions had to be made concerning fabrication techniques and final Sail configuration. Therefore, the discussion that follows contains items pertinent to several manufactur-ing methods and both sail concepts.

(1)   Sail Contour and Smoothness (Square Sail)

A particular problem was foreseen with respect to the topography of the Square Sail. It was visualized that

Table 4-23. Simulated Solar and Space Radiation Test
Requirements for Determination of Sail
Performance

Data Required	Environment or Conditions
1. Physical and Thermal Character-istics (Bi-axial) • Tensile strength • Tear strength • Yield strength • Modulus • Elongation/Shrinkage • Creep • Fatigue characteristics • Bond strengths (shear and peel) • Specific heat	• Thermal. A wide temperature range is expected with brittle-ness a possible problem at the lowest temperature and coating and seam bond failure or film decomposition at the highest temperature. Data is required at -100°C, 20°C, 100°C, 200°C, 300°C, 400°C. • Vacuum. Do thermal test tem-perature applications at low ambient pressure to include desorption effects on mate-rials. Restrict atmospheric air contact with samples during physical property tests. • Solar Radiation. Tests are required after maximum inten-sity U.V., I.R. and x-ray exposure and after various accumulated exposure times. • Accumulative environments. Physical property tests should be made at various significant stages of the mission at vacuum ambient pressure and with the appropriate Sail tem-perature and cumulative solar radiation. Note: These properties should be obtained after exposure to the individual and combined thermal-vacuum-solar environments anticipated.
2. Electrostatic Characteristics • Resistance (Tri-axial) • Capacitance (Transverse) • Breakdown Voltage (Transverse)	Test electrostatic properties over anticipated Sail temperature range and after solar radiation expo-sure. Include Sail sheet, seams and ripstops in test samples. Include smooth and wrinkled sam-ples. Observe warping characteristics.

Table 4-23. Simulated Solar and Space Radiation Test
Requirements for Determination of Sail
Performance (Continuation 1)

Data Required	Environment or Conditions

3. Optical Characteristics
 	
  • Reflectivity
 	
    - Specular Reflection
 	
    - Total Reflection
 	
  • Emissivity
	• Optically smooth, clean Sail material
	
	• Mechanically or impingement eroded Sail material
	
	• Wrinkled Sail material
	
	• Dust coated Sail material
	
	• Accumulative environments. Optical characteristics should be determined at various significant stages of the mission at the appropriate Sail temperature, cumulative solar radiation and cumulative simulated erosion and micrometeoroid puncture.
	
	Note: These properties affect the propulsive and thermal balance characteristics of the Sail. Prelaunch handling, deployment and the space environment affect the surface of the Sail. Include Sail sheet, seams and ripstops in test samples. Optical properties are required.

the deployed Sail, if allowed to relax, would take on
an irregular shape, because of the following factors:

(a) Effect of internal stresses present in the coated
film material before Sail fabrication.

(b) Effect of stresses introduced by Sail fabrica-
tion processes.

(c) Creasing (permanent set) introduced during
packaging, shipping, and storing.

(d) Effect of stresses introduced during
deployment.

(e) Shrinkage as a function of time and exposure.

(f) Differential thermal expansion while deployed.

It was further presumed that, if the deployed Sail were simply restrained without actual tension, the billowing pressure of the solar flux would be insufficient to remove undesirable contour irregularities, either micro- or macroscopically. In short, it would seem necessary to operate the Sail under slight tension to insure the required surface contour and smoothness. This was not a simple requirement.

If the Sail were pre-tensioned in a structural support of fixed dimensions, the tension will tend to be relieved by the creep of the Sail material. The inherent shrinkage tendency would seem to provide a counteracting effect, however, it is doubted (from past experience) that this effect will be useful. It was apparent that some mechanical means would be required to maintain tension automatically or retension from time to time.

Analysis of this problem would depend upon testing to determine the pertinent structural characteristics of the Sail material as a function of the space environment.

(2) Differential Shrinkage

Assuming the Sail film material is supplied in bolts, wound under, some nominal tension, there will be relaxation/shrinkage if this tension is relaxed during Sail fabrication. At the time when two Sail sections are joined, they should have identical potentials for subsequent relaxation (short and long term), to avoid puckering and distortion of Sail shape.

(3) Overstressing

The inherent fragility of the ultrathin Sail material calls for innovative processes for Sail manufacturing and handling. Tension must not be allowed to exceed the yield point at any time, as this would cause thinning and result in distortion of thermal balance.

Also, the optical and electrical integrity of Sail coatings will be affected by stretching. Tests were required to establish a maximum allowable tensile load or stretch. Also required would be a means of verifying that this load limit was not exceeded during fabrication or handling.

(4) Puncturing/Cutting/Tearing

The Sail film material is highly susceptible to rupture from sharp instruments, corners, snags, foreign particles, etc. Positive quality control measures must be applied to eliminate such hazards from the fabrication and packaging environments and to verify physical integrity of the finished Sail.

(5) Cleanliness

During Sail fabrication, the material will be fully exposed to the ambient atmosphere, including any particulents that are present in the form of dust, smoke, and volatiles. There will be a tendency for these contaminants to deposit on the material surface. The problem may be aggravated by electrostatic forces. An evaluation is required to determine the air filtering requirements for the fabrication area.

A general criterion for all of the fabrication planning should be to avoid having to clean the Sail surfaces, as this would lead to another set of problems including explosion safety, health hazards, and Sail surface deterioration. All lubrication systems in the Sail assembly area must be non-contaminating.

(6) Electrostatic Charging

(a) Safety. Fabrication and packaging of the Sail presents a problem in industrial electrostatic charge control. Classical safety considerations would dictate that the entire fabrication area be free of flammable dust and vapors, regardless of measures taken to dissipate charge cumulations. It would be desirable for the techniques used in splicing, reinforcement and mending to comply with the above rule. Flammable solvents should be avoided.

(b) Forces. Aside from safety considerations, electrostatic forces acting on the bare Sail material would tend to make it unmanageable during fabrication, packaging, and deployment. Also, the Sail would be contaminated by the attraction of airborne particles.

(c) Breakdown. There is the possibility of potential electrical breakdown through the Sail material, with unknown long-term effects, possibly from repeated breakdown along pre-established paths.

(d) Remedies. It is not clear that conventional industrial static eliminators are the answer to this problem. The opportunity for reaccumulation throughout the fabrication and packaging processes appears formidable. One helpful measure would be to maintain high relative humidity, but this conflicts with the requirement for minimizing surface chemical degradation. The best solution is to make both surfaces of the Sail "conductive" via coatings. Then simple provisions can be made to avoid charge cumulation. In connection with this approach, it is essential to measure the reduction of conductivity caused by creasing and crumpling of candidate coatings.

(7) Fabricability/Reproducibility

(a) The Sail design will impose dimensional tolerances to assure that the fabricated Sail will fit the interfacing structure. Therefore, answers are needed to the following questions:

1. What Sail dimensional deviations can be expected with a given material and fabrication process?

2. Can the interface design accommodate the
    foregoing deviations, or will it be necessary
    to trim the Sail to size after (or during)
    fabrication?

3. How will the problem of Sail thermal
    expansion/contraction be handled with
    respect to: (1) Sail acceptance inspection?
    (2) Sail deployment?

(b) The huge size and fragility of the Sail pose unpre-
cedented fabrication problems, hence, fabrication
concepts should be viewed as tentative and initial
fabrication efforts as experimental. A crucial
failure mode associated with Sail manufacture is
failure to detect and reject a defective product.
Another serious failure is a fabrication defect
that cannot be repaired. It is submitted,
therefore, that prime attention should be given
to the following items when evaluating Sail fab-
rication concepts:

(1) Plans for in-process quality control and end-
 product verification and (2), potential manu-
 facturing defects and associated repair processes.

(8) Blocking

Assuming that the Sail is packaged in a tightly compressed
configuration, either folded or rolled, it is important to account for
any adhesive effects which accompany unfurling. Such effects may be a
function of storage time, initial compaction, or vacuum degassing.
They may also be different for unfurling in vacuum than in air, and may
depend upon the rate of unfurling and angle of pull. Blocking is also
discussed in the section on Joining and Handling where a test is pro-
posed to determine these characteristics.

(9) Ascent Temperature Profile

The ascent temperature profile may not pose a threat to the
Sail. Routine analysis will cover the purely temperature aspects.

However, secondary effects to be evaluated include (1) freezing of condensed moisture, (2) congealing of lubricants, and (3) binding caused by differential expansion/contraction. Any of these could cause deployment failure.

(10) Ascent Pressure Profile

The Sail is assumed to be stowed in a compact configuration, either folded or rolled. The latter is the proposed method for the Heliogyro. It is uncertain how much air or other gas will be trapped between layers or in the bonded joints during the stowing process. During ascent to space vacuum, any trapped gas will tend to expand, with possible damage to the Sail and/or the Sail container.

Therefore, it will be necessary to devise a test to simulate the reaction of the stowed Sail when exposed to vacuum. A vacuum expansion test should also be made on samples of all bonded joints. Note that the container vents must be designed so as not to be obstructed by possible expansion of the Sail package.

If a problem is found, one solution might be to vacuum degass the complete Sail. This could be done as a conditioning operation to remove as much air as possible or as a quality assurange check to verify compatibility with the stowage container, or for both reasons. Small perforations in the Sail sheet at predetermined intervals might also be considered as a means for minimizing the potential of this problem.

(11) Coating Susceptibility

Analysis of Sail performance requires that working limits be established for the values of optical and thermal properties of the Sail material. This is made difficult by various adverse environments which work to alter the initial values. For the period from Sail fabrication through deployment, the most critical environments are those which threaten the surface coating characteristics, as follows.

CRITICAL ENVIRONMENTS	POTENTIAL DAMAGE TO COATING
(a) Exposure during fabrication to ambient air at normal levels of contamination and humidity.	Oxidation, other chemical reactions.
(b) Fabrication, handling and packing, including exposure to tools, fixtures, containers, chemical processes, heat processes, foreign matter.	Puncturing, cutting, tearing, stretching, creasing, wrinkling, cracking, sloughing, abrasion, overheating, chemical reaction.
(c) Transportation and storage, including jolting and vibration in folded condition. Also, breathing caused by diurnal temperature changes, constricted ventilation because of tightly-packed and/or contained condition.	Abrasion, moisture condensation, fungus growth, accelerated chemical reactions, sticking or blocking.

CRITICAL ENVIRONMENTS	POTENTIAL DAMAGE TO COATING
(d) Deployment, including tensile and peeling loads associated with unfolding layered stack, and contact with structure.	Abrasion, stretching, cracking, debonding, tearing

Unless more is known about the ability of the Sail material to withstand these environments, it will be necessary to take extreme control measures and then to assume that degradation has been precluded or limited to some arbitrary level. This approach tends to be expensive on the one hand and to lack credibility on the other. Appropriate tests would provide indications of the levels of protection required to keep the Sail optical-thermal parameters within prescribed limits.

It was proposed that tests be conducted on the coated Sail material to determine changes in optical-thermal properties as a function of various treatments, as follows:

1. Stretching-relaxation, uni- and bi-axial.

   One-shot samples, load increased incrementally.

2. Creasing-flattening.

   Samples with different crease spacings and representative compactions.

3. Random crumpling - flattening.

   Test with various degrees of compaction and repetition.

4. Abrasion.

   Test to simulate fabrication processes and transportation vibration.

5.   Atmospheric exposure.

     Samples in controlled S.L. atmospheres at different
     temperatures and humidities. Test at intervals over an
     extended period.

6.   "Blocking" effects.

     Samples folded and pressed together to simulate bottom
     layers of stored Sail. Test after an extended period
     in storage environment. Measure sticking tendency as
     well as optical-thermal changes.

4.4.1.2   Failure Preventive Action Integration. After a potential
failure mode had been identified, evaluated, and found to require pre-
ventive action, there was the task of integrating the requirement into
the Sail fabrication program. Such action may involve any or all phases
of the fabrication program. To stress the possible number of places
where preventive action might be appropriate, a hypothetical fabrication
program outline was developed which was useful as a checklist or as
the basis for a matrix to insure complete integration of preventive
actions. This hypothetical outline included: design criteria and
requirements; engineering drawings and specifications; design verifica-
tion requirements; manufacturing, including procurement, production
planning and control and quality control; and operations.

4.4.1.3   Space Failure Modes Analysis. The first step in analysing
space failure modes was to develop a generalized fault tree.
(Figure 4-23). This provided a picture of the interrelationships
between failure causes and effects. Failures that include "upset
thermal balance" as an effect, appear most significant as they boot-
strap through the system causing further performance degradation.

     A failure interaction matrix was developed.   Figure 4-24
is a reduction of the large working chart where approximately 200 items
were compared one against the other to record that: 1) a failure mode
definitely exists, 2) a failure mode possibly exists, 3) a failure mode
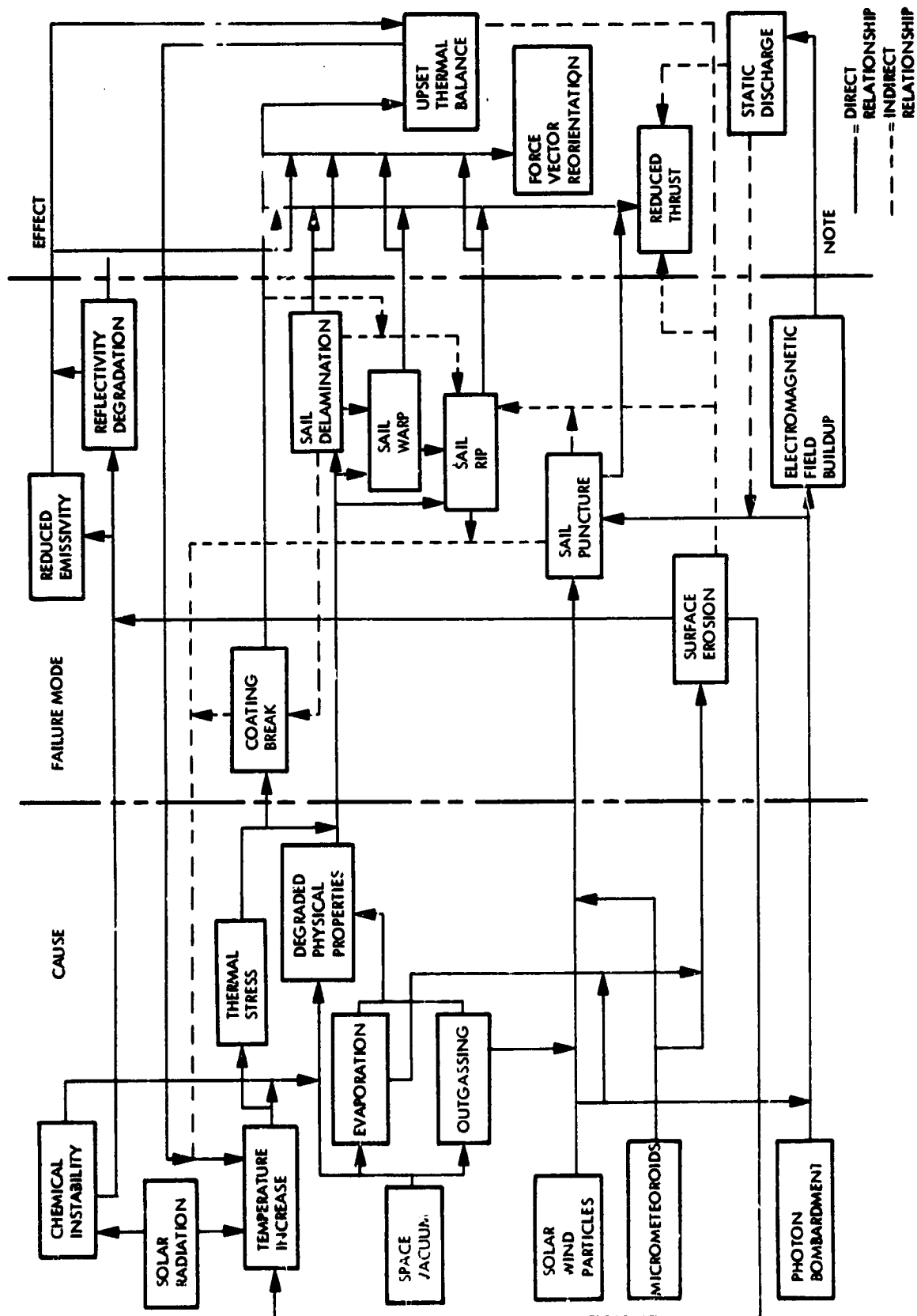does exist. Arithmetical summaries were made of the in-space failure

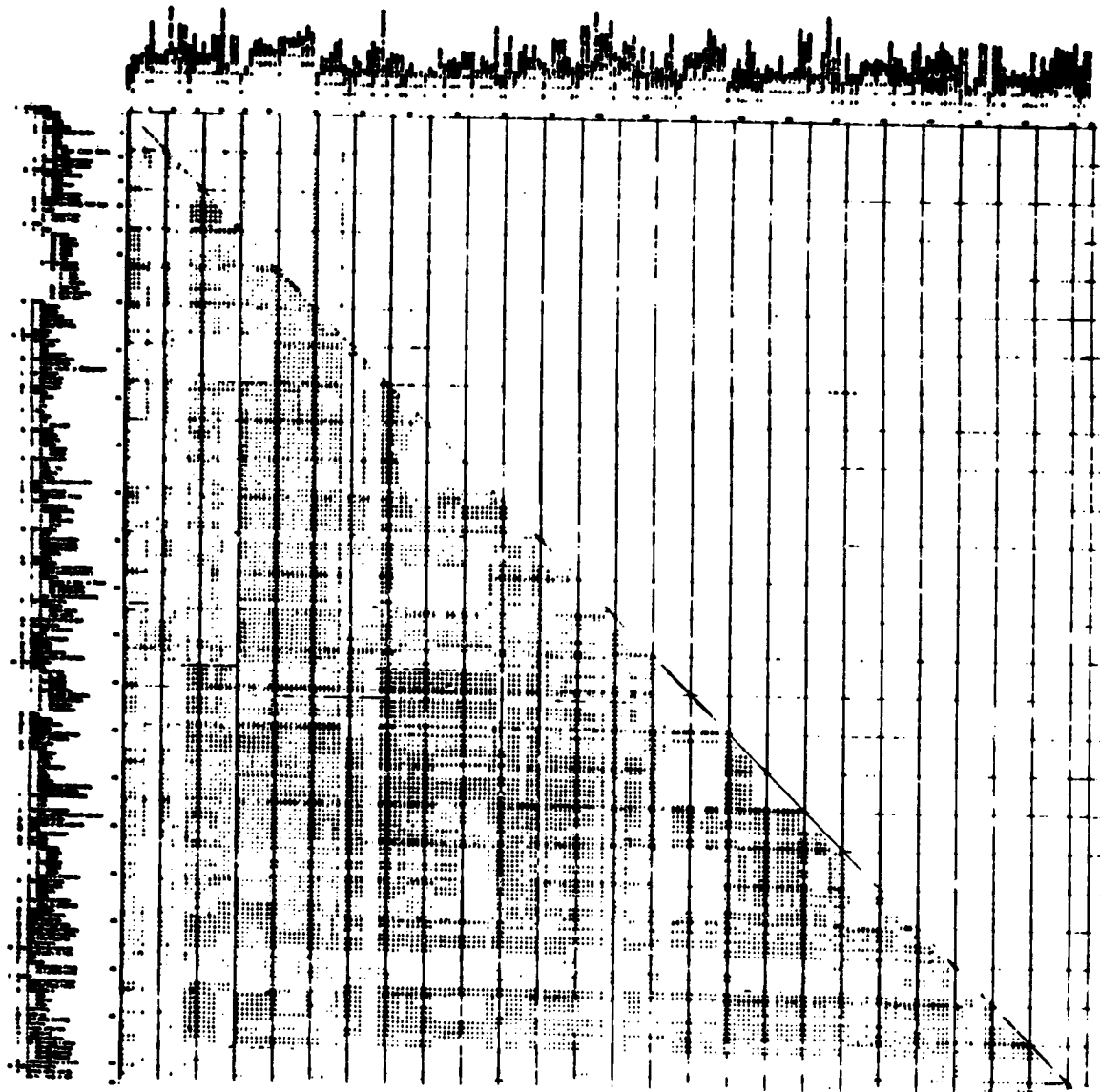Figure 4-23. Generalized Fault Tree Solar Sail Sheet Space Failure Modes

Figure 4-24. Failure Interactions Work Sheet

interaction matrix. It is significant that "synergistic" interactions ranked first in a summary of items of positive and probable failure interactions. An individual Sail property may be satisfactory at a given environmental condition; however, mission success requires all properties to be satisfactory over the accumulative mission history. The Sail will experience an accumulation of solar radiation, erosion and cyclic loading. In addition, wrinkling, solar dust coating, creep, and possible warping from static charge will affect Sail shape and influence propulsive efficiency and thermal balance. Physical property tests, electro-static property tests and optical characteristics tests as depicted in Table 4-23 should be made at various significant stages of the mission at vacuum ambient pressure and with the appropriate Sail temperature and cumulative solar radiation.

The arithmetical summary was exercised to develop a failure interaction "order of significance" of primary subjects. A tabulation of the ranked order of significance in the categories; components, characteristics, environment, and failure interaction frequency is given in Table 4-24.

A correlation was then begun of the high probability failure interaction modes with test data requirements to identify significant characteristics. Plans were to obtain the necessary test data and then perform analyses to demonstrate that the Sail design could accommodate the suspected failure modes and accomplish the mission.

The aforementioned correlation was performed, resulting in several pages of tables giving a review of the high probability failure modes and interactions with assignments to various technical specialty groups such as materials, structures and dynamics, attitude control and mission design, to perform either tests and analyses to verify the Sail design. These are included in Appendix II.

Table 4-24. Failure Interactions Order of Significance

Sail Sheet Material Failure Interactions

Components Order of Significance

1. Film
2. Bonds
3. Rip Stops
4. Reflective Surface

Characteristics Order of Significance

1. Contaminants	14. Substrate Bonds
2. Mat'l. Specs.	15. Foldability
3. Aging	16. Polymer Orientation
4. Life-Time Prediction	17. Pin Holes
5. Temp. Characteristics	18. Electrical
6. Processing Specs.	19. Ionization of Sail Mat'l.
7. Tolerances	20. Resistance to U.V.
8. Thermal Expansion	21. Optical
9. Strength	22. Coating Interactions
10. Uniformity	23. Pigmentation
11. Bend Radius	24. Reproducibility
12. Attractive Forces	25. Mass
13. Coating Thickness	

Environment Order of Significance

●1. Thermal	●11. Trajectory
o2. Sail Loading	x12. Launch Loads
o3. Shape	o13. Center of Pressure
o4. Reefing	o14. Vibrations
●5. Space Vacuum	●15. X-Ray
●6. Electrical Charge	o16. Solar Wind
o7. Reorientation	●17. Micrometeoroids
●8. Occultations	●18. Cosine Angle (Sun)
o9. RCS Dynamics	x19. Condensation on Surfaces
●10. Photons	x20. Human Handling

Table 4-24. Failure Interactions Order of Significance (Continuation 1)

Environment Order of Significance (Cont.)

NOTE

● = space environment

o = space loads environment

x = latent ground & launch environment

Failure Interaction Frequency

1.	Puncture	6.	Surface Erosion
2.	Coating Failure Leading to Base Failure	7.	Crosslinking
3.	Debonding	8.	Depolymerization
4.	Cratering	9.	Desorption
5.	Dust (Solar Coating)		

4.4.2   Long-Term Service Projections from Predictive Tests and Analyses

4.4.2.1   Evaluation Methodology. The properties of materials in general, and polymers in particular are manifestations of their chemical state and morphological states. The chemical state and morphological state may change as a result of aging and the changes will be reflected changes in properties. Thus, the rates of chemical changes and morphological changes provide the basic guidelines for service life prediction, even though the correlation between structures and properties may not be linear.

As a result, the properties of the materials may show systematic deterioration. Since it is essential that the selected materials and the fabricated Sail have a very small rate of performance degradation in space to assure mission success, an effort was directed towards analyzing available test data of the Solar Sail materials. This data had been published in the literature or generated from the test programs performed specifically for the film, coatings, or bond joints that were conducted to evaluate service life in the anticipated space environment.

The Solar Sail materials may degrade as they are exposed to various individual and combined stresses such as:

(1)   Thermal

(2)   Mechanical

(3)   Environmental, ---e.g., UV, ionizing radiation, contamination.

Most of the parametric tests that were conducted were made to enable performance characterization rather than long-term prediction. Thus, in this portion of the Sail performance evaluation, predictive models were formulated based on chemical-physical theories. The predictive models also provide a basis for accelerated test program design. The plan was to check the validity of the model through comparison with actual test results and subsequent modification where appropriate. The verified models were then to be used as a basis for materials evaluation and selection.

Chemical degradation rate served as the basis for service life prediction and for formulation of predictive models for the basic film. For Kapton and other high temperature polymers selected as the most viable candidates, information about morphological changes is almost nonexistent and as a result these effects on the service life were not taken into account. Formation of paracrystalline structure accompanying improved tensile strength has been reported for polyimide annealed at temperature ranges of $150-400°C$[1,2]. Therefore, it is expected that morphological changes of the basic film caused by thermal annealing in space may improve the mechanical properties. The morphological changes may cause slight changes of the Sail dimensions but these can be easily accommodated by minor design modification such as the use of springs between tendon and Sail sheet on the blade panels of the Heliogyro.

The adhesive joint service life prediction requires quantitative knowledge of aging, of interfacial chemistry, and viscoelastic

properties of the adhesive as well as changes in the fracture mechanics of the adhesive joint caused by aging[3]. Since this quantative aging information was not available, a predictive model was adopted for the predictive testing design. This model has been shown to give reasonably good life prediction for five structural adhesives[4].

Initially, only the effects of thermal stress and high vacuum on aging were considered in preparing the models. Since the estimated stress level of the Sail is only 3000 psi during handling and considerably less ($\sim$0.5 psi) during flight, the effect of stress on aging is expected to be negligible. UV and ionizing particles are detrimental to the bare polymer films but these effects are negated through proper adjustment of the metal coating thicknesses.

4.4.2.2   Basic Film Predictions.

(1)   Thermal Degradation of Kapton

Polypyromellitimide (Kapton) will be thermally degraded at elevated temperature. Different reaction mechanisms accompanying different degradation rates will occur at various temperature ranges. Pyrolytic studies[5] and mass-spectrometric studies[6,7] of the thermal degradation of Kapton in vacuum and in inert gas (helium and nitrogen) environment have concluded that the major mechanisms are:

> (a)   Hydrolysis of amide groups (due to incomplete cyclization),
>
> (b)   Decomposition of isoimide groups, and
>
> (c)   Decomposition of imide groups

Activation energies and frequency factors for the reactions are summarized in Table 4-25 and Table 4-26 presents the proposed degradation mechanisms. The extent of degradation of Kapton due to the latter two mechanisms at 250°C, in two years, will be negligible and only the hydrolytic breakdown will cause severe degradation of Kapton. However, the hydrolytic degradation may be reduced by heating Kapton film at elevated temperature in inert gas or under vacuum to remove the absorbed water and to maximize imidization of the uncyclized amide units.

Table 4-25. Thermal Degradation of Kapton H-Film

Chemical Degradation	Frequency Factor (sec. $^{-1}$)	Activation Energy (kcal/mole)	Reference
Thermal Breakdown of imide groups in Kapton under vacuum (400-822°C)	$10^{15.9}$	69.3	5
Thermal Breakdown of isoimide groups in Kapton under vacuum (below 500°C)	10^{11}	47.9	5
Thermal Degradation of Kapton H-Film in nitrogen (426-510°C)	-	62±9	6
Hydrolysis of Amide Group at 150-160°C	-	10-20	7

The cyclization is very slow at temperatures below 150°C. At higher temperature, the cyclization is characterized by an initial rapid reaction followed by a slower cyclization process[8]. It has been reported that heating Kapton film at 250°C under high vacuum for one hour resulted in almost complete cyclization[7]. Thus, by preheating the Kapton film at temperatures in the range of 300 to 350°C under vacuum for a few minutes, may stabilize the film to the extent that thermal degradation at 250°C for two years is negligible.

The degradation reactions appear to be the first-order reactions[5-7]. Consequently the degradation kinetic equation may be expressed as[9].

$$\frac{dWi}{dt} = A_i e^{-\Delta H_i/RT} Wi \qquad (1)$$

where Wi = weight fraction of species i, Ai = frequency factor, ΔH_i = activation energy, R = gas constant and T = absolute temperature. From equation 1 one obtains

$$\frac{Wi(t)}{Wi(o)} = e^{-t/\tau_i} \qquad (2)$$

Table 4-26.   Proposed Degradation Mechanisms

(a) MECHANISM OF THERMAL DEGRADATION OF IMIDE GROUPS IN H-FILM
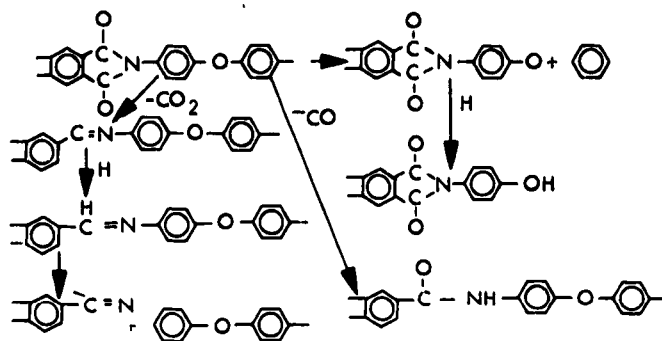
(b) THERMAL DEGRADATION OF ISOIMIDE IN H-FILM.
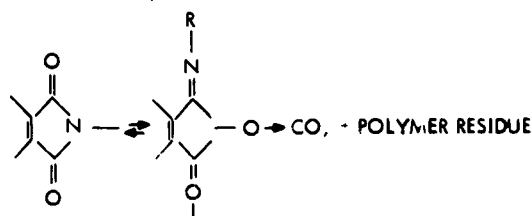
and

$$W(t) = \sum W_i(t) = \sum W_i(o) e^{-t/\tau_i} \qquad (3)$$

where

$$\tau_i = \frac{1}{A_i} e^{\Delta H_i / RT} \qquad (4)$$

$W_i(o)$ and $W_i(t)$ are the initial weight fraction of i species at time zero and time t respectively. W(t) is the weight fraction of the sample at time t. Equation 3 resembles the equations used to represent the viscoelastic properties of polymers and, consequently, time-temperature superposition should also be applicable in this case.

Figure 4-25 shows the superimposed curve using the isothermal weight loss data of Kapton reported by Heacock and Beer[9]; $520^{\circ}C$ was chosen as reference temperature. The shift factor (a) follows the Arrhenius equation and gives an activation energy of 57.6 Kcal/mole, as shown in Figure 4-26, which is between the activation energy of isoimide decomposition and that of imide decomposition (see Table 4-25). This is probably due to the fact that, although decomposition of imide groups is the dominating mechanism at this temperature range, decomposition of isoimide still makes some contribution to the isothermal weight loss and thus the activation energy obtained is in between.

Using the time-temperature superposition principle one could estimate the amount of weight loss at $250^{\circ}C$ in two years from the data in Figure 4-25. The amount is nearly zero.

NASA-Ames Research Center reported an activation energy of 49 - 50 kcal/mole of thermal degradation of Kapton in vacuum at 300-$400^{\circ}C$ temperature range from measurements of the optical density of the film at $6000\overset{\circ}{A}$ wavelength[10]. Judging from the magnitude of the activation energy and the temperature range of decomposition, it appears likely that this is due to the decomposition of isoimide groups.

Tests carried out at JPL reported substantial weight loss of Kapton (0.049% in 4 hours at $250^{\circ}C$ and 0.27% in 18 hours at $300^{\circ}C$[11]. This probably is due to the fact that these samples had not been given sufficient heat treatment (annealing) to remove the trapped H_2O, CO_2 and solvent or other organic compounds. Also as mentioned earlier, annealing tends to make imidization more complete and thus eliminates the weak sites for possible decomposition, e.g. hydrolysis, to occur at low temperature.

Based on these analyses, Kapton appears to have the thermal stability required for the Solar Sail mission. However, a thermal annealing treatment of the Kapton film prior to Sail fabrication may be necessary to prevent hydrolytic breakdown.
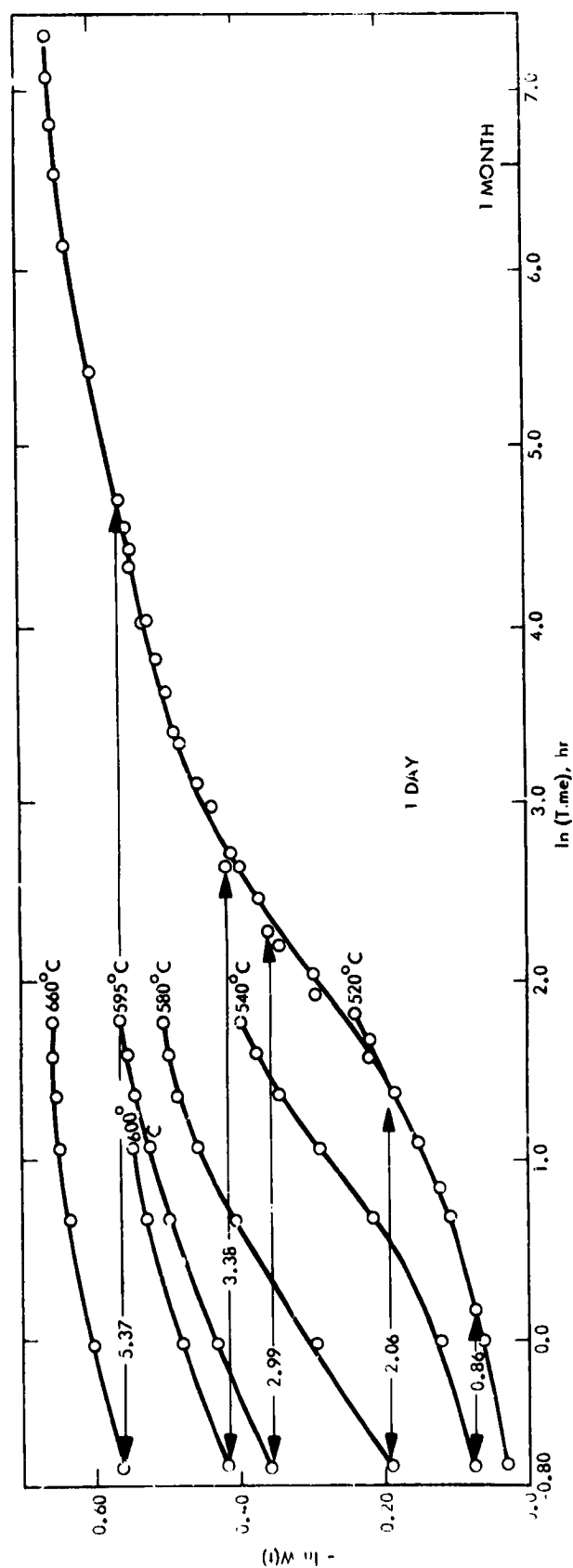
Figure 4-25. Isothermal Weight Loss of Kapton versus Time
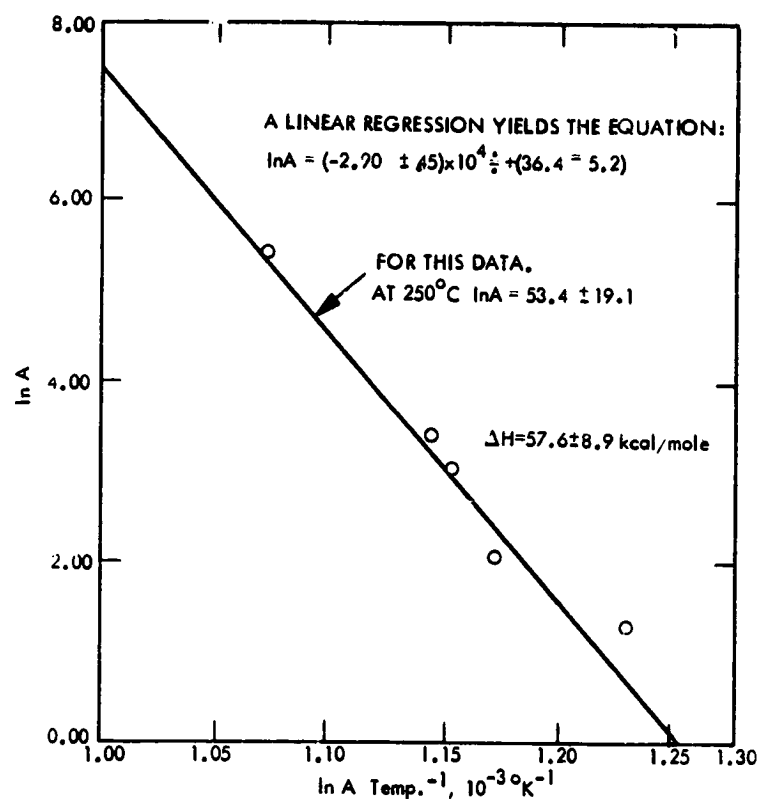
Figure 4-26. Graph of the Shift Factor lnA, vs. Temp^{-1}

(2)   Effects of Thermal Aging on Mechanical Properties of
       Kapton

Deterioration of mechanical properties as a consequence of
thermal aging can be represented by the Arrhenius equation, as shown
in Figure 4-27a and 4-27b[12]. The kinetic parameters of deterioration
are summarized in Table 4-26[12-13]. One may note that the activation
energy for samples with thermal treatment before aging is between those
of imide breakdown and isoimide decomposition and close to that from
isothermal weight loss measurement, while for samples without the heat
treatment the activation energy[13] is very close to that reported for
hydrolysis of amide groups[7]. This seems to indicate a close correla-
tion between chemical degradation and mechanical properties deteriora-
tion. Using the kinetic data presented in Table 4-26, the tensile
strength and the ultimate elongation of Kapton aged at 250°C are calcu-
lated as a function of aging time, as shown in Figures 4-28, 4-29 and
4-30.

Figure 4-27a. Effect of aging in air at 300°C on the physical pro-
perties of H-film. Linear relationships are apparent
for each property.
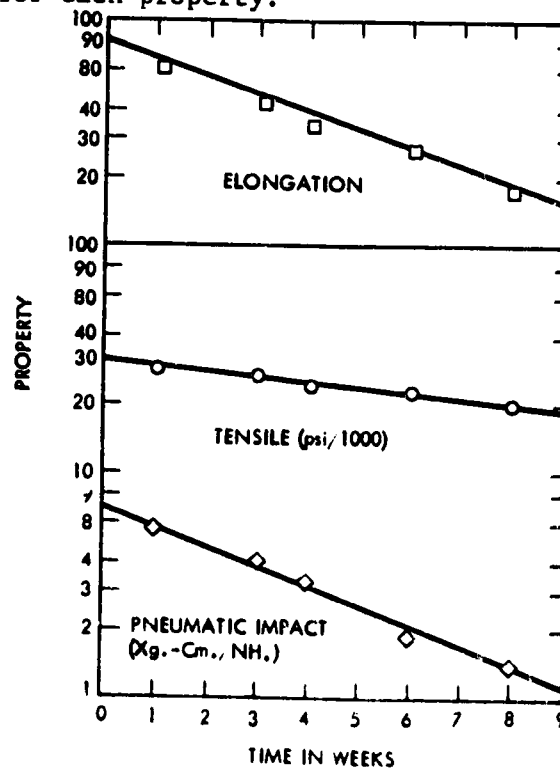
Figure 4-27b. Arrhenius plot of physical property deterioration.
Again a linear relationship is obtained.

Table 4-26. Property Deterioration Rate Parameters In Helium

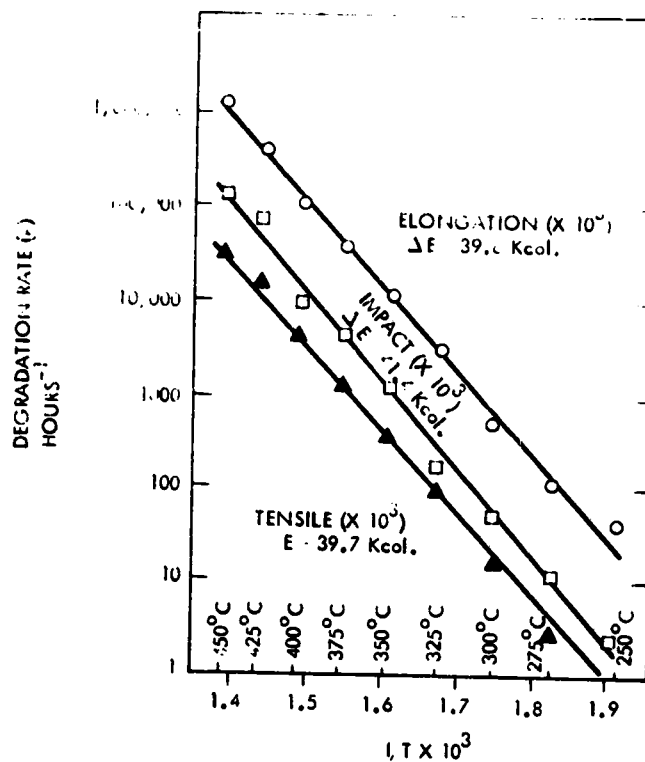| Property	P_o	ΔE K_{cal}	K_{100} $1/hr$
A) Sample Outgassed at Elevated Temperature Before Aging			
Elongation (%)	70	55.4 ± 1.7	0.0050
Impact Strength (kg-cm/mil)	6	51.1 ± 2.7	0.0029
Tensile (psi/1000)	23	55.5 ± 1.3	0.0019
B) Sample Not Outgassed Before Aging			
Tensile Strength and Elongation	--	17 ± 4	--

From these results, one may conclude that at 250°C in two years, Kapton will not have detectable deterioration of its mechanical properties, a conclusion in agreement with chemical degradation results.

(3) Creep, Thermal Expansion Coefficient and Thermal Shrinkage of Kapton

It appears that morphological changes of Kapton due to thermal aging may be the factors which will affect long term creep, thermal expansion and thermal shrinkage (shrinkage occurs at constant temperature), because chemical degradation is expected to be negligible. Data on rate of morphological changes of Kapton are not available presently. However, the morphology of the Sail film materials may be stabilized by proper thermal treatment.

Long term creep of Kapton H film under a load of 10 psi at 250°C was calculated from stress relaxation data reported by Shen et. al.[14], and is shown in Figure 4-31. The approximate equation proposed by Leaderman[15].

$$D(t) = (\sin m\pi)/m\pi\ E(t) \tag{5}$$

$$m = \frac{d \log E(t)}{d \log t} \tag{6}$$

$$(t) = {}_o D(t) \tag{7}$$
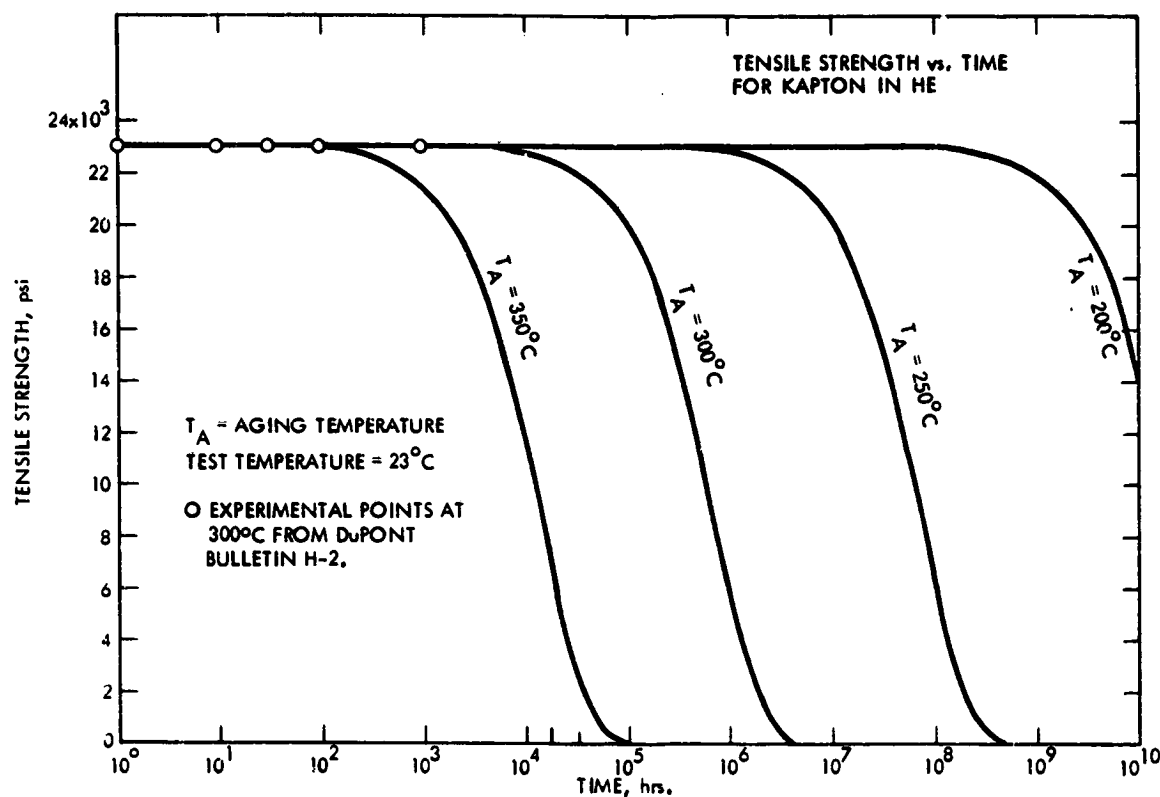
Figure 4-28. Tensile Strength vs. Time for Kapton in He

was used for the calculation, where $D(t)$ = tensile creep compliance,
$E(t)$ = relaxation modulus, σ_o = applied stress and $\epsilon(t)$ creep. The
experimental data, which were measured under a load of 50 to 200 psi,
were converted to 10 psi. The experimental data, after the conversions,
were further multiplied by a factor of 4.3 to take into account the
fact that the Young's Modulus reported in reference 16 is higher than
that reported in reference 14 by a factor of 4.3.

The samples were annealed at 300°C for a week in high
vacuum prior to the experiment. Agreement of the experimental data and
the calculated values is reasonably good. The large scatter of the
experimental data is believed due to thermal fluctuation of the sample
chamber and ground vibration.
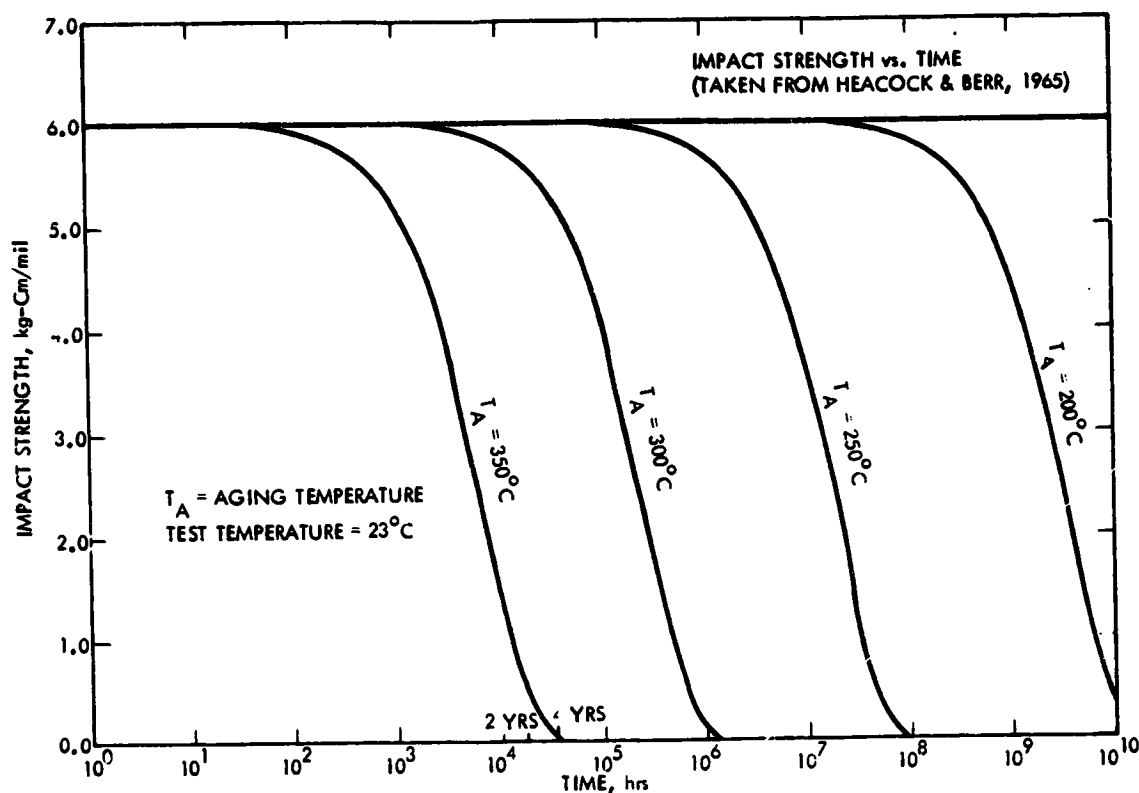
Figure 4-29.   Impact Strength vs. Time for Kapton in He

To check the predicted creep at times inaccessible to experiments at 250°C, creep measurements at higher temperature were performed.   Figure 4-32 presents predicted creep at various temperatures and experimental values at 300°C and 45°C.   Again, agreement is fairly good.

Table 4-27 summarizes the dimensional change of basic film due to creep, thermal expansion and thermal shrinkage.   Long term thermal shrinkage of Kapton is not known.   The creep is calculated with an assumed load of 50 psi, which was the estimated maximum load on the square Sail configuration.   The actual load during the cranking orbit was estimated to be even less.
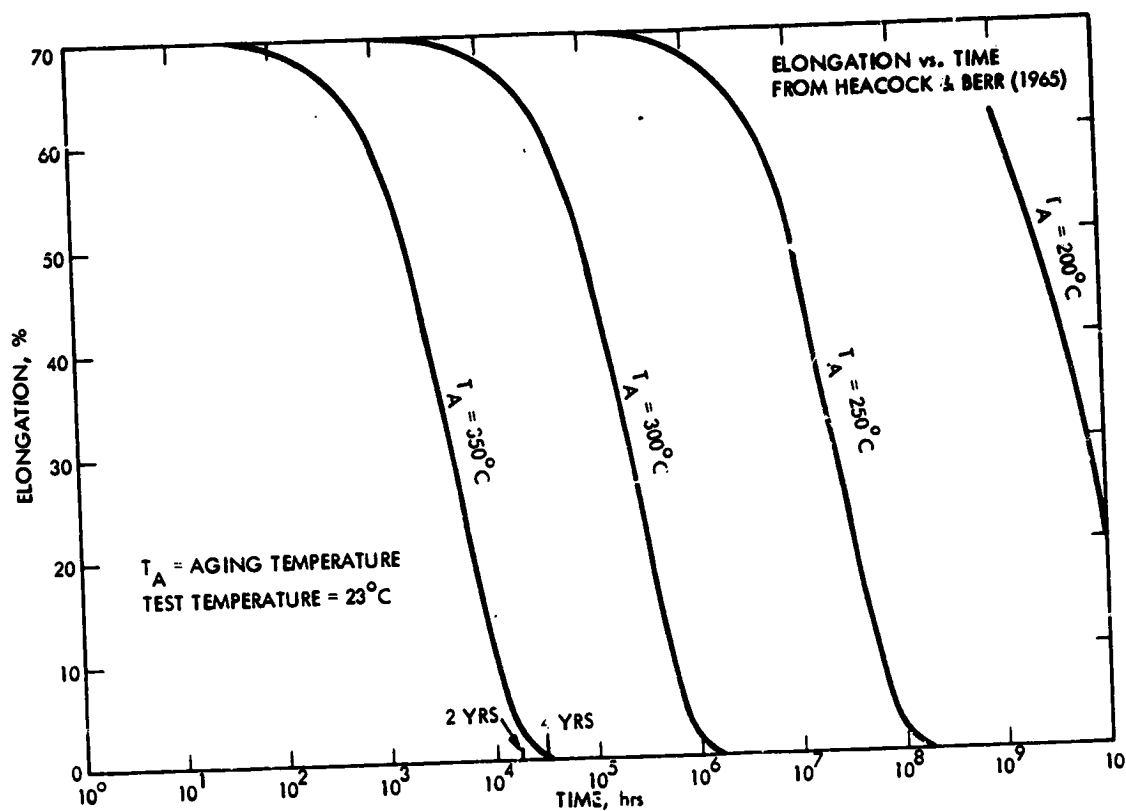
Figure 4-30. Elongation vs. Time for Kapton in He
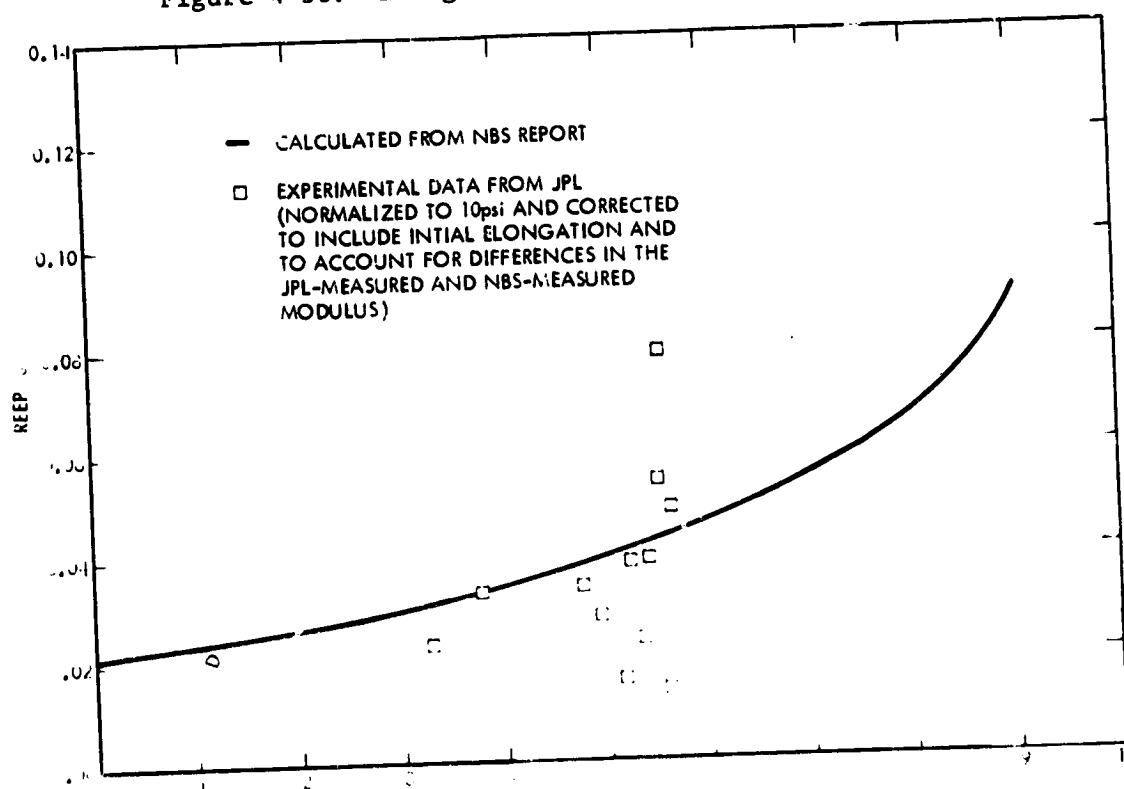
Figure 4-31. Extrapolation of Creep vs Time for Kapton at 250°C
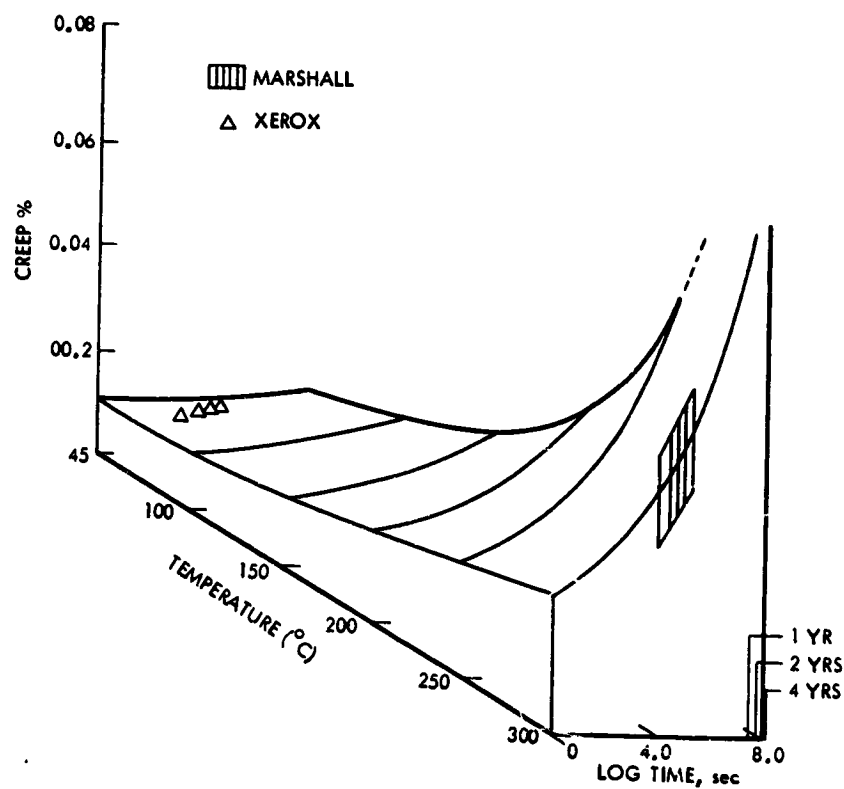
Figure 4-32. Predicted Creep of Kapton at Various Temperatures

Table 4-27. Dimensional Changes Due to Creep, Thermal
Expansion and Thermal Shrinkage

Creep @ 59 psi* at 250°C in two years.	Thermal Expansion (from -100° to 250°C)	Thermal Shrinkage (in N_2 at 264°C for three days)
3.3×10^{-3} in/in	1.02×10^{-2} in/in	-3.3×10^{-3} in/in**
	$(2.9 \times 10^{-5}$ oc$^{-1})$	

*calculated value
**S.D. Hong, Solar Sail Monthly Report, July 1977

(4) Tensile Strength of Kapton as a Function of Mission Time

From the discussion and data in the portion on the effects of thermal aging on the mechanical properties of Kapton, one may express the tensile strength of basic film during the mission as

$$\sigma = \sigma_o(T, t_o)e^{-Kt}{}_o \tag{8}$$

where $K = Ae^{-\Delta H/RT}$, and t_o = mission time. Since the temperature during the mission is estimated to be below 250°C, and the Sail is expected to be exposed to the high temperature for about two years, as shown by Figure 4-32, using the kinetic parameters in Table 4-26, one has

$$e^{-Kt}{}_o \approx 1 \tag{9}$$

So $\sigma = \sigma_o(T, t_o)$. The tensile strength may increase due to annealing. In general the tensile strength of glassy polymers is found to linearly depend on temperature, as shown in Figure 4-33. From Figures 4-32 and 4-33, the tensile strength of Kapton film as a function of mission was calculated, as shown in Figure 4-34. In calculating Figure 4-34, yield strength instead of breaking strength was used. The target requirement of 4000 psi and 50 psi were estimated values during ground handling and during cranking around the sun. One can see that the safety margin is about 160.

4.4.2.3 Adhesive Joint

(1) Model for Lifetime Prediction

The performance of adhesive joints is a complex function of bonding chemistry in the interface, viscoelastic properties of the adhesive and fracture mechanics of the adhesive joint. A detailed analysis of fracture mechanisms in an adhesive joint for lifetime prediction under some specified service conditions require quantitative knowledge of the relevant chemical, physical and mechanical factors previously cited. Since these detailed elements of quantitative knowledge are not available, a modified Prot model was used for proof testing.
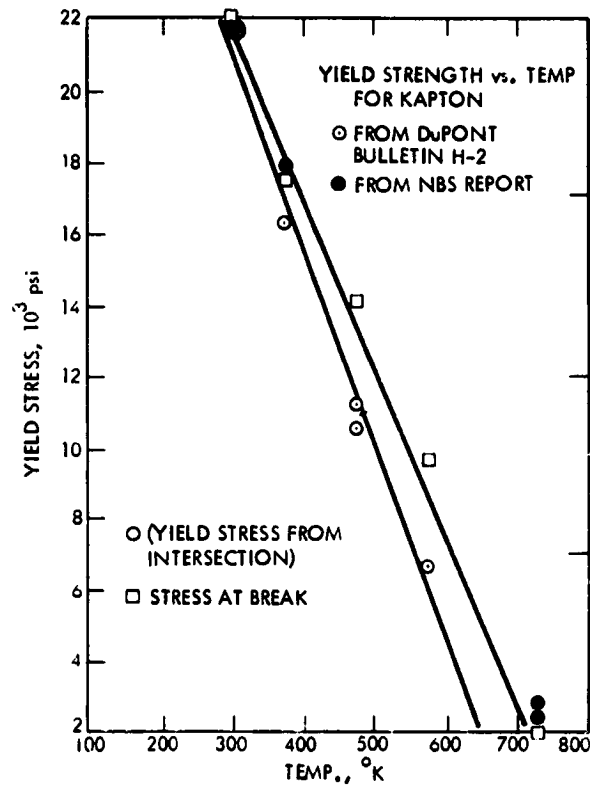
Figure 4-33. Yield Strength vs. Temperature for Kapton

According to this modified Prot accelerated test scheme,[17] the time to break, t_b, of a structural joint under stress, S_b, may be given by

$$t_b = \frac{K}{(S_b - 2EL)} \tag{10}$$

where

K = material constant

EL = endurance limit

S_b = applied shear stress
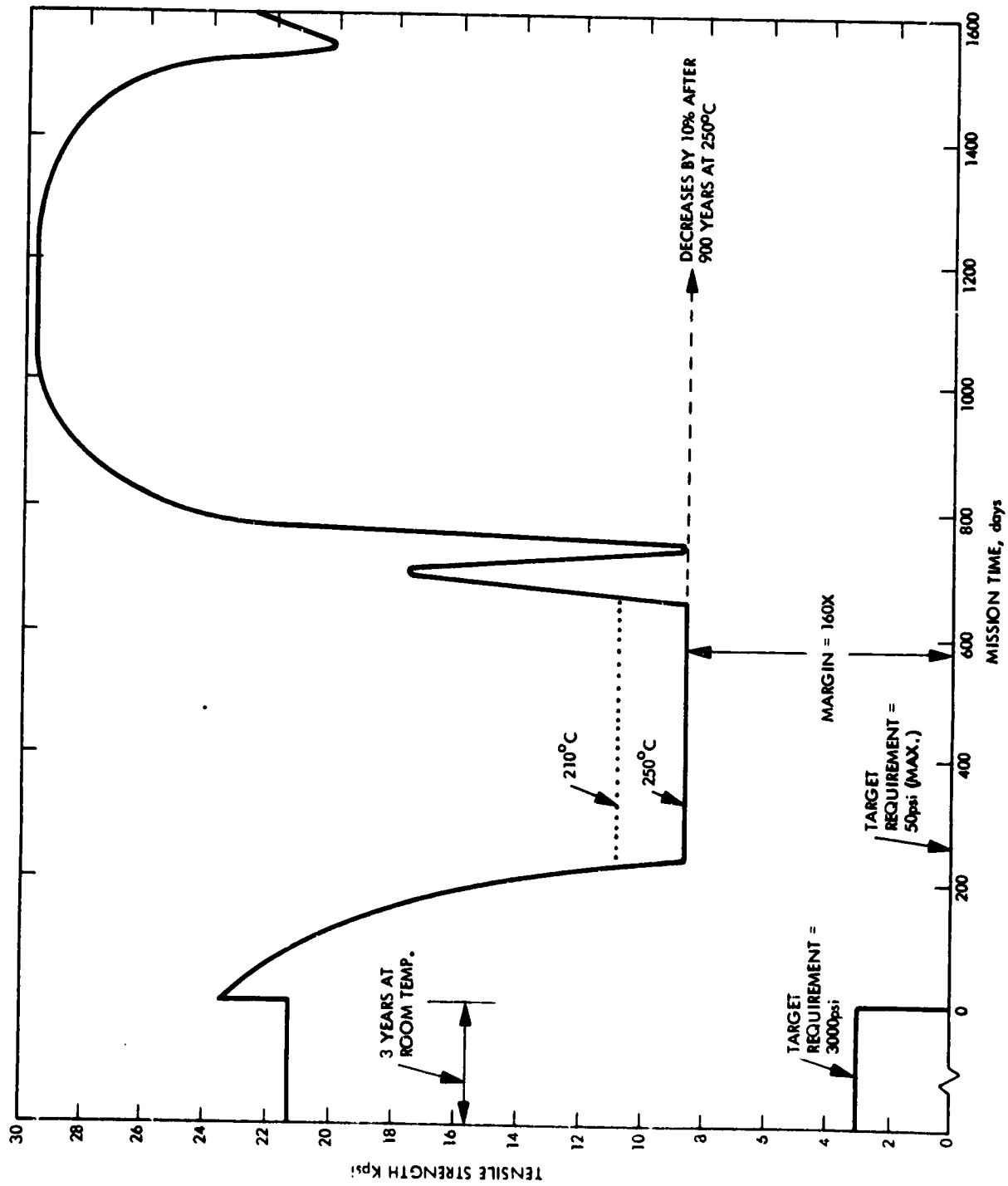
Figure 4-34. Sail Film Tensile Strength as a Function of Time During the HCRM

Recently, Lewis, Kinmonth, and Kreahling[4] applied the modi-
fied Prot model to test five types of structural adhesive joints
(adhesive on aluminum substrate). They found that, within statistical
scattering, the ratio of EL and lap shear strength (designated hereafter
as LSS) is a constant independent of temperature, geometry and modulus
of the bulk adhesive. Their results from long-term tests (up to 36,000
hours) have reasonably good agreement with the prediction from short-
term accelerated load tests. Thus, despite theoretical short-comings,
the method seems to be a reasonable model for predicting the lifetime of
an adhesive joint.

Because of time limitations, it was not possible to restruc-
ture the instrument to measure the endurance limit of the adhesive
joint. Thus, we will assume that the ratio of endurance limit and lap
shear strength (LSS) of the adhesive joint is the same value as recom-
mended by other investigators.

$$EL/LSS = 0.25 \qquad (11)$$

The value of this ratio may change as a result of aging of the adhesive
joint. This will have to be determined experimentally. However, we
will assume for the NR-150B2G adhesive joint, the one selected as the
"benchmark" design for the Solar Sail, that the ratio of endurance
limit and lap shear strength does not change due to aging. Combining
Eqs. 10 and 11, one obtains:

$$t_b = \frac{2K}{2S_b - LSS} \qquad (12)$$

Eq. 12 implies that, if the lap shear strength of adhesive joint (LSS),
remains higher than $2S_b$, the adhesive joint will never fail. The cri-
terion of LSS larger than $2S_b$ will be used as a measure of service life
of the adhesive joint.

(2) Analysis of Test Results

The predicted shear strength of adhesive joint as a func-
tion of mission time is shown in Figure 4-35. The prediction was
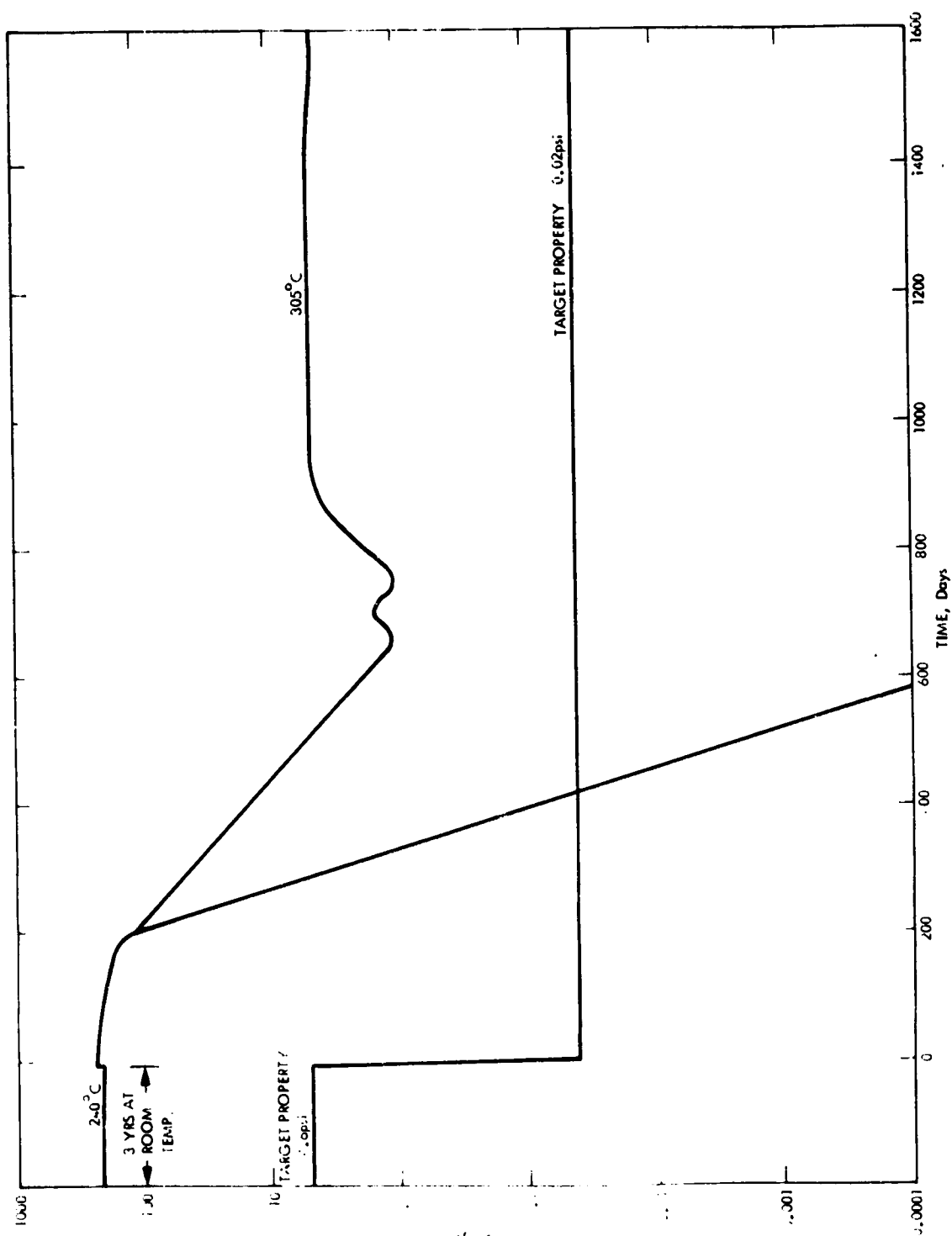
Figure 4-35. Predicted Shear Strength of Adhesive Joint vs. Time

calculated using the degradation rates of the accelerated aging tests presented in the section of this report on joining and handling with the following assumptions:

(a) No degradation occurs at temperatures below 220°C (there are no data available to assess degradation at lower temperature)

(b) Temperature dependence of the shear strength of an adhesive joint is linear.

(c) The degradation rate follows the Arrhenius equation.

The shear strength of the adhesive joint at temperatures other than 250°C and -60°C was obtained by interpolation. Because of the limited amount of test data available, there is great uncertainty in the magnitudes of the calculated degradation rates. Thus the predicted shear strength of the adhesive joint that is shown in Figure 4-35 should be considered to be tentative. The target properties represent $2S_b$ (see eq. 12), where S_b is estimated to be 3000 psi during ground handling and 10 psi during the cranking orbit.

Figure 4-36 shows the degradation rates for adhesive joints that were aged at 240, 270 and 305°C. It is apparent from this data that samples aged at the higher temperatures have the lower degradation rates. This is just the opposite to what one would expect for thermal degradation behavior.

The shear strength of the adhesive joint may be affected by:

(a) Chemical changes in the interface and in the bulk of the adhesive,

(b) Development of weak bond layer, and

(c) Transcrystalline structure in the interface.

Since no morphological studies were made of the interface for the polyimide, the effects of a weak bond layer and a transcrystalline structure on the long-term shear strength of the adhesive joint are not
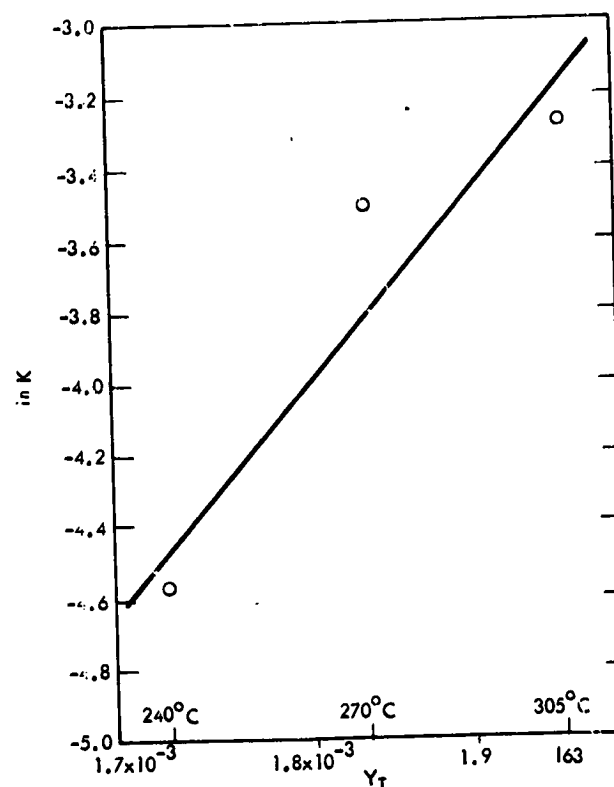
Figure 4-36. Adhesive Joint Degradation
Rates at Three Temperatures

certain. On the other hand, the chemical characteristics of the inter-
face may be affected by the presence of solvents and the degree or
extent of curing. It is generally well known that strong solvents can
deteriorate interfacial bonding while extended post curing enhances
bonding. It is speculated that the apparent abnormal degradation
behavior observed for the aged adhesive joints may be attributed to
the combined effects of curing, degradation and the presence of the
solvent N-methylpyrolidone in the interface. The boiling point of
n-methylpyrolidone is 202°C. When it is mixed with NR150-B2G adhesive,
the boiling point is expected to be higher than 202°C (probably close
to or even higher than 240°C). Consequently, the amount of solvent left
in the adhesive (and the interface) will be increased for samples aged
at lower temperatures. Furthermore, the samples aged at the higher
temperatures probably received better curing in the relatively short
aging period. This may explain the lower degradation rate for the
samples aged at the hi   er temperatures.

REFERENCES

1. E. Sacher and D.G. Sedor, J. Polym. Sci., Polymer Physics Ed., 12, 629, (1974).

2. K.N. Vlasova, M.L. Dohrokhtova, L.N. Suvorova and I.N. Emelyanov, Soviet Plastics, No. 10, 26 (1971).

3. Aerospace Structural Adhesive, NMAB ad hoc Committee on Structural Adhesives for Aerospace Use, July, 1974, Chap. 9.

4. R.F. Lewis, R.A. Kinmonth and R.P. Kreahling, J. Adhesion, 3, 249 (1972).

5. F.P. Gay and C.E. Berr, J. Polym. Sci., A-1, 6, 1935 (1968).

6. C. Arnold and L.K. Borgmann, Ind. Eng. Chem. Prod. Res. Develop., 11, 322 (1972).

7. A.S. Teleshova, E.N. Teleshov and A.N. Pranednik, Polym. Sci., USSR, 13, 2593 (1971).

8. J.A. Krenz, A.L. Endrey, F.P. Gay and C.E. Sroog, J. Polym. Sci., Part A-1, 4, 2607 (1966).

9. I.J. Goldfarb and W.L.S. Lawkhaf, AFML-TR-73-253, Air Force Materials Laboratory, Wright-Patterson Air Force Base, Ohio, 1972.

10. A.H. Heimbuch, Sail Materials Adivsory Group Meeting at Jet Propulsion Laboratory, July 11-12, 1977.

11. M.N. Sarbolouki, Monthly Report, May, 1977.

12. J.F. Heacock and C.E. Berr, SPE Transactions, 5, 105 (1965).

13. R.K. Traeger and E.A. Salazar, Polym. Preprints, 12, 292 (1971).

14. A.D. Mair, M.C. Shen and A.V. Toholsky, ONR Tech. Rept. RLT-83, Frick Chemical Lab., Princeton Univ. Princeton, NJ (AD 604010) (1964).

15. H. Leaderman, in Rheology, edited by F.R. Eirich, Vol. II, Academic, NY 1958.

16. Bergfjork and Pennell, Modern plastics, March 1977.

17. H.S. Loveless, C.W. Deeley and D.L. Swanson, SPE Transaction 2, No. 2, April 1962.

4.4.3   Space Effects Testing

Simulated space environment testing was generally performed only on the prime Sail film candidate materials, either uncoated (for worst case purposes, e.g. to simulate areas where coatings are absent via cracking, peeling, etc.) or coated with the "benchmark" metallizations (aluminum and chromium). Testing was performed in various areas to determine the effects of:

(1)   thermal degradation

(2)   ultraviolet radiation

(3)   gamma and neutron radiation

(4)   combined particle and ultraviolet radiation

(5)   electrostatic charging

Additionally, computer simulations were performed of the absorbed nuclear radiation dose over the mission.

In the conduct of the tests, there were cases where specimen size detrimentally influenced the test results. For example in the series of tests at Boeing to establish the effects of UV and proton radiation on "free standing" metallized films, the thin, narrow, test strips tended to curl and twist in the radiation beam. This severely impacted the thermal balance of the specimens and greatly accelerated the thermal degradation. Long narrow strips resulted from an attempt to maximize the number of test conditions—(combinations of film types and coatings). The available sample area exposed in the special test chamber was limited. It was concluded that in future tests, the film samples should be larger in dimension and possibly be framed. A major problem faced in the Sail program was the extremely short time limit for obtaining data, which may have preempted sound experimental procedures.

Kapton, the primary candidate for the Solar Sail basic film, is thermally stable in vacuum to temperatures in excess of 500°C, but does undergo some thermal darkening near 400°C and up. These temperatures are much higher than the expected highest Sail temperature of near 260°C

where the temperature control coatings are employed. Despite its excellent thermal stability, Kapton has been experimentally observed at both JPL and NASA-ARC to be readily degradable by solar UV at temperatures above 260°C. Exposure of the bare film in vacuum to 11 suns of UV while trying to control the specimens at 260 to 300°C resulted in film blackening and burn-through in less than 1 day.* Darkening also occurs at 1 sun, but the rate is much slower. Thus, for the Solar Sail application, Kapton must be protected from solar UV, e.g., by the reflective coating: tentatively selected as approximately 1000Å of aluminum. Later testing indicated that an increase to 1100 to 1200Å might be required to achieve UV opacity. Exposure of coated films to UV and particulate radiation under controlled and known temperature conditions at JPL and NASA-MSFC have not identified a problem area. (Exposure testing at Boeing and Brookhaven was plagued with thermal runaway preventing the drawing of any conclusions).

To raise the backside emittance and aid electrostatic charge dissipation, coatings are applied; ∿100Å of chromium or ∿1000Å or Indium-Tin Oxide (ITO) are the most promising. It is uncertain whether chrome at 100Å can provide adequate radiation shielding for the Kapton film. ITO deposited by vacuum deposition techniques yields conductive coatings, but ion-plated (Endurex) ITO coatings are occasionally insulating. It is believed that the conductivity of this coating is strongly related to the proper mix of the oxygen with the tin and the indium.

4.4.3.1   Thermal Degradation. Preliminary tests for thermal degradation of he Sail film materials were performed on the two final candidate basic film polymers: Kapton H and C-G B100. These tests consisted of weight loss measurements with subsequent analysis of the off gassing products during thermal aging and determination of water absorption rates. Groups of cleaned and degassed bare film samples were placed in

---

*
Later analysis attributed this apparent carbonizing of the films to a "thermal runaway" condition. It was noted that in some locations on the samples where there was lack of good thermal contact between them and the copper heat dissipation block, burn spots or gathered areas appeared which darkened preferentially in the solar radiation, changing their absorptive properties in the process, thus leading to even higher temperatures and eventual carbonizing and burn-through.

vacuum-sealed glass containers for the thermal aging. Analysis of the gasses evolved was accomplished using standard mass spectrographic techniques. The results of this initial series of tests are summarized in Table 4-28.

Thermogravimetric analysis (TGA) was also performed at NASA-ARC on Kapton at a heating rate of 10°C/Min, in a nitrogen atmosphere. The Kapton film showed no initial weight loss until 470°C with the onset of significant degradation beginning at 570°C. Figure 4-37 shows literature TGA curves for Kapton heated in both air and under a vacuum of 10^{-6} torr, indicating the onset of thermal degradation in air at about 450°C and in vacuum at about 550°C. The latter vacuum result essentially duplicates that of the NASA-ARC determination under nitrogen.

In non-oxidizing environments, Kapton is apparently stable to temperatures up to 470°C, well above the highest expected Sail film temperature of near 260°C. Above 400°C, Kapton is observed to darken. This was investigated at NASA-ARC with samples of Kapton heated in vacuum at temperatures ranging from 400°C to 600°C. After exposure to high temperature for a period of 10 minutes, the optical density at 750 nm and at 510 nm of the samples was measured in a double beam spectrophotometer with a sample of virgin Kapton in the reference beam. The electron spin density was also measured. These quantities were plotted versus reciprocal temperature (see attached Figure 4-38). The activation energy is similar for both the darkening of the samples and the production of unpaired electron spins. This suggests that the darkening which occurs when Kapton is heated results in, or is accompanied by, the simultaneous production of a free radical.

Subsequently, a detailed test plan was developed at JPL for more lengthy and thorough diagnostic testing in which a series of coated and uncoated Kapton and B100 film samples, placed in vacuum sealed glass containers, were exposed at various temperatures for varying lengths of time. The Kapton had been directly manufactured by duPont to a thickness of 0.12-0.16 mils. The B100 had been directly manufactured to a thickness of approximately 0.13 mils by Schweitzer. The test matrix included exposure times of 3, 6, 14 and 28 days at temperatures of 240, 270 and

Table 4-28. Results of Preliminary Weight Loss and Water Absorption Measurements on Candidate Sail Film

Material	Weight Loss, %				% Water Absorption	Order of Dominant Species in Evolved Gas
	Thermogravimetric Analysis Under Continuous Vacuo of 10^{-4} torr		In Vacuo (Sealed glass containers)		Soaked in Deionized Water	
	4 hrs @ 250°C	18 hrs @ 300°C	168 hrs @ 300°C	168 hrs @ 320°C	336 hrs @ 25°C	
Alkaline etched Kapton film	0.05	0.27	0.2 - 0.3	0.5	—	CO_2, CO, N_2, H_2O and traces of benzene
Direct produced Kapton film	—	—	—	—	2.9	
Hand cast B100 film	0.05	0.27	0.2 - 0.3	0.5	2.9	CO_2, CO, N_2, H_2O and traces of indane derivative

Note: All film approximately 2.5 μm thick, uncoated.
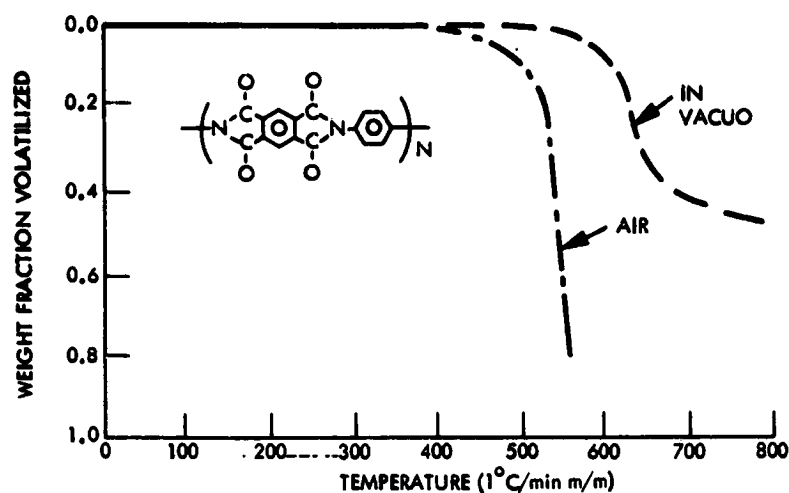
a. Programmed TGA curves in static air and in vacuo for an experimental polyimide nominal bar thickness 0.9-mil. Final cure was 350°C for 1 hour in air. Sample source Dr. Vernon L. Bell, NASA, Langley Research Center.
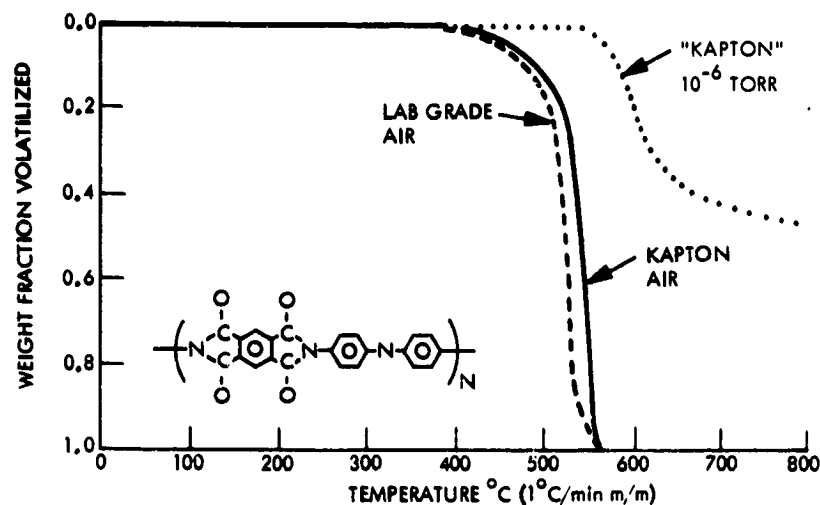
b. Programmed TGA curves in static air and in vacuo for a polyimide ether. The thermogram displayed in broken lines was taken with a nominal 0.9-mil film made in this laboratory. It had a final cure of 1 hour at 300°C. The 0.9-mil Kapton film is from the E.I. duPont de Nemours Company. The difference in the two air thermograms illustrates the improvement that can be made in a new polymer when large-scale processing and curing techniques are used.

Figure 4-37. TGA Curves for Kapton Heated in Air and in Vacuo.
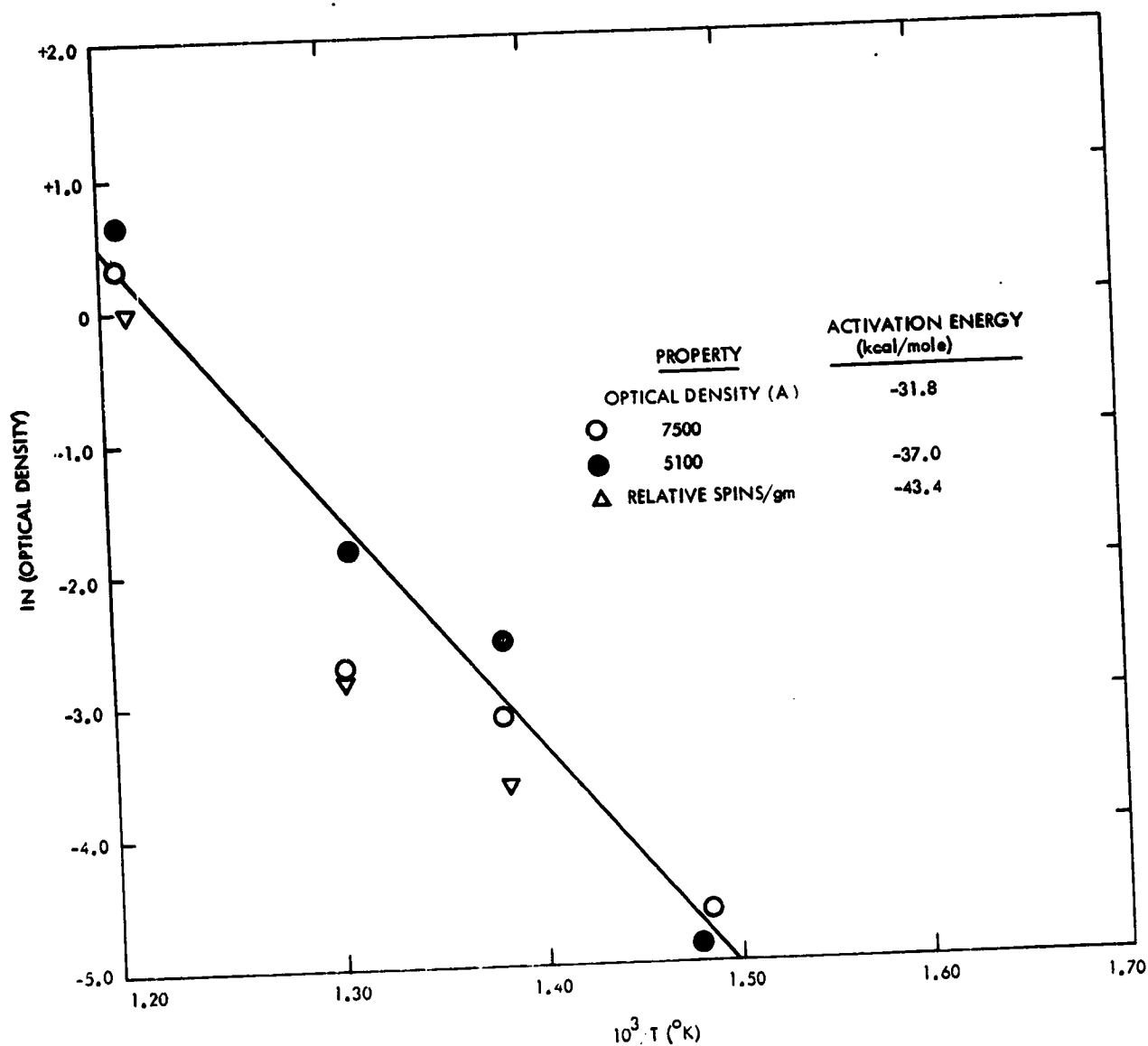
Figure 4-38. Thermally-Induced Darkening of Kapton Film.

305°C. After exposure, the sample films were removed from the containers and subjected to the following types of testing:

(1)   Weight Loss

(2)   Dimensional Changes

(3)   Evolved gas pressure and its mass spectra

(4)   Fourier Transformation Infrared Transmission Spectro-
       scopy (FT-IR)

(5)   Dichroism

(6)   Mechanical Properties

    (a)   dynamic tensile modulus at 25°C

    (b)   static tensile modulus at 250°C

    (c)   ultimate tensile at 250°C

    (d)   elongation at yield at 250°C

    (e)   tear initiation strength at 250°C

The data from this series of tests were examined and the results were as follows. After thermal aging at 240°C, there was a gradual improvement of the majority of the properties for both the Kapton and the B100 films. There were small dimensional changes ($\sim$0.2% shrinkage) and slow gradual weight loss. Thermal aging at 270°C resulted in even more improvement in the properties than was observed at 240°C. The dimensional change was $\sim$0.5% for the Kapton at the end of 28 days, accompanied by a gradual weight loss. The B100 results at 270°C were similar to the Kapton except the dimensional change was 0.6% at the end of 28 days. At 305° aging, there was a gradual deterioration of the Kapton properties (except static tensile modulus). The dimensional change was $\sim$1% with a slow, continuous weight loss ($\sim$5.6% at the end of 28 days. For the B100, aged at 305°C, there was improvement in some properties and deterioration in others (notably tear initiation and static tensile modulus). The dimensional change was $\sim$1.5% at 28 days. This was accompanied by a slow, continuous weight loss of $\sim$3% at 28 days. In examining this data, <u>it is very important to note</u> that the property comparisons were against the initial room temperature properties for a particular film. The initial properties of the Kapton film were superior to those of B100 and even in cases where there was noted improvement of B100 properties, these properties did not exceed those of the Kapton. These observations concluded that in terms of resistance of uncoated film to thermal degradation at 250°C, that the Kapton was clearly superior to the B100. At 270°C, the Kapton was clearly superior to the B100. At 270°C both films appeared to perform well within the B100 improving, apparently through cross-linking after 10 days of exposure. Up to and including 270°C, both films satisfied the target requirements. At 305°C, deterioration of properties begins

with the Kapton (with a higher glass transition temperature) demon-
strating superior performance.

The thermal aging tests on the metallized film samples were
not as conclusive. There was only a limited amount of metallized,
directly manufactured thin gage Kapton available for test and also (as
noted previously) the narrow metallized film specimens of both materials
curled severely during test precluding the conduct of many of the
mechanical tests. The following comments apply to the thermal degrada-
tion testing of these metallized films:

(1)   the evolution of gas as evidenced by weight loss
       appeared greater than for bare film

(2)   the dimensional changes* were more pronounced, espe-
       cially for the B100 where it was approximately 2.6%.

(3)   the mechanical properties (where measurements could be
       made) were very similar to the bare films

4.4.3.2   Ultraviolet Radiation. Samples of 2.5 μm (0.1 mil) Kapton,
under a continuously pumped vacuum of 10^{-7} to 10^{-9} Torr, were exposed
to 16 suns of UV radiation at a nominal temperature of 250°C. These
bare Kapton samples blackened and burned through within 4 hours of
exposure. Temperature was monitored from the change in resistance of
a thin metallic strip deposited on the backside of the films.

The experiment was repeated with benchmark metallized Kapton
film, irradiating the aluminized side. After 120 hours of continuous
exposure at 280°C, no visible damage occurred to the film. Modulus and
loss tangent measurements were carried out and compared with controls.
There was no detectable change in film modulus, but there was a slight
increase in loss tangent observed for the exposed film which suggested a
decrease in the metallized band strength. The electrical resistivities
of the metal coatings underwent no significant change during the exposure.

_____
*The dimensional instability of the B100 is believed to be related to
 the uniaxial stretching it received during its fabrication. This
 problem may be alleviated by an annealing operation.

4.4.3.3   Combined Particle and Ultraviolet.   Testing was conducted at the Boeing Aerospace Company (under contract to JPL) to expose selected samples of coated and uncoated Solar Sail film candidate materials to combined ultraviolet and proton radiation. Uncoated film samples were initially exposed to 11 suns and 1.3 Kev protons at a rate of 3×10^9 protons per cm^2-second. The tests were designed such that the temperature for the uncoated films was to be controlled at 300°C. The coated films were to be exposed to a proportionally increased 16 solar winds proton flux and the solar UV was increased to 16 suns, and the planned temperature was to be decreased to 260°C. The reasons for this were as follows. When the Boeing tests were started on the uncoated films, the initial Sail trajectory was scheduled for ∿0.33 AU, which corresponds to nearly 11 suns, and the Sail film system temperature was estimated at about 300°C. After the uncoated film testing was started, but before the coated film testing, the Sail trajectory was changed to 0.25 AU, which

Table 4-29.   Photothermal Effects in Etched Kapton[a]

Sample	Treatment [b,c]	Absorbtance of 730 nm[d]
Alkali-Etched	330 hr @ 350°C	0
	330 hr @ 350°C + UV	0.028
	357 hr @ 363°C	0
	357 hr @ 363°C + UV	0.033
	344 hr @ <50°C + UV	0.031
	3 hr @ 470°C[e]	0.32
Plasma-Etched	330 hr @ 350°C	0
	330 hr @ 350C + UV	0.011
	357 hr @ 363°C	0
	357 hr @ 363°C + UV	0.029

[a]Etched to ∿2.5 μm (0.1 mil) thickness from 25 μm starting material

[b]Indicated temperatures are those of top of hot plate, except where noted

[c]UV signifies ultraviolet equivalent of 1 Sun

[d]Relative to absorbtance at 750 nm for control

[e]Actual temperature in immersion cell

corresponds to nearly 16 suns. The revised Sail temperature estimates were lowered to 260°C however, because of the demonstration of a lower equilibrium temperature for the Sail film system with the use of an emittance increasing chromium coating on the back-side of the film.

The specialized combined radiation effects test chamber (CRETC) facilities at the Boeing Radiation Effects Laboratory (BREL) were modified to meet the test requirements. An "In Situ Mechanical Property Test Apparatus" was designed and fabricated to fit the CRETC II sample exposure chamber so that polymer test samples would face the incoming, combined beams from existing radiation sources placed around the CRETC II. This sample apparatus is shown in Figure 4-39 before integration with the CRETC II vacuum chamber.

Uncoated Film Experiments

The purpose of exposive uncoated films was to determine the effects of the combination of UV, proton and elevated temperature on unprotected film, in the event there were areas in the Sail where metallization might be missing because of problems (cracks, creases, etc.) associated with stowage and deployment. This represented a worst case analysis.

Test Procedures

Test strips of polyimide films were "draped" over temperature controlled, copper cylindrical sections (heated to and controlled at 300°C) and weighted with ∿1-gram masses, resulting in ∿100-psi loading throughout an initially scheduled 65-day irradiation period. Table 4-30 lists the eight materials that were exposed during the tests. Relatively small changes in sample length could be documented using photographs of the weights' positions as a function of time. Simultaneously, the irradiated sample faces would be photographed to document changes in appearance.

The test plan intended to expose separate samples of each of the materials in Table 4-30 for four time periods, 1, 14, 30, and 65 days, followed by chemical testing using Electron Scanning for Chemical Analysis (ESCA) and dynamic mechanical testing on a Rheovibron viscoelastometer to
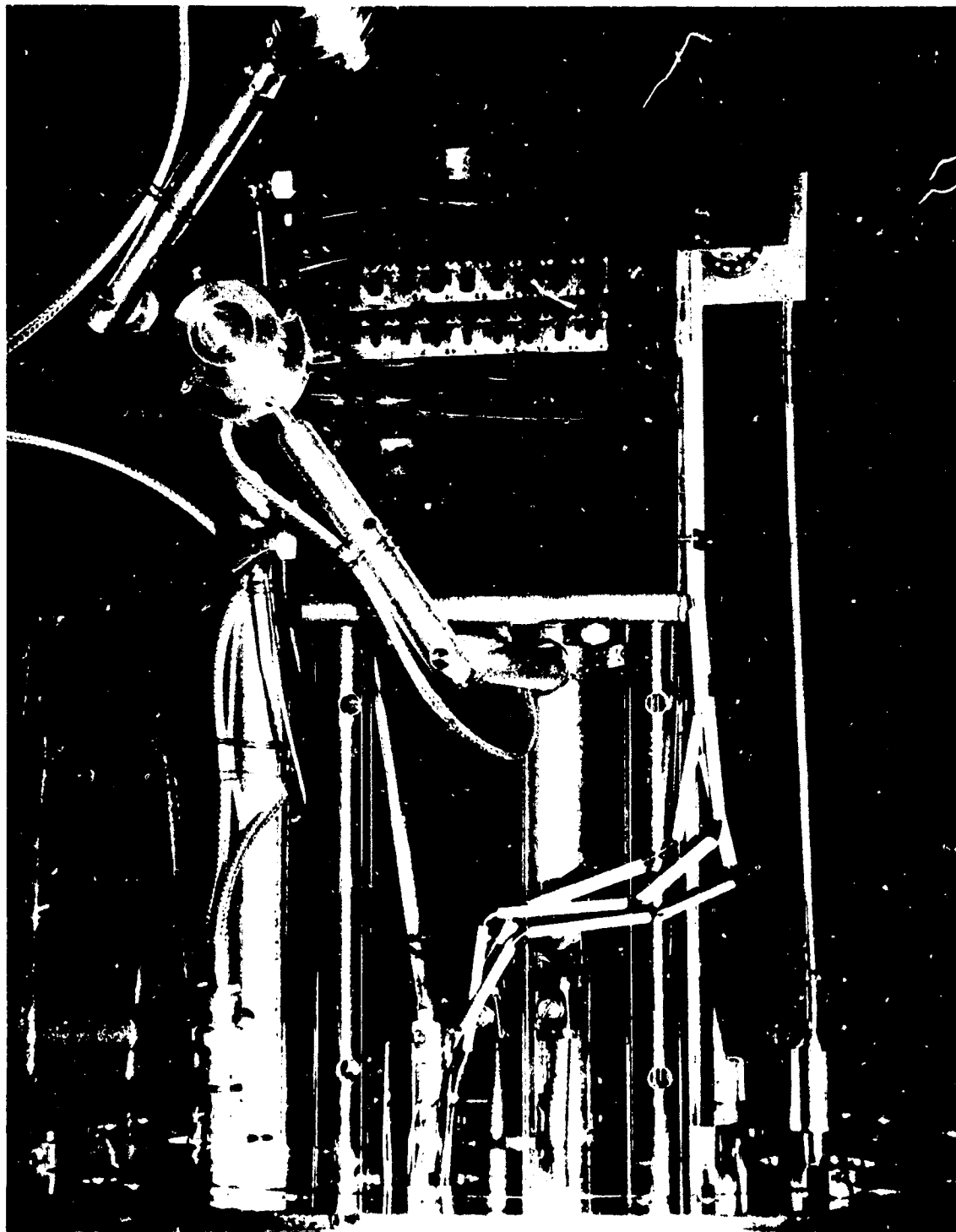
Figure 4-39.   In Situ Mechanical Property Test Apparatus

Table 4-30. Solar Sail Film Materials Irradiated in Boeing CRETC II Tests

Test Sample No./Type	Film Material	Source Sample	JPL Log No.	Measured [3] Thickness (mils)	Calculated Sample Loading (lb/in²)
1	Plasma-etched commercial Kapton[1] polyimide, etched side up	NASA-Ames	141	0.165	91.5
2	Solvent-cast Kapton-type polyimide,[1] *glass side up	NASA-Langley	66	0.06	168
3	Commercial Kapton, NR-150-B2G adhesive bond, pristine (unetched) side up	Dupont/ JPL	118	----	
4	Alkaline-etched commercial Kapton,[1] 24-hr/600°F post cure, unetched side up	Dupont/ JPL	82	0.07	144
5	Electro-cast polyimide,[1] smooth side up	TRW	135	0.055	147
6	Ciba-Geigy solvent-cast B100[2] polyimide, *glass side up	JPL/ Ciba Geigy	140	0.300	
7	Upjohn No. 2080[2] solvent cast polyimide, *glass side up	JPL	85	0.017	59.2
8	Commercial Kapton,[1] no post cure, alkaline-etched side up	Dupont/ JPL	106	0.147	68.4

1 Thermosetting polyimide.   2 Thermoplastic polyimide.   3 1 mil=25.4 μm.

*Refers to the smooth side of the film that was in contact with a glass plate during fabrication (casting) of the film

determine the elastic modulus values. The ESCA and Rheovibron test specimens were prepared and mounted on the copper fixture specially built by Boeing for this test.

Sixteen "strip" samples were loaded by means of attached weights at their lower ends and 16 smaller ESCA test samples were placed in intermediate rows in the test fixture for exposure. Figure 4-40 is a closeup photo showing all four rows of specimens, for a total of 32 test samples.

The basic plan involved shielding the top two rows of samples during the first 13 days of proton and "UV" exposure and then raising the shield for an additional day of exposure. The movable shield is shown "open" or "up" at the top of Figure 4-39. Thus, the top two rows of samples were exposed for one day and the bottom two rows received up to 14 days of irradiation. Because of the extensive degradation which occurred in the 14 day test period, tests planned for 30 and 65 days were cancelled.
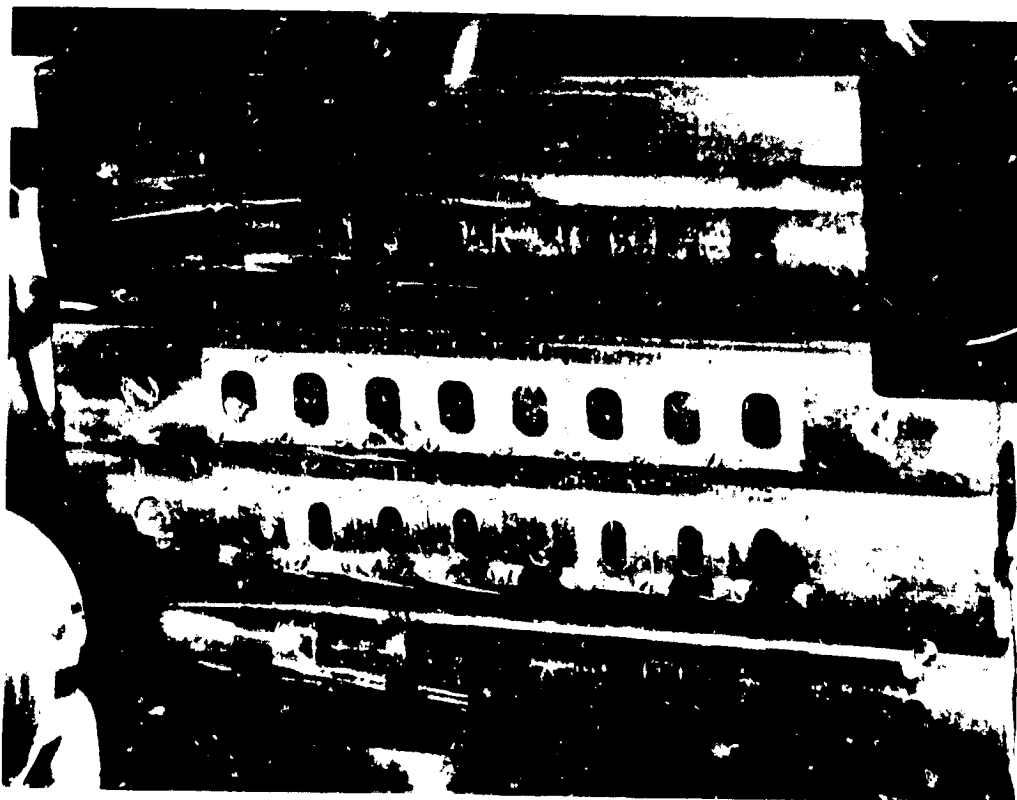
Figure 4-40. Array of Tensile and ESCA Test Samples Prepared From Uncoated Polyimides.

Interior to the Boeing test facility, a Spectrolab Spectro-sun X-25 simulator was modified to produce 11-sun (electromagnetic radiation, including the solar UV continuum (~0.25 to 0.40 micrometers, or 5 to 3 eV) from the simulator's zenon arc-discharge source. Figure 4-41 is a uniformity map of the simulator's output beam as measured during final calibration. The positions of the bottom two rows of samples during their exposure period of 13 days are also shown as overlays on the simulator's output beam pattern in this figure. The "UV" beam was later shifted to expose the upper two rows of samples, which if overlaid on Figure 4-41 would occupy an equal area.

The 1.3-keV proton beam from the CRETC II proton source was checked out relative to the sample array size. Figure 4-42 indicates the proton beam uniformity along the two Farraday cup tracks. The sweep of these tracks across the sample array was apparent from Figure 4-40. The "100%" proton radiation rate used during the "first test stage" was 4×10^9 protons/cm^2-sec. As seen in Figure 4-42, it is possible that the top two rows received somewhat more intense proton radiation.

Vacuum levels during the experiment were limited only by sample outgassing characteristics. Vacuum as measured by an ionization gauge ranged from 10^{-8} to 10^{-7} torr during peak outgassing periods.

A side view of the sample block would show, from top to bottom, an upper row of "strip" (weighted) samples; two rows of ESCA samples, behind which are the weights and ref- e.ence lines for the upper row of strip samples; and the lower row of weighted samples. This sample arrangement is sketched at the right. Inside the uppermost and lowermost curved contact surfaces are electrical heaters, to provide the elevated test temperatures for the weighted samples. A thermo-couple measures the temperatures of

SAMPLES 1A TO 8A

TEMPORARY SHIELD (1ST 13 DAYS OF 14-DAY TEST)

ESCA A

UV, PROTON

RADIATION

ESCA B

SAMPLES 1B TO 8B

HEATER (TOP & BOTTOM)
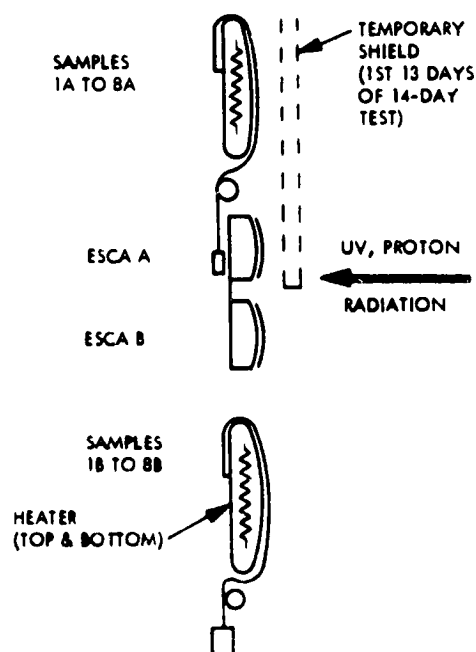
each row of weighted samples. A third thermocouple measures the temper-
ature of the block on which the two rows of ESCA samples are mounted.

Results on Uncoated Samples

The results of these set of tests were somewhat contradictory
between the 24-hour exposures and the 14-day exposures. Generally, the
most dramatic changes occurred during the first 48 hours of exposure in
the chamber when some samples shrank (Upjohn 2080, ∿5%, and Ciba-Geigy
B-100, ∿2%), and the Upjohn material quickly discolored. However, at
the thirteenth day when the shield was raised from the one-day exposure
samples, (to expose these to UV and proton irradiation) the same results
did not occur. In fact, degradation was visually judged to be just
about as severe after one-day of exposure on these samples as on the
14-day exposure specimens. It is believed that the temperature and high
vacuum (for the previous 13 days) conditioned these specimens to the
point that when they were exposed to the UV and protons, they degraded
very quickly.

Aside from the fact that the radiation profile varied from
the center to the edges of the beam (Figures 4-41 and 4-42), the thermo-
setting type polyimides (Kapton and TRW electrocast) generally appeared
to withstand the environment better than the thermoplastic polyimides
(Upjohn 2080 and Ciba-Geigy B100).

As previously mentioned, because of the rapid darkening and
general degradation of these uncoated materials, exposure testing was
terminated after 14 days. The copper block fixture with the specimens
intact was then returned to JPL for disassembly and further specimen
diagnosis. The following general visual observations were noted during
disassembly at JPL:

> (1) All ESCA sample masks were easily disassembled and
>   cleanly removed. Black fragments of samples No. 3,
>   No. 5, and No. 8 (14 day exposures) adhered to their
>   masks and were found to be slightly adherent, but
>   removable.
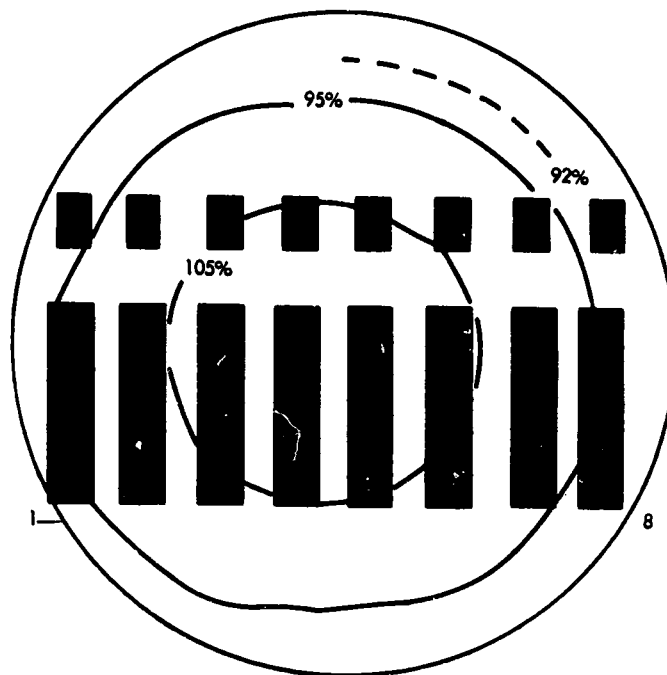
Figure 4-41. Uniformity of Ultraviolet Radiaton (Actual Size of
11-Sun Beam)
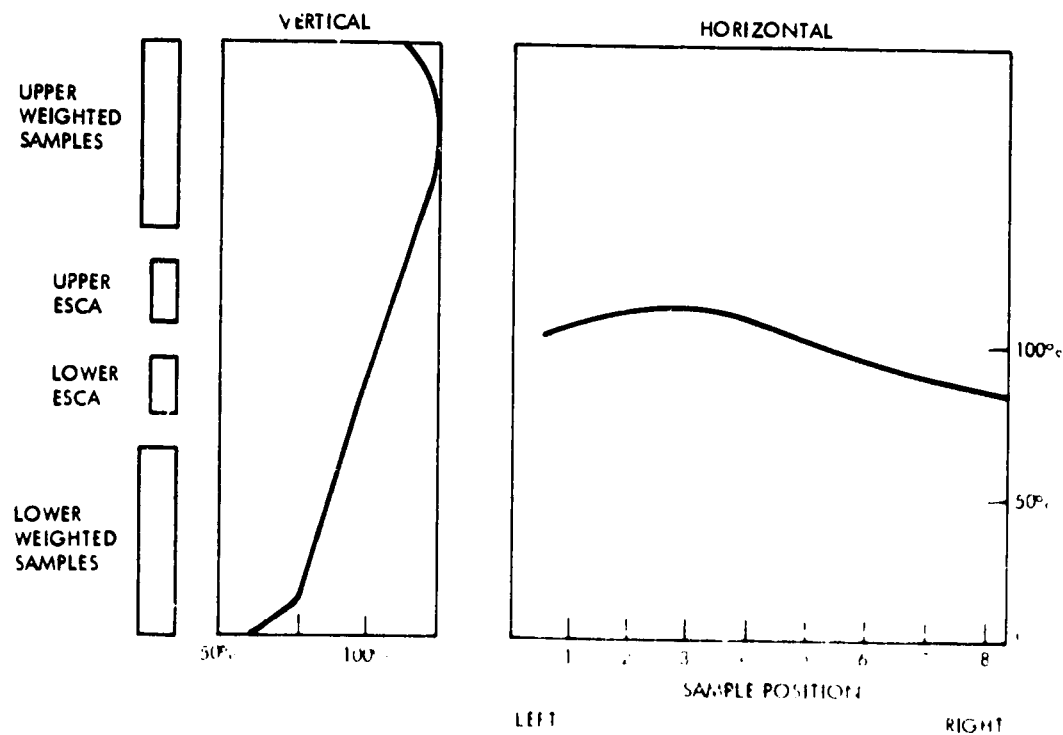
Figure 4-42. Proton Uniformity Along Near-Horizontal and
Near-Vertical Arcs

(2) All ESCA samples exhibited various degrees of electro-
static attraction for the copper surfaces, and with few
exceptions, were easily removed. Typically, the charred
or black portions of the films were more adherent to the
copper block. The most notable exception was sample
No. 2 (14 day) whose edges under the mask were badly
stuck to the copper block, but surprisingly the irra-
diated area was not stuck and easily lifted off. Again
sample No. 2 (1 day) was found to be brittle, easily
broken when handled, and exhibited some evidence of
clinging at the edges which were under the mask. As a
generalization, the 1 day samples seemed to exhibit
more overall adherence to the copper block than the 14
day samples, but the difference was small.

(3) The 1-day Rheovibron (weighted) samples were in general
easily removed from the copper block, exhibiting to
various degrees electrostatic clinging and some stronger
bonding (but removable) involving only charred or black
areas of the films.

(4) With the exception of samples No. 6 and No. 7, the 14-
day Rheovibron samples were removable, but overall there
was a greater tendency toward more adherence, consisting
of electrostatic clinging and charred bonding. Samples
No. 6 and No. 7 were strongly bonded to the copper
block. Sample No. 3 readily fell off the block, and
samples No. 1 and No. 8 exhibited very slight electro-
static clinging.

(5) With specific attention to only the areas of the ESCA
and Rheovibron samples which were exposed to radiation,
clinging which was of a type judged to be greater than
or different from electrostatic clinging, occurred only
when encountered with the charred or black portions of
the film.

(6) Sample No. 6, the Ciba-Geigy polyimide, after 1 day of
radiation exposure underwent a decrease in width from
an initial 5.61 mm to 3.77 mm, and an increase in
thickness from an initial 7.41×10^{-3} mm to about
20×10^{-3} mm.

ESCA Analyses

Various questions and concerns were raised and expressed
about this test, a key question centered on whether or not copper acted
in any way, such as a catalyst, to either promote or accelerate the
radiation damage. Accordingly, ESCA analysis centered on two areas,
detection for copper in the irradiated films and the direction of radia-
tion damage through the films, either from the irradiated side through
to the copper side, or from the copper side outward toward the radiation
source.

The results of the ESCA analysis of these materials were as
follows:

(1) Copper in concentrations ranging from 3 to 5 atomic
percent was found on all surfaces of the materials,
but not in the bulk of the materials.

(2) The radiation exposure caused the materials to carbo-
nize, as determined by the decreases in concentrations
of the non-carbon elements. Carbonization is more evi-
dent on the radiated surfaces, then on the back sur-
faces, but the gradient of carbonization, although dis-
cernable, is not great. It could not be determined
from these tests whether the proton or UV radiation
caused the carbonization. However, in some tests con-
ducted at TRW,[1] proton irradiation was identified as
the cause of optical degradation to Kapton film.

(3) Evidence from these tests indicate that radiation
damage to the materials proceeded from the radiation

exposed side of the samples toward the back side which is in contact with the copper block.

(4) It is speculated that proton bombardment caused sputtering of the copper, which may be the mechanis by which copper deposited on the surfaces of the samples not in contact with the copper block. This same mechanism of metal transfer has been observed by the ESCA people when they are Argon etching. Argon striking metal masks causes sputtering of the metal and deposition onto surrounding surfaces. The mechanism by which copper deposited on the back side of the films is not explained.

Rheovibron Analysis

Only Rheovibron samples No. 1, No. 6, and No. 8 after 1 day, and samples No. 1 and No. 8 after 14 days had sufficient length and body for mechanical testing on the Rheovibron. The modulus results on these exposed samples, along with those for the controls, are tabulated in Table 4-31. Because of degraded condition of the samples, all that can really be said is that the modulus values decreased from exposure, again strongly pointing out the need for reflective, protective coatings on the polymer films.

Metallized Film Experiments

For the second set of tests conducted at the Boeing Radiation Effects Laboratory, several changes were made. First, the test samples were metallized films of the two major candidate polymers; Kapton-H and Ciba-Geigy B100. Ten benchmark coated samples of these films (1000Å of aluminum on the front surface and 125Å of chromium on the back) were irradiated with 1.3-keV protons and UV, visible, and IR radiation at a 16-sun rate. Test conditions differed from the first test set in that the samples were suspended in the chamber in such a manner that their irradiated zones were "free-standing", i.e., not in contact with any temperature control mechanism, nor any portion of the vacuum chamber or other apparatus. The test was designed such that each sample

Table 4-31. Modulus Values of Boeing Test Materials (Rheovibron Analysis)

A. Before Exposure

Boeing Sample No.	JPL Log No.	Sample Designation	Modulus PSI x 10^{-5}
1	141	Ames O_2 Etch	5.06
2	66	LaRC Cast Polymide	5.02
3	118	Joint	Not Measured
4	82	KOH Etch with Post Cure	5.04
5	135	TRW Electrocast	4.33
6	140	Ciba Geigy B100X	2.69
7	85	Upjohn 2080	4.19
8	106	KOH Etch W/O Post Cure	4.96

B. After Exposure

Boeing Sample No.	Exposure Time, Days	Modulus PSI x 10^{-5}
1	0	5.06
	1	4.94
	13	2.06
6	0	2.64
	1	2.07
8	0	4.96
	1	4.64
	13	2.34

was to acquire a steady-state temperature as determined by (1) its absorption and emission characteristics, (2) the proton and "UV" exposure rate, and (3) the rate of receiving secondary radiation from nearby surfaces.

The metallized samples are listed in Table 4-32. A total of ten specimens with Rheovibron test size dimensions were fabricated, some with built-in defects where the aluminum coating was intentionally deleted in a thin horizontal segment or gap of varying width across the approximate mid-points of these specimens. Also included was a sample bonded joint of each material.

Figure 4-43 is a closeup photograph of the 10 metallized films prior to irradiation. Identification of sample type for its position in the chamber is given in Figure 4-48. The photograph is taken

Table 4-32. Aluminized Samples for Second Test Stage

TYPE I   TYPE II   TYPE III

GAP

ALUMINIZED KAPTON
REFLECTOR, CHROMIUM
EMITTER, NO BREAK
IN Al METALLIZATION

ALUMINIZED KAPTON
REFLECTOR WITH GAP
IN Al & NONE IN Cr
EMITTER

BOND JOINT, Al
REFLECTOR & Cr
EMITTER
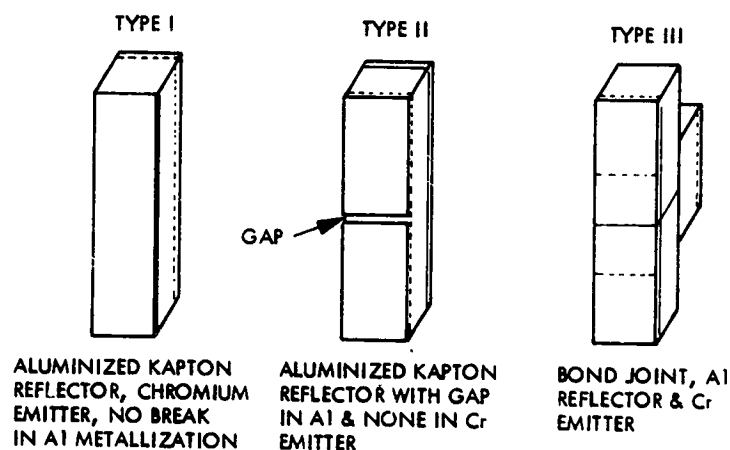
	Description	Spec Type	JPL Designation	Boeing Chamber Position	Sample Thickness
Direct manufac-tured Kapton Polyimide with Benchmark Coating[1]	No gap	I	340D	13	0.16 mil
	1-mil Gap	II	340A	17	0.16 mil
	2-mil Gap	II	340B	15	0.16 mil
	5-mil Gap	II	340C	9	0.16 mil
	Bond	III	306D	14	0.16 mil
Direct manufactured (P.J. Sweitzer) Ciba-Geigy B100 Polyimide with Benchmark Coating[1]	No Gap	I	306D	14	0.12 mil
	1-mil Gap	II	306A	10	0.12 mil
	2-mil Gap	II	306B	12	0.12 mil
	5-mil Gap	II	306C	18[2]	0.12 mil
	Bond	III		16	0.12 mil

[1] Benchmark coating consisted of 125Å of Cr on the emitting side of film and 1000Å of Al on the reflecting (sun) side.

[2] This sample (No. 18) was cut for irradiation testing in a direction 90° from the direction of cut of the other Ciba-Geigy samples. The others were cut with the long direction parallel to the machine direction. This specimen was in the transverse direction. This sample was dimensionally much more stable than the other Ciba-Geigy samples (see Figure 4-43).
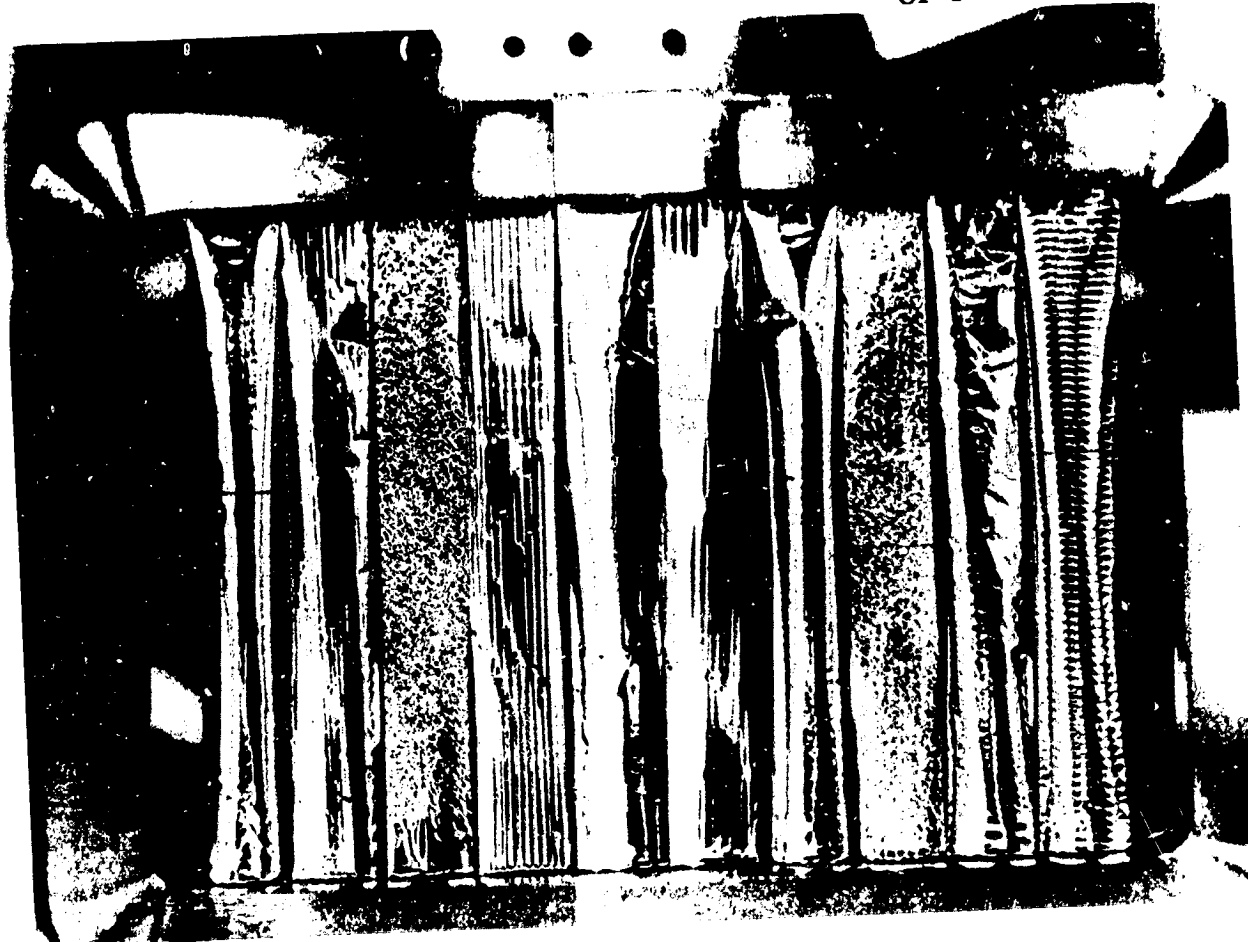
Figure 4-43. Metallized Polyimide Film Samples Before 16-Sun
UV/Proton Irradiation

from the side to be exposed to UV and protons. The gaps that were
intentionally put in the aluminum overcoating by selective masks during
vapor deposition are visible in some samples. Views of the reverse side
of the sample apparatus as modified for this experiment (Figure 4-44)
show the 1-gram mass below each sample and show horizontal grid markings
that allowed sample length changes to be measured in situ during exposure.

Many of the details involved in setting "UV" exposure inten-
sity and attempting the temperature calibration for the chamber are left
for the discussion in Appendix III.

Test Results on Metallized Samples

A principal objective of these tests was to expose the
temperature-sensitive films to no more than 16 total suns. During pre-
irradiation photography of the samples' initial conditions it was

4-141
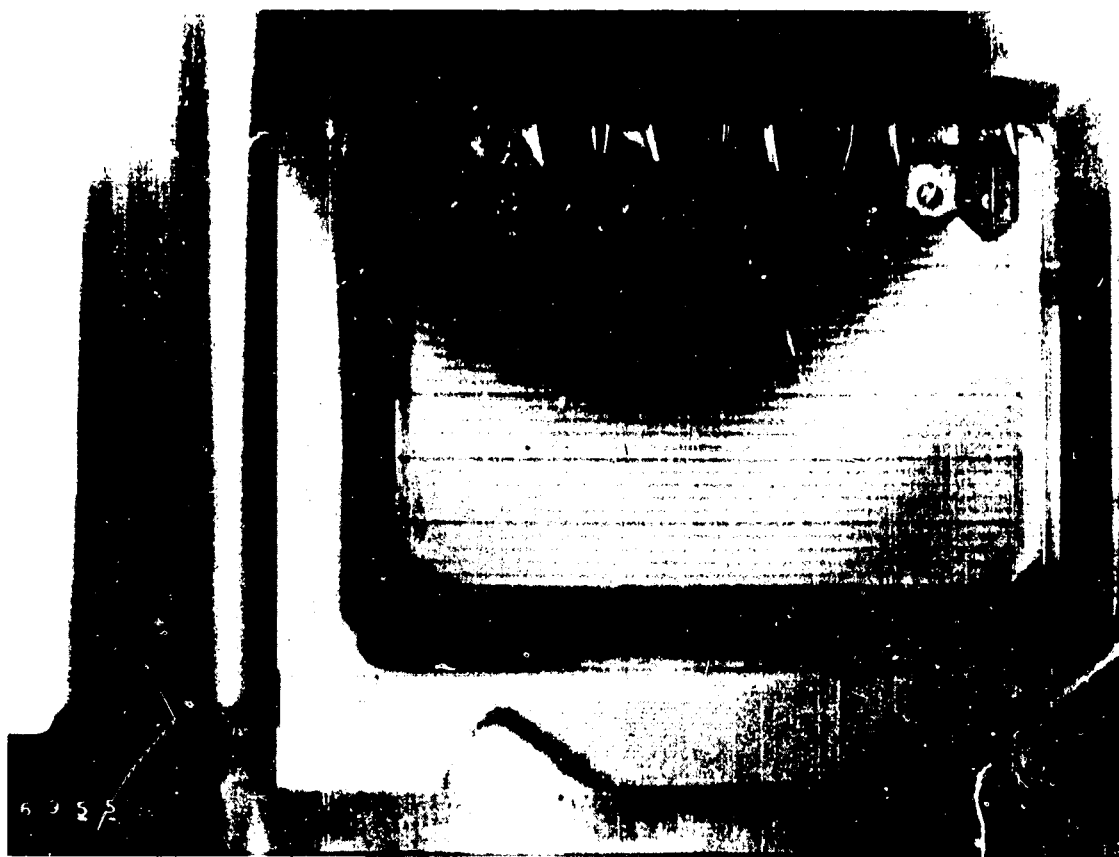
Figure 4-44.   Weight Positions Below Suspended Metallized Polyimide
Films Prior to Exposure

determined that the Ciba-Geigy polymers that were "longitudinally cut"
had already shrunk appreciable under illumination by the photo lighting
source.   Irradiation by the solar simulator continued the length shrink-
age in these samples and to a lesser extent in the Kapton films.   Data
on sample length changes, as reduced from periodic photographs of sample
weight positions in situ before, during, and after the 1100-hour exposure
period, is presented for Kapton films in Figure 4-45 and for Ciba Geigy
films in Figure 4-46.   Since the current through the UV source lamp must
periodically be increased to compensate for lamp aging, and since optical
surfaces between the source lamp and the samples must periodically be
cleaned, Figure 4-45 includes a charting of these adjustments to show
the degree of correlation between small intensity adjustments and sample
lengths.   The main coincidence of sample length changes and solar simula-
tor intensity increases is seen in Figure 4-45 to be after 22 hours of
exposure when, as described in Appendix III, the rationale for setting "UV"
exposure intensity was modified.   Figure 4-46 compares the stability of
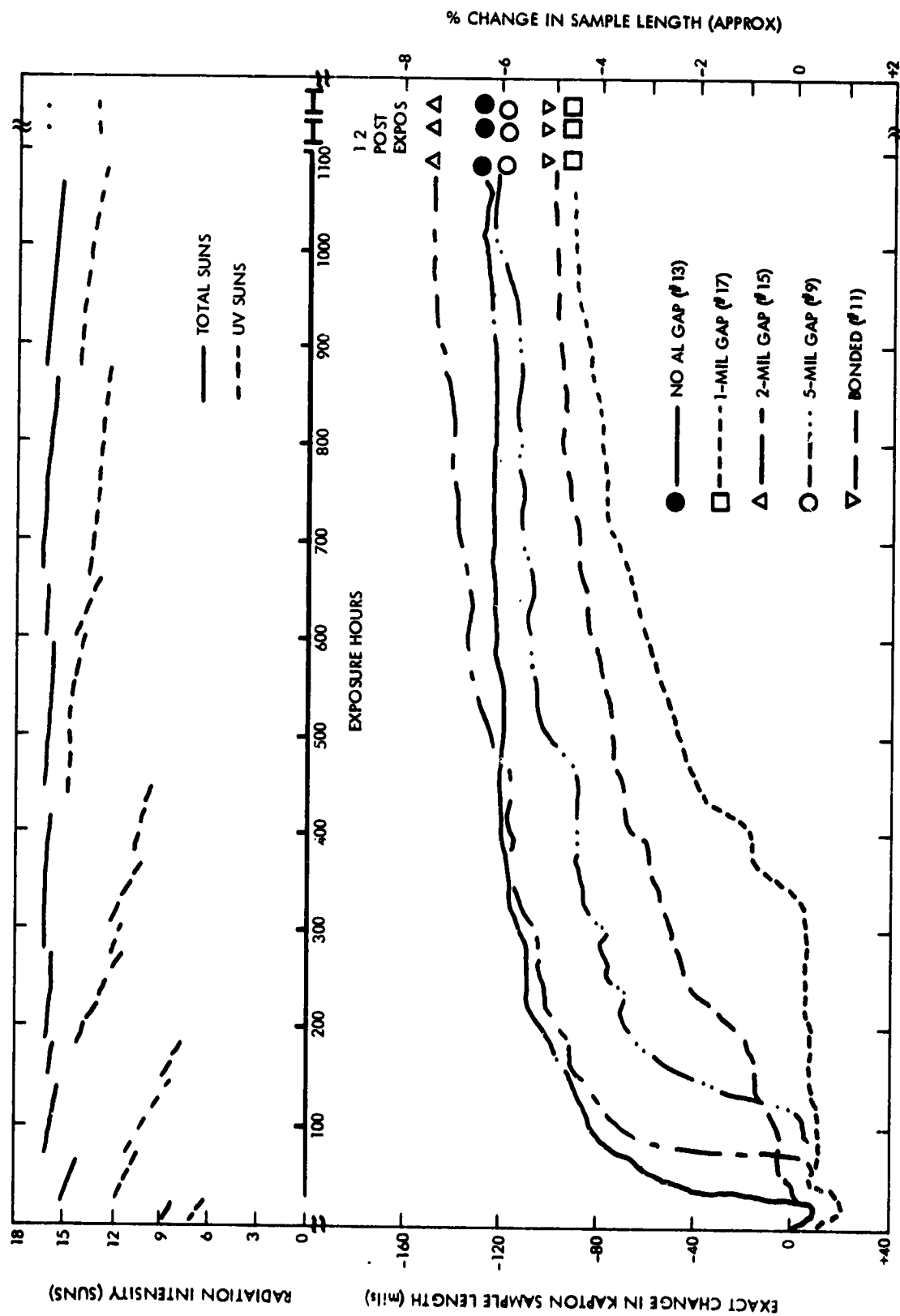
Figure 4-45. Changes in Radiation Intensity and Kapton Sample Lengths During 1100-Hour Test
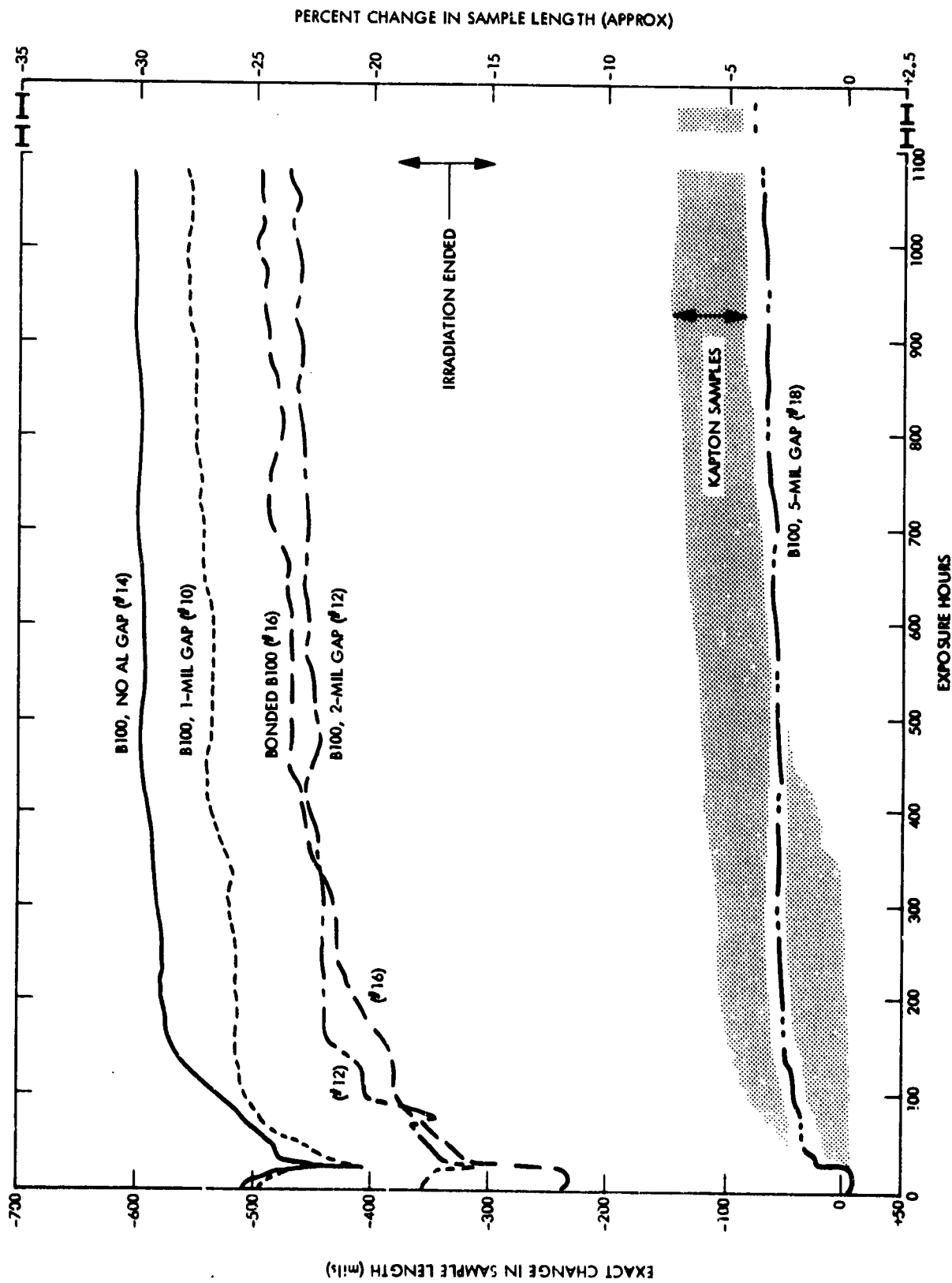
Figure 4-46. Changes in Metallized Kapton and B100 Film Lengths During 1100-Hour Test

sample length among Kapton samples as a group, individual Ciba-Geigy
samples cut longitudinally, and Ciba-Geigy sample No. 18 cut transversly.

The irradiated surfaces of all ten specimens were affected
by the proton/UV exposure. This was most noticeable in the Ciba Geigy
B100 specimens. After the first 20 hours of exposure approximately 80%
of the Ciba Geigy samples' irradiated lengths had shortened ∿5% narrowed,
as their transition temperature was exceeded. The transverse-cut Ciba
Geigy sample (No. 18) appeared to be an exception to this statement
about shortening, although it did neck down soon after the exposure
intensity was increased to 16 suns. The shape of the solar simulator
beam is indicated in Figure 4-48, and the uniformity of the proton beam
is shown in Figure 4-49. Toward the end of the experiment, extensive
curling, warping, and twisting has affected both the Kapton and the Ciba
Geigy materials, as shown in Figure 4-47.

Shrinkage of a sample in both the width and length dimension
implies an increase in material thickness (which was not measured) and/or
loss of volatile molecules through outgassing in the vacuum test chamber.
Vacuum gauge indications confirm the latter.

Insufficient thermal conditioning of the Ciba-Giegy test
samples before delivery to Boeing for irradiation may have been a factor
in their greater instability. The Ciba Geigy test samples were "soaked"
at 250°C in vacuum for 5 minutes. It is believed that a longer condi-
tioning period might have improved the dimensional stability of the Ciba
Geigy material tested.

After completion of 45 days of exposure, all 10 samples were
extensively deteriorated, friable, and best described as resemblying
pyrolyzed cigarette paper. With the exception of specimen No. 11
(Table 4-32), a bonded joint Kapton sample, all of the initially flat
samples were tightly curled. The condition of the samples suggested
deterioration resulted from high temperatures, not radiation.

Considering the degraded condition of the specimens, analysis
by ESCA and Rheovibron was ruled out, along with planned aluminum peel
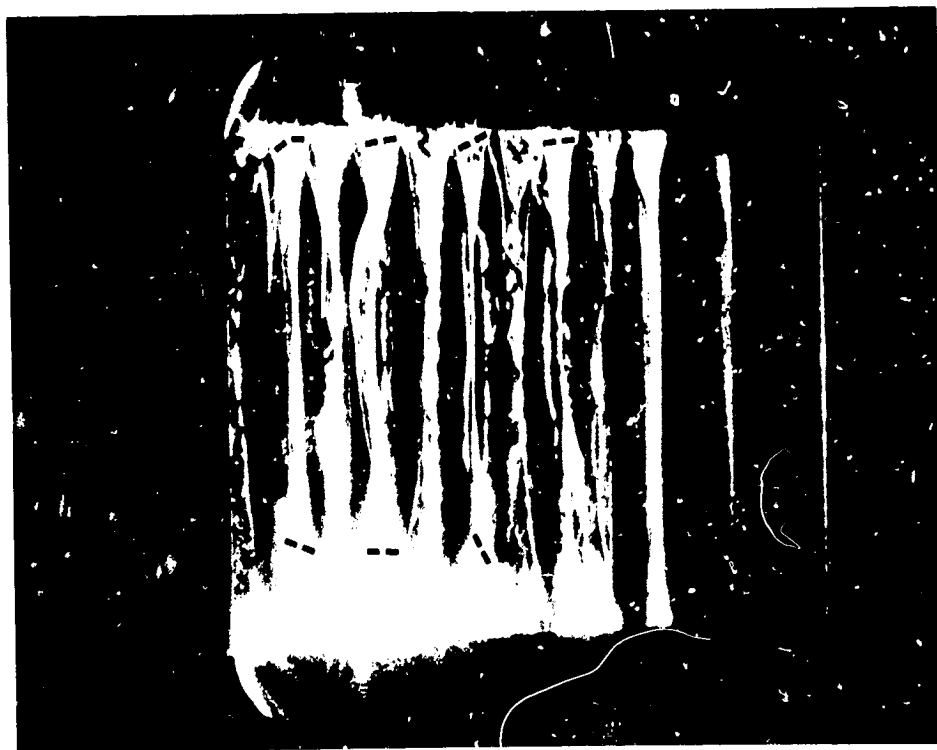
Figure 4-47. Metallized Films After 1000 Hours Exposure

strength measurements at Rockwell. There was however one specimen, Kapton sample No. 17 (Table 4-32) which was completely intact, although tightly curled. By patient and careful handling, this specimen was successfully mounted intact in an Instron test machine and found to have a breaking load of near 1.5 grams. This film sample was intentionally fabricated to have a 1 mil gap of missing aluminum, the gap running width-wise across the sample and therefore normal to the applied load. So presumably the deteriorated Kapton carried the mechanical load, and based on its initial cross sectional area, this breaking load calculates to a stress of 150 psi. The tensile strength of control Kapton is nearly 20,000 psi.

As inferred earlier, it was evident from the condition of the specimens that the desired temperature level (260°C) for the test had been exceeded, thus causing thermal effects to contribute heavily to the degradation observed in some of the test materials.

ORIGINAL PAGE IS
OF POOR QUALITY

KAPTON

CIGA-GEIGY
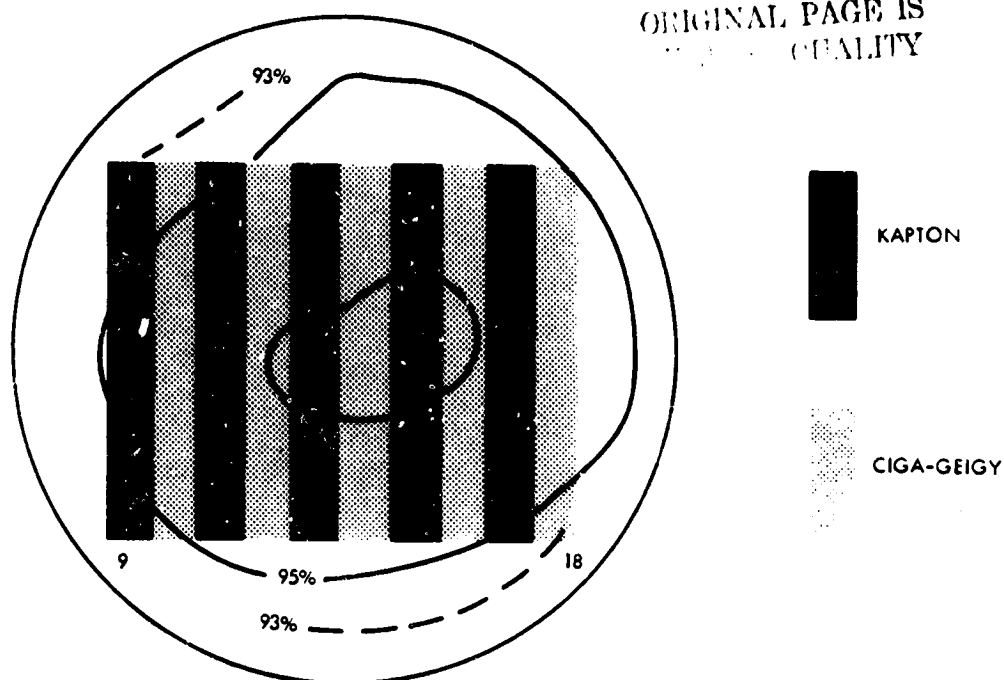
Figure 4-48. Uniformity of Solar Simulator Beam Actual Size
of 16-Sun UV Beam
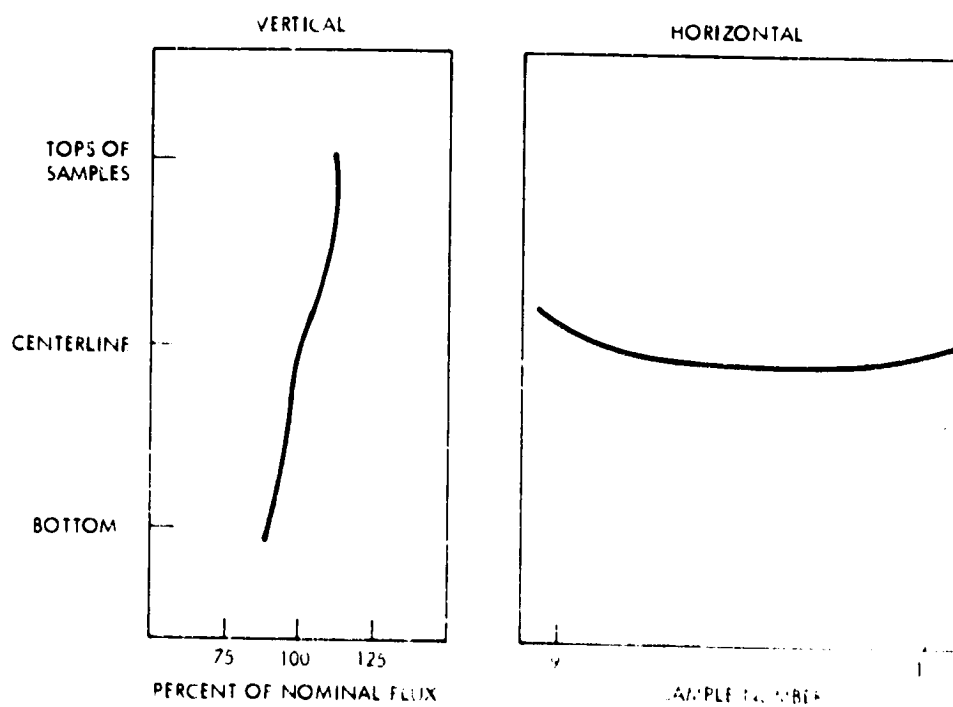
Figure 4-49. Proton Uniformity Along Near-Horizontal and
Near-Vertical Arcs

The major contributor to the excess temperatures in this test was again the specimen configuration. The curling and twisting of the narrow film strips altered their radiative exchange properties and resultant equilibrium temperatures. Some film samples rotated enough that the more absorbing emissive side was facing the radiation rather than the intended reflective surface. Sample changes such as these depend on incident radiation levels and on interactions with the test chamber as well. Test chamber limitations point out that laboratory simulation is not duplication of space. The surrounding chamber is not a true black body. In this program, highly reflective nickel plating had been used to cover the copper sample block for the second test, since in the earlier tests copper and Kapton had previously been found chemically incompatible.

In connection with future Solar Sailing material studies and development, samples more closely simulating planar sheets should be irradiated. Long, narrow samples are particularly susceptible to warping and twisting. Tensile-loaded samples having widths approaching their exposed lengths should be exposed to radiation pertinent to the application environments. Even framing of test materials for overall circumferential dimensional control should be considered.

From the test chamber standpoint, further control over the reflective and radiative properties of surfaces surrounding test specimens should be exercised during future experiments of the type performed for this program. Boeing has developed improved test techniques and configurations, including use of wider samples and chamber surfaces with controlled reflectance (Reference 2).

4.4.3.4 _Gamma and Neutron Radiation._ Brookhaven Laboratories in Upton, Long Island, N.Y. offered to irradiate Solar Sail materials in their nuclear pile, which is a source of gamma and neutrons. The dose rate is 10^8 Rads every 12.8 minutes. Two entry ports into the reactor core were made available to JPL, which are designed as V15 and V16. V15 was to be used to irradiate Sail materials at levels of 10^8, 10^9, and

10^{10} Rads, and V16 was to be used to irradiate only at a level of 2×10^{11} Rads. The port geometry of V15 permits irradiation of 14 materials, each sealed in separate quartz tubes, under a 0.5 atm. of helium, while V16 permits only two materials, again each sealed in a separate quartz tube under a 0.5 atm. of helium. The 14 materials to be irradiated in V15 at each of the three irradiation levels are listed in Table 4-33. Without prior experience, it was estimated that 0.5 atm. of helium would yield a material temperature of approximately 150°C. This was experimentally monitored by using bare Mylar (sample No. 14) as a temperature check, which has a melting point near 250°C.

There was concern that chromium could become sufficiently radioactive after exposure in V15 to prevent handling. This was not in fact realized. The materials were somewhat radioactive after exposure, but the level dropped well below 1 mr at 1 cm (the limit below which materials legally may be handled in a routine manner) within 2 to 3 weeks.

Irradiation and Visual Examination. Experimentally, many of the 14 Solar Sail materials which were to be irradiated at 10^8, 10^9, and 10^{10} Rads in the V15 core of the Brookhaven pile were overheated and destroyed due to temperature control problems with the experiment. Included were samples No. 1 through 7 to be exposed at 10^8 Rads, samples No. 2, 4, 5, 6, and 7 to be exposed at 10^9 Rads, and all 14 samples to be exposed at 10^{10} Rads. Due to space limitations in the V15 core, only two duplicates of seven samples at a time could be irradiated at any of the discrete radiation levels. The arbitrary sequence started out with samples No. 1 to 7 at 10^{10} Rads, followed by samples No. 8 to 14 at 10^{10} Rads, samples No. 1 to 7 at 10^8 Rads, and samples No. 1 to 7 at 10^9 Rads. At this point the thermal runaway condition was detected, and corrective procedures implemented.

The next batch then consisted of samples No. 8 to 14 to be exposed at 10^8 Rads, which were in the reactor for about 12-13 minutes. Upon removal from the pile, it was found that reactor water had leaked

Table 4-33.   Samples for Brookhaven Tests

Sample No.	Description	JPL Log #
14	Bare Mylar	463
13	Ciba-Geigy P100 (bare)	299
12	Ames O_2 etched Kapton (bare)	424 old (195)
11	JPL chem etched Kapton (bare)	423
10	CGS production 0.16 mil B100 (bare)	422
9	Production Kapton 0.15 mil (bare)	421
8	Bonded 0.5 mil Kapton (Benchmark plated) NR 150 Joints (3 ea. tube)	340
7	Kapton, Cr only	340
6	Benchmark 0.3 mil Kapton	427
5	Benchmark Direct Manfg Kapton 0.12 mil	425
4	Ion plated, Benchmark coating, chem etched Kapton	429
3	0.1 mil Kapton Al only	234
2	Benchmark plated CGS direct production 0.12 mil B100	426
1	Benchmark plated, 0.5 mil CGS B100	428

into and filled the aluminum capsule which contains the seven quartz sample tubes. Thus the outside surfaces of the quartz sample tubes for this batch were presumed to be at the reactor water temperature of near 60°C. However, inspection of the Mylar in sample tube No. 14 found it to be only slightly tan in color (radiation coloring), but fused hard and very brittle on touch. This evidence indicated that the Mylar had been heated to a temperature in excess of its 250°C melting point.

Further, film sample No. 10, of CGS B-100, initially wrapped in a loose cylindrical shape, was found to be tightly shriveled for some length along its cylindrical axis, and then flared out to its initial

shape (bell bottom appearance) where the material was in contact with the bottom of its quartz tube, which was in turn in direct contact with the aluminum capsule. This evidence indicated that the temperature gradient from the tube along the length of the sample had a temperature range from 60° to somewhere above 325°C, the glass transition temperature (Tg) of the material. Thus, even with temperature control techniques and the presence of leaked reactor water, the best guess is that gamma heating from the reactor still caused these sample materials to be at temperatures somewhere between 250 and 350°C. Nevertheless, all samples from No. 8 through 13 were generally in good shape and handleable.

The next batch was samples No. 8 to 14 to be exposed at 10^9 Rads, which was in the reactor for about 2 hours. No reactor water leakage occurred during this exposure. The Mylar in tube 13 was charred, black, and totally disintegrated. The CGS B-100 in tube No. 10 had the identical bell bottom appearance as observed for the 10^8 Rad exposure level. Temperatures for this batch are estimated to have been in excess of 300°C, and with the exception of Mylar, all the remaining samples are slightly discolored to various degrees, but appear to be in good mechanical shape and were returned to JPL.

At Brookhaven, the temperature control techniques implemented in V15 cannot be used in V16, and thus thermal runaway in V16 was expected. Brookhaven therefore irradiated four samples (2, 5, 9, 10) to 3×10^{10} Rads in the V15 core. These materials were found to be brittle after the exposure, but a judgment could not be made as to the relative contribution of temperature or radiation to the material degradation.

Mechanical Testing. Mechanical testing on the Rheovibron was done only with the bonded Kapton joints which had been irradiated to 10^8 and 10^9 Rads. These materials are designated as Brookhaven sample No. 8 (Table 4-33). Three each of the samples were irradiated at each level. The Rheovibron test results for three controls, and the three samples from each radiation level and tabulated in Table 4.34.

Table 4-34. Rheovibron Analysis of Brookhaven Irradiated
NR 150 Bonded 0.5 mil Kapton Joints

(Brookhaven Sample No. 8)

		Dynamic Force	Loss Tangent
Controls	{	73	0.010
		70	0.014
		<u>71</u>	<u>0.010</u>
Average		71	0.011
10^8 Rads	{	69	0.014
		71	0.009
		<u>67</u>	<u>0.009</u>
Average		69	0.010
10^9 Rads	{	69	0.010
		70	0.010
		<u>62</u>	<u>0.007</u>
Average		67	0.009

On the Rheovibron, the "Dynamic Force" is inversely proportional
to modulus, the calculation of which also requires knowledge of the sam-
ple dimensions. Since the bonded joint is fabricated in a double con-
figuration, the selection of appropriate dimensions for a modulus calcu-
lation is not straightforward. Recognizing this in advance, all nine
samples were cut out of a common bonded film, and all were sliced to the
same length and width dimensions. Hence, dynamic force can provide com-
parative information, and form the data of Table 4-34, there is a sug-
gestion that the modulus (strength) of the bonded joint samples increased
with radiation exposure, at least up to 10^9 Rads. Whether the slight
increase in modulus is related to the adhesive joint, or to the base
Kapton film is not resolvable here, but it is known that the modulus of
Kapton film will slightly increase with radiation exposure up to a dos-
age of about 3×10^9 Rads, there being no data at higher rates.

"Loss Tangent" is a property of materials undergoing dynamic test-
ing which relates to the dissipation of mechanical energy. It was pre-
viously observed (see Reference 3) that the loss tangent was related to

the quality of an adhesive joint, with the loss tangent increasing as the joint deteriorated, and that it decreased as bond strength quality of the joint improved. The hypothesis to explain this suggests that friction develops between debonding areas, which increases mechanical energy dissipation and therefore the value of the loss tangent. Examination of the loss tangent data in Table 4-35 is suggestive of subtle decreases in loss tangent, which would indicate at the very least no bond deterioration, and possible some bond strength improvement.

The Brookhaven reactor puts out a gamma heating rate of near 9 watts per gram of irradiated material. For plastic films such as Kapton, this translates into a material heating rate of near 8°C/second. Thus in one minute, temperatures of the samples could be approaching 4...°C. Given that poor heat transfer conditions exist between the sealed samples and the outside reactor cooling water (maintained at 60°C), thermal degradation of the test materials is a major concern. Because of this, experimental results on Brookhaven irradiated materials might not provide a fair evaluation of the Solar Sail materials.

4.4.3.5   Proton Tests.   The absorbed dose, calculated for the entire mission as a function of position in the film is shown in Figure 4-50. The range of reported threshold doses for mechanical damage to Kapton is also shown. Based on this data, no bulk degradation would be expected through most of the thickness of the film. The high surface dose could produce mechanical damage in the Kapton, and potential catastrophic degradation of the aluminum adhesion.

In order to reduce the uncertainty in the threshold dose and to obtain an initial assessment of the expected properties of the film at various depths, a series of proton tests was carried out by MSFC. Samples of 0.1 mil (chemically etched from 0.3 mil commercial film) Kapton with aluminum and chromium coatings were irradiated with 440 keV protons to total absorbed doses of 10^8, 10^9, 10^{10} and 5×10^{10} rads. No significant changes were detected up to 10^{10} rads.
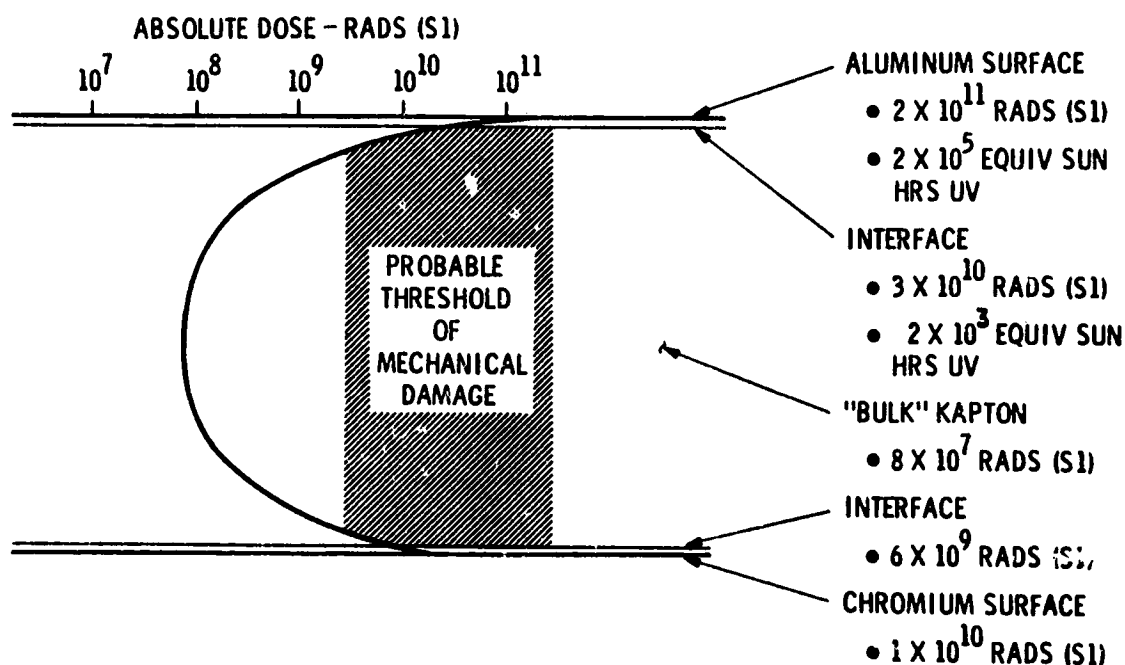
Figure 4-50. Absorbed Radiation Dose as a Function
of Position in Sail Film

The sample irradiated to 5×10^9 showed no apparent effects when removed to an N_2 purged bag at completion of the exposure. Within approximately 20 minutes it had broken into two pieces and by the following morning into small fragments.

From Fig. 4-50 it is obvious that this result raised concern about the integrity of the surface of the Kapton and the Kapton/aluminum interface for the Benchmark design. The concern did not extend to the viability of the Sail for the HCRM since significant additional attenuation of the radiation, down to acceptable levels (for HCRM) could be achieved with increased aluminum thickness and substitution of ITO for Cr on the back side.

The observed degradation·at 5×10^{10} rads raised several questions which would have required resolution for a HCRM but which were never addressed:

- Where, between 10^{10} and 5×10^{10} rads is the threshold?

- What is the nature of the (delayed) failure; is it characteristic of what would happen during the mission or the result of some secondary process?

- Would the damage adversely affect the Kapton/Aluminum adhesion?

- What levels of conservatism are in the curve in Figure 4-50? (Comparable profiles by MSFC indicated lower dose levels).

4.4.3.6   Electrostatic Control/Dissipation. Metallic or conductive semiconductor coatings appear quite promising as a means for dissipating electrostatic charge and enhancing the thermal emittance of the Solar Sail. The main points are:

(1) Thin metallic films (e.g., a few hundred angstroms of Cr, Al, etc.) are suitable to dissipate charge and improve thermal emittance.

(2) ITO ($In_2O_3SnO_2$) appears to be the most promising oxide semiconductor since SnO_2 requires a 300°C heat treatment and may be unstable,

(3) Sb doped SnO_2 is quite superior to SnO_2,

(4) The composition and vacuum deposition conditions can significantly affect the resistivity of ITO coatings,

(5) ITO coatings appear stable to UV radiation (1300 UVSH) and high temperatures.

(6) Vacuum deposition works well for both metals and semiconductors and is suitable for scale up process.

(7) The use of thin metal or semiconductor films to improve the thermal emittance involves an approach which combines the benefits of using high resistivity (high

emissivity) materials in an interference filter type
configuration.

(8) The most promising backside coating from both electro-
static dissipation and thermal emittance appears to be
~100Å Cr or ~1000Å ITO. A potential problem with this
thickness of chrome is an increase in resistivity with
creasing, it becomes oxidized and non-conducting in air
at elevated temperatures, and may not provide enough
particulate radiation protection to the Kapton film.

No problems with ITO related to space performance have been
identified. The only problem seems related to its conductivity as dic-
tated by the coating technique. Vacuum deposited ITO conducts, but
occasionally coatings of the ion-plated ITO were insulating. This is
most likely a function of coating technique where the oxygen content
entering the chamber strongly influences the morphology of the coating.
The major drawbacks of ITO for the Sail was the deposition thickness
required (1000Å) posed processing problems (multiple passes to achieve
desired thickness) and the experimental status of the coating technology.

4.4.3.7   Computer Simulation of Absorbed Dose.

Halley's Comet Rendezvous. A computer simulation of the absorbed
nuclear radiation dose over the HCRM was performed using a JPL derived
environmental particle distributions analysis. The purpose of this
effort was to estimate the magnitudes of the space radiation effects on
the Solar Sail film and surface coatings. The four primary degradation
environments were:

(1) Earth's Radiation Belts

(2) Solar Wind

(3) Solar Flares

(4) Cosmic Rays

The particle interactions, fluence peak flux and dose distributions
through the film were computed using a shield computer program.

The general earth-solar wind relationship is shown in Figure 4-51. The solar wind direction, is canted with respect to the earth's proton and electron belts. The radiation effects analysis takes into account the orientation existing from launch, January 1982 to Halley's Comet rendezvous in March-April 1986. The fluences expected for a HCRM are shown in Table 4-35. The solar protons tend to occur in conjunction with sunspot maximum which should peak around 1980 and diminish until 1986. (Figure 4-52.)

I: the computer simulation, the basic environmental distribution shown in Figure 4-51 was used at the 95% level whenever an option is given. The results (Figures 4-53, 4-54, 4-55, and 4-56) show the flux, fluence, dose rate, and dose distributions through the benchmark coated polymer film.

Passage Through the Earth's Radiation Belts. A calculation was performed to determine the amount of dose received by a single fast passage through the earth's Van Allen belts. The dose profile from protons and electrons impinging on a single side, i.e., the aluminum is shown in Figure 4-57. The radiation dose is low compared to the levels obtained over the total mission, most of which is received during the cranking orbit at 0.25 AU.

Surface Erosion Calculations. An investigation of the effect of high energy protons and electrons on the aluminum and chromium metallization of the benchmark configuration was also performed. Because of their heavier mass, high speed protons were considered to be capable of inflicting the greater damage. The results are as follows:

Percent of Atoms Removed

Aluminum (10^3 Å)	Chromium (125 Å)
0.25	1.46

Worst case assumptions were used in this study but the effects were found to be negligible. The main elements formed by direct activation were Si^{27} and Mn^{52}, both position emitters.
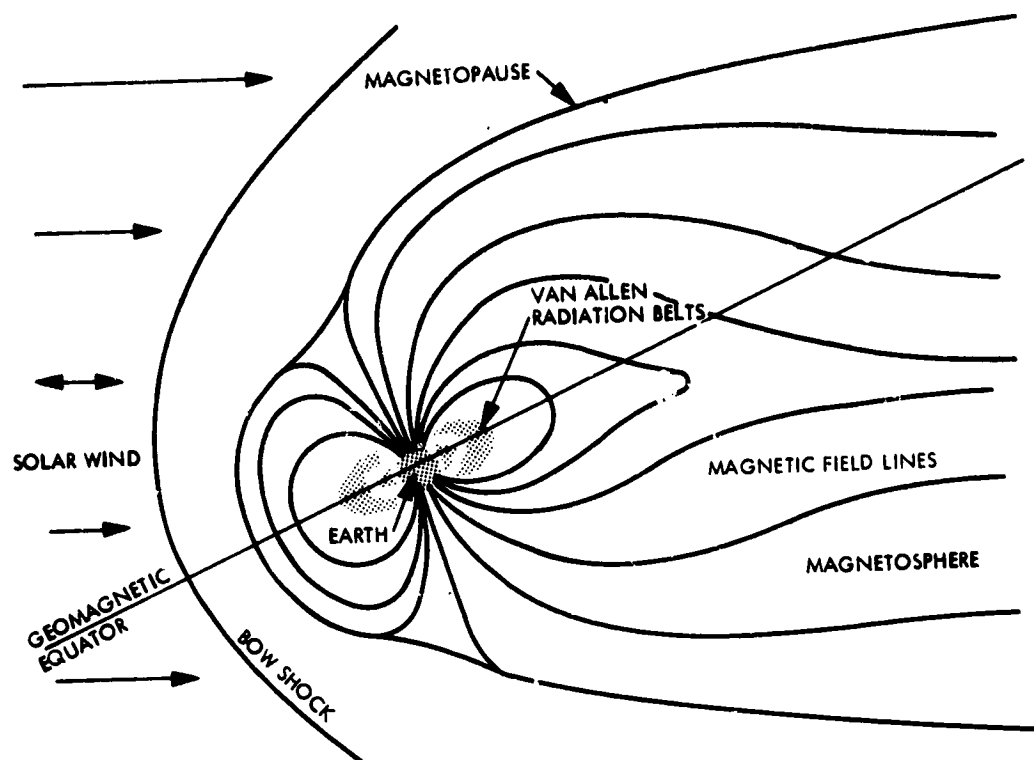
Figure 4-51. Earth-Solar Wind Relationships
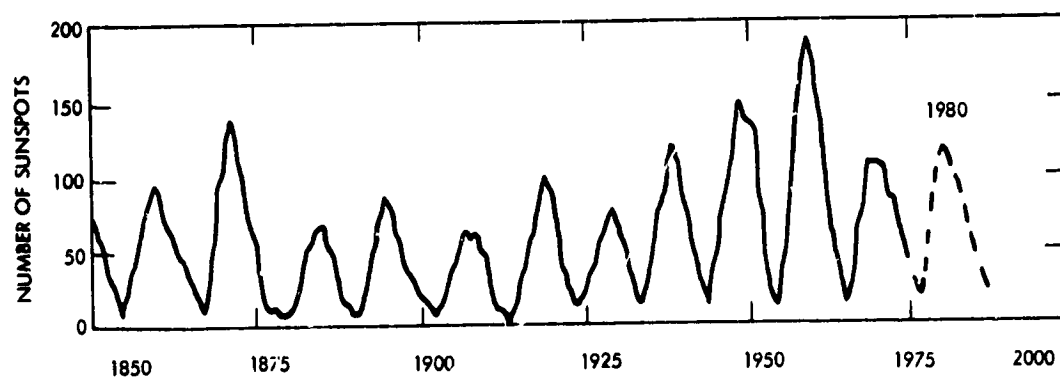
Figure 4-52. Predicted Sunspot Activity
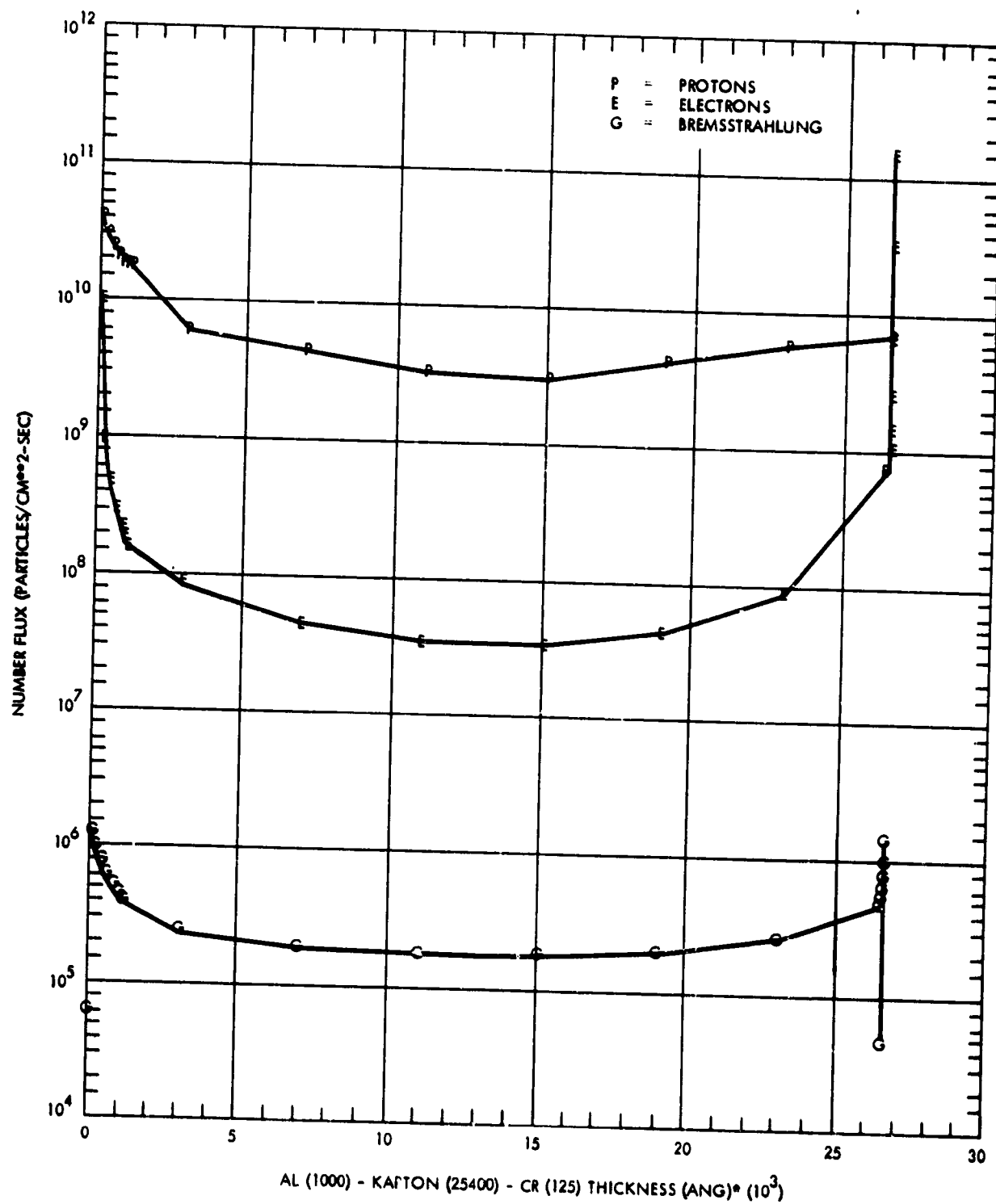
Figure 4-53. Particle Flux (0.25AU) - Solar Sail (2 Sides Inc)
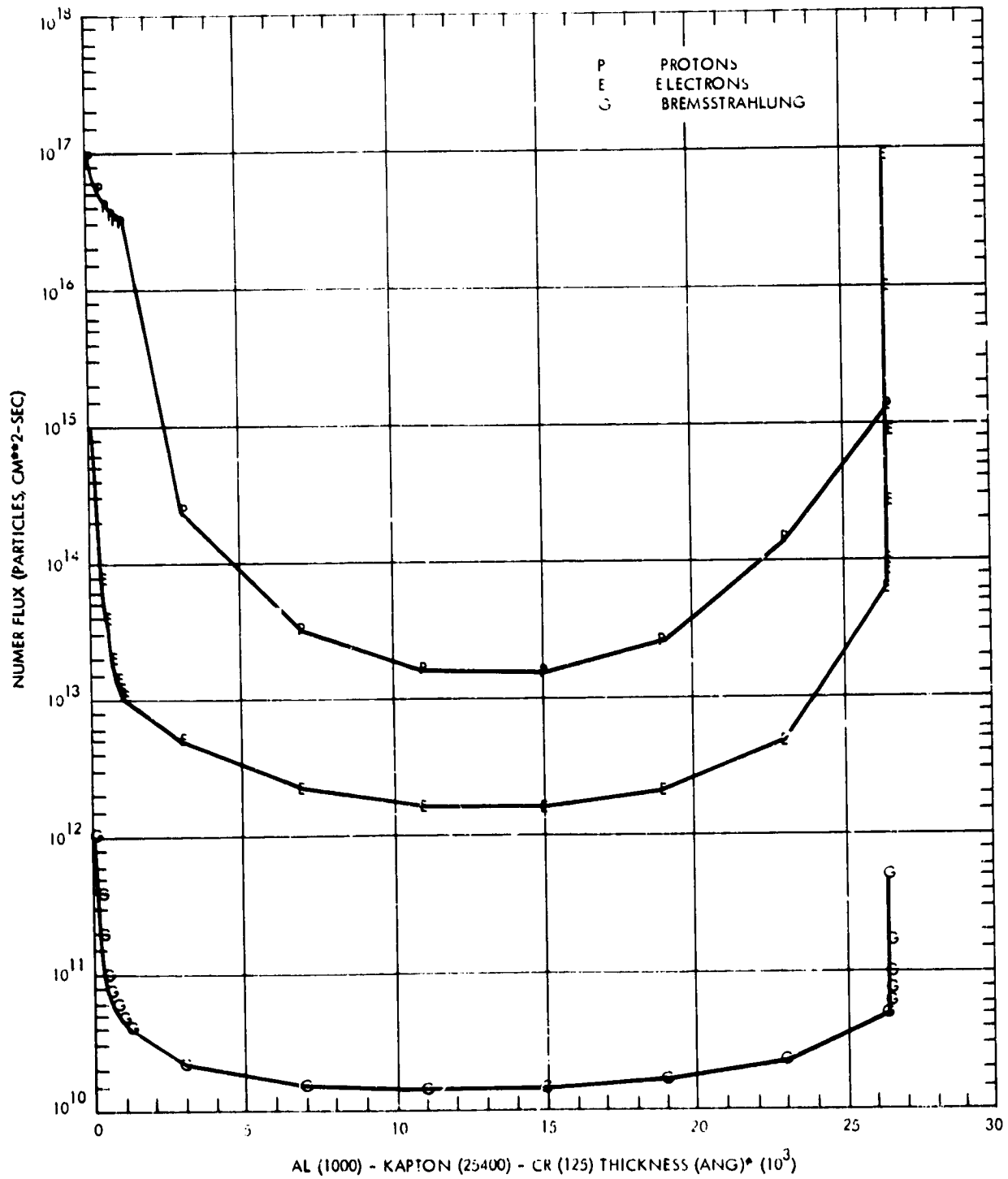
Figure 4-54. Particle Fluence (0.25AU) – Solar Sail (2 Sides Inc)
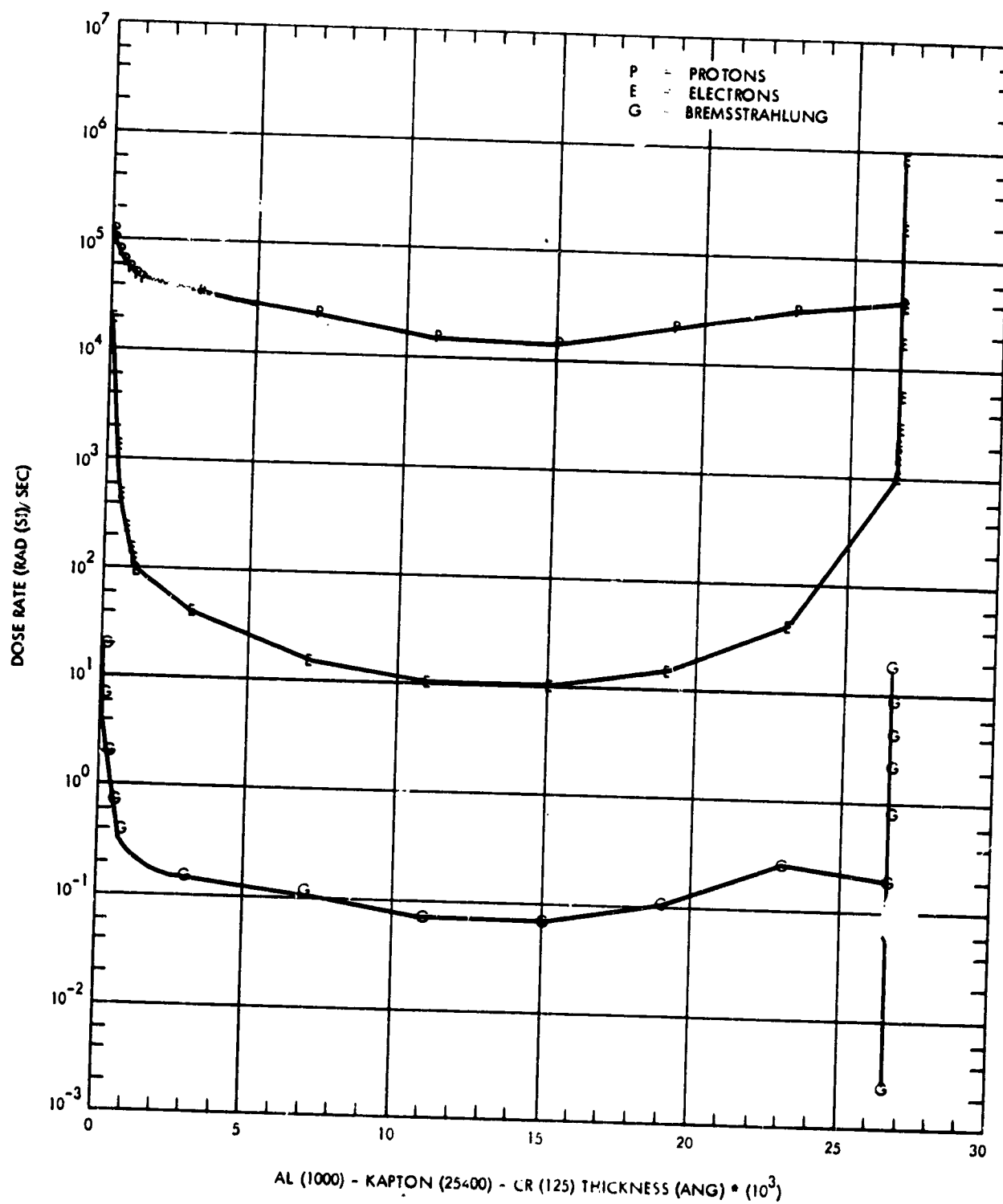
Figure 4-55.   Dose Rate (0.25AU) - Solar Sail (2 Sides Inc)
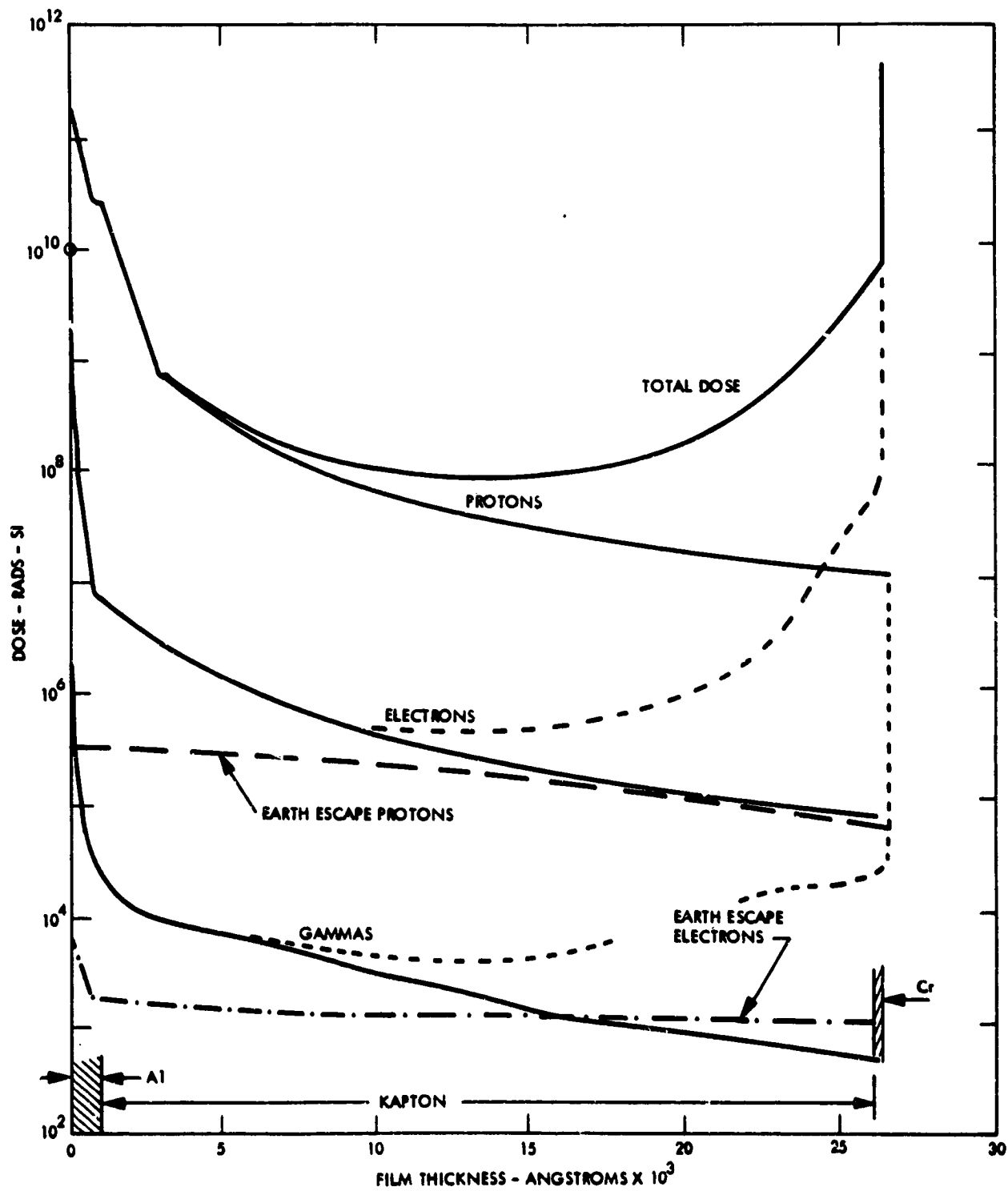
Figure 4-56. Dose vs Solar Sail Thickness

Table 4-35. Fluences for Halley's Comet/Solar Sail Mission

Particles	Environment	Energy, E	Integral Fluence, F (cm^{-2})			
			Probability that F is Not Exceeded			
			50%	75%	90%	95%
Inter-planetary Protons	Solar Wind	0	1.9(17)			
		900	1.9(17)			
		1 keV	1.5(17)			
	Intermediate Energy Protons	10 keV	3.0(15)			
		100 keV	5.9(13)			
		1 MeV	1.2(12)	1.2(12)	1.2(12)	1.2(12)
		1.4 MeV	6.6(11)	6.6(11)	6.6(11)	9.6(11)
		2.8 MeV	2.0(11)	2.0(11)	4.4(11)	6.0(11)
		8.5 MeV	9.4(10)	9.4(10)	2.1(11)	2.9(11)
	Solar Proton Events and Cosmis Rays	10 MeV	7.8(10)	8.7(10)	1.9(11)	2.6(11)
		30 MeV	1.0(10)	3.1(10)	6.8(10)	9.2(10)
		60 MeV	3.4(9)	9.9(9)	2.0(10)	2.8(10)
		100 MeV	1.0(9)	2.4(9)	4.8(9)	6.6(9)
		1000 MeV	2.1(8)	2.1(8)	2.1(8)	2.1(8)
Inter-planetary Electrons	Solar Wind	0	1.8(18)			
		10 eV	1.8(18)			
		20 eV	1.6(18)			
		30 eV	1.2(18)			
	Intermediate Energy Electrons (Solar and Jovian)	100 eV	1.8(17)			
		1 keV	8.5(14)			
		10 keV	4.0(12)			
		100 keV	2.0(10)			
		1 MeV	9.3(7)			
	Cosmic Rays	10 MeV	2.2(7)			
		100 MeV	2.0(7)			
		1000 MeV	7.4(6)			
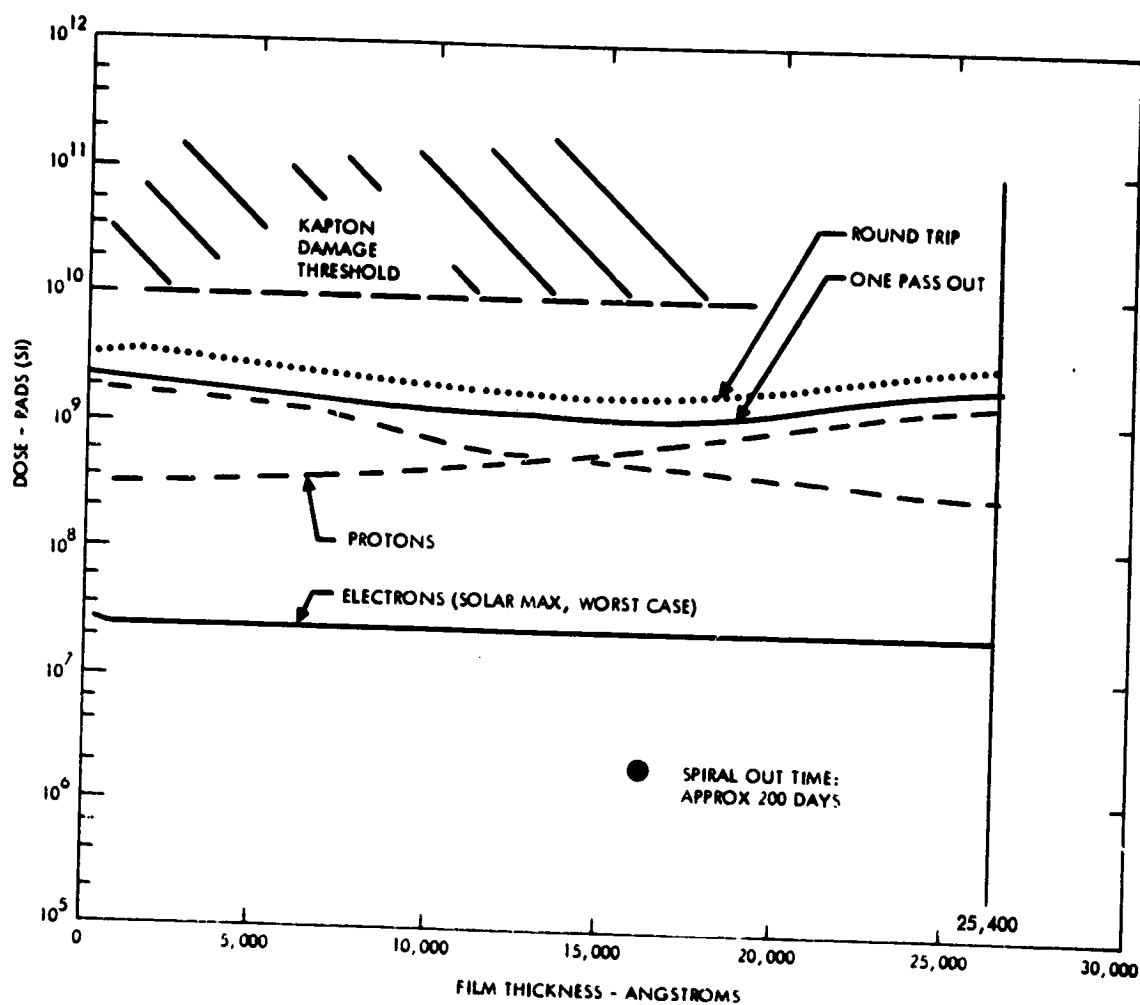
Figure 4-57.   Film Dose vs Thickness Earth Spiral

Percent of Atoms Activated

Aluminum (10^3 Å)   Chromium (125Å)

6 x 10^{-6} 1.10^{-7}

For the environment postulated, both effects are estimated to be negligible.

Future Work.   The preliminary evaluation of the effect of space radiation on thin Solar Sail films were completed in this initial effort.   The primary environmental effects that have been treated are absorbed dose computer simulation supplemented by limited radiation testing and theoretical damage calculations.

Although major concern areas were identified, future work needs to be performed in evaluation of subtle radiation effects that remain. Examples are: ion effects on coatings, high energy particle reactions, surface contamination effects, free radical formation, diffusion phenomena and synergistic effects. These and other areas are potential investigation topics that should be pursued both theoretically and experimentally in order to verify practicality of the Solar Sail concept.

4.4.3.7 <u>Miscellaneous Analytical Methods</u>. To obtain more information about the surface chemistry and physics, and adhesion and interfacial mechanics of the Sail film and its bonds; a study was conducted (under contract to JPL) by the Rockwell Science Center, Thousand Oaks, Ca. The purpose of this study was to investigate and analyze Sail film materials by means of some special refined diagnostic and analytical techniques developed by Rockwell.

Their technical approach was divided into two phases: analytical tools and high stress (accelerated) testing. The tools consisted of:

(1) Ellipsometry - a technique for analyzing and investigating interfaces

(2) Water contact angle - provides information on the surface conditions of polymers and metals.

(3) Surface potential differences - to investigate surface effects of metals

(4) Photoelectron emission - another method for characterizing and investigating metal surfaces.

The information obtained from the use of these techniques is basically derived from comparative analysis and was to be used primarily in investigating Solar Sail materials before and after space effects testing to simulate the space and solar radiation at 16 suns intensity. For example, the test specimens from the previously discussed tests conducted at the Boeing Co. and at Brookhaven Labs were to be further analyzed using these "tools". For reasons given in the section discussing

these latter tests, the resultant specimens were not suitable for further analytical study. However, Rockwell was able to demonstrate that the four analytical techniques were capable of yielding reproducible and characteristic readings on control samples of the film materials.

In the area of high stress testing, Rockwell conducted experimental work to develop the following types of accelerated tests:

(1) Coating Integrity - Exposure to polar solvents - metallized (Al and Cr) films heated in polar solvents should eventually separate or delaminate from the polymer substrate. The time-to-delaminate can be considered a measure of coating bond strength, for a fixed solvent and temperature condition. Alternatively, intermediate exposure times should result in reduced bond strength which could be used to calibrate the tools.

(2) Temperature cycling - metallized film was thermally cycled from room temperature to 250°C once every 6 minutes.

(3) Thermal shock - metallized films were heated to 260°C and allowed to stabilize at that temperature. They were then quenched in liquid nitrogen. This step was repeated through several cycles.

(4) Vibration - strips of metallized film were placed in slight tension by clamping the ends between two fixed grips. The center of the film strip is then attached to a vibrating piston operating at 40 Hz and an amplitude of 0.25 inch.

These four tests were devised to simulate the mechanical and thermal environments that the Sail film might experience both in the pre-launch and mission environments. They found that the surface characterization of the film changed with some of the degradation processes, e.g., thermal cycling, vibration cycling. However, the changes observed were not relatable to physical degradation that might occur under

anticipated Solar Sail service conditions. Visual observations of the metallized film material after exposure to drastic thermal and mechanical shock or cycling indicated that it was very stable. However, the analytical tools developed, indicated that in some cases the chromium layer was detrimentally affected. This was also observed viaually at times.

At the time that work was suspended on the Sail program, Rockwell had demonstrated the capability of their sophisticated analytical tools to characterize the Sail film materials on control specimens. Unfortunately, they were not able to verify their findings by characterizing samples that had been exposed to simulated space and solar radiation, e.g., the Boeing and Brookhaven tests.

REFERENCES

1. Kurland, R., et al., "Properties of Metallized Flexible Materials in the Space Environment, Final Report," SAMSO TR 78-31, January 1978.

2. Fogdall, L.B., and Cannady, S.S., "Study of Front-Surface Aluminized Kapton Films Under Combined Electron, Proton, and Ultraviolet Radiation," Boeing Document D180-24073-1 (in preparation).

3. Murayama, T. and Lawton, E.L., "Dynamic Loss Energy Measurement of Tire Card Adhesions to Rubber", J. Appl. Poly Science, 17, p. 669 (1973).

4.5   SUPPORTING STRUCTURES

At the time the Heliogyro design concept was adopted for the Solar Sail vehicle, the structural materials for the previously pursued square sail were still under study and not sufficiently finalized to warrant inclusion in this report. The following discussion of supporting structures is, therefore, limited to the Heliogyro version. The information presented in this section is directed at the consideration of Solar Sail propulsion in the future, which will definitely employ the Heliogyro concept in view of its high efficiency and unique maneuverability.

For the convenience of the reader, the discussion includes some essential design aspects, even though they may have been covered earlier in this report.

4.5.1   Identification of Structural Components

From the viewpoint of overall design and material requirements, the Heliogyro structures may be divided into three major subassemblies: (1) the hub structures which provide the structural support, the deployment mechanism and the pitch control of the blades, (2) the flap hinge brace assembly which may be considered as blade root structure, and (3) the blades. These subassemblies and their major components are identified in Figure 4-58 with the nomenclature used throughout this chapter.

An overview of the individual structural components is presented in Table 4-36, together with the quantity per vehicle, the largest dimension and the identification code of the section in which they are discussed. For completeness, the table includes a few non-structural components (in parentheses).
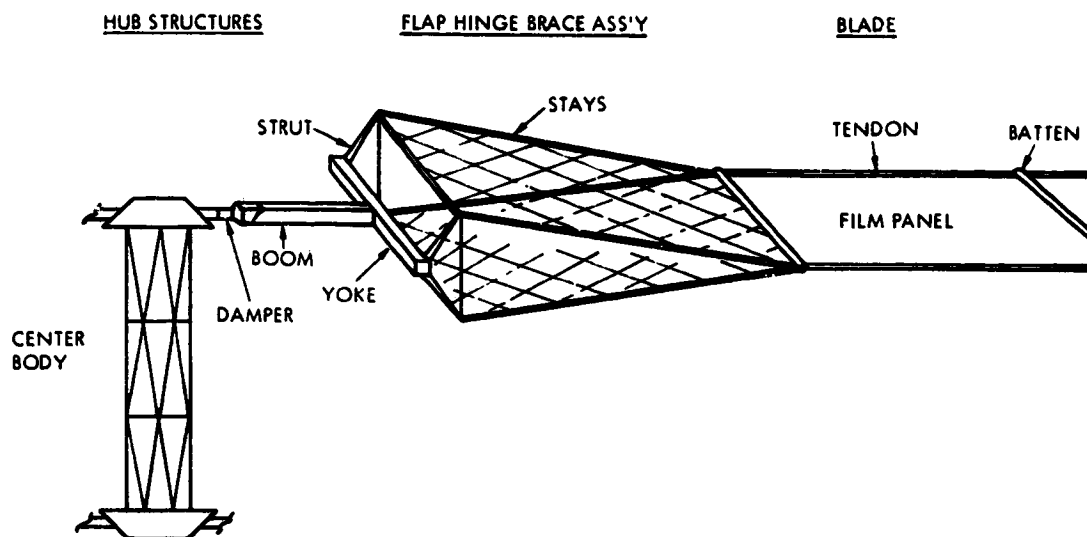
Figure 4-58. Major Heliogyro Structural Components

4.5.2 Material Requirements and Generic Materials Selection

The most basic requirements of structural materials for
overall systems efficiency are high strength and/or stiffness, low mass
(weight) and high dimensional stability throughout the temperature
range from near-sun orbit to aphelion. These requirements can be
translated into the following material properties:

High Strength to Weight Ratio

High Stiffness to Weight Ratio

Low Thermal Expansion Coefficient

In the early part of the study, aluminum, titanium and polymer-base com-
posites were considered as candidate materials. A first-order analysis
was performed on the basis of merit functions representative of the

Table 4-36. Major Heliogyro Components

Components	Qty.	Max. Dim. (in)	Section
HUB Structures			
Center Body	1	9.55	4.5.4.1
(Spacecraft)	(1)		
Boom	12	4.75	4.5.4.2
Yoke	12	8.2	4.5.4.2
Damper	12	0.15	4.5.4.3
Reel	12	8.1	4.5.4.4
(Pitch Motors)	12	0.4	
Flap Hinge Brace Assembly			
Struts and Tie Bars	48	3.5	4.5.4.5
Stays	24	172.0	4.5.4.5
Blade			4.5.4.6
Tendons	24	7,340.0	4.5.4.7
Battens	1,068	8.0	4.5.4.8
x) Cross-Tendons	11,520	8.1	4.5.4.9
x) (Film Panels)	5.760	15.0	(4.5.4.9)
(End Mass)	12	8.0	

x) applicable only to one optional design (individual film panels suspended with cross-tendons.)

above postulated requirements. The comparison of the candidate materials with regard to the strength merit function F_{tu}/ρ, the stiffness merit function E/ρ and the thermal dimensional stability merit function $1/\alpha\epsilon$ indicated a distinct superiority of graphite/polymer composites, as illustrated in Figure 4-59. However, the high temperatures encountered during flight phase II (solar cranking orbits) limited the choice of the composite matrix to polyimides. Graphite/polyimide composites were, therefore, selected as the preferred structural material to be applied wherever feasible.
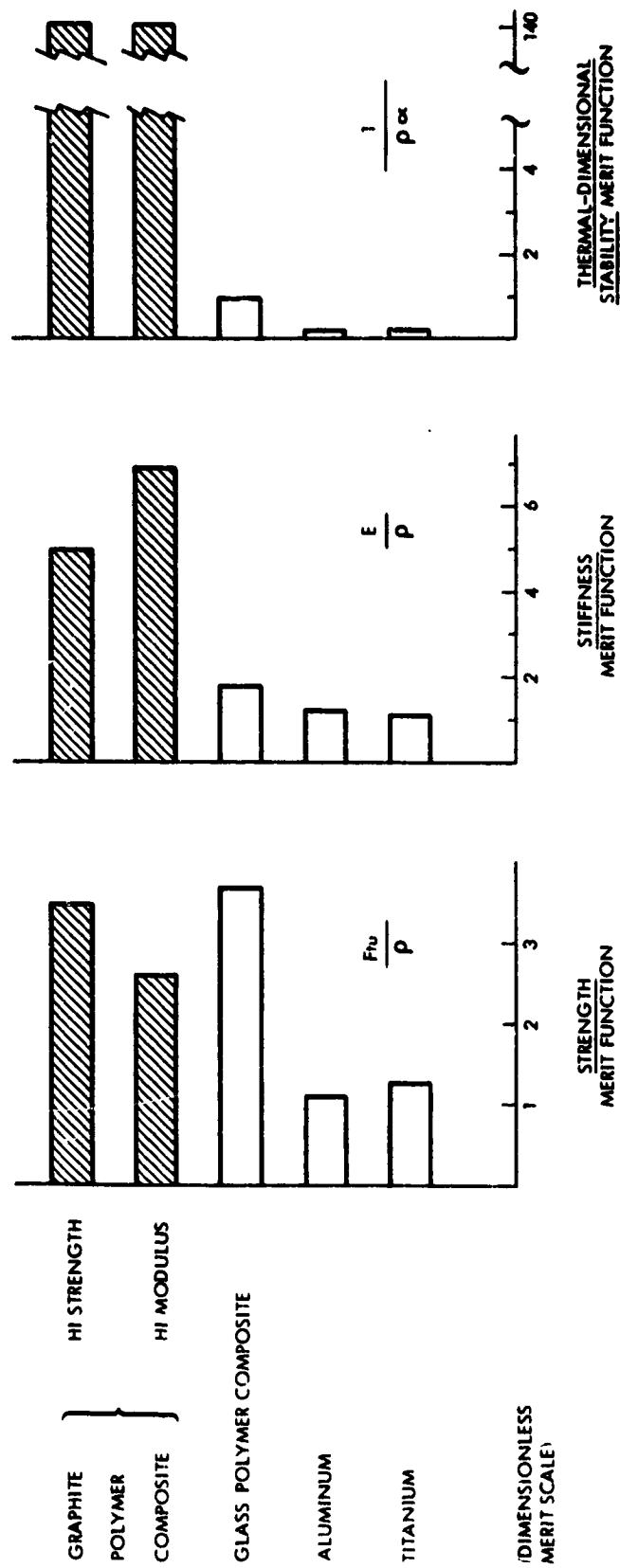
Figure 4-59. Property Merit Functions of Candidate Materials Illustrating
Superiority of Graphite/Polymer Composites

4.5.3   Selection of Graphite/Polyimide Composites

The selection of specific polyimide types as composite
matrix material was based on three criteria: (1) maximum temperature
capability, (2) curing requirements and reproducibility, and (3) adapta-
bility to joining. An evaluation of various commercially available
polyimides led to the selection of the following types:

Polyimide	Max. Temp.	Joining
NR-150-B2	$330^{\circ}C$ ($620^{\circ}F$)	Thermoplastic
PMR-15 } LARC-160 }	$290^{\circ}C$ ($550^{\circ}F$)	Adhesive Bonding

DuPont NR-150-B2 emerged as the most attractive matrix
material since it combines hightest temperature resistance with ease of
joining due to its thermoplastic characteristics; however, the curing
cycle is somewhat complex, and effective joining by thermoplastic
methods has not been adequately demonstrated in composite applications.
PMR-15 (NASA-Lewis) and the alternate LARC-160 (NASA-Langley) offer the
advantage of highly reproducible curing characteristics, yet exhibit
more limited high--temperature capabilities; since both are thermoset-
ting, joining can only be accomplished by adhesive bonding. Ultimate
matrix selection is governed by the temperature and joining requirements
of specific components.

The choice of graphite fibers depends likewise of the
requirements of the specific component. Tension-critical components
call for a high strength fiber, such as HTS, Celion 6000, Modmore II or
Thornel 1000, and stiffness-critical components for a high-modulus
fiber, such as HMS or GY-70. All candidate fibers exhibit an extremely
low (negative) thermal expansion coefficient, which can be adjusted to
zero in multiple-layer composites by an appropriate orientation
pattern.

The extreme time limitations of the Heliogyro program (5
months) did not permit an experimental evaluation of the selected

materials. All property definitions were, therefore, derived from data provided by material producers, from NASA-sponsored experimental evaluation programs and from theoretical studies. The tentatively adopted design data for various graphite/polyimide composites and structural component categories (as of the time of program termination) are summarized in Table 4-37 (primary data source: Reference 3).

4.5.4   Materials for Individual Structural Components

This section defines the materials selected for individual components on the basis of structural loads, temperatures, operational considerations and producibility. The temperature data are based on the following optical properties of graphite/polyimide composites:

Uncoated	Absorptance	0.80
	Emittance	0.80
Al-Coated	Absorptance	0.15
	Emittance	0.05

Total Emittance (Near-flat, sun
        facing side Al-coated)   0.85

Note that the data for the Al-coated composite are somewhat highe.. than for the Al-coating of the film (0.12 and 0.03), accounting for surface degradation during assembly and operation.

4.5.4.1   Center Body.

The center body, which serves as central hub for the blades, is a tubular truss structure, 9.55m in length and 1.5 m in diameter (Figure 4-60). The length of the individual tubings (truss elements) varies from 0.7 to 1.3 m and the diameter from 2.5 to 10 cm.

Temperatures: Since the center body as a whole remains at a constant sun angle, the tubings can be selectively coated to minimize material temperatures. However, due to the varying orientation of individual truss members, the temperatures vary from app. 230 to 325°C (450-620°F). This temperature range dictates the use of NR-150 as matrix material.

Table 4-37. Properties of Graphite - Polyimide Composites Based on Test Data, Except (=) Engr. Estimates

Component / Construction	Dens. ρ g/cm³	Material Polyim.	Material Fiber	Temperature Level	°C	°F	Tension Ftu (ksi)	Tension E (msi)	Compression Ftu (ksi)	Compression E (msi)
Tendon Tapes										
Unidirectional, 1 mil thick, 0.6-2.1 cm wide	1.58	NR 150-B2 (710) (LARC 160)	HTS (Celion 6000)	MAX	234	454	130	17.5	44	16.0
				RT	24	75	130	18.0	82.5	16.0
				MIN	-100	-150	120	17.5	82.5	15.5
Batten Tapes x)										
Unidirectional, 1 x 1 mm and, 0.5 x 1 mm	1.60	NR 150-B2 (710) (LARC 160)	HMS (CY 70)	MAX	260	500	129	25.5	(50)	26
				RT	24	75	131	26.0	(60)	27
				MIN	-100	-150	124	25.5	(55)	(27)
Tubings ≤ 10 cm dia ≤ 30 mil thick (0, +45, -45, 0, 0, 0)	1.59	NR 150-B2	HMS (CY 70)	MAX	320	610	89	17.5	37	18.2
				RT	24	75	91	18.0	45	19.3
				MIN	-100	-150	80	17.3	41	19.3
Tubings < 5 cm dia (0, +45, -45, 0, 0)	1.59	NR 150-B2	HMS (CY 70)	MAX	320	610	80	16	35	16.5
				RT	24	75	83	16.5	42	18
				MIN	-100	-150	73	16	38	18

x) Assuming thermal shielding of battens
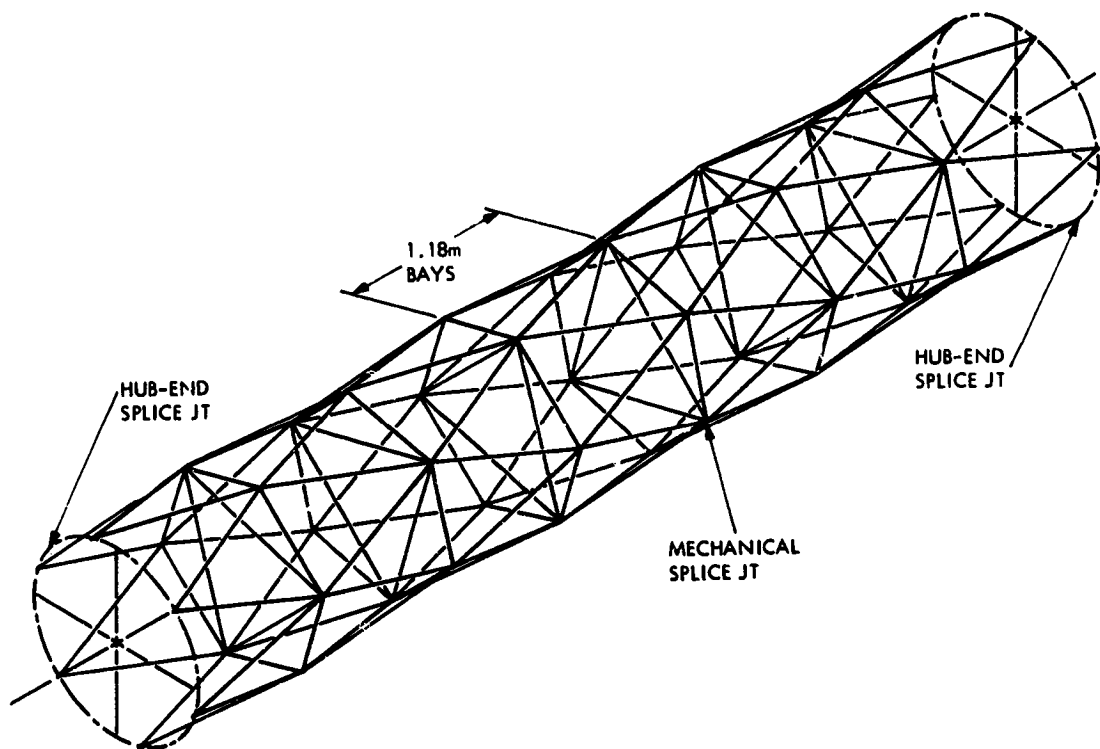
Figure 4-60. Center Body

Loads: The center body is primarily stiffness-critical with high compressive loads, calling for a high-modulus fiber.

Base Material: Composite tape, 2.5-3.5 mil thick, with the following composition:

Matrix: NR-150-B2

Fibers: GY-70 or HMS

Tubing Construction: The tubings are manufactured from the base material tapes by multiple lay-up in 0°, $+45^o$ and -45° orientation, with a maximum permissible number of 0° layers to increase stiffness and compressive strength. This may necessitate an "unbalanced" lay-up

pattern, which is acceptable for tubings. Composite wall thickness and number of layers are as follows:

Tubing Diam. mm (in)	Wall Thickn. mm (mil)	No. of Layers
25 (1)	0.38 (15)	5
50 (2)	0.56 (22)	7
75 (3)	0.76 (30)	9
100 (4)	0.76 (30)	9

Assembly: Individual tubings are connected with titanium alloy brackets. The necessary adhesive bonding requires pressure which can be easily applied to the first bracket by the use of an expandable and retractable internal mandrel (Figure 4-61A). A problem arises for the second bracket, as the closed system precludes the insertion of a mandrel. The use of slightly tapered tubings (advantageous also in tubing fabrication) and brackets generates sufficient pressure as the tubing is inserted in the bracket (Figure 4-61B). The bracket holes are drilled to exact distance after bonding.

4.5.4.2   Booms and Yokes. The function of these two components is the deployment and retention of the blade. They are essentially box-beams with rectangular cross-section and one open (longitudinal) side (see Figure 4-58). Outisde dimensions are as follows:

	Boom	Yoke
Length (m)	4.75	8.2
Cross-section (m)	0.4 x 0.4	0.4 x 0.5

The original design as one single unit with flat/thin walls, produced by composite lay-up techniques in one operation, appeared quite feasible. It was, however, later replaced by a tubular design in view of the more predictable stiffness characteristics and the higher confidence in producibility. The length of individual tubings ranges from 0.35 to 0.6 m with outside diameters of 25 to 38 mm (1 to 1.5 in.).
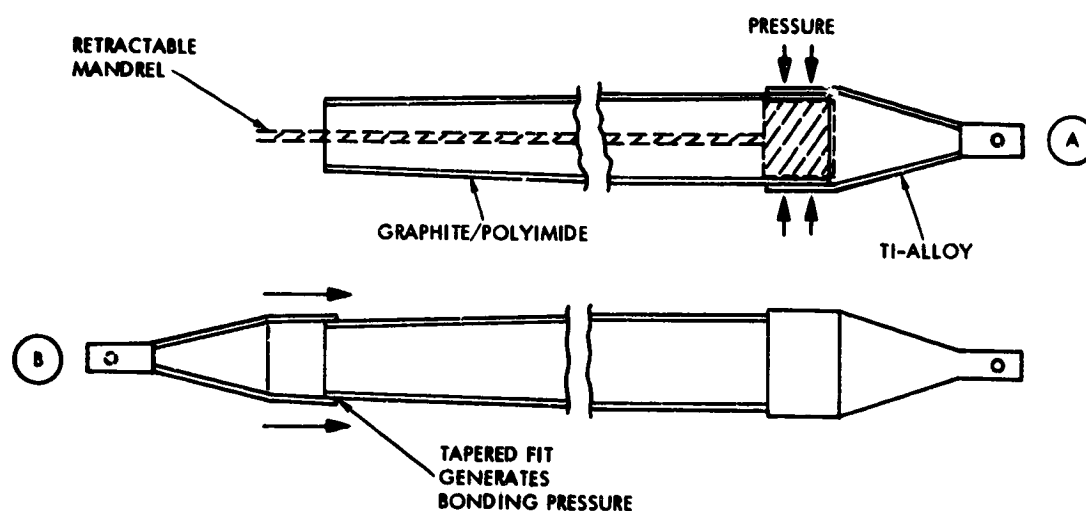
Figure 4-61. Assembly of Truss Members (Adhesive Bonding
of Tubings to Brackets)

Temperatures: Booms and Yokes are subjected to the same cyclic pitch-
ing and, consequently, sun angle as the blade (for details on thermal
cycling see section 4.5.4.6). Even with partial Al-coating, excessive
composite temperatures up to 400°C (750°F) would be encountered at the
transient minimum sun angle of 10°. during high-pitch periods. Further
studies and computer analyses showed that these unacceptable tempera-
tures can be reduced to less than 315°C (600°F) by covering the tubings
with HRSI insulation, (as used in the space shuttle), which is a low-
density felt-like material composed of fine quartz fibers. An insula-
tion thickness of 2 mm, representing a 20% weight penalty, reduces the
temperatures for 25-100 mm diam. tubings to 280-305°C (530-580°F),
respectively.

Materials: Since these temperatures as well as the loads are similar
to the center body, the tubings for booms and yokes can be produced

from the same base material and by the same techniques as specified for the center body (section 4.5.4.1).

4.5.4.3 Damper. The damper, located between the inboard end of the boom and the pitch control mechanism, has a length of app. 0.15 m and a diameter of app. 0.4 m. The use of silicone rubber together with a simple heat shield appears to present no problem.

4.5.4.4 Reels. The reel, located inside the yoke, provides stowage for the blade and the flap hinge brace assembly prior to deployment. It has a length of 8.1 m and a diameter (at the spindle) of 0.3 m. It is primarily stiffness-critical and exposed to comparatively moderate temperatures. It is preferably produced from HMS fiber and LARC 160 or PMR-15 polyimide, except for the titanium tubing axle.

4.5.4.5 Flap Hinge Brace Assembly. This assembly provides the transfer and re-distribution of torsional and bending loads between the blade (first batten) and the yoke. Major structural components are: four struts, two tie-bars and two "stays" in the form of wide-mesh systems with edge tendons extending from the tie-bars to the first batten. The entire assembly is stowed on the reel (partly in the reel spindle) and is self-erecting upon full blade deployment.

The length of the struts and tie-bars is 3.5 m and 8.0 m, respectively. There are stringent limitations on the size and shape of their cross-section, as they have to fit into the reel spindle for stowage. Since they are further exposed to high compression and bending loads at appreciable temperatures, the use of NR-150-B2 and GY-70 fiber is mandatory for composite fabrication.

For the 172 x 8 m wire mesh panels, both quartz filaments and metal wire have been considered as alternate materials. The edge members may be fabricated from the same materials. The extension of the blade tendons to serve as edge members would be most straightforward, yet may be precluded by excessive differences in thermal expansion.

The wire mesh requires a certain redundancy to compensate for potential
micrometeoroid damage.

4.5.4.6   **Blades**. The blade represents the actual sail of the Helio-
gyro. It is stiffened in longitudinal or spanwise direction by the
centrifugal tension generated by the vehicle rotation and an end mass.
Figure 4-62 gives an overview of blade configuration and major data.
The total length from the flap hinge brace assembly to the end mass is
7,340 m at a constant width of 8 m. The centrifugal tension increases
from 12 N at the end mass to 764 N at the root (reel). The half-load
point, which is frequently used as reference value, is at 71% of the
total length in the spanwise direction (r/R = 0.71).

Since the ultrathin sail film cannot be subjected to any
structural loads, the tension is carried exclusively by two edge members,
designated as "tendons".
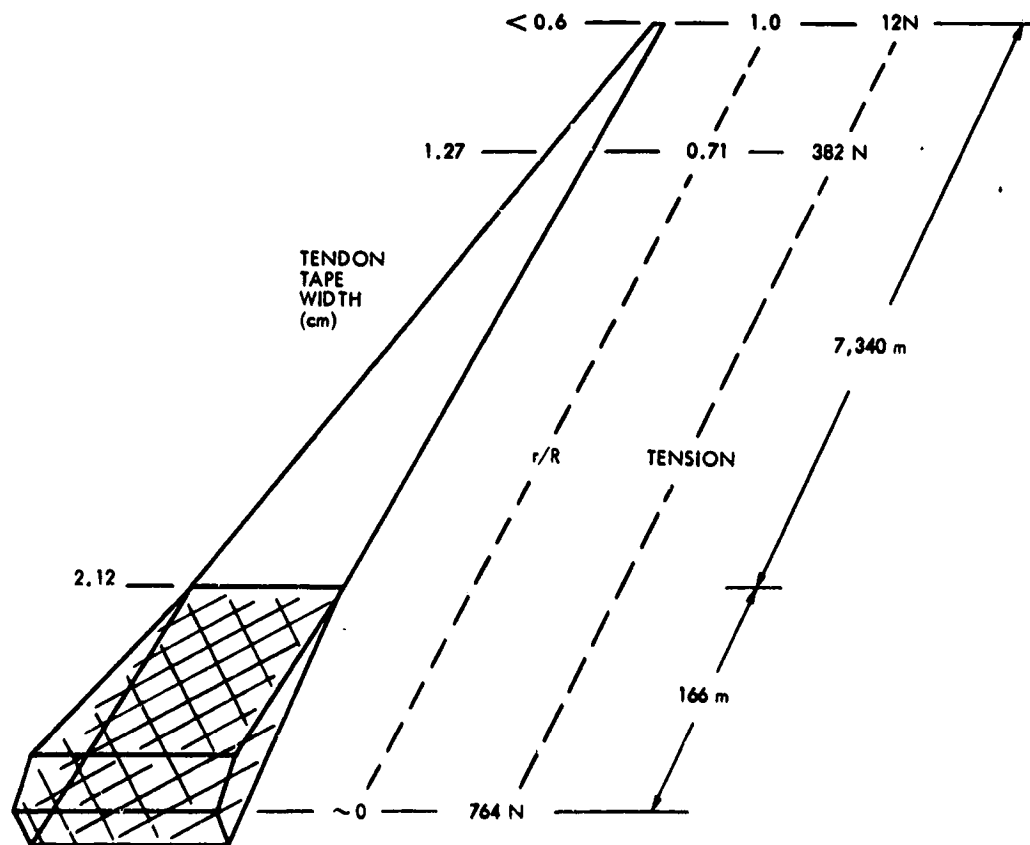
Figure 4-62. Heliogyro Blade - Tendon Data

The chordwise tension, generated by the solar pressure on the film - regardless of the mode of film attachment - has to be absorbed further by chordwise compression members or "battens", spaced at irregular intervals. There are a total of 89 battens in each blade, with an average spacing of 80 m. For the purpose of material definition and the mode of film attachment, the blade may be considered as consisting of 89 individual panels, in which tendons and battens provide a reasonably stiff framework for the suspension of the sail film.

Several designs for these blade panels have been evaluated in considerable detail. Three designs which had been defined to the level of preliminary manufacturing drawings are shown in Figure 4-63. In the first, the film is bonded to the tendons, resulting in a catenary edge curvature. Difficulties in maintaining film flatness led to the second design concept, in which individual film panels of app. 15 m length are attached to the tendons by means of clotheline-like cross-tendons.
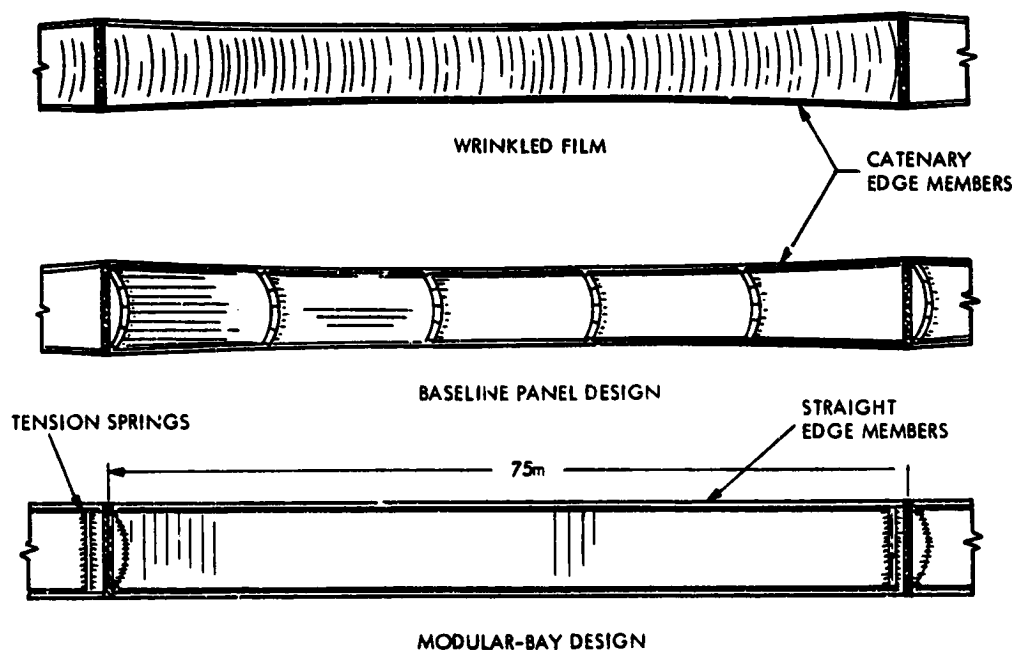
Figure 4-63. Blade Design Evolution

While this concept still requires catenary tendon curvature, it assures reasonable film flatness. In the latest design, the film is essentially attached to the battens, which illuminates the necessity of tendon curvature. It requires, however, a rather complex attachment mechanism to the battens or, rather, the batten/tendon intersect points.

Blade Temperatures: The temperatures encountered in the blade can be defined rather accurately due to the essentially two-dimensional configuration and the well predictable (programmed) change of position. This applies particularly to the tendons and the sail film.

During the cranking orbit, the blade is subjected to continuous pitching around the basic (coning) sun angle of 35°. Each pitch cycle has a duration of 465 seconds (2 revolutions). There are two types of pitch maneuvers, and consequently, thermal cycling as follows:

> (1) Continuous low pitch of $\pm 10^\circ$ (sun angle varying between 25° and 45° maximum). Total low-pitch time is 9.720 hours, comprising 75,180 thermal cycles.
>
> (2) 16 periods of high-pitch between 10° and 50°. Total high-pitch time is 384 hours representing 2,970 thermal cycles.

The two types of thermal cycles are illustrated in Figure 4-64 for the film, together with the associated temperatures. The cycle characteristics of the tendons are identical, except that temperatures are $8-11^\circ C$ lower (primarily due to the high emittance of the graphite-polyimide composite).
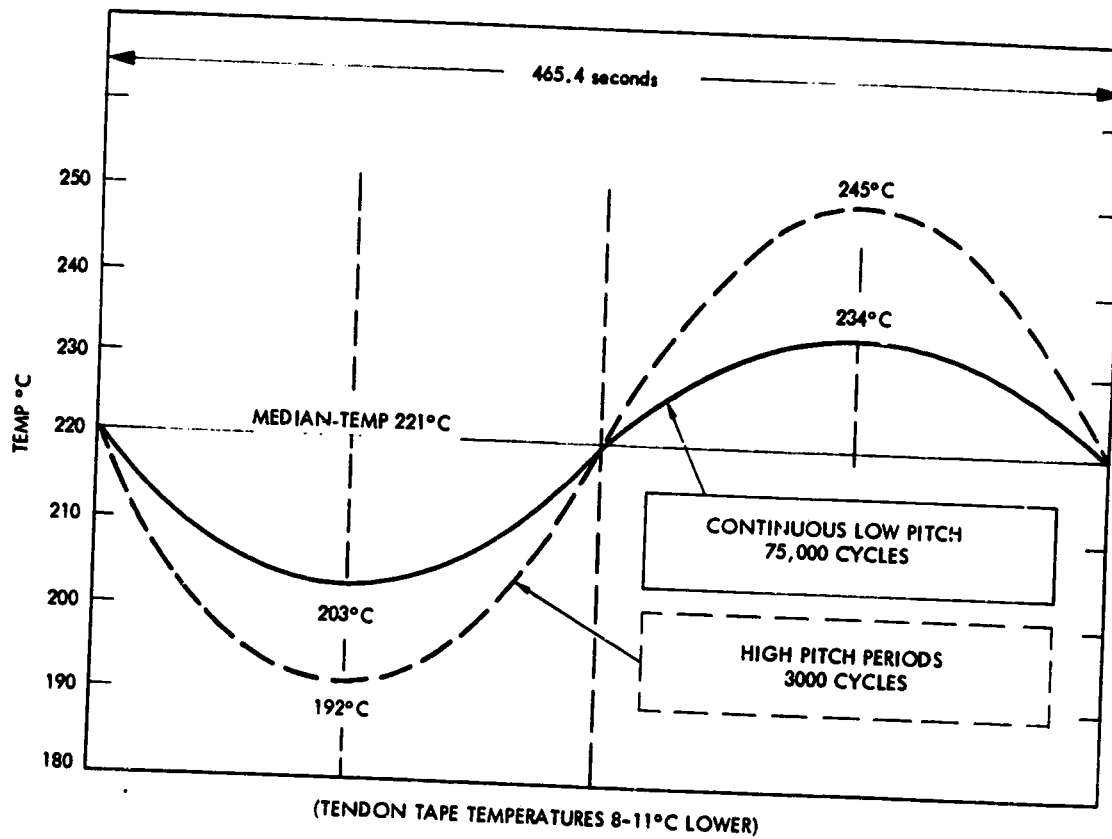
Figure 4-64. Blade Temperature Cycles (Near Sun)

The temperature computations were based on the following optical properties of film and tendon tapes:

Material	Property	Film	Tapes
Al-Coating	α_s	0.12	0.15
	ε	0.03	0.05
Cr-Coating	α_s	0.75	----
	ε	0.60	----
G/Pi Composite	α	----	0.80
	ε	----	0.80
Total Emittance	ε_o	0.03	0.85

The somewhat higher values for the Al-coating of the tapes account for surface degradation due to handling and rubbing on the reel. The values of the Al- and Cr-coatings are based on accurate measurements carried out by TRW; the values for the graphite-polyimide composite of the tapes are engineering estimates. The temperature maxima of 234°C for the film and 224°C for the tendons with excursions to 245°C for only 96 hours total are well within the capabilities of the selected composite materials, representing a substantial safety margin. Cumulative time vs. temperature is illustrated in Figure 4-65.

The temperature profile of the blade over the entire sail cruise time of 1,599 days is shown in Figure 4-66. As indicated, sub-zero temperatures are encountered during cruise phase III (aphelion) for approximately 750 days (18,000 hours), dropping down gradually to a minimum of -128°C. These low temperatures can be substantially relieved by blade reversal due to the high solar absorptance of the then sun-facing Cr-coating (film) and the uncoated side of the composite tapes. A temperature increase in the low-temperature regime is desirable with regard to shrinkage (localized effects as well as overall blade dimensions) and with regard to potential enbrittlement of the polyimide.

Temperature minima at aphelion for not-reversed and reversed blades are as follows:

		Film (°C)	Tapes (°C)
Not Reversed	– Median	-128	-131
	– Transient	-133	-130
Reversed	– Median	-44	-57
	– Transient	-52	-65
ΔT by Blade Reversal		81-84	71-74
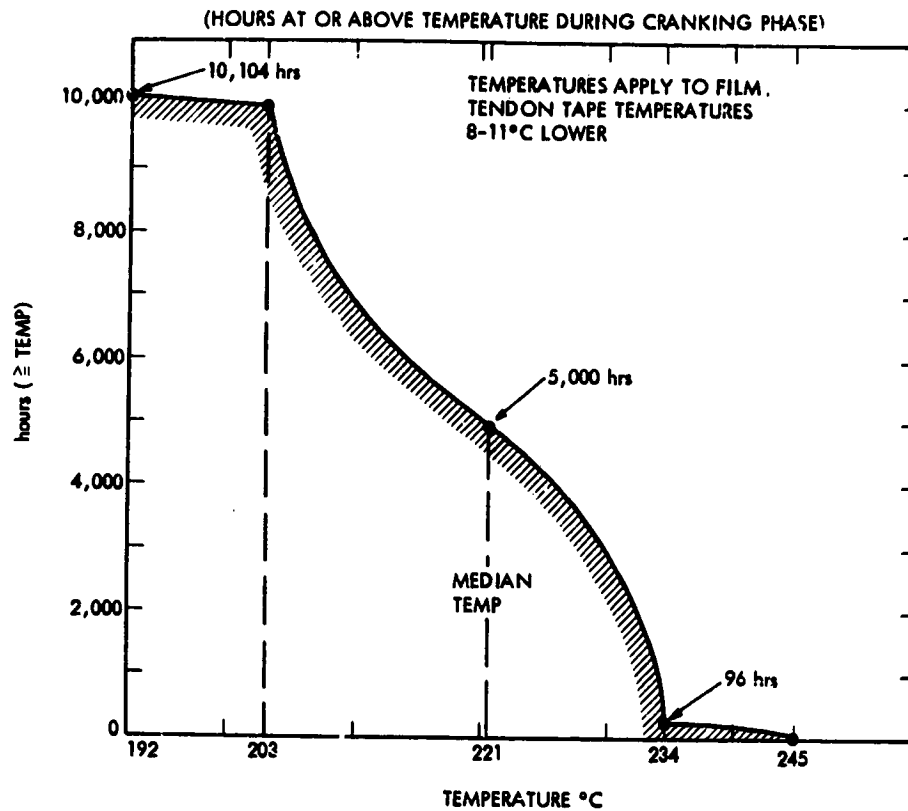
Figure 4-65. Cumulative Time at High Temperatures (Blade)
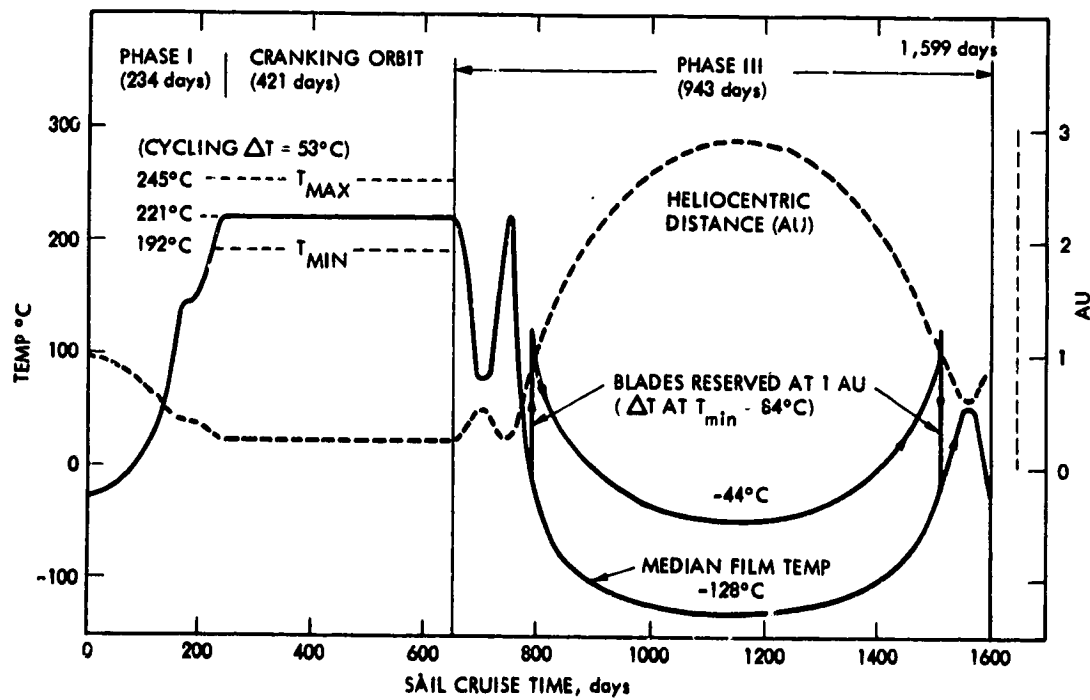
Figure 4-66. Blade Temperature Over Entire Mission Time

It is apparent that the blade temperature rises sharply during reversal and drops equally sharp during return to its original position. Temperature limitations of these excursions dictate a finite range for the timing of the reversal maneuvers. In Figure 4-67 this range is defined in terms of heliocentric distance and days past launch (shaded area). It represents various options between two limiting conditions for reversal and turnback:

a. Temperature is allowed to rise to the temperature of the cranking orbit (221°C). In this case the temperature has dropped to +42°C before reversal.

b. Temperature is allowed to drop to the minimum temperature encountered by the reversed blade at aphelion (-44°C). In this case the temperature rises from -44°C to +85°C during the maneuver.
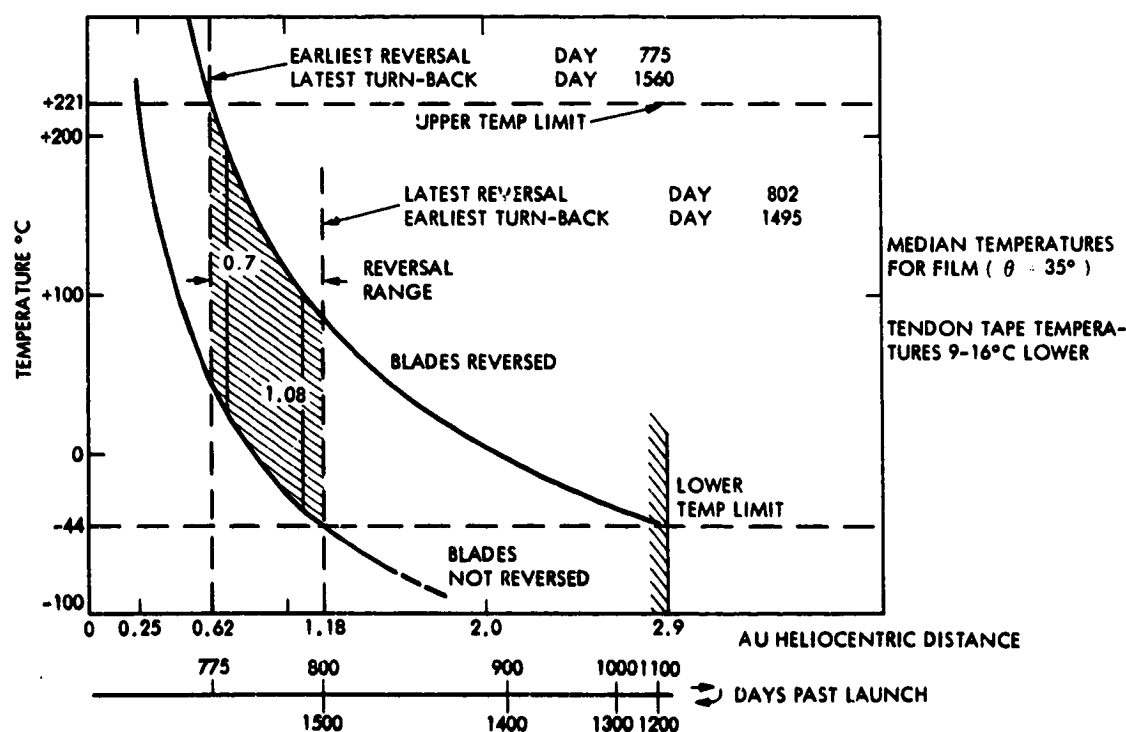
Figure 4-67. Range for Blade Reversal and Turn-Back

To provide a safety margin against overshoot or undershoot, the following two options are recommended (see Figure 4-67).

	Option A	Option B
Heliocentric Distance (AU)	0.70	1.08
Temperature – Maneuver Start	+20°C	-33°C
– Maneuver Completed	+195°C	+100°C
Days past Launch – Reversal	778	795
– Turn-back	1,545	1,520

4.5.4.7   Tendons. The primary criteria for materials selection and configuration of the tendons, representing the most delicate Heliogyro components next to the film, are

(1)   Load (tension) carrying capability at the cyclic temperatures defined in the foregoing paragraph.

(2)   Lowest thickness to minimize build-up on the reel during stowage.

(3)   Adequate resistance to meteroid impact.

It was clear from the outset, that a unidirectional graphite-polyimide composite is the ideal tendon material in view of its high strength at the encountered temperatures and almost zero thermal expansion. Since it further exhibits high creep resistance, the only dimensional change is due to elastic strain in the order of 0.2%, resulting of a total growth of the blade length upon full deployment by app. 15 m.

Base Metal Form: The prime criterion for base material form is the necessity of minimized thickness to prevent excessive stacking height during stowage on the reel (maximum permissible reel diameter is 0.6 m, which limits the stacking height to 0.15 m, including battens). Unidirectional graphite/polyimide tape of 1 mil thickness was adopted as target material, which was considered the ultimate feasible in view of the 0.3 mil diameter of the individual graphite fiber. Since this represented a substantial advancement of the state of art (limited to

minimum thickness of 2.5 mil), a developmental program was initiated jointly with Ferro Corporation which led to the successful production of 1-mil graphite/polyimide tape in continuous lengths up to 800 m.*

Tendon Design: The configuration of the tendons is solely determined by resistance to micrometeoroid damage. From the viewpoint of load carrying capability, a single 1-mil tape of a median width of 25 mm would be adequate. However, a single hit by a larger micrometeroid at one point of the total 7,340 m tendon length during the 4.38 year mission would result in the loss of the blade. This dictates a redundant tendon design consisting of several narrower tapes arranged so that the load is re-distributed in the case of the failure of one member.

The evaluation of various tendon designs was based on an integrated meteroid flux for the total mission time as defined in Figure 4-68 in terms of particles/m^2 vs. particle size. Further assumptions were a directionality factor of 1, an average particle density of 0.5 g/cm^3 and a mean impact velocity of 32.6 km/sec.

In a redundant (multi-tape) tendon, catastrophic failure occurs by either of three modes:

    (1)   Failure of an excessive number of redundant elements

    (2)   Simultaneous failure of more than one element at load transfer points (tape joints).

    (3)   Catastrophic failure of the entire tendon by a single large meteoroid hit.

It was found that no tendon design with less than 4 elements meets the requirement of appreciable resistance to catastrophic failure after failure of one edge element. The slope at tape intersect points, further, should be 0.059 or less to prevent combined axial and bending

---

*1-mil tape was also produced with epoxy and polysulfone matrix. An attractive spin-off of this capability is the potential of producing ultrathin multi-ply composites, as demonstrated by the successful manufacture of 7-ply panels with a wall thickness of only 9 mil.
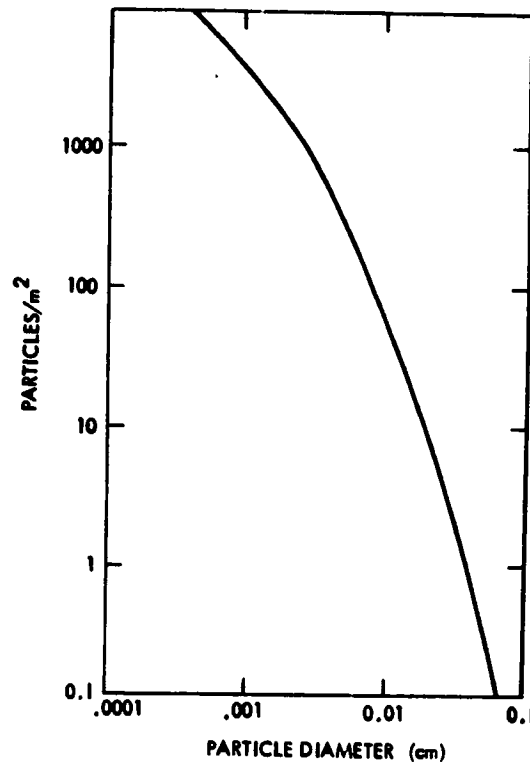
Figure 4-68. Meteoroid Environment, Expected Number of
Impacts during Entire Mission as Related
to Particle Size

stress in the doubled area from exceeding the axial stress in the
unspliced region. This is also the highest slope that produces no
compression.

These criteria led to the finally adopted tendon design
illustrated in Figure 4-69. It is composed of two straight edge tapes
and several diagonal tapes at an angle of app. 2° and intersecting in
2.5 m intervals. The 0.27 m wide cross-section consists of 5 and, in
some regions, 6 tapes (average 5.6 tapes). The width of the individual
1-mil thick tapes varies from 2.1 cm at the root to 0.6 cm at the tip
of the blade, with a median width of 1.27 cm and a median weight of
2.89 g/m.

The failure sensitivity of individual tendon elements as
related to meteroid size is illustrated in Figure 4-70. It can be seen
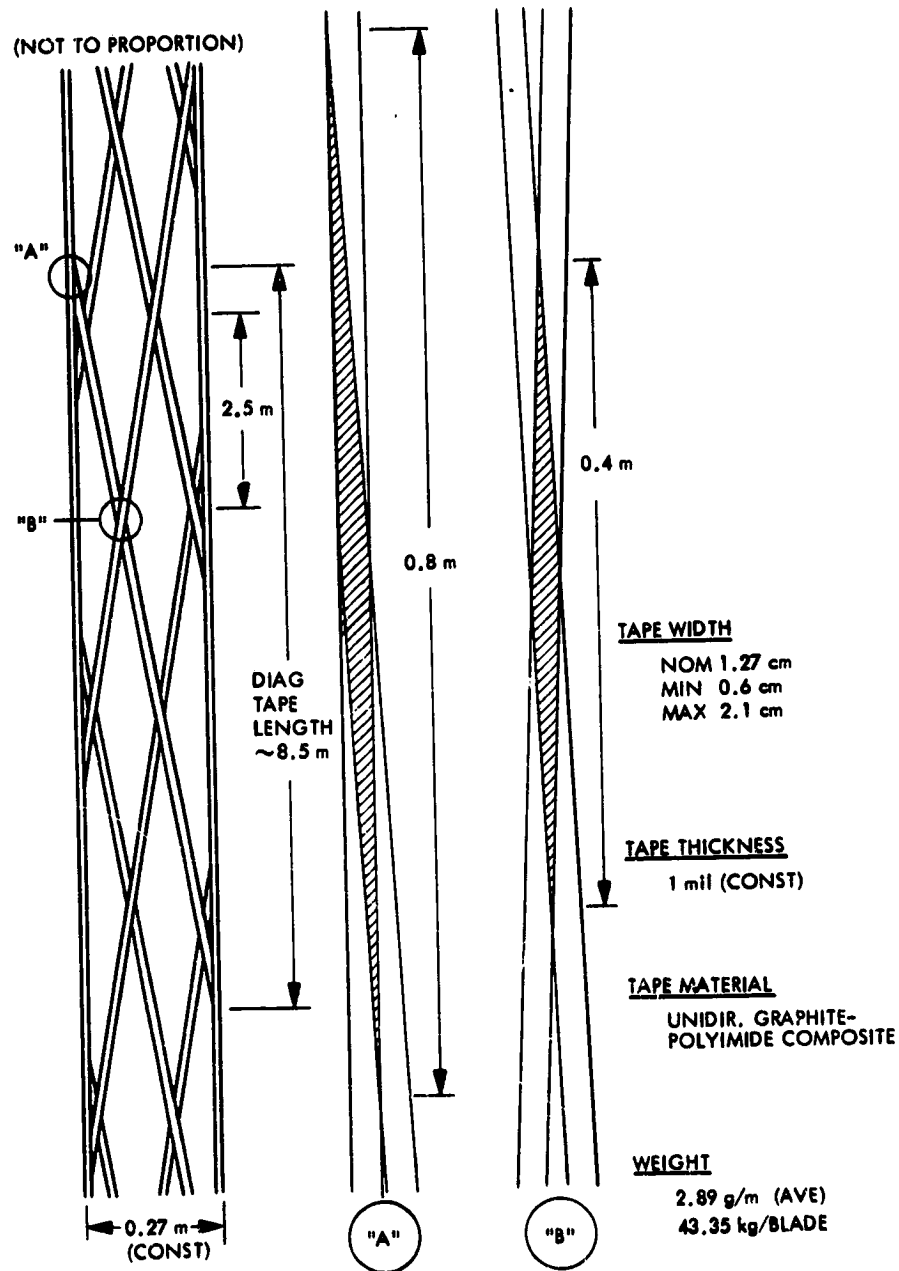
Figure 4-69. Tendon Design - Tape Data

that failure of an appreciable fraction of elements occurs only in the
size range between 0.1 and 1 mm. Below this range the particles are too
small to cause damage, while above 1 mm the probability of hig becomes
negligible. Assuming very conservatively the complete meteroid size
spectrum up to the cm-regime, the fraction of elements failing during
the entire mission is 0.29%. The total expected failure rate per meter

720-9
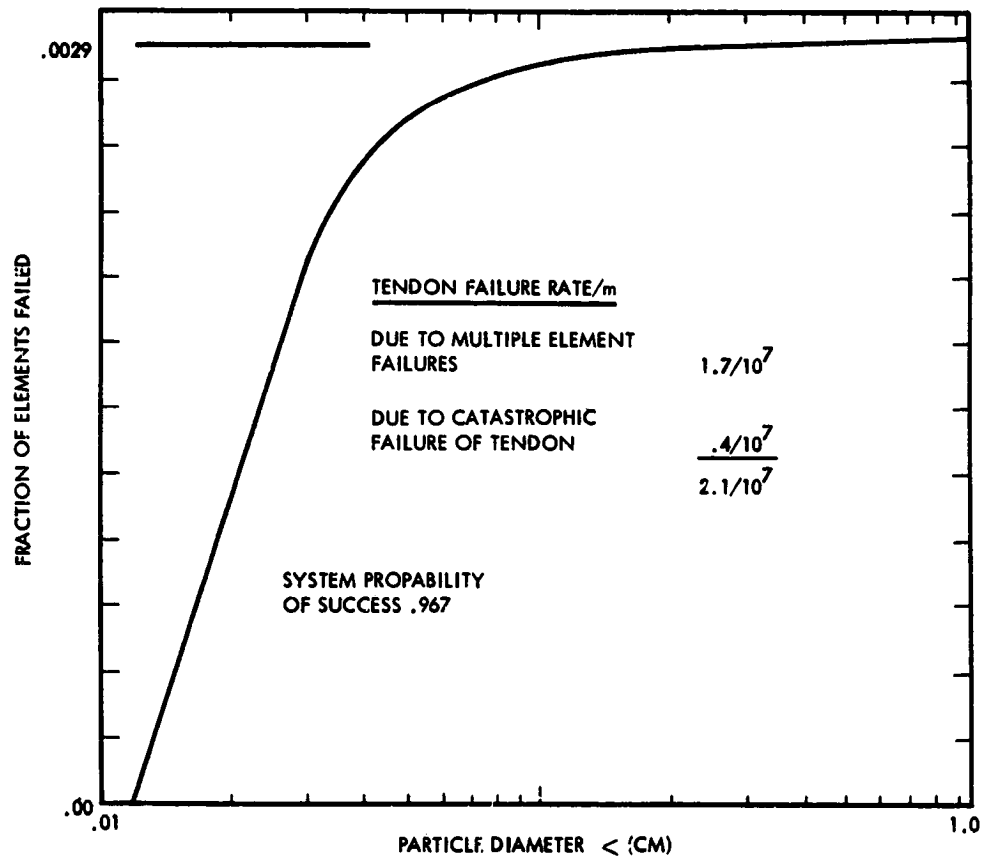
Figure 4-70. Fraction of Elements Failed
Due to Meteroid Impact

of tendon is in the order to 2.1 x 10^{-7}. Rates by failure mode are as follows:

Multiple Element Failure	1.7 x 10^{-7}
Catastrophic Tendon Failure	0.4 x 10^{-7}

On the basis of these data, the overall probability of tendon survival has been computed (conservatively) to 0.967.

According to Table 4-37, the tendon tapes exhibit a minimum tensile strength of 120,000 psi. On the basis of this value, the safety factor of the virgin tendons against rupture is app. 2.5, which decreases gradually with the meteroid-induced disablement of individual members of 1.2 at the end of the mission.

Summary of Tendon Material:

Base Material: Composite of NR-150-B2 polyimide and high-strength graphite fibers, preferably Celion 6000 or Modmore II.

Composite Form: Unidirectional single tape with a uniform thickness of 25 μm (1 mil) and a maximum width of 2.1 cm.

Joining Method: Thermoplastic (fusion).

4.5.4.8 **Battens.** To counteract excessive catenary curvature of the tendons, i.e., to keep the blade edges reasonably straight, chordwise compression members ("battens") are required at variable intervals, ranging from 15 m near the tip to 120 m toward the flap hinge (root). Primary design criteria are (1) Stiffness against bending/buckling at a maximum chordwise compressive load of 12N, (2) Capability of compacting at low pressure to a flat configuration of minimum thickness for roll-up on the stowage reel, and (3) low weight.

In the final design, the 0.12 m diam. x 8.0 m long cylindrical batten was to be constructed from 0.5 x 0.5 mm graphite/polyimide tapes, arranged in a 45 spiral lattice and chordwise longerons (Figure 4-71). To accommodate both, the cylindrical and flattened configuration, the batten is assembled from two lengthwise halves, connected with 6-mm titanium hinges. Assembly and curing of one half-batten on a smaller (8 cm diam) mandrel provides sufficient spring action for positive self-erection upon deployment from the reel.

Heat-shielded by a strip of standard sail film, the batten temperature does not exceed 250°C (480°F). This moderate temperature permits a wide choice of polyimides as tape matrix. In view of the high stiffness requirements, the use of a high modulus fiber, such as HMS or GY-70 is mandatory. Compressive strength and modulus are included in Table 4-37.

720-9

DIAM   DEPLOYED 12 cm

WIDTH   FLATTENED 18.8 cm

THICKN.   FLATTENED ∼ 1.5 mm

TITANIUM HINGES

GRAPHITE/POLYIMIDE SPIRALS

GRAPHITE/POLYIMIDE LONGERONS
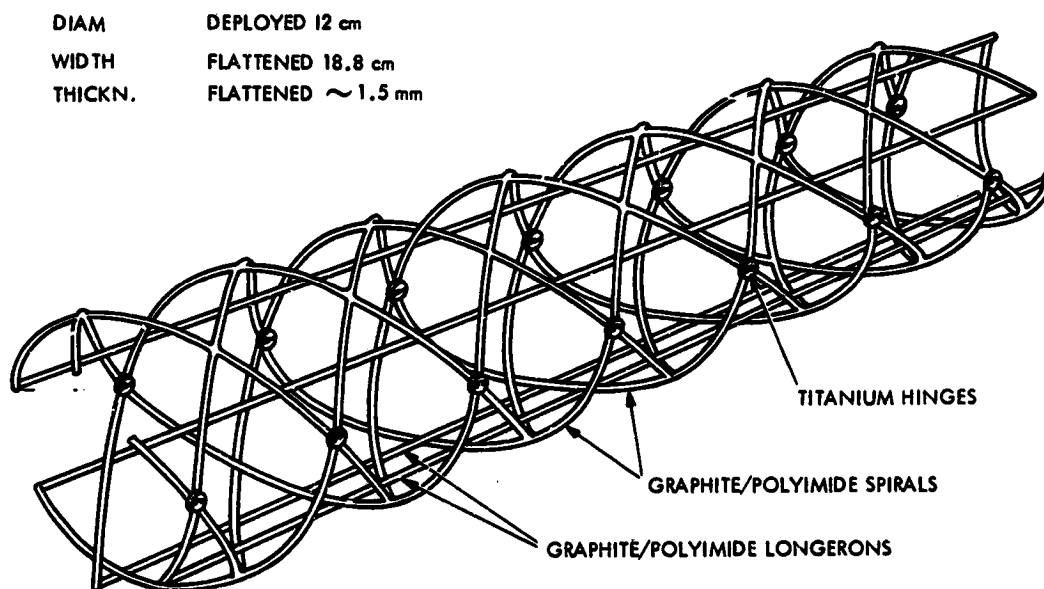
Figure 4-71.   Batten Construction
(Circular Section)

4.5.4.9   Cross-Tendons.   In one of the alternate blade designs, the
sail area is composed of individual 15-m long film panels which are
attached to the tendons by means of two cross-tendons, as illustrated
in Figure 4-72. Since the temperatures, loads and joining require-
ments of the 3 mm wide cross-tendons are essentially identical to those
of the tendons, the same 1-mil tape material can be applied. With
regard to meteroid damage, the use of two tapes provides adequate redun-
dancy for high survival probability of at least one tape, sufficient
for the moderate load. The cross-tendons are joined with the main
tendons by thermoplastic bonding, while the film is attached by adhe-
sive bonding.
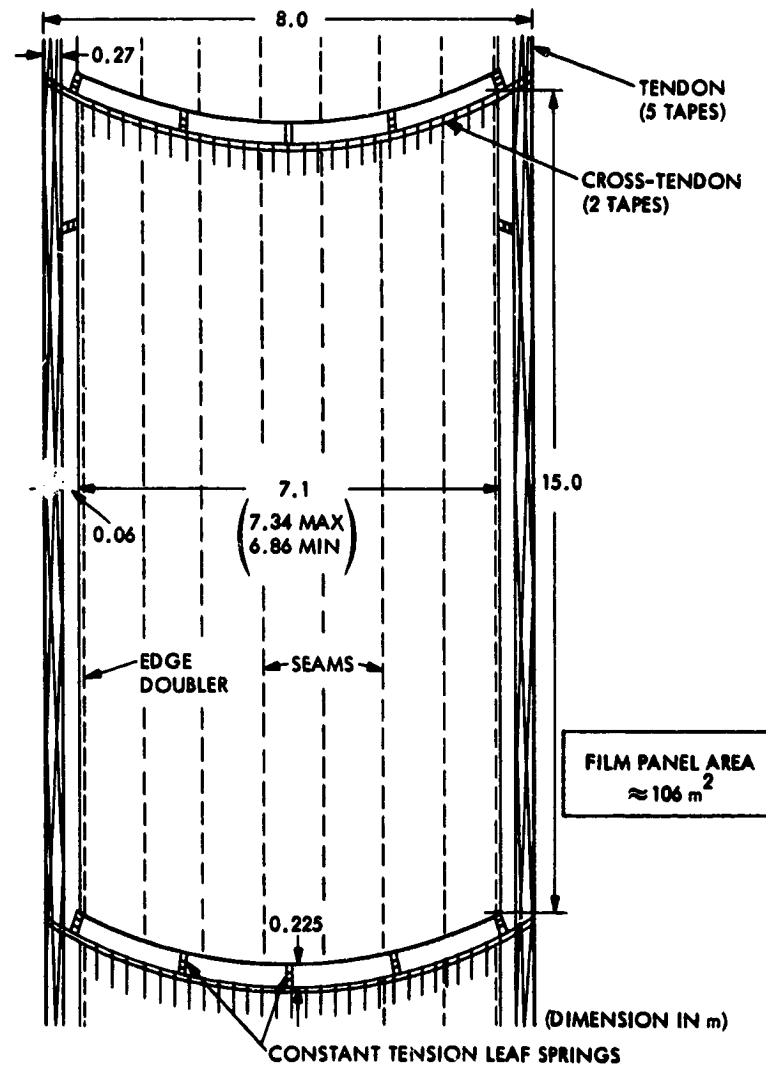
Figure 4-72.   Film Panel Suspension with
Cross-Tendons

4.5.5   Blade Assembly. A short paragraph is devoted to the assembly
of the blade, since it is possibly the most demanding and complex man-
ufacturing task ever to be undertaken.   In view of the delicate nature
of the components and the sensitivity of the materials to degradation
by mere handling, the entire 7.5 km long blade has to be fabricated in
one single continuous operation, from base material forms to the

finished product, rolled up on the flight reel and ready for deployment in space. This calls not only for very exacting individual manufacturing operations, but on-the-spot quality assurance, since the commonly practiced inspection and qualification of the end product is not possible. A simplified flow chart of the blade assembly, identifying only major operations, is presented in Figure 4-73. More detailed information can be obtained from Reference 2, which also includes conceptual tooling design.

4.5.6   Base Material Specification and Quantities. In the following, the most significant base materials for major structural components are summarized with regard to material type, material form and quantities required for the Halley mission. Quantities include the flight
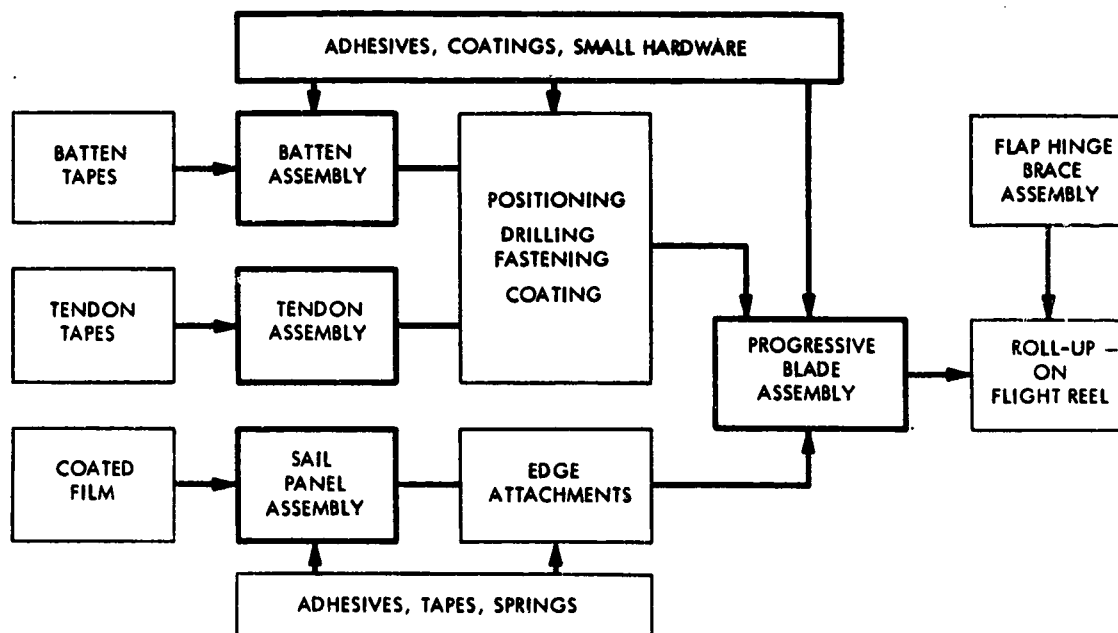
Figure 4-73. Blade Assembly Flow Chart

vehicle, ground test articles as well as manufacturing waste and
represent the total demands for material producers.

(1) Tubings

Material: Prepreg tape of NR-150-B2 polyimide and HMS
or GY-70 graphite fibers. Tape thickness
63-88 μm (2.5-3.5 mil).

Composite Construction: Multiple Lay-up in 0° and
45° orientation.

Tubing Dimensions: 2.5-10 cm (1-4 in) diameter,
0.38-0.76 mm (15-30 mil) thick, in lengths of
0.8 to 1.5 m. (2.6-5 ft)

Quantity: 4,750 m (15,580 ft)

Weight: app. 255 kg (560 lbs)

(2) Tendon Tapes

Material: Prepreg tape of NR-150-B2 polyimide and
high-strength graphite fibers (Celion 6000 or
Modmore II).

Form: Unidirectional tape of 25 μm (1 mil) thickness
and 0.6 to 2.1 cm (0.32-0.83 in) width.

Quantity: app. 1.5 million m (∿5 million ft).

Weight: app. 780 kg (1,700 lbs)

(3) Batten Tapes

Material: Prepreg tape of PMR-15 or LARC-160 polyimide
and HMS or GY-70 graphite fibers.

Form: Unidirectional tape of 0.5 x 0.5 mm (20 x 20
mil) cross-section.

Quantity: app. 225,000 m (738,000 ft)

Weight: app. 83 kg (181 lbs)

REFERENCES

1. Heliogyro Preliminary Design, Final Report, MacNeal-Schwendler Corporation Report No. MS-404, 24 August 1977. Vol. I – MacNeal-Schwendler Reports.

2. Ibid. Vol II – Astro Research Corporation Reports.

3. Development of Design Data for Graphite-Reinforced Epoxy and Polyimide Composites, General Dynamics-Convair Report No. GDC-DBG-70-005, May 1974.

Chapter 5

CONCLUSIONS AND RECOMMENDATIONS

The feasibility of space-stable, very large area, highly reflecting film systems at 3.3 gm/m^2 (>300 m^2/Kg) has been demonstrated. A reasonable probability of comparable films approaching 1.6 gm/m^2 (>600 m^2/Kg) has been indicated.

NASA has decided, for reasons other than high performance Sail material feasibility, not to attempt a Halley Comet Rendezvous Mission (HCRM) and to concentrate on development of ion propulsion for other "low thrust" missions. Reversal of the decision on the former (HCRM) is not only unlikely, it is rapidly becoming (if not actually already) impossible because of the lack of the time necessary for further development and manufacturing scale-up to meet the required launch date. Since ion propulsion is judged to: 1) be closer to demonstrated technology readiness and 2) have greater growth potential (i.e. to nuclear electric propulsion), there are no plans for Solar Sail development in the foreseeable future.

The ultra-light weight, reflective film technology developed for the Solar Sail and the future projection of this technology may have a significant impact on other future space missions. Specific identified potential applications are: 1) reflecting solar concentrator surfaces for the heat engine version of sattelite power station (SPS); 2) reflectors for the concentrated photovoltaic version of SPS and 3) Solares, space reflectors for terrestrial solar power stations. Potential other applications include antenna membranes and light-weight, high temperature, radiation resistant, multi-layer insulation.

Some discrete points in current and projected thin-film technology are shown in Table 5-1, with an estimate of calendar time and dollars to reach technology readiness for missions requiring $\sim 10^6 m^2$. Requirements for a few 10's or 100's of m^2 can probably be met in much shorter time and with significantly less resources.

720-9

Table 5-1.   Current and Projected Thin Film Technology

Film System Area/Mass (Incl. Relf. Coatings)	Current Status	Estimated Projection to Large Scale Technology Readiness*		Notes
		Time	Dev/Equip $	
11 gm/M^2 (90 m^2/Kg)	Nov. 76	—	—	Current technology
3.2 gm/M^2 (>300 m^2/Kg)	Feasibility Demonstrated	2-3 Yrs	$10M	Baseline for study completed July 1977
1.6 gm/M^2 (>600 m^2/Kg)	Probable	5 Yrs	$10-30M	Reasonable probability
1.0 gm/m^2 (1000 m^2/Kg	Lower Limit of Practical Terrestrial Mfg.	5 Yrs	$30M	Practical limit
(0.2-0.5 gm/m^2	Mfg. in Space	10 Yrs	TBD	Mfg. in low-G and vacuum of space

*Note: A few 10's or 100's of square meters could be made in time
         with resources.

The estimated limit of practical terrestrial manufacture
(1 - 1.5 gm/m^2) is based on extrapolation of technology and handling
experience. Lighter weight films could be made but the handling con-
straints for terrestrial manufacture, assembly, launch stowage and sub-
sequent space deployment would make large scale applications impactical.

Reinforced or unsupported films in the range of 0.2 -
0.5 gm/m^2 could be manufactured and used in the low -g and atmosphere
free environment of space.

The significance of reduced film area density on the feasibility of very large area space structures is illustrated in Figure 5-1, which shows the number of shuttle flights required to launch $10^8 m^2$ reflector film and associated structure. The value of $10^8 m^2$ is the approximate size of the collector for the heat engine version of SPS and also the minimum practical area for a single SOLARES reflector array. For this illustration, it was assumed that the structure mass is directly proportional to the film mass and equal to twice the film mass.
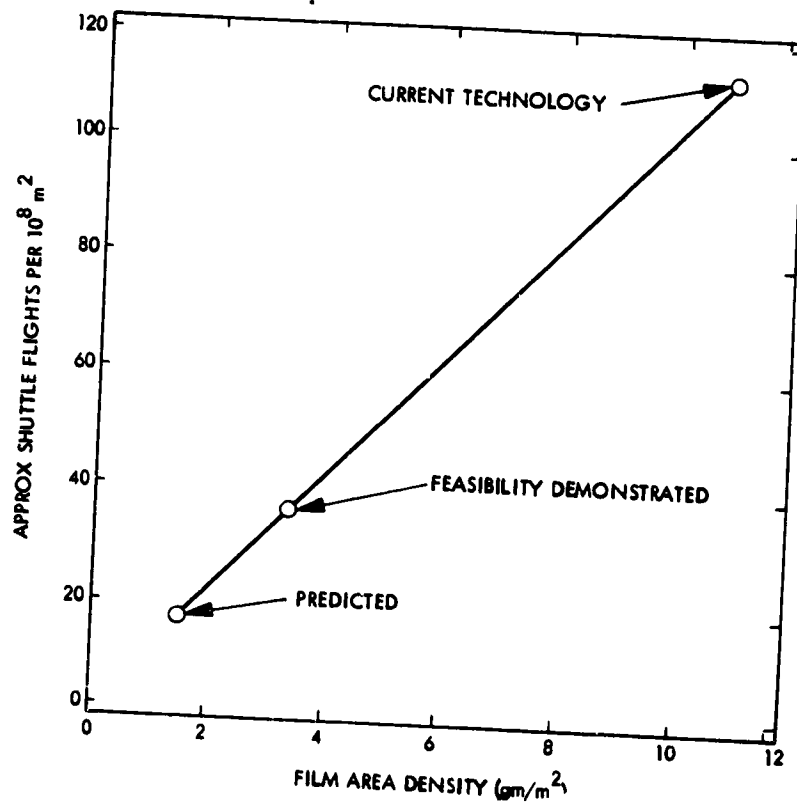
Figure 5-1. Shuttle Flights vs Area Density for Thin Films

APPENDIX I

FABRICATION OF A SAIL SHEET PANEL

The panel is fabricated by bonding four 1.0 foot wide x
7.5 feet long strips of coated 0.3 mil Kapton film into a sheet. Butt
joints will be spliced with coated 0.3 mil Kapton doublers 0.5 centi-
meter wide x 7.5 feet long. The doublers will have NА-150-B2G adhesive
coated (sprayed) on the aluminum surface to a thickness of 0.1 to
0.15 mil. Adhesive for making all bonded joints is only applied to
the doublers.

Brown Kraft paper is used as a carrier to enable us to move
the cure the assembly without causing the layup to separate or creep
out of tolerance. Strips of brown Kraft approx. 5/8 in. wide x 7'7"
are placed over the doublers in the layup in order to assure that
adhesive flash cannot get onto the curing facility.

Solvent tacking is accomplished by spraying a very small
amount of solvent (ethyl alcohol or ethanol) onto the joint at the spot
on which the doubler is to be tacked. Before the alcohol dries, the
doubler must be properly located and lightly pressed onto the alcohol
wetted spot. Hold a light pressure for a few seconds and then release
it.

Soldering iron tacking is accomplished by pressing a heated
soldering iron onto a piece of brown Kraft paper placed over the spot
to be tacked. Hold heat and pressure on the spot until the paper
starts to darken or discolor under the iron. (15-20 seconds.)

Step by Step Assembly Procedure

1) Procure a sheet of 1/4, 3/8, or 1/2 inch plywood 4 ft. x 8 ft.

2) Cover the smooth side of the plywood with brown Kraft Paper stretched tight and wrinkle free. Tape the paper firmly to the plywood around the peripheral edges. A longitudinal splice is probably required in the paper. Make sure it is located between the bond joints and between the paper and the plywood. Use 1 in. masking tape.

3) Cut a strip of coated Kapton 7 ft. 8 in. long.

4) Lay it flat, (do not stretch it too hard) on a smooth surface convenient for spray painting. (The back of the sheet of plywood with a strip of paper on it might do.)

5) Spray NR-150-B2G on the aluminum coated side to a width of about 6 in. so that a strip 6 in. x 7 ft. 8 in. is coated 0.1 to 0.15 mil with the adhesive.

6) Air dry the adhesive for two hours or more.

7) Oven dry the adhesive for 5 to 15 minutes at $225^{\circ}F$.

8) Cut (carefully) the strip of adhesive coated Kapton into doublers 0.3 in. wide x 7 ft. 8 in. long (a total of 11 doublers are required for the panel, seven for the butt joints and one for each peripheral edge.)

9) Cut four strips of coated Kapton 1 ft. x 7 ft. 8 in.

10) Carefully trim the edges straight and to a width of 11.5 inches.

11) Carefully lay the first stip of coated film on the stretched taped paper. Locate it (with the chromium side up) 1 in. in from the edge of the plywood sheet and 2 in. from one end. Pull it tight (do not stretch) and tape each end in 3 places.
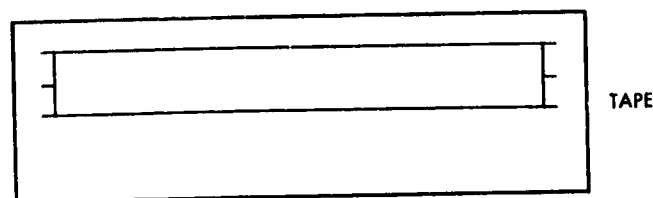
TAPE

12) Carefully lay the next strip so that the longitudinal edges butt but do not overlap – and tape in place. (You will probably be able to get the two strips to butt at the ends only.)

13) Tack one end of (adhesive tack) a doubler to the abutted strips at one end. Be careful to located the doubler so that one half its width is on each strip. (We placed a straight edge on one strip one half a doubler width from the joint and used the edge to locate the doubler.)

14) Progressively each 4 in. (approx) bring the strip edges into contact (do not overlap) and adhesively tack the doubler to them.

15) When the joint is completely adhesively tacked, soldering iron tack the joint in at least 8 places.

16) Lay the next strip (step 12) and repeat operations 13 thru 15.

17) Repeat operation 16

You should now have four 11.5 in. x 7 ft. 8 in. strips taped to the plywood (or the paper on the plywood) and the three joints tacked securely.

18) Slide a sheet of paper between the film assembly and the paper it is taped to. The purpose of this added paper is to prevent slitting the bottom (carrier) paper as the strips are slitted for the four additional seams (joints). The paper should extend from end to end in order to protect the carrier paper fully.

720-9

APPENDIX II

REVIEW OF HIGH PROBABILITY FAILURE MODES AND ASSIGNMENT FOR SPECIALIST CONFIRMATION

Specialist Organization Identification

1. Materials

2. Structures and Dynamics

3. Attitude Control

4. Design and Hardware

5. Spacecraft

6. Mission Design

7. Temperature Control

8. Power

720-9

Solar Sail Sheet Material Failure Interactions

Review of High Probability Failure Modes
and Assignment for Specialist Confirmation

Failure Interaction	Review Coordination	
	Test Group Data Required	Affected* Investigative Organizations
THERMAL ENVIRONMENT		
Interaction of the sail with the thermal environment is the most significant consideration for this mission since sail strength and susceptibility to applied load failure modes is a function of temperature.		
I. Environments		
A. Sail Loading		
It is particularly important that these failure interactions be considered against the sail characteristics with the appropriate accumulated environmental history.		
1. Reduced strength at high temperatures can result in sail tearing or deformation under load. Creep at high stress locations reduces load capability, affects propulsive efficiency and attitude control.	1	1,2,3,4,6,7
2. Brittleness at low temperatures can result in coating or sheet cracking during sail reorientation or reefing.	1	1,2,4
3. Worst case dynamic loading after deployment is probably $180°$ rotation per day in the high temperature cranking orbit. Stress loads can tear or deform sail.	1	1,2,3,4,6

*from II-1

720-9

Review of High Probability Failure Modes and Assignment for Specialist Confirmation (Cont.)

Failure Interaction	Review Coordination	
	Test Group Data Required	Affected* Investigative Organizations
4. The 180° rotation per day in cranking orbit is the major repeated loading sequence for the sail. Fatigue failure is a possibility.	1	1,2,3,4,6
5. Reefing is a potential cause of fatigue failure. Additional considerations are local stress concentrations, folding, and wrinkling.	1	1,2,3,4
B. Trajectory		
The flight path affects gross and cyclic heating/cooling of the sail. Sun approach distance is limited by the high temperature strength of the film material. Potential degradation of optical properties by the time of the cranking maneuver may restrict the minimum AU and reduce performance. Occultations from passing in front of a planet may cause sail overheating from loss of cooling emission. Occultations from passing behind a planet may damage sail coatings from differential expansion/contraction of coating and film or may reduce gross sail temperature limiting sail orientation or reefing for a time after emergence.	1,3	1,3,6
II. Characteristics		
Sail response to the thermal environment at a given mission milepost depends upon changes in sail characteristics as the result of accumulated solar radiation, space vacuum and temperature history prior to that point.		

*from II-1

720-9

Review of High Probability Failure Modes and Assignment for Specialist Confirmation (Cont.)

Failure Interaction		Review Coordination	
		Test Group Data Required	Affected* Investigative Organizations
A.	Materials Specifications and Process Specifications	1,2,3	1,2,3,4,6,7
	The sail must retain strength and integrity at temperatures from -100°C to 315°C. Materials must be homogeneous, without contaminants, solid inclusions or voids that will weaken, upset thermal balance, or distort the sail in the space thermal environment. Process specifications must prevent residual stresses, gas or air inclusions in adhesives, and uneven material thicknesses that will weaken, upset thermal balance, or cause unplanned sail distortion in the space thermal environment.		
B.	Aging	1,3	1,2
	Hardening or embrittlement of the sail after accumulated UV and vacuum exposure may increase its susceptibility to fatigue failure from repeated loading. Of particular concern are areas where coatings have cracked allowing direct film exposure to solar radiation.		
C.	Temperature	1	1,2
	1. Expansion/contraction (non-isotropic) of the sail adds to the stresses of dynamic and steady state loading.		
	2. Differential expansion/ contraction of the sail due to the non-isotropic properties of Kapton causes higher stresses in one plane. Warping may result affecting sail		

*from II-1

II-4

Review of High Probability Failure Modes and
Assignment for Specialist Confirmation (Cont.)

		Review Coordination	
	Failure Interaction	Test Group Data Required	Affected* Investigative Organizations
	thermal balance/control or attitude control.		
3.	Differential expansion/ contraction of the sail components (coatings and film) may crack the coatings exposing the film directly to solar radiation.	1	1
4.	Expansion/contraction after deployment may open cracks along creases formed in packing and storage.	1	1
5.	Outgassing of the Kapton film at high temperatures may cause eruptions in the coatings — reducing propulsive efficiency, revising sail thermal balance and exposing film to direct solar radiation.	1,3	1,2,6,7
6.	Expansion of trapped air pockets in adhesives may degrade sail seam strength by local rupture of the bonds.	1	1
D. Strength		See I.A.	See I.A.
	Sail strength varies with temperature and the cumulative solar radiation exposure. Reduced strength at high temperature and brittleness at low temperature are analyzed under item I.A. above for failure modes under load.		

ORIGINAL PAGE IS
OF POOR QUALITY

*from II-1

Review of High Probability Failure Modes and
Assignment for Specialist Confirmation (Cont.)

Failure Interaction	Review Coordination	
	Test Group Data Required	Affected* Investigative Organizations
E. Isotropic Properties Variation of characteristics with axis causes unequal load distribution and possible sail distortion and warping. Analysis is under I.A. and II.C.2 above.	See I.A., II.C.2.	See I.A., II.C.2.
F. Electrical The sail electrical properties of surface resistance, capacitance, and transverse breakdown voltage vary with temperature.		
1. Static discharge from one coated surface to the other through the film can rupture the film and break the coating surface. Propulsive efficiency is reduced, thermal balance is disturbed and the film is exposed to direct solar radiation.	2	1
2. If coated surfaces become like charged, the coatings may be pushed apart, breaking the bond with the film. The separated materials may be severely damaged by dynamic loading, reefing, and differential thermal expansion.	1,2	1,2
3. Static charge over the non-uniform constructed, differentially heated/cooled sail may warp the sail affecting propulsive efficiency, thermal balance and attitude control.	1,3	1,2,3,4,7
G. UV Resistance Susceptibility to UV radiation damage may be temperature	1,3	1,2,6

*from II-1

Review of High Probability Failure Modes and
Assignment for Specialist Confirmation (Cont.)

	Review Coordination	
Failure Interaction	Test Group Data Required	Affected* Investigative Organizations
sensitive. UV damage to either coatings or film will affect strength and possibly electrostatic and optical characteristics. Analyses in I.A. above and II.H. below will determine failure modes.		
H. Optical		
Reflectivity and emissivity is a function of sail temperature and the accumulative influence of solar radiation, space erosion and mechanical surface irregularities.		
1. Loss of specular reflectivity reduces propulsive efficiency.	3	1,6
2. Reduced emissivity changes the sail thermal balance, raising sail temperature. Increased sail temperature reduces strength and increases creep. Reduced load capability may result in sail tearing. Deformation from creep affects propulsive efficiency and attitude control.	1,3	1,2,3,4,6,7
3. Combined reduction of reflectivity and emissivity magnifies effects of II.H.2 above.	1,3	1,2,3,4,6,7
III. Failures		
The following sail sheet failure modes, due to all causes, have been identified in order of frequency. Generally only thermal environmental causes are considered in this section.		

*from II-1

Review of High Probability Failure Modes and
Assignment for Specialist Confirmation (Cont.)

	Review Coordination	
Failure Interaction	Test Group Data Required	Affected* Investigative Organizations
A. Puncture Puncture probability from space debris (micrometeoroids, cosmic dust) is likely unaffected by the sail temperature, however, punctures expose film edges and coating bond edges directly to the space environment. The puncture may become an initial source of coating bond or seam bond separation.	1,3	1,2
B. Coating Failure Leading to Base Failure Cracking, peeling, separating, cratering of the metallic coatings that results in direct exposure of the basic film material to the space environment reduces sail strength and accelerates aging.	1	1,2
C. Debonding Excessive heating, differential expansion/contraction and outgassing of the polymer of adhesive entrapped air bubbles can delaminate coatings from the film or cause separation of seams and joints. Reduced sail strength and possible attitude control disturbance results.	1,3	1,2,3
D. Cratering Polymer outgassing can cause surface coating eruptions. The results would be reduced propulsive efficiency, revised sail thermal balance, direct exposure of the film to solar radiation, and possible attitude control influence.	1,3	1,2,3,6,7

*from II-1

Review of High Probability Failure Modes and
Assignment for Specialist Confirmation (Cont.)

		Review Coordination	
Failure Interaction		Test Group Data Required	Affected* Investigative Organizations
E. Dust (Solar Coating)		1,3	1,2,6,7
Dust coating of the sail reduces reflectivity and increases absorb-tivity. Sail temperature increases in all mission phases leading to reduced sail strength and poten-tial sail failure under load. Reduced specular reflectivity affects propulsive efficiency.			
F. Erosion		1,3	1,2,6,7
Reduced reflectivity and increased absorbtivity from erosion increases sail temperature in all mission phases. Reduced strength at high temperature may result in sail failure under load. Reduced specular reflectivity affects propulsive efficiency.			
G. Crosslinking/Deploymerization		1	1
Polymer exposure to direct solar radiation where surface coatings have been damaged or from exposure through the coatings may result in revised molecular structure and physical properties. Susceptibil-ity to damage may depend upon tem-perature level and accumulated radiation exposure.			
H. Desorption		1,3	1
Polymer degradation from desorp-tion of CO_2, H_2O, N_2 and other gases increases with temperature. In addition to revised physical properties after outgassing, the gaseous products may rupture coat-ing surfaces, tear seam bonds or chemically react with coatings and adhesives.			

ORIGINAL PAGE IS
OF POOR QUALITY

*from II-1

Review of High Probability Failure Modes and
Assignment for Specialist Confirmation (Cont.)

Failure Interaction	Review Coordination	
	Test Group Data Required	Affected* Investigative Organizations
SPACE VACUUM ENVIRONMENT		
The vacuum environment of space results in evaporation of materials, volatile components of materials and the layer of absorbed gas on the surface of the material. Evaporation of one or more components of the material results in changes in the bulk mechanical and physical properties.		
IV. Environments		
Failure interactions must be considered for sail properties reflecting the appropriate accumulated environmental history.		
A. Thermal	1,3	1,2,3,6,7
The rate of desorption and evaporation increases with temperature. Outgassing revises physical properties, affecting sail strength. In addition, the gaseous products may rupture coating surfaces, tear seam bonds or chemically react with coatings and adhesives affecting propulsive efficiency and attitude control.		
B. Photons	1	1,2,3,4,7
Evaporation in vacuum is dependent upon the cumulative ultraviolet radiation exposure. Revised molecular structure from UV exposure may increase mass loss and embrittle sail material. Reduced flexibility results in coating or sheet cracking during sail reorientation or reefing.		

*from II-1

Review of High Probability Failure Modes and
Assignment for Specialist Confirmation (Cont.)

	Review Coordination	
Failure Interaction	Test Group Data Required	Affected* Investigative Organizations
C. Micrometeoroids	1	1,2,4
Punctures from micrometeoroids expose film and coating bond edges to space vacuum. The puncture may become an initial source of coating bond or seam separation.		
V. Characteristics		
Sail response to the vacuum environment depends upon changes in sail characteristics as the result of accumulated solar radiation, space vacuum and temperature history at the time of interest.		
A. Materials Specifications and Process Specifications	1,3	1,2,3,4,6,7
The sail must provide a service life of 4-1/4 years minimum in space vacuum. Materials must not have gas or air pockets that can expand in vacuum to rupture the sail. Process specifications must prevent gas or air inclusions in adhesives since these can expand in vacuum, rupture sail sheet and coatings, reducing sail strength, upset thermal balance and cause sail distortion.		
B. Temperature	1	1,2,4,7
Vacuum exposure may change the physical properties and thermal characteristics of the sail material. Changes in specific heat and thermal expansion coefficient affect sail temperature and thermal balance.		

*from II-1

Review of High Probability Failure Modes and
Assignment for Specialist Confirmation (Cont.)

	Review Coordination	
Failure Interaction	Test Group Data Required	Affected* Investigative Organizations
C. Strength	See IV.A.	See IV.A
Sail strength is affected as physical properties change from outgassing or bonds are disrupted by rupture or chemical action. The effects on propulsive efficiency and attitude control together with failure modes under load are analyzed under item I V.A. above.		
D. Substrate Bonds	See IV.A.	See IV.A.
Bond rupture from outgassing of entrapped gas or polymer decomposition products reduces sail strength, affects propulsive efficiency and attitude control as analyzed under item IV.A. above.		
E. UV Resistance	1	1,2
Susceptibilityto UV damage may change as polymer outgassing progresses. This may be due to basic polymer characteristics or to increased UV exposure (direct) because of coating rupture. UV damage to film or coatings will affect strength characteristics. Analyses under IV.A. above will determine failure modes.		
F. Optical	1,3	1,2,3,6,7
The space vacuum environment has an indirect influence upon sail reflectivity and emissivity. These properties are not directly affected by vacuum exposure but by the results of surface changes from outgassing eruptions.		

*from II-1

Review of High Probability Failure Modes and
Assignment for Specialist Confirmation (Cont.)

Failure Interaction	Review Coordination	
	Test Group Data Required	Affected* Investigative Organizations
Optical changes affect thermal balance, propulsive efficiency and attitude control.		
VI. Failures		
The order of frequency of sail failure modes has been established from the interaction of all causes. Generally, only vacuum environmental causes are considered in this section.		
A. Puncture	1	1,2
Probability of puncture is likely unaffected by the vacuum environment, however, punctures expose film and coating bond edges directly to the space environment. The puncture may become an initial source of coating bond or seam bond separation.		
B. Coating Failure Leading to Base Failure	1	1,2
Cracking, cratering, of the metallic coatings from outgassing results in direct exposure of the basic film material to the space environment reducing sail strength and accelerating aging.		
C. Debonding	1	1,2,3
Outgassing of the polymer or adhesive entrapped air bubbles can delaminate coatings from the film or cause separation of seams and joints. Reduced sail strength and possible attitude control disturbance results.		

*from II-1

Review of High Probability Failure Modes and
Assignment for Specialist Confirmation (Cont.)

		Review Coordination	
Failure Interaction		Test Group Data Required	Affected* Investigative Organizations
D. Cratering		1,3	1,2,3,6,7
Polymer outgassing can cause surface coating eruptions. The results would be reduced propulsive efficiency, revised sail thermal balance, direct exposure of the film to solar radiation, and possible attitude control influence.			
E. Crosslinking/Depolymerization		1	1,2,4
Polymer exposure to direct solar radiation where surface coatings have been damaged by outgassing may result in revised molecular structure and physical properties. Susceptibility to damage may depend upon accumulated radiation exposure.			
F. Desorption/Outgassing		1,3	1,2,3,4,6,7
Polymer degradation from outgassing of CO_2, H_2O, N_2 and other gases depends upon ambient pressure and temperature. In addition to revised physical properties after outgassing, the gaseous products may rupture coating surfaces, tear seam bonds or chemically react with coatings and adhesives.			

*from II-1

Review of High Probability Failure Modes and
Assignment for Specialist Confirmation (Cont.)

	Review Coordination	
Failure Interaction	Test Group Data Required	Affected* Investigative Organizations
The preceding considerations of in-space sail failure modes under the influence of thermal and space vacuum environments have described failure modes common to those caused by other environments. To avoid descriptive redundancy, the following failure interactions under the influence of space radiation, solar wind. and micrometeoroid environments, will reference the applicable preceding failure descriptions and add only unique failure interaction descriptions.		
PHOTON ENVIRONMENT		
The infrared and ultraviolet radiations are potentially the most destructive portions of the solar spectrum. IR radiation is essentially heat that must be dissipated by a high emissivity backside sail coating. UV radiation can alter the molecular structure, and thereby the physical and thermal properties, of the organic sail film and adhesives.		
VII. Environments Thermal	See I,II, III, and IV.A.	See I,II,III, III, and IV.A.
Sail strength and susceptibility to applied load failures is a function of temperature. Tests and analyses of Sections I, II, III, and IV.A. are applicable. Damage to film, bonds or coatings from accumulated UV exposure can reduce sail strength at all temperatures.		

*from II-1

Review of High Probability Failure Modes and
Assignment for Specialist Confirmation (Cont.)

Failure Interaction	Review Coordination	
	Test Group Data Required	Affected* Investigative Organizations
VIII. Characteristics		
The accumulated UV exposure at a given mission milepost will affect sail characteristics and response to the thermal vacuum and loads environment.		
A. Materials Specifications and Process Specifications	1,3	1
The solar sail mission includes operation in the high intensity radiation environment of a 0.25 AU solar orbit. The basic film and adhesives must be stable in the UV environment and UV stable coatings must limit maximum sail temperature to 315°C.		
B. Aging	See II.B.	See II.B.
C. Temperature	See II.C., and V.B.	See II.C., and V.B.
D. Strength	See I.A., and IV.A.	See I.A., and IV.A.
E. Coating Thickness		
Coating thin spots resulting from the manufacturing process or erosion can cause local hot spots from IR radiation and expose adhesive and film to direct UV radiation. Potential effects are upset thermal balance, reduced local strength, and reduced propulsive efficiency.		
F. Substrate Bonds	1,3	1,2,6,7
Bond strength may be reduced from local direct exposure to space radiation as discussed in VIII.E. above.		

*from II-1

Review of High Probability Failure Modes and
Assignment for Specialist Confirmation (Cont.)

Failure Interaction	Review C-ordination	
	Test Group Data Required	Affected* Investigative Organizations
G. Optical	1,3	1,6,7
Optical properties of the sail will be affected if IR or UV exposure causes swelling of the film or adhesive such that reflective surfaces are distorted or ruptured, or if pigmentation changes occur affecting transmittance. Effects of optical property disturbance are upset thermal balance and reduced propulsive efficiency.		
IX. Failures		
A. Puncture	See III.A., VI.A.	See III.A., VI.A.
B. Coating Failure Leading to Base Failure	See III.B., VI.B.	See III.B., VI.B.
C. Debonding	See III.C., VI.C.	See III.C., VI.C.
D. Cratering	See III.D., VI.D.	See III.D., VI.D.
E. Dust (Solar Coating)	1	1
Dust coating will increase sail temperature in all mission phases. Susceptibility to UV damage may be temperature sensitive.		
F. Erosion	1	1
Reduced reflectivity from erosion will increase sail temperature. UV damage may be temperature sensitive.		

*from II-1

Review of High Probability Failure Modes and
Assignment for Specialist Confirmation (Cont.)

Failure Interaction	Review Coordination	
	Test Group Data Required	Affected* Investigative Organizations
G. Crosslinking/Depolymerization	See III.G., VI.E.	See III.G., VI.E.
H. Desorption/Outgassing	1 See also III.H., VI.F.	1 See also III.H., VI.F.
Polymer degradation from outgassing of CO_2, H_2O, N_2 and other gases increases from IR induced temperature increases. The revised film and adhesive material may be more sensitive to UV damage.		

SOLAR WIND ENVIRONMENT

Corpuscular radiation from the sun is
called the solar wind. Interplanetary
dust and gas is blown outward from the
sun by the solar wind.

X. Environments		
A. Shape	1	1,3,6
The gross response of the sail shape to the solar wind can affect propulsive efficiency and attitude control.		
B. Temperature	1	1,3,6
Sail response to solar wind caused loads will depend upon physical properties at the applicable temperature.		

*from II-1

Review of High Probability Failure Modes and
Assignment for Specialist Confirmation (Cont.)

	Review Coordination	
Failure Interaction	Test Group Data Required	Affected* Investigative Organizations
C. Electrical Charge		
1. The ionized particles of the solar wind may create a static charge on the front (sun) side of the sail. Static discharge may occur rupturing the film as considered in II.F.L. The static charge may warp the sail as considered in II.F.3.	See II.F.1, II.F.3	See II.F.1, II.F.3
2. The charged particles may degrade reflectance characteristics with influence on thermal balance and propulsive efficiency.	1	1,6,7
XI. Characteristics		
A. Materials Specifications and Process Specifications	1	1
Solar wind density is low, variable and patchy due to irregularities of sun surface eruptions and the interplanetary magnetic field. The materials selection must consider the probable maximum electron energy and fluence of the solar wind environment.		
B. Aging	1,2,3	1,2,4,7
The ionized particles of the solar wind may contribute to hardening or embrittlement aging of the sail. Conversely, aging from UV exposure may affect the charging characteristics of the sail. Aging would affect sail strength and thermal balance.		

*from II-1

Review of High Probability Failure Modes and
Assignment for Specialist Confirmation (Cont.)

		Review Coordination	
Failure Interaction		Test Group Data Required	Affected* Investigative Organizations
C.	Strength	1	1,2,4
	Sputtering from collision of solar wind ions and erosion from collision with solar wind-borne dust may erode the front side of the sail. Tensile and yield strengths may be reduced. Aging from electron collisions may reduce sail fatigue strength.		
D.	Electrostatic Forces	1,2,3	1,3,6,7
	Collision with solar wind ions will either tend to neutralize the static charge on the sail front or will create a static charge. In either case the sail shape can be influenced affecting thermal balance, propulsive efficiency and attitude control.		
E.	Coating Thickness	1,3	1,3,6,7
	Erosion from sputtering or particles, as considered in XI.C. above, may reduce coating thickness. Optical properties will be affected. Coating thickness, including tolerances, must accommodate the erosion, retaining satisfactory optical properties and protecting the basic film.		
F.	Electrical	See II.F.1, II.F.3	See II.F.1, II.F.3
	Coating erosion by the solar wind may change sail electrical properties of surface resistance, capacitance, and transverse breakdown voltage. Failure interactions are as considered in II.F.1 and II.F.3. above.		

*from II-1

Review of High Probability Failure Modes and
Assignment for Specialist Confirmation (Cont.)

Failure Interaction	Review Coordination	
	Test Group Data Required	Affected* Investigative Organizations
G. Optical	1,3	1,6,7
Degradation of optical properties from solar wind caused sputtering and erosion will affect sail thermal balance and reduce propulsive efficiency.		
XII. Failures		
A. Puncture	1,3 See also III.A., VI.A.	1,2,4,6 See also III.A., VI.A.
Solar dust impact may puncture as well as erode the sail. Puncture will reduce sail strength and propulsive performance.		
B. Coating Failure Leading to Base Failure	See III.B., VI.B.	See III.B., VI.B.
C. Cratering	1,3	1,2,4,6,7
Cratering in the solar wind environment is caused by the sputtering from ion collisions. Effects are reduced sail strength and propulsive efficiency in addition to potential thermal balance effects from reduced reflectivity.		
D. Dust (Solar Coating)	See III.E.	See III.E.
E. Erosion	See III.F.	See III.F.

*from II-1

Review of High Probability Failure Modes and
Assignment for Specialist Confirmation (Cont.)

	Review Coordination	
	---	---
Failure Interaction	Test Group Data Required	Affected* Investigative Organizations
MICROMETEOROID ENVIRONMENT Micrometeorite impact will most certainly puncture the sail. Behavior of the sail material under hypervelocity particle impact should be determined. Characteristics of the hole created will influence failure modes from this environment. Flight path planning will avoid known space debris belts.		
XIII. Environments		
Thermal The thermal environment does not affect the susceptibility to micrometeorite impact but sail strength and load capability degradation from punctures will be amplified at high temperature. Sail brittleness at low temperatures may amplify damage from a micrometeorite impact by shattering or cracking film and coatings beyond impact particle dimensions.	1 See also I,II,III, IV.A., IV.C.	1,2,4 See also I,II, III,IV.A., IV.C.
XIV. Characteristics		
A. Strength Sail load capability is reduced by micrometeorite puncture.	1	1,2,4
B. Optical Micrometeorite puncture reduces reflective surface area affecting propulsive efficiency. The puncture characteristics on the sail back side may affect emittance beyond the reduction in area due to the puncture. Thermal balance is therefore a potential problem area.	1,3	1,6,7

*from II-1

Review of High Probability Failure Modes and
Assignment for Specialist Confirmation (Cont.)

Failure Interaction	Required Coordination	
	Test Group Data Required	Affected* Investigative Organizations
XV. Failures		
A. Puncture	1	1,2,4,6,7
Sail puncture from micrometeorite impact reduces sail strength and propulsive efficiency and may affect thermal balance. Exposure of film and bond edges directly to the space environment may initiate bond separations around the puncture.		
B. Coating Failure Leading to Base Failure	1	1,6,7
Hypervelocity micrometeorite impact may shatter, peel, exposad or craze the reflective coatings near the puncture. Such action would expose the basic film material directly to the space environment potentially hastening degradation. Propulsive and thermal performance losses would be greater than that due just to the puncture area.		

*from II-1

APPENDIX III

IRRADIATION CHAMBER CALIBRATION EXPERIMENT

This experiment was designed by JPL and Boeing to compare solar illumination obtainable in the laboratory with the intensity of radiation anticipated for a Solar Sail in space. A series of experiments was eventually performed, by which conventional means of doing UV dosimetry in the laboratory were checked against a calorimeter designed to have solar absorptance (α_s) and thermal emittance (ϵ) coefficients similar to those of the candidate Solar Sail film materials. The calorimeter was delivered to Boeing and installed inside the CRETC II sample exposure chamber just in front of the test film sample plane (Figure A-1).
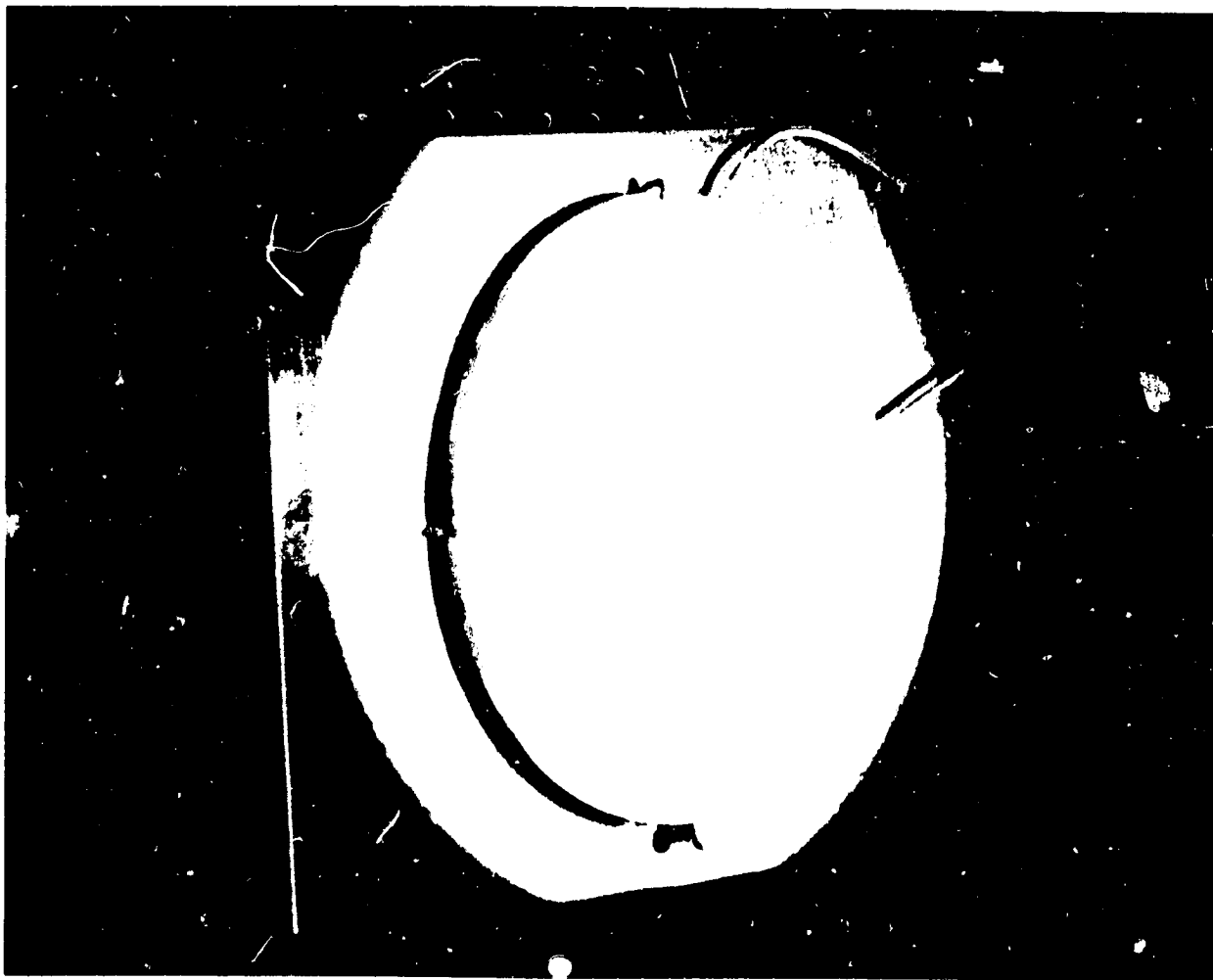

Figure A-1. Aluminized Kapton Calorimeter Exposed to 16-Sun Solar Simulator Beam

A Solar Sail film in a plane, receiving radiation on its front side and emitting radiation on both sides, would equilibrate at a temperature T such that

$$T^4 = \frac{\alpha_s \ (SC)(SR)}{\sigma \ (\varepsilon_f + \varepsilon_b)}.$$

where SC is the solar constant, SR is the sun rate, and σ is the Stefan-Boltzmann constant. It can be shown that Solar Sailing under near-sun conditions (namely, SR = 16 times the solar intensity at Earth's orbit) results in an equilibrium temperature of approximately +250°C for aluminized Kapton that has an emittance-enhancing coating on the back side. On this basis a calorimeter closely simulating a Solar Sail film in α and ε characteristics could be used in a vacuum chamber to set the intensity of radiation from a solar simulator, provided secondary (bounce) radiation in the chamber were comparable to view factors (spacecraft geometry) in space.

The calorimeter discussed above is a circular disk with a diameter of two in. and thickness of 0.1 in. Hence it approximates a Solar Sail film in a plane. It was fabricated by TRW with 2 chromel-alumel thermocouples on the unirradiated side, one at the center and the second 0.707 in. from the center — the radius which divides the calorimeter's total area into halves. Assuming edge losses of heat are small around the perimeter of the calorimeter, its thermocouple(s) will indicate the same equilibrium temperature as stated above for the case of irradiation and partial absorption on its front side and thermal emission from both sides (front and unirradiated back).

The irradiation source must be discussed from the stand-point of its spectral content, since absorption on the front face of a Solar Sail or the calorimeter varies with the wavelength. It is pre-sently impractical to obtain total irradiation levels like 16 suns (to simulate near-sun Solar Sailing trajectories) along with "close filtering" spectral matches using a simulator mobile enough to be com-bined with an ultra-high-vacuum chamber and charged particle accelerator. (That is, the nearly immobile X-75 and X-200 style solar simulators

that have enough energy tu trade for close spectral filtering are not
currently available, and the more mobile, X-25-type power limitations
must be settled for.) As a result, the relatively large emission from
a xenon arc in the near infrared (0.8 to 1.2 micrometers) is utilized
along with the desired continuum across the visible and near-ultraviolet
wavelength regions. Table A-1 shows the relative spectral energy appli-
cable to the start of exposure of metallized film samples.

Table A-1. X-25 Solar Simulator Relative Output

Bandwidth (micrometers)		Scaled Data	Data Matched to 1 Solar Const. (watts/m^2)	Engineering Standard (watts/m^2)	% Deviation
0.25	0.35	4.7	27.3	58.5	−53.3
0.35	0.40	06.7	38.9	56.9	−31.6
0.40	0.45	8.5	51.3	89.6	−40.9
0.45	0.50	10.7	64.6	100.9	−36.0
0.50	0.60	22.8	137.7	177.0	−22.2
0.60	0.70	22.4	135.3	151.5	−10.7
0.70	0.80	19.5	117.8	123.6	−4.7
0.80	0.90	33.0	199.3	99.3	+100.7
0.90	1.00	32.2	194.5	82.6	+135.5
1.00	1.20	22.2	134.1	120.7	+11.1
1.20	1.50	18.1	109.3	111.8	−2.2
1.50	1.80	10.5	63.4	66.9	−5.2
1.80	2.20	8.6	51.9	43.8	+18.5
2.20	2.50	4.1	24.8	19.9	+24.6

The three bands with the longest wavelengths partially repre-
sent emission from the incandescent electrodes of the xenon arc source
lamp. This we eliminate by insertion of a water window between the
solar simulator and the sample exposure chamber, since pure water
absorbs wavelengths longer than ~1.4 micrometers and transmits shorter

wavelengths down to approximately 0.2 micrometers. "Scaled data" represents energy arriving at the detector on a modified Beckman DK-1/ spectro-radiometer measuring system. This data is tnen matched to the spectral shape of the solar constant in space (air mass zero) in accordance with NASA/IES engineering standards. The deviations of spectral power obtainable, compared with the ideal represented by latest measurements of actual solar output, are included in Table A-1.

Between the first and second test stages for the space radiation test, program, Boeing modified the in situ mechanical property test apparatus to provide for insertion of the disk calorimeter in front of the sample plane, and removal at any time using an in situ remote manipulator. As the metallized film experiment was about to begin, the calorimeter disk was moved into the solar simulator's "UV" beam. The group of 10 test samples intervened between the calorimeter's emitting back surface and the water-cooled sample block, modifying the effective emittance of the calorimeter an unknown amount. It was determined that the solar simulator needed to be set at an output level considerably lower than that indicated as 16 suns by a pyrheliometer, if a calorimeter equilibrium commonly used for this type of dosimetry then indicated that approximately nine total suns and seven UV suns were incident on the sample (or calorimeter) plane under these conditions.

In the second test set, after 22 hours of exposure the decision was made to return to the usual pyrheliometer dosimetry as a basis for setting solar simulator output intensity. This decision acknowledged that the presence of an array of test samples between the calorimeter and the water-cooled sample block effectively altered the properties of the calorimeter so that its indicated temperature should not be used as a basis for setting the solar simulator's output level. The solar simulator output was accordingly increased to an intensity of 16 total suns as determined by pyrheliometer dosimetry readings. The calorimeter was not reintroduced into the "UV" beam at this time, because it was known that the solar simulator intensity was now great enough to degrade the calorimeter materials thermally. That is, previous short-time insertions of the calorimeter into such an intense

beam had shown by the slope of the response curve on a strip chart recorder that an equilibrium temperature substantially above ±330°C would be reached.

At the end of the metallized films (Test Set No. 2) experiment the solar simulator output level, which was still being maintained at 16 total suns using pyrheliometer dosimetry, was again compared with indicated calorimeter temperature. The output level of the solar simulator had been adjusted and the optics cleaned from time to time throughout the 1100-hour exposure period of the "second test stage." The final-output dial settings, not easily relatable to the output settings at 22 hours, understandably also resulted in calorimeter temperature indications too high to be sustained safely. The array of samples at test end was quite twisted and irregular in shape. Portions of the back surfaces of some test samples were seen to be facing the radiation sources. In such areas greater absorption occurred, due to the existence of the emissive coating. This led to higher temperatures than planned for the specimens. The twisting modified the calorimeter's effective emittance to an unknown and different degree than at the start of the experiment. It was determined that the only precise data that could be obtained would be a comparison of the calorimeter's temperatures for cases of samples present and samples absent (for a certain reduced simulator output level). Subsequently an equilibrium temperature of +334°C was obtained from the calorimeter with samples still present and a certain solar simulator dial setting. After the ten test samples had been removed a calorimeter thermocouple temperature of +330°C was obtained with the same dial setting. All temperature readings noted here were obtained using the thermocouple at the center of the calorimeter's unirradiated side. Readings from the thermocouple closer to the unirradiated side's edge were consistently 3°C less.

With the ten test samples removed, an outgassed film was clearly observable on the water-cooled sample block just behind the test sample plane. The patterns of outgassed material were typical of thin film interference coatings. As with all other phases of the program, high quality color photographs were taken to document the

condition. Color enlargements were subsequently forwarded to JPL.
Figure A-2 is a reproduction of the patterns of outgassed molecules.
Close examination of the original photos shows the patterns can be
related to polyimide sample placement and subsequent twisting during
the 1100-hour irradiation period. Even the elevated positions of the
1-gram weights below the shortest (Ciba-Geigy) metallized samples can
be discerned from a close examination of the photos.

The emittance of the thin film pattern of outgassed mole-
cular matter was not measured. It has been estimated, however, as
being substantially greater than the emittance of the nickel-plated,
water-cooled sample block. The small $4^{\circ}C$ difference in calorimeter
equilibrium temperatures when the cases of samples present and samples
absent are compared shows that the array of narrow, twisted test samples
following 1100 hours of irradiation had net radiative exchange chara-
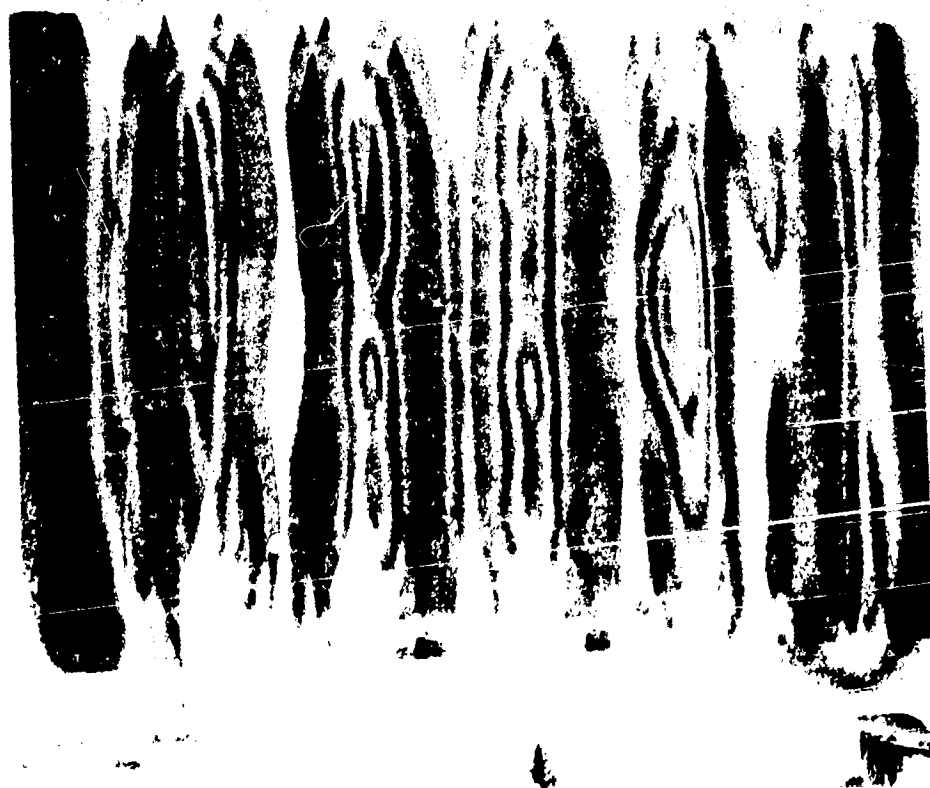acteristics not unlike the outgassed thin film pattern.

Figure A-2. Outgassed Thin Film Pattern Behind Metallized
Polyimide Films Irradiated for 100 hours.

III-6

APPENDIX IV

LIST OF PUBLICATIONS (CONTRACTOR REPORTS)

1. E.J. Bradbury, D.M. Bigg, Chong Wan, D.L. Chambers and F.A. Sliemers, "Survey and Assessment of Monolithic Film Materials and Associated Manufacturing Processes for a Solar Sail.", Battelle Columbus Laboratories Interim Summary Report, JPL Contract 954659, May 2, 1977.

2. L.B. Fogdall and S.S. Cannaday, "Simulation of Space Radiation Effects on Polyimide Film Materials for High Temperature Applications", Boeing Aerospace Co., Final Report, JPL Contract 954701, November 1977.

3. E.E. Luedke, "Thermophysical Properties of Solar Sail Materials", TRW Defense and Space Systems Group Interim Technical Report for the Period 12/1/76 to 3/31/77, JPL Contract 954660, TRW Sales No. 31750.000.

4. E. Luedke, "Thermophysical Properties of Solar Sail Materials" TRW Defense and Space Systems Group 2nd Interim Technical Report, 4/1/77 to 6/30/77, JPL Contract 954660, TRW Sales No. 31750.000.

5. B. Schneier, T.V. Braswell, and R. Vaughn, "Feasibility Demonstration for Electrocasting of Ultrathin Polyimide Films", TRW Defense and Space Systems Group, Final Report No. 32052-6009-RU-00, JPL Contract 954771, August 1978.

6. R.H. Forester, "The Production of Ultrathin Polyimide Films for the Solar Sail Program and Large Space Structure Technology, A Feasibility Study", Midwest Research Institute, Final Report MRI Project No. 4437-N, JPL Contract 954849, June 1978.

7. E. Luedke, "Thermophysical Properties of Solar Sail Materials", TRW Defense and Space Systems Group, Summary Final Report, period 7/77 to 7/78, JPL Contract 954660, TRW Sales No. 31250.000.

8. E.J. Bradbury, R.J. Jakobsen and F.A. Sliemers, "Analysis and Assessment of Film Materials and Associated Manufacturing Processes for a Solar Sail," Battelle Columbus Laboratories, Summary Final Report, JPL Contract 954659, February 1978.

9. R.E. Howe, "Feasibility of Continuous Etching of Kapton Film for Solar Sail," June 1977, P.O. No. A41901B(GP), Surface Activation Corp.

10. T. Smith, "Study of Changes in Properties of Solar Sail Materials from Radiation Exposure," Rockwell International Science Center, Interim Report No. 1, Subcontract No. 954776, July 1977.